

DEVELOPING NOVEL 1,2-AZABORINE BUILDING BLOCKS & THE BASIC SCIENCE OF 1,2-AZABORINES AS HYDROGEN-BOND DONORS

Yao Liu

A dissertation
submitted to the faculty of
the Department of Chemistry
in partial fulfillment
of the requirements for the degree of
Doctor of Philosophy

Boston College
Morrissey College of Arts and Sciences
Graduate School

February 2022

DEVELOPING NOVEL 1,2-AZABORINE BUILDING BLOCKS & THE BASIC SCIENCE of 1,2-AZABORINES AS HYDROGEN-BOND DONORS

YAO LIU

Advisor: Professor Shih-Yuan Liu

ABSTRACT: The overarching theme of this dissertation is developing 1,2-azaborine motif as a novel arene pharmacophore. The first chapter of this dissertation is about exploring the synthesis and characterization of a new α -boryl diazo family-diazomethyl-1,2-azaborine and its diverse reaction chemistry. As a remarkable 1,2-azaborine building block, it can undergo a variety of classical diazo reactions including C–H activation, O–H activation, [3+2] cycloaddition, halogenation, and Ru-catalyzed carbonyl olefination. In the second chapter, we take a closer look at the hydrogen bond donor ability of 1,2-azaborines. A congeneric series of 1,2-azaborine ligands was used to probe the strength of hydrogen bonding as a function of ligand's steric effects. The results of this study provide fundamental reference data for establishing 1,2-azaborines as potential pharmacophores. Lastly, 1,2-azaborine as a new ligand for T4 lysozyme double mutant L99A/M102 was investigated, and a new mode of ligand-protein interaction was discovered and evaluated by X-ray crystallography and ITC.

ACKNOWLEDGMENTS

First and foremost, thanks to my advisor, Prof. Liu for his guidance, support and patience with me throughout my entire PhD process. I will be forever grateful for everything he taught me, from practice of being meticulous to critical thinking skills in scientific research. I am sure the knowledge and skills that I acquired in the past six years will serve me well in my future scientific research journey. I will never forget his help in the process of job searching and graduation.

Thanks to Prof. Zhang and Prof. Chatterjee for serving as the members of my thesis defense committee and taking the time to read and review my thesis and offer your suggestions. I learned a lot from your questions and comments.

My sincerest thanks to my mentors and colleagues in Liu lab throughout my study: Dr. Peng Zhao, Dr. Kiran Unikela, Dr. Andrew Baggett, Dr. Zachary Giustra, Dr. Jacob Ishibashi, Dr. Yuanzhe Zhang for mentoring me and offering me valuable advice, help and company in difficult times, and my junior colleague Xinyu Yang for giving me suggestions with job searching and encouragements. Thanks to all group Liu members in 013 for creating a fun and friendly working environment.

Special thanks go out to Dr. Marek Domin, Dr. Bo Li, TJ for helping me with my experiments and providing expert advice. And BC administration team (Lynne Houlihan, Dale Mahoney) for always being so helpful.

Finally, I own an incredible amount of gratitude to my Parents, Chunxiang Jiang and Pin Liu. They offered me unconditional support and love which made this PhD process possible.

To My Mom and Granny

TABLE OF CONTENTS

LIST OF ABBREVIATIONS	v
Chapter 1 Diazomethyl 1,2-azaborine and its derivatives.....	1
1.1 Introduction to synthesis of diazo compounds	1
1.2 Heteroatom-containing diazo compounds.....	7
1.2.1 Phosphine-substituted diazo reagents.....	7
1.2.2 α -boryl diazo reagents	9
1.2.3 α -Diazo silicon compounds.....	11
1.3 Reactions of diazo compound	13
1.3.1 Diazo compounds stability.....	13
1.3.2 [3+2] Cycloaddition of diazo compounds	14
The theory about the conservation of orbital symmetry in concerted reaction.....	16
1.3.3 Perturbation theory	17
1.4 Diazo compounds as carbene precursors.....	22
1.4.1 Fisher and Schrock carbene.....	25
1.4.2 Ru-catalyzed carbonyl olefination	27
1.4.3 C-H bond activation of diazo compounds	30
1.4.4 Metal carbene C-H insertion mechanism	31
1.4.5 Diazo X-H insertion reactions.....	36
1.4.6 Halo functionalization of diazo compounds.....	40
1.4.7 Diazo compounds utility in total synthesis	43
1.4.8 Reaction of diazo compounds with organoboron compounds	45
1.5 Diazomethyl-1,2-azaborine compounds as a new class of α-boryl diazo compounds.....	47
1.5.1 Synthesis of Diazomethyl-1,2-azaborine.....	48
1.5.2 Diazomethyl-1,2-azaborine as a new versatile 1,2-azaborine building blocks.....	50
1.5.3 Experimental section.....	60
Chapter 2 Understanding the hydrogen bond donor capability of 1,2-azaborines	109
2.1 Introduction to 1,2-azaborine chemistry	109
2.1.1 Basic electronic structure of 1,2-azaborines	109
2.1.2 Synthesis of 1,2-azaborine: A brief historical perspective	110
2.1.3 Late-stage functionalization of 1,2-azaborine.....	112
2.1.4 The application of 1,2-azaborine in biomedical research	116
2.2 Hydrogen bonding in molecular binding recognition.....	118
2.3 Engineered T4 double mutant lysozyme as arene recognition cavity	122
2.4 H-bonding between 1,2-azaborine and T4 double mutant lysozyme cavity.....	130
2.5 The measurement of hydrogen bonding strengths.....	132
2.6 Introduction to isothermal titration calorimetry.....	134
2.7 Double mutant cycle analysis review.....	135
2.8 Exploring the strength of a hydrogen bond as a function of steric environment using 1,2-azaborine ligands and engineered T4 lysozyme receptors	136
2.8.1 The relationship of hydrogen bonding strength with the steric demand of the ligand.....	136

2.8.2 Experimental details.....	144
2.9 Binding of 1,2-azaborine to L99A/M102H T4 lysozyme: the presence of a water bridge.....	159
2.9.1 The role of water bridge in the intermolecular hydrogen bonding network.....	159
2.9.2 The protein X-ray crystal structure of 1,2-azaborine in T4 lysozyme L99A/M102H cavity.....	162
2.9.3 Isothermal titration calorimetry data	166
2.9.4 Experimental session	169

LIST OF ABBREVIATIONS

Å	Angstrom
Ac	Acetyl
aq	Aqueous
Ar	Aryl
atm	Atmosphere(s)
ATP	Adenosine triphosphate
B ₂ Pin ₂	bis-Pinacolatodiboron
Bn	Benzyl
Boc	tert-Butoxycarbonyl
bp	Boiling point
Br	Broad
Bu	Butyl
Bz	Benzoyl
d	Doublet
DART	Direct analysis in real time
dba	Dibenzylideneacetone
dd	Doublet of doublets
DFT	Density functional theory
DIPEA	Diisopropylethylamine
DMF	N,N-Dimethylformamide
dt	Doublet of triplets
DTBP	Di-tert-butyl peroxide
dtbpy	4,4'-Di-tert-butyl-2,2'-bipyridyl
dppf	1,1'-Bis(diphenylphosphino)ferrocene
EDTA	Ethylenediaminetetraacetic acid
ee	Enantiomeric excess
eV	Electron volts
ESI	Electrospray ionization
Et	Ethyl
Eq	Equation
equiv	Equivalent(s)
FT	Fourier transform
GC	Gas chromatography
h	Hour(s)
Het	Hetero
HPLC	High performance liquid chromatography
HRMS	High resolution mass spectrometry
<i>i</i> -	Iso
IPTG	Isopropyl-β-D-thiogalactopyranoside
IR	Infrared
LB	Luria–Bertani
m	Multiplet

M	Molar
mCPBA	meta-Chloroperbenzoic acid
Me	Methyl
Mes	Mesityl
min	Minute(s)
Ms	Mesyl
MTBE	tert-Butylmethyl ether
NMI	N-Methylimidazole
NMO	N-Methylmorpholine N-oxide
NMR	Nuclear magnetic resonance
OD	Optical density
Pd/C	Palladium on carbon
<i>p</i> -ABSA	4-Acetamidobenzenesulfonyl azide
Ph	Phenyl
ppm	Parts per million
Pr	Propyl
PPTS	para-Toluenesulfonic acid
q	Quartet
RT	Room temperature
S	Singlet
S _E Ar	Electrophilic aromatic substitution
S _N Ar	Nucleophilic aromatic substitution
t	Triplet
<i>t</i> -	Tertiary
TBAF	tetra-Butylammonium fluoride
TBS	tert-Butyl dimethyl silyl
THF	Tetrahydrofuran
TCL	Thin layer chromatography
TMS	Trimethylsilyl
Ts	<i>para</i> -Toluenesulfonyl
UV	Ultraviolet

Chapter 1 Diazomethyl 1,2-azaborine and its derivatives

Chapter 1 describes my work on diazomethyl 1,2-azaborine, a new α -boryl diazo compound. To provide context of my work, I attempted to summarize the synthesis of diazo compounds (Section I Introduction to synthesis of diazo compounds) and their reaction diversity (Section II Reaction of diazo compound). The review of classical reactions that diazo compounds can engage will be mainly focused on the Ru-catalyzed carbonyl olefination, [3+2] cycloaddition, C–H activation, O–H insertion and halogenation reactions. Included in Section II are the reaction of metal carbenoids that can be generated from the decomposition of diazo compounds. Section III describes the synthesis and reactivity studies of diazomethyl 1,2-azaborine. Portions of Section 1.3 has appeared in a publication.¹

1.1 Introduction to synthesis of diazo compounds

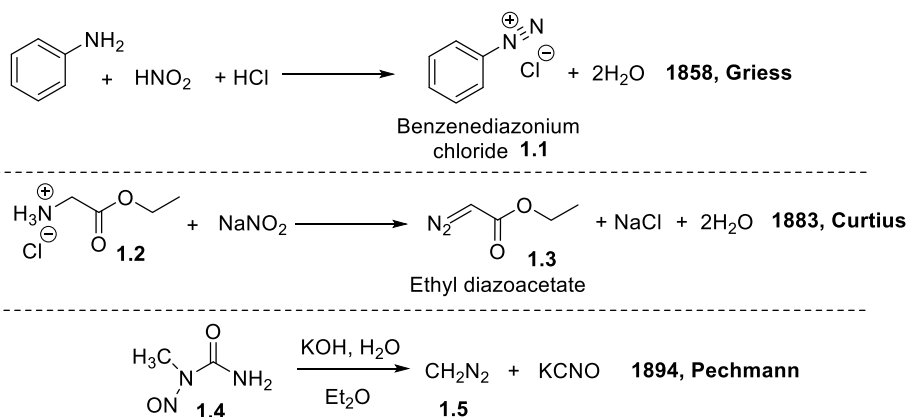
Diazo compounds were discovered in 1858 by Peter Griess² who initially prepared diazonitrophenol and established the conditions of the diazotization process by treating aromatic amines with nitrous acid that give benzenediazonium chloride **1.1**. The subsequent synthesis of azo dyes from the azo coupling of diazonium salt had made a huge contribution in the development of dye industry (Scheme 1.1). The first aliphatic diazo compounds³ was synthesized in 1883; Curtius synthesized ethyl diazoacetate **1.3** by diazotization of glycine hydrochloride **1.2**. In 1894, Von Pechmann synthesized diazomethane **1.5** for the first time by base cleavage of N-Methyl-N-nitrosourethane.⁴ Aliphatic diazo compound synthesis marked a new milestone and opened the wide field of diazo chemistry.

¹ Liu, Y.; Puig de la Bellacasa, R.; Li, B.; Cuenca, A. B.; Liu, S.-Y. *J. Am. Chem. Soc.* **2021**, *143*, 14059-14064.

² Heines, S. V. *J. Chem. Ed.* **1958**, *35*, 187.

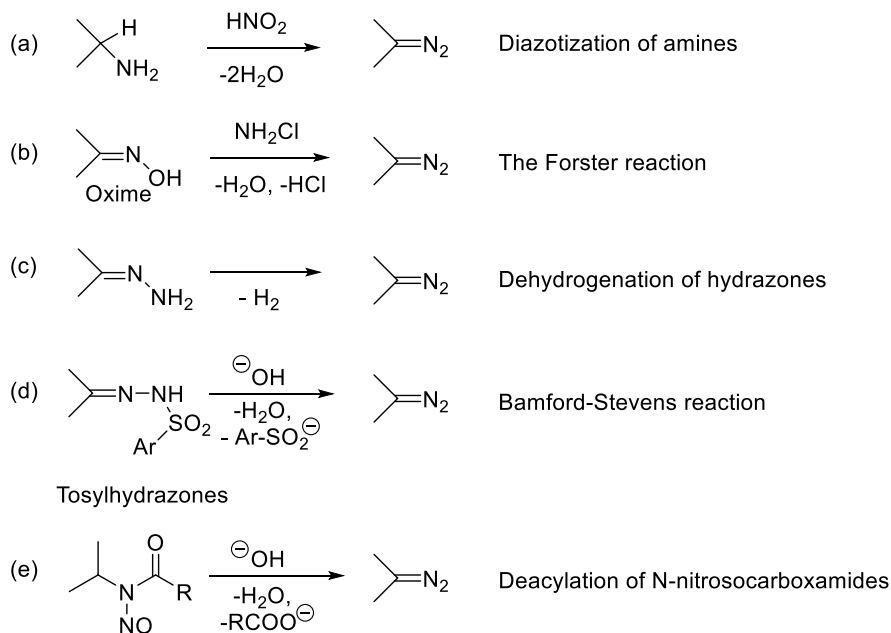
³ a) Regitz, M., *Diazo compounds: properties and synthesis*. Elsevier: 2012. b) Curtius, T. *Ber. Dtsch. Chem. Ges.* **1883**, *16*, 2230-2231. c) Arndt, F. *Org. Synth.* **1943**, *2*, 165.

⁴ Pechmann, H. *Ber. Dtsch. Chem. Ges.* **1894**, *27*, 1888-1891.



Scheme 1.1. History of diazo compounds.

Conventional synthetic methods⁵ for diazo compounds (Scheme 1.2) include: a) diazotization of amines,⁶ b) the Forster reaction,⁷ c) dehydration of hydrazones,⁸ d) the Bamford-Stevens reaction,⁹ e) deacylation of N-nitrosocarbox-amides.^{3a}



Scheme 1.2. Traditional diazo compound synthetic methods.

⁵ REGITZ, M. *Synthesis* **1972**, 1972, 351-373.

⁶ Butler, R. *Chem. Rev.* **1975**, 75, 241-257.

⁷ Meinwald, J.; Gassman, P. G.; Miller, E. G. *J. Am. Chem. Soc.* **1959**, 81, 4751-4752.

⁸ Holton, T. L.; Schechter, H. *J. Org. Chem.* **1995**, 60, 4725-4729.

⁹ Bamford, W.; Stevens, T. *J. Am. Chem. Soc.* **1952**, 924, 4735-4740.

Recent developments of novel methods and improved procedures for accessing aliphatic diazo compounds have been continuously reported in the literature (Scheme 1.3). The base-assisted diazo-group transfer from azide onto activated methylene compounds¹⁰ (Regitz diazo transfer) is a popular method. Several sulfonyl azides and a few other electron-deficient organoazide derivatives such as *p*-tosyl azide, methanesulfonyl azide¹¹ and *p*-acetamidobenzenesulfonyl azide (*p*-ABSA)¹² were used previously as suitable diazo transfer reagents for activated substrates i.e., methylene group bears two strong acceptor substituents such as acyl-, cyano-, nitro-, sulfonyl- and phosphoryl- groups. Imidazole-1-sulfonylazide **1.6** is among one of the most recently developed¹³ reagents, which can be converted into an insoluble sulfonamide that allows easy separation from the diazo compound than *p*-tosyl amide (Scheme 1.3, eq 1). However, less activated substrates such as α -diazocarboxylate and diazomethyl ketone derivatives are not accessible by direct diazo-group transfer onto carboxylic esters and ketones. Regitz and co-worker developed a “deformylating diazo-group-transfer” strategy.¹⁴ An additional electron-withdrawing group was installed before the diazo-transfer to activate these substrates (Scheme 1.3, eq 2). Danheiser and co-workers¹⁵ used a more efficient activation reagent CF₃CO₂CH₂CF₃ for the synthesis of Seyferth-Gilbert reagent **1.7** (Scheme 1.3, eq 3). A TiCl₄-mediated benzoylation method developed by Taber¹⁶ enabled the efficient preparation of various α -diazocarboxylate compounds such as **1.8** (Scheme 1.3, eq 4).

¹⁰ a) Heydt, H. *Science of Synthesis*, Vol. 27, Thieme, Stuttgart, **2004**, 843 – 915. b) Regitz, M. *Angew. Chem. Intern. Ed. Engl.* **1967**, *6*, 733-749.

¹¹ Taber, D. F.; Ruckle, Jr., R. E.; Hennessy, M. J. *J. Org. Chem.* **1986**, *51*, 4077-4078.

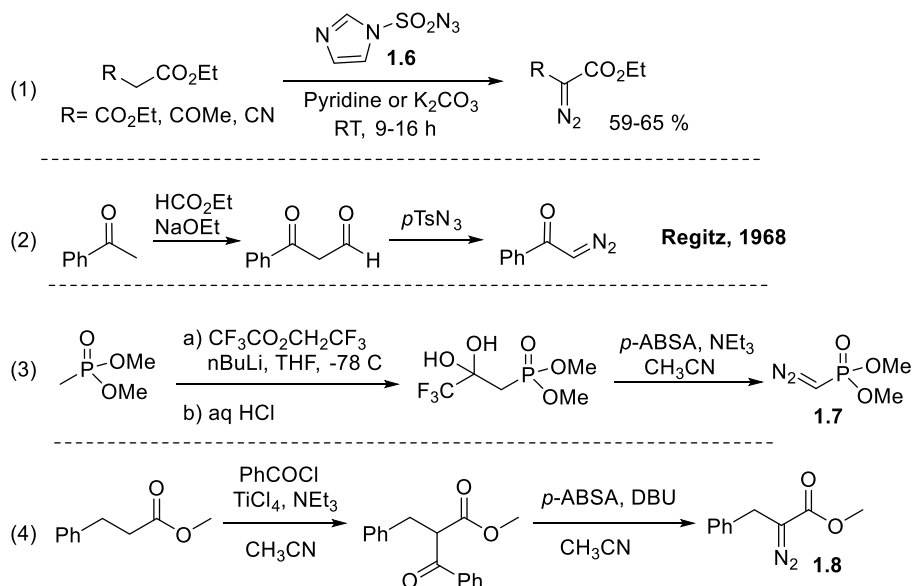
¹² Davies, H. M. L.; Cantrell, Jr., W. R.; Romines, K. R.; Baum, J. S. *Org. Synth.* **1992**, *70*, 93-100.

¹³ Goddard-Borger, E. D. Stick, R. V. *Org. Lett.* **2007**, *9*, 3797 – 3800.

¹⁴ a) Regitz, M.; Rüter, J. *Chem. Ber.* **1968**, *101*, 1263-1270. b) Regitz, M.; Menz, F. *Chem. Ber.* **1968**, *101*, 2622 – 2632.

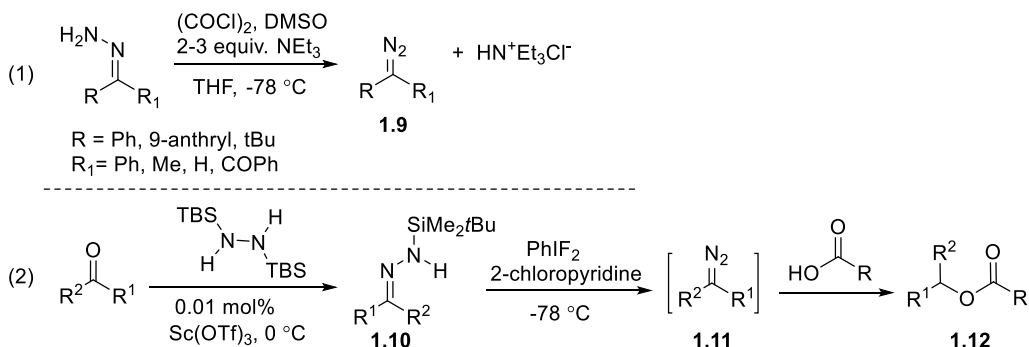
¹⁵ Brown, D. G.; Velthuisen, E. J.; Commerford, J. R.; Brisbois, R. G.; Hoye, T. R. *J. Org. Chem.* **1996**, *61*, 2540–2541.

¹⁶ Taber, D. F.; Sheth, R. B.; Joshi, P. V. *J. Org. Chem.* **2005**, *70*, 2851–2854.



Scheme 1.3. Diazo group transfer synthesis methods.

Diazo compounds have also been prepared by the oxidation of hydrazones. Heavy-metal-based oxidants¹⁷ such as lead tetraacetate, mercury oxide, manganese dioxide and silver(I) oxide are traditional reagents for dehydrogenation of hydrazones. A metal-free alternative reagent chlorodimethylsulfonium chloride¹⁸ (Swern reagent) was utilized for the preparation of different aryl- or alkyl- substituted derivatives of diazomethane **1.9** (Scheme 1.4, eq 1). (Difluoroiodo) benzene¹⁹ is another metal-free oxidant for the oxidation of *N*-(*tert*-butyldimethylsilyl) hydrazones **1.10** (TBSHs), in this case, diazoalkane **1.11** was generated in situ and reacted with carboxylic acid to form the ester adduct **1.12** (Scheme 1.4, eq 2).



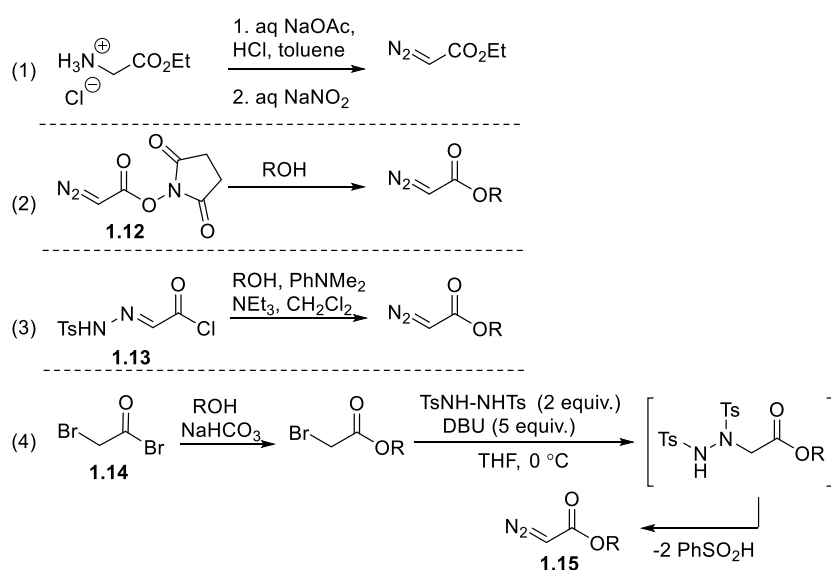
Scheme 1.4 Synthesis of diazo compounds by metal-free dehydrogenation of hydrazones.

¹⁷ Holton, T. L.; Schechter, H. *J. Org. Chem.* **1995**, *60*, 4725-4729.

¹⁸ Javed, M. I.; Brewer, M. *Org. Lett.* **2007**, *9*, 1789-1792.

¹⁹ Furrow, M. E.; Myers, A. G. *J. Am. Chem. Soc.* **2004**, *126*, 12222-12223.

Scheme 1.5 shows some common methods that are used to prepare α -diazoacetate derivatives. The industrial production of ethyl diazoacetate involves the diazotization of ester of glycine (Scheme 1.5, eq 1). Cleavage of activated carboxylic acid derivatives 2-diazo-3-oxocarboxylates **1.12** and **1.13** is a frequently used strategy of diazoacetylation of alcohols (Scheme 1.5, eq 2 and eq 3).²⁰ Another similar diazoacetylation method was introduced by Fukuyama and coworkers in 2007,²¹ and allows the convenient conversion of alcohol substrate into α -diazoacetate **1.15** in a single step starting with α -bromoketones **1.14** in the presence of a base by using N,N-ditosylhydrazine, a stable crystalline reagent (Scheme 1.5, eq 4).



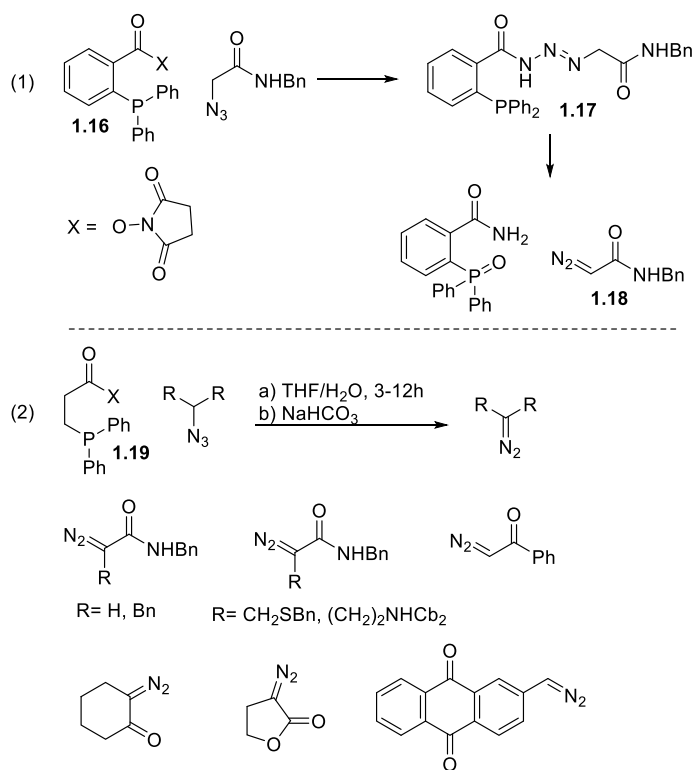
Scheme 1.5. Synthesis of α -diazoacetates by diazoacetylation of alcohols.

Raines discovered a phosphine mediated conversion of organoazides into diazo compounds.²² Triarylphosphine succinimidyl ester **1.16** reacts with an α -azido amide to give acyl triazene intermediate **1.17**, which undergoes fragmentation to yield α -diazoacetamide **1.18** in the presence of NEt_3 or saturated aqueous NaHCO_3 (Scheme 1.6, eq 1). (Diphenylphosphanyl)propionate **1.19** was ultimately identified as the optimal reagent to use for the discovered reductive fragmentation reaction, and various diazo compound derivatives could be generated (Scheme 1.6, eq 2).

²⁰ a) Corey, E. J.; Myers, A. G. *Tetrahedron Lett.* **1984**, *25*, 3559-3562. b) House, H. O.; Blankley, C. J. *J. Org. Chem.* **1968**, *33*, 53-60. c) Ouhia, A.; Rene, L.; Guilhem, J.; Pascard, C.; Badet, B. *J. Org. Chem.* **1993**, *58*, 1641-1642.

²¹ Toma, T.; Shimokawa, J.; Fukuyama, T. *Org. Lett.* **2007**, *9*, 3195-3197.

²² Myers, E. L.; Raines, R. T. *Angew. Chem. Int. Ed.* **2009**, *48*, 2359-2363.

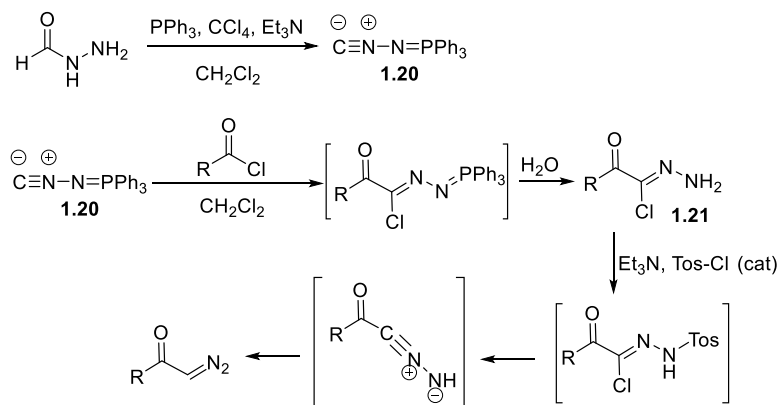


Scheme 1.6. Phosphane-mediated conversion of organoazide into diazo compounds.

In 2000, Aller²³ and co-workers reported the synthesis of α -diazoketones from the reaction of an acid chloride with *N*-isocyanoiminotriphenylphosphorane **1.20**, a thermally stable solid reagent (Scheme 1.7). An optimized²⁴ procedure was reported to prepared **1.20** from formic acid hydrazide and PPh₃/CCl₄. Reagent **1.20** reacts with an acid chloride to afford an addition product, which is then hydrolyzed to give the isolable diazo precursor hydrazidoyl chloride **1.21**, which can then be subsequently converted to α -diazoketone in the presence of base and a catalytic amount of *p*-toluenesulfonyl chloride.

²³ Aller, E.; Molina, P.; Lorenzo, A. *Synlett* **2000**, 2000, 526-528.

²⁴ Bio, M. M.; Javadi, G.; Song, Z. J. *Synthesis* **2005**, 2005, 19-21.



Scheme 1.7. Synthesis of α -diazoketones by acylation of N-isocyano-tripheylphosphoranimine.

1.2 Heteroatom-containing diazo compounds

1.2.1 Phosphine-substituted diazo reagents

In early 1970s, Seyferth²⁵ discovered dimethyl (diazomethyl) phosphonate **1.22** that is known as the Seyferth-Gilbert reagent (Scheme 1.8, eq1). In 1977, Colvin²⁶ demonstrated that aromatic aldehydes **1.23** can be transformed into the corresponding homologous acetylenic derivatives using **1.22** (Scheme 1.8, eq2). Gilbert²⁷ studied its reaction mechanism and expanded the reaction scope of this reagent to base-promoted homologation of ketones or aldehydes to form alkyne **1.24** (Scheme 1.8, eq3).

The Seyferth-Gilbert reagent has some drawbacks that limits its application: it is not readily available and has a short shelf-life. Thus, there is incentive for developing a more stable and easily accessible reagent. Ohira²⁸ found the anion of Seyferth-Gilbert reagent could be generated in situ from 1-diazo-2-oxopropyl phosphonate **1.26** under basic conditions. Then Bestmann and co-workers²⁹ made a major improvement for the synthesis of this reagent. Thereafter, **1.26** became known as Bestmann-Ohira reagent.³⁰ Some efficient and facile methods for preparation of Bestmann-Ohira reagents were reported

²⁵ Seyferth, D.; Marmor, R. S.; Hilbert, P. *J. Org. Chem.* **1971**, *36*, 1379-1386.

²⁶ Colvin, E. W.; Hamill, B. J. *J. Chem. Soc. Perkin Trans. I* **1977**, *8*, 869-874.

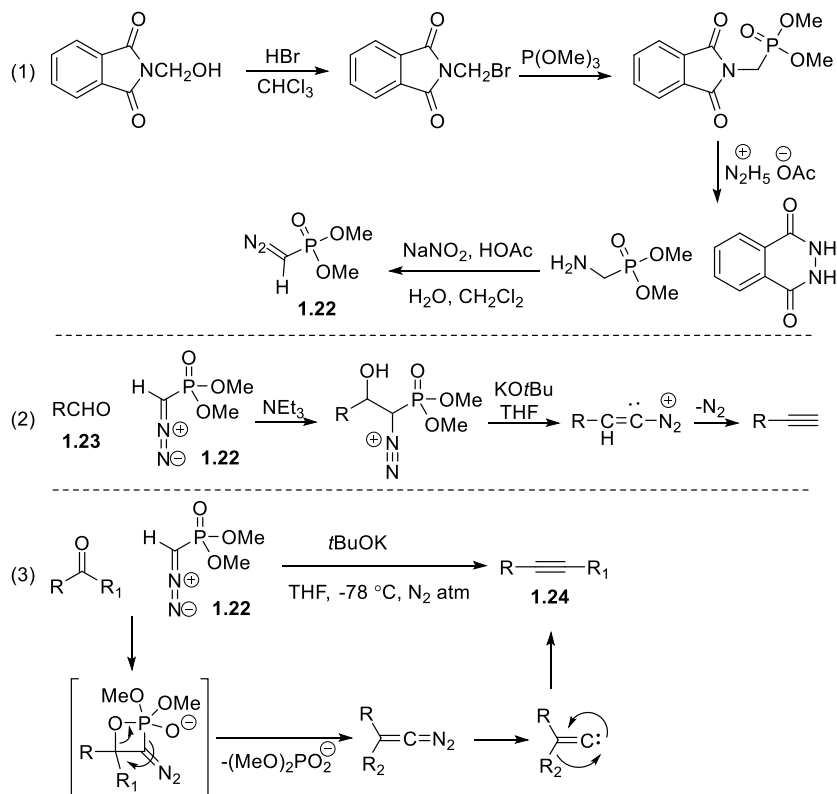
²⁷ Gilbert, J. C. *J. Org. Chem.* **1982**, *47*, 1837-1845.

²⁸ Ohira, S. *Synth. Commun.* **1989**, *19*, 561-564.

²⁹ Roth, G. J.; Liepold, B.; Mueller, S. G.; Bestmann, H. J. *Synthesis* **2004**, *01*, 59-62. b) S. Müller, B. Liepold, G. J. Roth, H. J. Bestmann, *Synlett*, **1996**, 521-522.

³⁰ Dhameja, M.; Pandey, J. *Asian J. Org. Chem.* **2018**, *7*, 1502-1523.

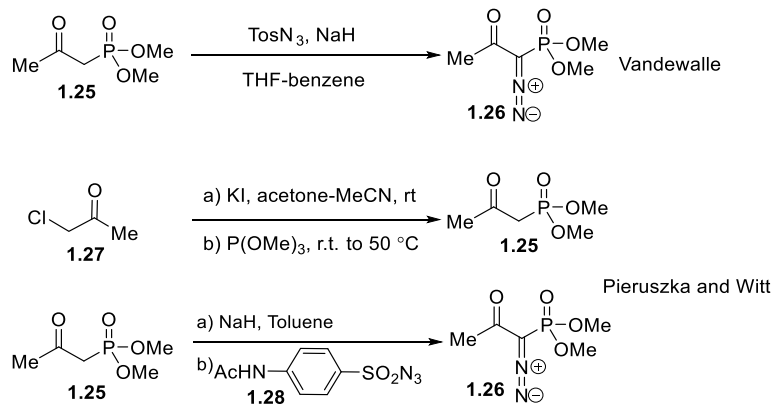
(scheme 1.9). Vandewalle³¹ used tosyl azide with NaH for effective diazo transfer to dimethyl-1-oxopropylphosphonate **1.25** to generate **1.26** in good yield. A reliable large scale preparation method for Bestmann-Ohira reagent from commercially available starting materials was published by Pietruszka and Witt³²: the synthesis involved the conversion of chloro acetone **1.27** to **1.25** followed by diazotization with **1.28** in the presence of NaH in 75% overall yield.



Scheme 1.8. Synthesis of Seyferth-Gilbert reagent and homologation reactions.

³¹ Callant, P.; Haenens, L. D'; Vandewalle, M. *Synth. Commun.* **1984**, *14*, 155–163

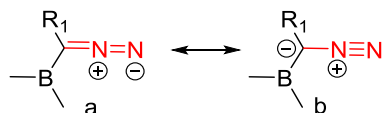
³² Pietruszka, J.; Witt, A. *Synthesis* **2006**, *24*, 4266–4268.



Scheme 1.9. Synthetic methods of Bestmann-Ohira reagent.

1.2.2 α -Boryl diazo reagents

The earliest report of an α -boryl diazo compounds is the Bpin substituted α -diazoacetate **1.29**, which was synthesized from 2-chloro-1,3,2-benzodioxaborole and ethyl diazolithioacetate in 1973.³³ The IR ν CN_2 stretching frequency of **1.29** can be observed at 2120 cm^{-1} (Scheme 1.10, eq 1). The predominant resonance forms of diazo compounds (structures a and b) are shown below, the diazo N-N bond stretching frequency is often investigated as a probe for the stability of α -carbanion. The higher the stretching frequency, the stronger the N-N bond will be and the resonance form of b will be more favored.

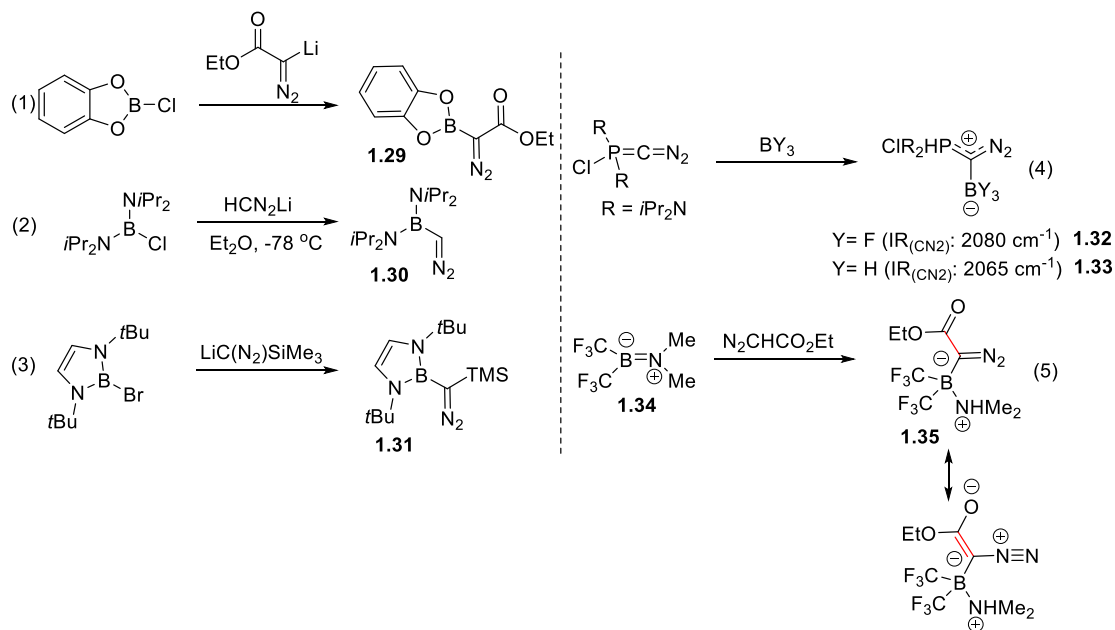


The synthesis of parental α -boranyldiazomethane **1.30** was accomplished by Bertrand in 1991.³⁴ The addition of bis(diisopropylamino)-chloroborane to the lithium salt of diazomethane at -78°C yielded **1.30** as a yellow oil after distillation (Scheme 1.10, eq 2). The compound has a ^{11}B NMR signal of 34.5 ppm and a strong IR absorption at 2070 cm^{-1} (ν CN_2). Two π -electron-donating heteroatoms attached to boron serve as an important factor to minimize the Lewis acidity of boron and prevent the decomposition of

³³ Schollkopf, U.; Banhidai, B.; Frasnelli, H.; Meyer, R.; Beckhaus, H. *Liebigs Ann. Chem.* **1974**, *11*, 1767– 1783

³⁴ Arthur, M. P.; Baccaredo, A.; Bertrand, G. *J. Am. Chem. Soc.* **1991**, *113*, 5856– 5857,

diazo derivatives via a Lewis acid mediated pathway.³⁵ In a similar approach, the 1,3,2-diazaborolyl(trimethylsilyl)diazomethane **1.31** was synthesized from 2,3-dihydro-1H-1,3,2-diazaborole bromide and lithio(trimethylsilyl) diazomethane (Scheme 1.10, eq 3).³⁶ The IR spectra of product **1.31** showed an CN₂ stretching vibration at 2048 cm⁻¹. Another way to quench the Lewis acidity of α -boryl diazo compounds is to form borate complexes.³⁷ The synthesis of first α -diazoalkylborates **1.32** and **1.33** was achieved³⁸ by addition of (diazomethylene)phosphorane with BF₃·Et₂O or BF₃·THF (Scheme 1.10, eq 4). The IR stretching frequencies for **1.32** and **1.33** were measured to be 2080 cm⁻¹ and 2065 cm⁻¹, respectively. In another example, the aminoborane **1.34** with two electron withdrawing CF₃ groups³⁹ reacts with ethyl diazoacetate to give borylated ethyl diazoacetate **1.35** in almost quantitative yield at -120 °C. The X-ray data of **1.35** shows that the boron atom and ethoxycarbonyldiazomethane group is in the same plane. This planarity and relatively short C-C bond (in red of **1.35**) length of 1.441 Å are characteristic for a delocalized π -electron system of α -carbanion (Scheme 1.10, eq 5).



Scheme 1.10. Synthesis of α -boryl diazo compounds

³⁵ a) Regitz, M.; Maas, G. *Diazo Compounds, Properties and Synthesis*; Academic Press: Orlando, 1986. b) Regitz, M. *Diazoalkanes*; Georg Thieme Verlag: Stuttgart, 1977. c) Regitz, M.; Maas, G. *Top. Curr. Chem.* **1981**, 97, 71.

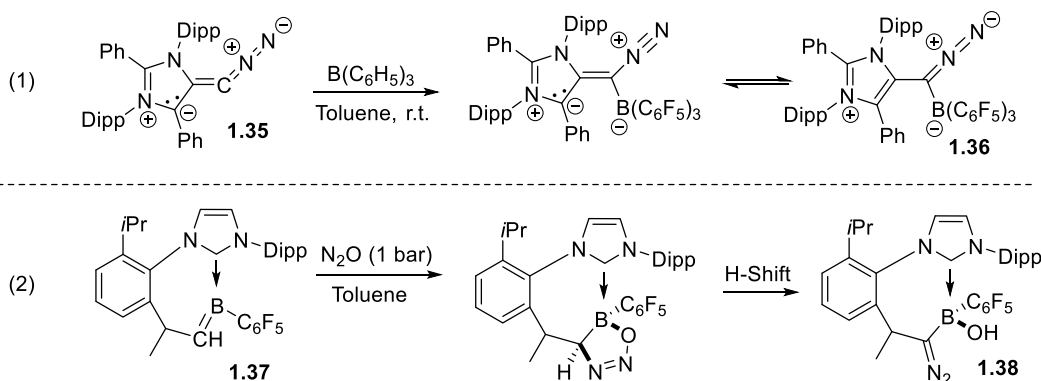
³⁶ Weber, L.; Wartig, H. B.; Stammler, H.-G.; Neumann, B. *Organometallics* **2001**, 20, 5248–5250

³⁷ Maza, R. J.; Fernández, E.; Carbó, J. J. *Chemistry (Weinheim an der Bergstrasse, Germany)* **2021**, 27, 12352.

³⁸ Sotiropoulos, J. M.; Baccaredo, A.; von Locquenghien, K. H.; Dahan, F.; Bertrand, G. *Angew. Chem., Int. Ed. Engl.* **1991**, 30, 1154–1156.

³⁹ Ansorge, A.; Brauer, D. J.; Bürger, H.; Hagen, T.; Pawelke, G. *Angew. Chem., Int. Ed. Engl.* **1993**, 32, 384–385.

Recently, Hansmann group⁴⁰ reported the synthesis of compound **1.35**, which is a room-temperature stable diazoalkane features a bent C–C–N geometry and the remarkable low characteristic infrared (IR) C=N=N stretching frequency at 1944 cm⁻¹ that fall out of the normal range of diazo compounds (2017-2180 cm⁻¹) and diazonium salts (2137-2306 cm⁻¹). Addition of the sterically demanding boron Lewis acid B(C₆F₅)₃ generates the C-bound diazo borane adducts **1.36**, and a significant IR shift was observed from 1944 to 2045 cm⁻¹ (Scheme 1.11, eq 1). Also recently, Erker reported a α -diazo boron complex **1.38** from the reaction of NHC-stabilized boraalkene **1.37** with N₂O.⁴¹ The N₂O acts as an 1,3-dipole and undergoes cycloaddition with **1.37** and followed by hydrogen shift to give **1.38** (Scheme 1.11, eq 2).



Scheme 1.11. Recent synthetic methods of α -boryl diazo compound.

1.2.3 α -Diazo silicon compounds

Trimethylsilyldiazomethane has been serving as a useful one-carbon homologation reagent in organic synthesis.⁴² It is traditionally prepared⁴³ via *N*-nitroso-*N*-trimethylsilylmethylurea **1.39** (Scheme 1.12, eq 1). Shioiri and coworkers⁴⁴ developed a scalable synthesis of trimethylsilyldiazomethane by diazo-transfer reaction of trimethylsilylmethylmagnesium chloride **1.40** with diphenyl phosphorazidate

⁴⁰ Antoni, P.; Golz, C.; Holstein, J.; Pantazis, D.; Hansmann, M. *Nat. Chem.* **2021**, *13*, 587-593.

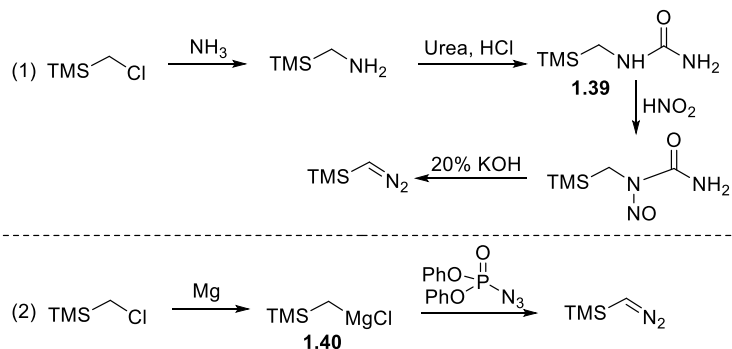
⁴¹ Chen, C.; Daniliuc, C. G.; Kehr, G.; Erker, G. *Angew. Chem., Int. Ed.* **2021**, *60*, 19905-19911.

⁴² Shioiri, T.; Aoyama, T.; Snowden, T.; Lee, D.; Gupta In *Encyclopedia of Reagents for Organic Synthesis*; Wiley, 2001.

⁴³ Seyferth, D.; Dow, A. W.; Menzel, H.; Flood, T. C. *J. Am. Chem. Soc.* **1968**, *90*, 1080-1082.

⁴⁴ Shioiri, T.; Aoyama, T.; Mori, S. *Org. Synth.* **1990**, *68*, 1.

(DDPA). The nucleophilicity of trimethylsilyldiazomethane is comparable to phenyl- α -diazomethane. α -diazo silicon compounds exhibit higher stability when compared to diazoalkanes.⁴⁵ While diazomethane is a gas (b.p. $-23\text{ }^{\circ}\text{C}$) and thermally labile and has been identified as a highly toxic and explosive material,⁴⁶ TMSCHN₂ as an alternative methylating reagent, is a stable liquid that is safe, easily to handle and can be prepared in large-scale.⁴⁷



Scheme 1.12. Preparative methods of trimethylsilyldiazomethane.

Other α -diazo silicon compounds are synthesized mainly through 3 different routes. Diazoacetate esters can undergo facile silylation reactions when treated with a nitrogen base and a chlorosilane⁴⁸ or silyl trifluoromethanesulfonate (Scheme 1.13, route A).⁴⁹ Similarly, lithium derivatives of diazo compounds prepared in situ can also undergo silylation reaction with triorganylsilyl chloride as reported by Kostyuk (Scheme 1.13, route B).⁵⁰ Additionally, the Bamford-Stevens reaction has been used for the synthesis of an α -diazo silicon compounds (Scheme 1.13, route C).⁵¹

⁴⁵ Lamoureux, G.; Agüero, C. *Arkivoc* **2009**, 251-264.

⁴⁶ Müller, S. T.; Wirth, T. *ChemSusChem* **2015**, 8, 245-250.

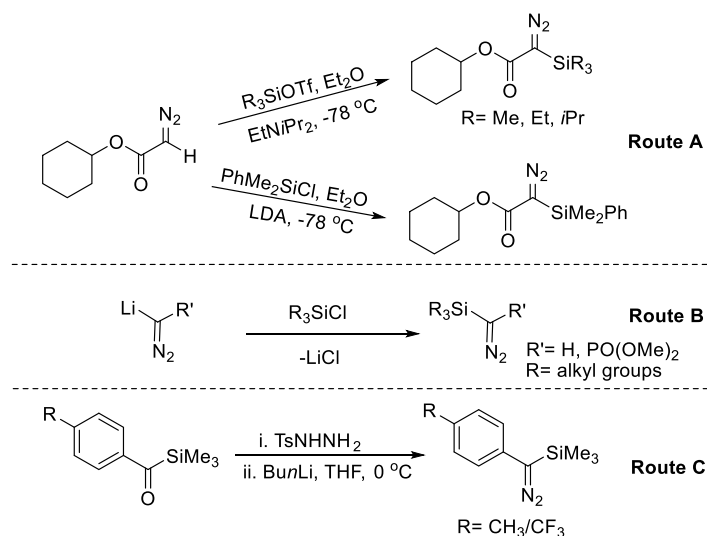
⁴⁷ Liu, H. Applications of Trimethylsilyldiazomethane in Synthetic Organic Chemistry. University of Illinois at Chicago, 2014.

⁴⁸ Maas, G.; Bender, S. *Synthesis* **1999**, 1175-1180.

⁴⁹ Fronda, A.; Krebs, F.; Daucher, B.; Werle, T.; Maas, G. *J. Organomet. Chem* **1992**, 424, 253-272.

⁵⁰ Kostyuk, A. S.; Ruderfer, I. B.; Baukov, Y. I.; Lutsenko, I. F. *J. Gen. Chem. USSR (Engl. Transl.)* **1975**, 45, 819-824.

⁵¹ Jin, F.; Xu, Y.; Ma, Y. *Tetrahedron Lett.* **1992**, 33, 6161-6164.



Scheme 1.13. Synthetic routes of α -silyl diazo compounds.

1.3 Reactions of diazo compounds

Diazo compounds have a wide range of reactivity as they can serve as 1,3-dipoles, carbene precursors and nucleophiles in the construction of various organic molecules.^{52a} Here we will be concentrating on reviewing those reactions that α -boryl diazo compounds was found to be engaging in (see Section 1.5). The commonly accepted reaction mechanisms and select examples of each reaction type are discussed for [3+2] cycloaddition, C–H insertion, carbonyl olefination with diazo compounds, X–H insertion, and diazo halogenation reactions.

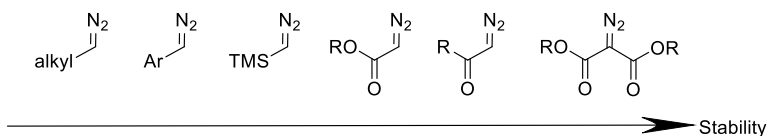
1.3.1 Diazo compounds' stability

Diazoalkanes are challenging to prepare and inherently unstable.⁵² Conjugation with an aromatic ring increases the thermal stability of the substituted diazomethane, but these compounds still decompose with time. Unlike diazoalkanes, α -diazocarbonyl compounds⁵³ are relatively thermally stable and they are easily prepared from readily available precursors. The decomposition of diazo compounds by Lewis acids

⁵² a) Ciszewski, L. W.; Rybicka-Jasińska, K.; Gryko, D. *Org. Biomol. Chem.* **2019**, *17*, 432-448. b) Cowell, G.; Ledwith, A. *Q. Rev. Chem. Soc.* **1970**, *24*, 119-167.

⁵³ Cheng, Q.-Q.; Doyle, M. *Adv. Organomet. Chem.* **2016**, *66*, 1-31.

is consistent with its basic nature.⁵⁴ Thus, the more delocalization of the negative charge on diazo carbon, the more stable the diazo compound is (Scheme 1.14).



Scheme 1.14. Reactivity trend of diazo compounds.

1.3.2 [3+2] Cycloaddition of diazo compounds

The cycloaddition of aliphatic diazo compounds was discovered⁵⁵ back in 1888. Huisgen proposed⁵⁶ the general concept of 1,3-dipole cycloadditions in 1958, where a formally zwitterionic molecule (i.e. the 1,3-dipole) undergoes 1,3-addition to an alkene or alkyne to form a five-membered heterocycle.⁵⁷ Diazo compounds such as α -diazocarbonyl compounds can act as 1,3-dipoles in [3+2] cycloadditions. In the absence of catalysts, diazo compounds undergo 1,3-dipolar cycloaddition reaction under mild conditions⁵⁸ with C=C bonds conjugated with carbonyl, amine, nitrile, nitro groups, or with double bonds as a part of a strained ring system to furnish pyrazolines. There are two proposed 1,3-dipole cycloadditions mechanistic pathway (Scheme 1.15) and the major difference is whether the two new σ bonds, that leads to the formation of five-membered ring upon the addition of 1,3-dipole (**a-b-c**) with the dipolarophile (**d-e**) are formed simultaneously or in a stepwise process.⁵⁷ The two-step mechanism involving polar intermediates was considered unlikely due to the lack of any dependence of the reaction rate on solvent polarity.^{51a} Fireshore came up a two-step mechanism involving a biradical intermediates.⁵⁹ Some evidence for a two-step cycloaddition mechanism that proceeds via polar intermediates was the reaction of *p*-methoxyphenyl diazomethane **1.41** with *p*-methoxystyrene **1.42**.⁵⁵ The *cis*- and *trans*-3,5-bis(*p*-anisyl)-1-

⁵⁴ a) Curtin, D. Y.; Gerber, S. M. *J. Am. Chem. Soc.* **1952**, *74*, 4052-4056. b) Bug, T.; Hartnagel, M.; Schlierf, C.; Mayr, H. *Chem. Eur. J.* **2003**, *9*, 4068-4076.

⁵⁵ Buchner, E. *Ber. Dtsch. Chem. Ges.* **1888**, *21*, 2637-2647.

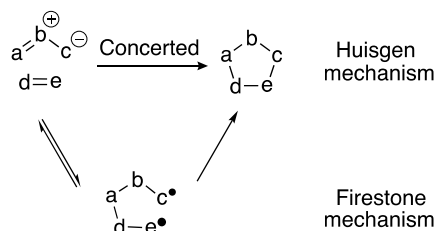
⁵⁶ a) Huisgen, R. *Angew. Chem., Int. Ed. Engl.* **1963**, *2*, 633-645. b) Patai, S., *Chemistry of alkenes*. **1964**. p. 739. c) Hoffmann, R.; Woodward, R. B. *Acc. Chem. Res.* **1968**, *1*, 17-22.

⁵⁷ a) Huisgen, R., Centenary Lecture. **1961**. b) Smith, L. I. *Chem. Rev.* **1938**, *23*, 193-285.

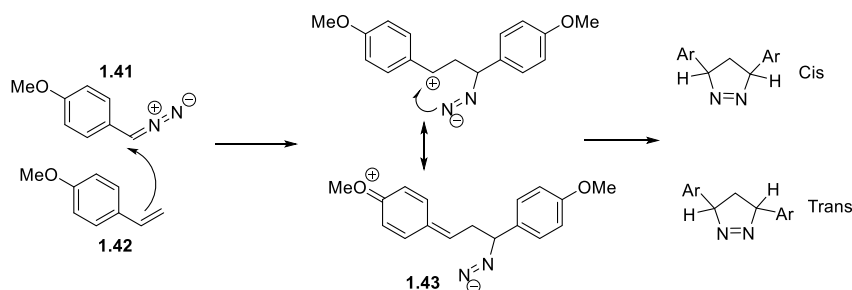
⁵⁸ Ye, T.; McKervey, M. A. *Chem. Rev.* **1994**, *94*, 1091-1160.

⁵⁹ a) Firestone, R. A. *J. Org. Chem.* **1968**, *33*, 2285-2290. b) Polansky, O. E.; Schuster, P. *Tetrahedron Lett.* **1964**, *5*, 2019-2022.

pyrazoline products were formed in almost equal amounts. The author pointed out that ⁶⁰ *p*-methoxy group stabilized the dipolar intermediate **1.43** and permitted the rotation around the styrene C=C bond for the generation of a mixture of *cis*- and *trans*- pyrazoline products (Scheme 1.16).



Scheme 1.15. Proposed 1,3-dipole cycloaddition mechanistic pathways.



Scheme 1.16. Significant evidence for the two-step cycloaddition of a diazo-alkane via a polar intermediate.

Other experimental data and mechanistic features suggest a concerted reaction pathway⁵⁷: 1) the rate and stereochemistry are not markedly influenced by solvent polarity, 2) reaction has low activation enthalpies (5-15 kcal/mol) and large negative activation entropies (-25 to -45 e.u.), 3) the stereochemistry of the reacting olefin (dipolarophile) is maintained, 4) reaction rates are markedly increased by conjugation of the reacting site in the dipolarophile, 5) reaction rate are reduced by the steric effect of all types of substituent, 6) cycloadditions of 1,3-dipoles to alkenes are stereospecifically suprafacial.^{51,61}

⁶⁰ Overberger, C.; Weinshenker, N.; Anselme, J.-P. *J. Am. Chem. Soc.* **1965**, *87*, 4119-4124.

⁶¹ a) Houk, K. *J. Am. Chem. Soc.* **1972**, *94*, 8953-8955. b) Woodward, R., R. Hoffmann. *Acc. Chem. Res.* **1970**, *57*, 17-22,

The theory about the conservation of orbital symmetry in concerted reaction stimulated numerous studies related to the [3+2] cycloaddition mechanism.^{62, 63} Huisgen proposed⁶⁴ concerted process involving a cyclic transition state oriented in two planes (e.g., for diphenyl diazomethane, Figure 1.1).

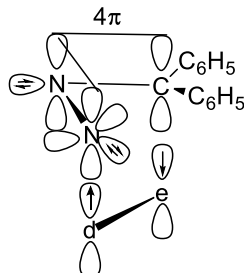


Figure 1.1. Transition state complex orientation for addition of diphenyl-diazomethane to a dipolarophile.

All 1,3-dipoles contain four π electrons in three conjugated p orbitals (see examples in Figure 1.2).⁶⁵ Similar to isoelectronic allyl anion, the four electrons occupy the two lowest molecular orbitals.⁶⁰ The bending of the linear 1,3-dipole of a diazo compound within the horizontal plane achieves the allyl anion geometry that can interact with the π bond of the dipolarophile. The orbital hybridization change from p to sp^3 and sp^2 orbitals are accompanied by uplifting of the middle diazo nitrogen until it reaches the 1-pyrazoline plane in the product. The “two plane” transition state orientation of Figure 1.1 in this 1,3-cycloaddition process mimics the [4+2] π electron addition during the Diels-Alder reaction.⁶⁶

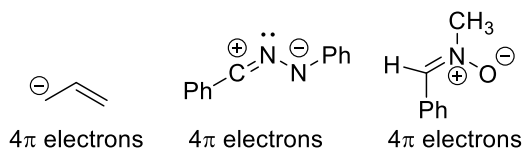


Figure 1.2. Diphenylnitrilimine and N-methyl-C-phenyl-nitrone as isoelectronic allyl anion structures.

⁶² Ledwith, A., Part (iii) Reaction mechanisms. *Annu. Rep. Prog. Chem. Sect. B: Org. Chem.* **1968**, 65, 143-170.

⁶³ a) Miller, S. I., Stereoselection in the Elementary steps of Organic Reactions. In *Advances in Physical Organic Chemistry*, Elsevier: 1968; Vol. 6, pp 185-332. b) Gill, G., The application of the Woodward–Hoffmann orbital symmetry rules to concerted organic reactions. *Q. Rev. Chem. Soc.* **1968**, 22, 338-389.

⁶⁴ Huisgen, R. *J. Org. Chem.* **2002**, 33, 2291-2297.

⁶⁵ a) Huisgen, R. *J. Org. Chem.* **1968**, 33, 2291-2297. b) Huisgen, R. *Angew. Chem., Int. Ed. Engl.* **1963**, 2, 565-598.

⁶⁶ a) Longuet-Higgins, H.; Abrahamson, E. *J. Am. Chem. Soc.* **1965**, 87, 2045-2046. b) Eckell, A.; Huisgen, R.; Sustmann, R.; Wallbillich, G.; Grashey, D.; Spindler, E. *Chem. Ber.* **1967**, 100, 2192-2213.

Woodward-Hoffman rules^{51b} for conservation of orbital symmetry is consistent with Huisgen's concerted mechanism. However, the nature of the orientation (a or b, Figure 1.3) is not adequately predicted by either concerted or biradical mechanisms.

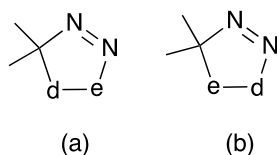


Figure 1.3. Orientation of dipolarophiles.

1.3.3 Perturbation theory

Reactivity of diazoalkanes in cycloaddition is markedly reduced by conjugating substituents and increased by alkyl groups.⁶⁷ On the other hand, conjugation substituents or ring strain of the dipolarophile strongly promotes its reactivity.^{59,68} MO perturbation theory provided an elegant solution for the above mentioned reactivity trends of diazo compounds toward dipolarophile during concerted additions.⁶⁹ According to MO theory, the energy separation of the frontier orbitals determines the reactivity of the cycloaddition process.⁷⁰

According to Sustmann's classification (Figure 1.4), diazomethane⁷¹ is a *Type I* 1,3-dipole, where the HOMO(1,3-dipole)-LUMO (dipolarophile) interaction controls the reactivity. Thus electron-withdrawing groups on the dipolarophile increase reactivity. As for the dipole diazomethane, electron donating substituents accelerate the cycloaddition (e.g. for aryldiazomethanes).⁷² In *Type II* Sustmann 1,3-dipole (e.g. methyl diazoacetate), the directionality of frontier orbital interactions is ambiguous. Thus, cycloaddition of diazo acetates is accelerated by both types of substituents on the olefin. For *Type III* 1,3-dipoles such as diazomalonate and diazo(phenylsulfonyl)acetates, the major frontier orbital interaction is

⁶⁷ Ledwith, A.; Parry, D. *J. Chem. Soc. C* **1966**, 1408-1410.

⁶⁸ Ledwith, A.; Shih-Lin, Y. *J. Chem. Soc. B* **1967**, 83-84.

⁶⁹ Parsons, P. J., *Synthetic Applications of 1, 3-Dipolar Cycloaddition Chemistry toward Heterocycles and Natural Products* Edited by Albert Padwa and William H. Pearson. Wiley: New York, Chichester. 2002. Hardcover

⁷⁰ a) Bihlmaier, W.; Huisgen, R.; Reissig, H.-U.; Vass, S. *Tetrahedron Lett.* **1979**, *20*, 2621-2624. b) Sustmann, R. I. 1, 3-dipolar cycloadditions. *Tetrahedron Lett.* **1971**, *12*, 2717-2720. c) Sustmann, R. *Phys. Org. Chem.* **1974**, *40*, 569-593.

⁷¹ Geittner, J.; Huisgen, R.; Sustmann, R. *Tetrahedron Lett.* **1977**, *18*, 881-884.

⁷² a) Samuilov, Y. D.; Movchan, A.; Soloveva, S.; Kononov, *Russ. J. Org. Chem.* **1984**, *20*, 2179-2182.

b) Fisera, L.; Geittner, J.; Huisgen, R.; Reissig, H. *Heterocycles* **1978**, *10*, 153-158.

HOMO (dipolarophile)-LUMO (1,3-dipole). Thus, electron rich olefins are predicted to be more reactive, as the electron donating substituents will raise the HOMO energy of dipolarophile.⁷³

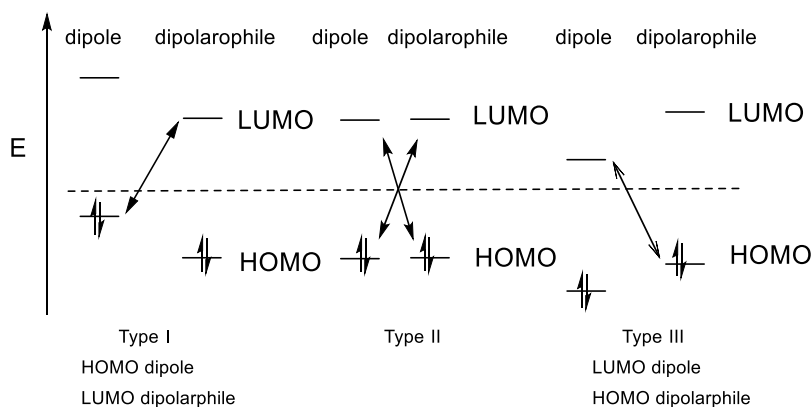


Figure 1.4. Sustainmann's classification of 1,3-dipolar cycloaddition.

Identifying the controlling frontier orbital interaction will help with predicting the product regiochemistry of 1,3-dipolar cycloaddition reactions.⁷⁴ Houk and coworkers applied the perturbation theory (focusing on the overlap terms arising from interactions of the frontier orbitals of the 1,3-dipole and dipolarophile) to 1,3-dipolar cycloaddition reaction. Substituents that raise the dipole HOMO energy (when R is X= π -electron donors such as -NR₂, -OR, or C= conjugating groups such as alkenes, alkynes) or lower the dipolarophile LUMO energy (R is C or Z= π -electron acceptors such as -COR, -SO₂R) will accelerate *Type I* cycloaddition reactions.

As can be seen from Figure 1.5, products A with the alkene substituent (dipolarophile) remote from "anionic terminus c" is generated from electron-deficient dipolarophiles (larger LUMO coefficients at unsubstituted carbon). On the other hand, product B with the substituent near the "anionic terminus c" is produced from electron-rich dipolarophiles (larger LUMO coefficient at substituted carbon). As an example, diazoalkanes are predominantly *Type I* 1,3-dipoles, thus conjugation -C and electron withdrawing substituent -Z on the dipolarophiles will thus accelerate reaction and produce 3-substituted 1-pyrazoline (a) (left side, Figure 1.5).⁷⁵ This phenomenon was attributed to the union of the larger HOMO coefficient at the

⁷³ Huisgen, R.; Geittner, J. *Heterocycles* **1978**, *11*, 105-108.

⁷⁴ Houk, K.; Sims, J. *J. Am. Chem. Soc.* **1973**, *95*, 7301-7315.

⁷⁵ a) Cowell, G.; Ledwith, A. *Q. Rev. Chem. Soc.* **1970**, *24*, 119-167. b) Kadaba, P. K.; Colturi, T. F. *J. Heterocycl. Chem.* **1969**, *6*, 829-834.

carbon of the diazomethane with larger LUMO coefficient at the unsubstituted carbon of the electron-deficient dipolarophiles. On the other hand, dipolarophiles with electron donating group -X are rather unreactive with diazo, for instance, enol ether reacts with diazomethane very slowly to give 4-substituted pyrazolines (b) (right side, Figure 1.5).⁷⁶

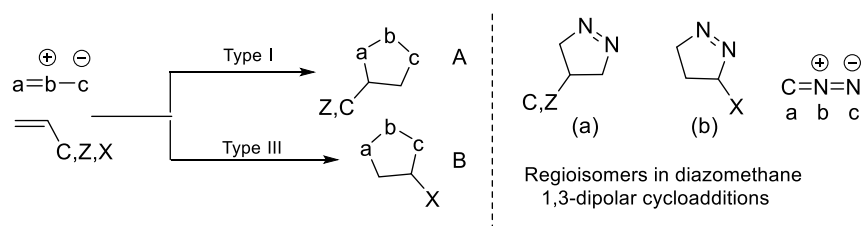


Figure 1.5. Regioisomer expected from HOMO or LUMO controlled 1,3-dipolar cycloaddition.

Substituents interacting with a π system can be roughly classified into three classes, on the basis of the perturbation orbital diagram⁷⁷: Z (π -electron acceptors such as -COR, -SOR, -SO₂R, -NO, and -NO₂), C (conjugating groups such as alkenes, alkynes, or aryl groups) and X (π -electron donors such as -NR₂, -OR, -SR, -F, -Cl, -Br, and -I).

The synthetic value of [3+2] cycloadditions of diazoalkanes has been examined (see reactions in Scheme 1.17). 1,3-dipolar cycloaddition reactions between diazoalkanes and alkenes initially form the unstable 1-pyrazoline cycloadducts, which would either undergo 1,3-proton migration to give thermal stable 2-pyrazoline product or release nitrogen to generate corresponding cyclopropane (Scheme 1.17, eq 1).⁷⁸ Pyrazolines can be synthesized from variety of different substrate olefins (such as hexafluorobicyclobutene **1.44**)⁷⁹ using diazomethane (Scheme 1.17, eq 2). Some other heterocyclic ring such as 1,5-diaryl-1,2,3-triazolines **1.45** was generated by the cycloaddition of diazomethane to Schiff bases (Scheme 1.17, eq 3).⁸⁰ The [3+2] cycloadducts of alkane diazo with 2-methyl naphthaquinone⁸¹ **1.46** can undergo base-catalyzed decomposition, providing a novel synthetic route to the highly reactive quinone methides **1.47** (Scheme 1.17, eq 4).

⁷⁶ Groen, S.; Arens, J. *Recl. Trav. Chim.* **1961**, *80*, 879-884.

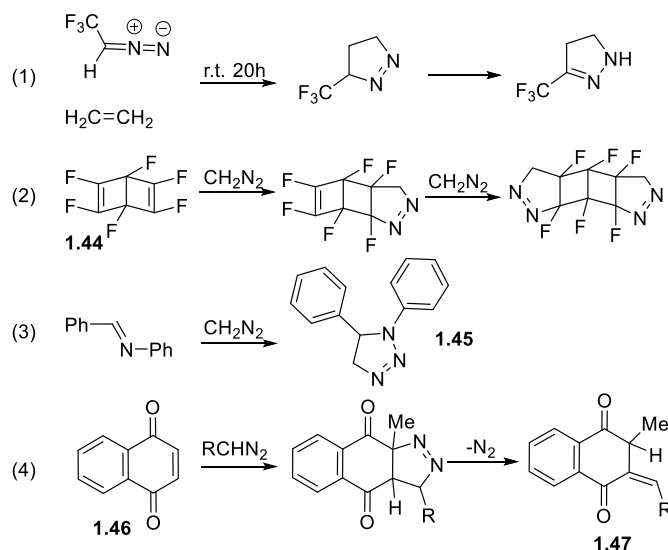
⁷⁷ Fleming, I., *Frontier orbitals and organic chemical reactions*. Wiley: **1977**.

⁷⁸ Nishiwaki, N., *Methods and applications of cycloaddition reactions in organic syntheses*. John Wiley & Sons: **2013**.

⁷⁹ a) Atherton, J.; Fields, R. *J. Chem. Soc. C* **1968**, 1507-1513. b) Barlow, M.; Haszeldine, R.; Morton, W. *J. Chem. Soc. D* **1969**, *16*, 931-932.

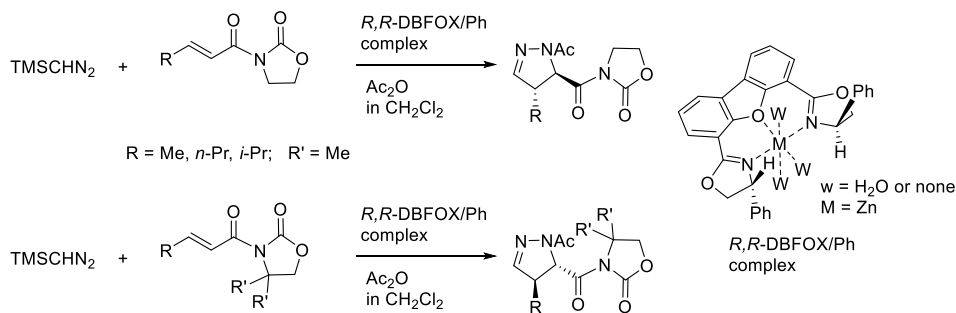
⁸⁰ Kadaba, P. K. *Tetrahedron* **1966**, *22*, 2453-2460.

⁸¹ Dean, F.; Houghton, L.; Morton, R. *J. Chem. Soc. C* **1967**, 1980-1984.



Scheme 1.17. Wide synthetic value of 3+2 cycloadditions of diazoalkanes.

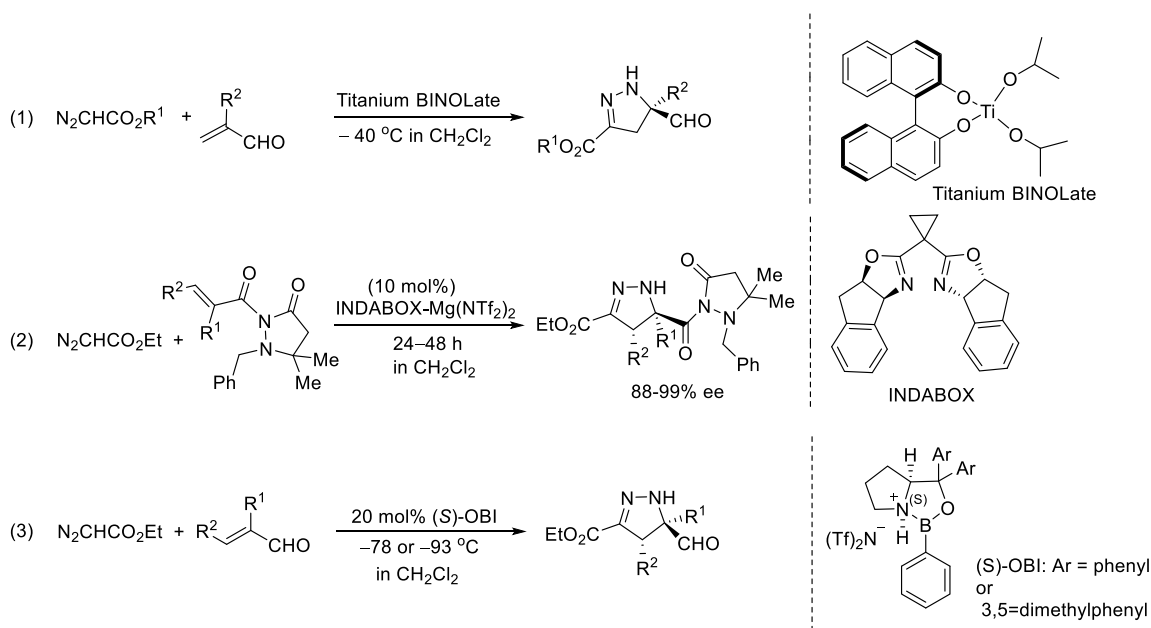
Trimethylsilyldiazomethane and diazoacetates was reported to undergo enantioselective cycloadditions in the presence of the chiral Lewis acids. In 2000, Kanemasa and Kanai⁸² reported the first Lewis acid-catalyzed enantioselective 1,3-dipolar cycloaddition reactions of diazoalkanes (Scheme 1.18) using transition metal aqua complexes (*R,R*-DBFOX/Ph) as the chiral Lewis acids.²² It is important to note that a complete switch of enantioselectivity has been observed by adding substituents *R'* to the achiral chelating auxiliary.



Scheme 1.18. Reactions of trimethylsilyldiazomethane with 2-alkenyl-3-oxazolidinone derivatives.

⁸² Kanemasa, S.; Kanai, T. *J. Am. Chem. Soc.* **2000**, *122*, 10710-10711.

Maruoka⁸³ and coworkers reported the chiral titanium BINOLate-catalyzed highly enantioselective 1,3-dipolar cycloaddition between diazoacetates and acroleins and generates chiral 2-pyrazolines with an asymmetric tetrasubstituted carbon center (Scheme 1.19, eq 1). In 2007, Sibi⁸⁴ group reported the enantioselective synthesis of 2-pyrazolines via INDABOX-Mg (II)-catalyzed cycloaddition reaction of diazo ester with less reactive α,β -disubstituted pyrazolidinone imides (Scheme 1.19, eq 2). In 2009, Ryu⁸⁵ and coworkers developed a chiral (S)-oxazaborolidinium ion (OBI) as a catalyst for the cycloaddition of diazo ester and acrolein giving highly functionalized chiral (5R)-pyrazolines in good yield with high (up to 99% ee) enantioselectivities (Scheme 1.19, eq 3).



Scheme 1.19. Asymmetric cycloaddition reaction between diazoacetates and α -substituted acroleins.

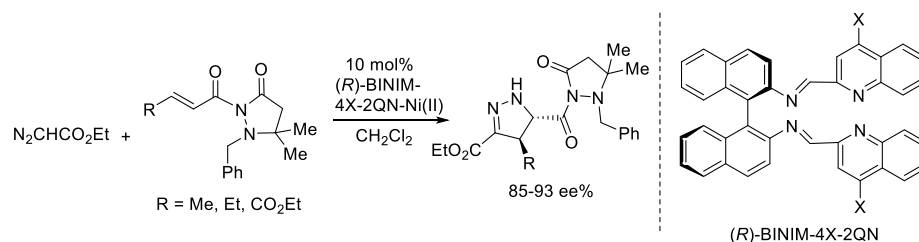
Suga⁸⁶ et al. demonstrated the 1,3-dipolar cycloaddition reactions between ethyl diazoacetate and pyrazolidinone derivatives with BINIM-Ni (II) catalysts for selective formation of 2-pyrazoline having a methine carbon substituted with a pyrazolidinonyl group in high enantioselectivity (Scheme 1.20).

⁸³ Kano, T.; Hashimoto, T.; Maruoka, K. *J. Am. Chem. Soc.* **2006**, *128*, 2174-2175.

⁸⁴ Sibi, M. P.; Stanley, L. M.; Soeta, T. *Org. Lett.* **2007**, *9*, 1553-1556.

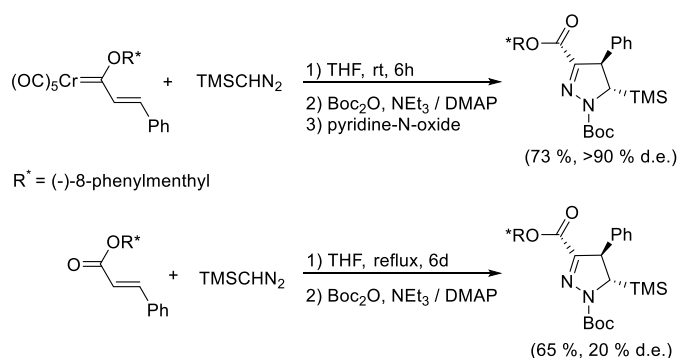
⁸⁵ Gao, L.; Hwang, G.-S.; Lee, M. Y. *Chem. Commun.* **2009**, *36*, 5460-5462.

⁸⁶ Suga, H.; Furihata, Y.; Sakamoto, A.; Itoh, K.; Okumura, Y.; Tsuchida, T.; Kakehi, A.; Baba, T. *J. Org. Chem.* **2011**, *76*, 7377-7387.



Scheme 1.20. Asymmetric cycloaddition reactions between ethyl diazoacetate and 2-(2-Alkenoyl)-1-benzyl-5,5-dimethyl-3-pyrazolidinone.

Fisher carbene complex⁸⁷ also react with 1,3-dipoles (diazomethane, nitrones and nitrilimines) to afford five-membered heterocyclic ring. α , β -Unsaturated fisher carbene complexes can serve as a C2 building block. The carbene fragment proceeds the cycloaddition reaction and enhances both the chemical yield and diastereomeric excess (Scheme 1.21).



Scheme 1.21. Trimethylsilyl diazomethanes as 1,3-dipoles in [3 + 2]-cycloaddition reactions with chiral alkenylcarbene complexes in comparison of cinnamates as their isolable analogues

1.4 Diazo compounds as carbene precursors

Diazo compounds can undergo decomposition to form carbenes, and there are widely applicable and reliable methods for the preparation of carbenes from different diazo compounds.⁸⁸ Carbenes have been defined as a class of intermediates possessing a neutral divalent carbon atom with six electrons on its

⁸⁷ a) Licandro, E.; Maiorana, S.; Papagni, A.; Gerosa, A. Z.; Cariati, F.; Bruni, S.; Moret, M.; Villa, A. C. *Inorganica chimica acta* **1994**, *220*, 233-247. b) Baldoli, C.; Del Buttero, P.; Licandro, E.; Maiorana, S.; Papagni, A.; Zanotti-Gerosa, A. *J. Organomet. Chem.* **1994**, *476*, 27-29.

⁸⁸ Xiang, Y.; Wang, C.; Ding, Q.; Peng, Y. *Adv. Synth. Catal.* **2019**, *361*, 919-944.

valence shell.⁸⁹ The two non-bonding electrons may have anti-parallel spins (singlet state) or parallel spins (triplet state). The relative energies of the two non-bonding orbitals determine the nature of ground state multiplicity (the orbital perpendicular to the plane defined by three atoms is the p orbital while the σ orbital is parallel to the plane).

If the two orbitals are degenerate, the electrons will occupy different orbitals with parallel spin.⁹⁰ Thus will be considered as a triplet ground state with σp configuration. When the two available orbitals are not equivalent, the two electrons would occupy the lower of the two-orbitals with paired spins to become a singlet carbene with σ^2 energy configuration (Figure 1.6, left). The magnitude of the energy difference between the triplet and singlet states determines the ground state multiplicity (S_0 or T_1). The differences between the energies of S_0 and T_1 may be tuned by electronic and steric effects of the substituents on the carbene center.⁹¹ In singlet, the electrons are paired up in the sp^2 lone pair, but for the triplet there is one electron in each of the sp^2 and p orbitals. As a consequence of spin conservation, most carbene precursors are considered as singlet carbenes and intersystem crossing may or may not occur before the individual carbene reacts with an acceptor.

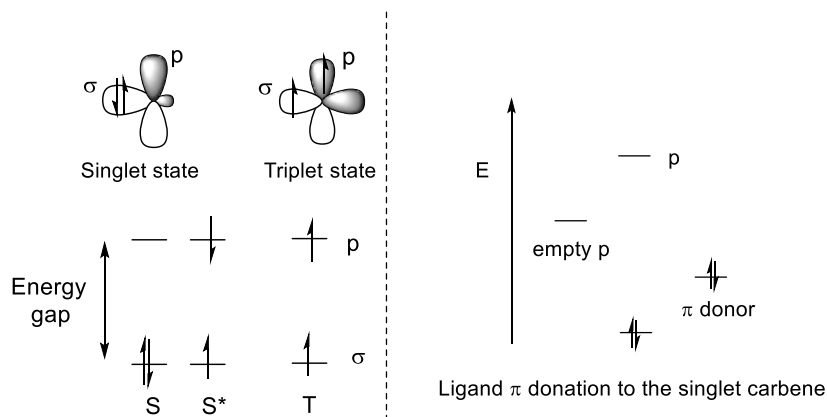


Figure 1.6. Electronic states of a carbene.

⁸⁹de Fremont, P.; Marion, N.; Nolan, S. P. *Coord. Chem. Rev.* **2009**, *253*, 862-892.

⁹⁰ Kirmse, W., *Carbene chemistry*. Elsevier: **2013**; Vol. 1.

⁹¹ a) Kirmse, W. *Angew. Chem. Int. Ed.* **2004**, *43*, 1767-1769. b) Tomioka, H., *Triplet carbenes*. Wiley-Interscience: Hoboken, NJ: **2004**.

The ground-state spin multiplicity dictates the fundamental reactivity of carbene,⁹² thus singlet carbene has a filled and a vacant orbital, and they are considered to possess an ambiphilic character. The electrophilic or nucleophilic character of singlet carbenes strongly depends on the substituents' electron donating or withdrawing capabilities. Substitution of the carbene carbon with two electron donating groups, such as -NR₂, -OR and -SR, make carbenes behave like nucleophiles in contrast to the electrophilic properties of many other divalent carbon intermediates. Singlet carbenes are stabilized by π electron donation from substituents into the vacant p orbital.⁹³ For π -electron donor substituents (-NR₂, -OR, -SR, -F, -Cl, -Br, and -I), the vacant carbene 2p orbital's interaction with the π donor can raise its energy, therefore increase the separation between the resulting antibonding p orbital and σ orbital, thus stabilize the singlet state (Figure 1.6, left).

Triplet carbenes have two singly occupied orbitals and the ground state is denoted as T₁. The π electron acceptors (such as -COR, -SOR, and NO₂) and conjugating substituents (alkenes, alkynes, or aryl groups) lower the gap between p and σ orbitals and can facilitate triplet ground state.⁹⁴ Triplet carbenes can be considered as di-radicals even though the interaction with two unpaired electrons give rise to some peculiarities.⁹⁵ It has been demonstrated by EPR studies that most aryl and diarylcarbenes have triplet ground state. Diazo compounds are used to generate triplet carbenes by photolysis.⁹⁶ Triplet carbenes can be trapped by oxygen to form ketones via a ketone oxide⁹⁷ intermediate. Triplet carbenes can also⁹⁸ rearrange/decompose to a simple radical by alkene dimerization, C-H insertion, cyclopropanation of alkenes and H-atom abstraction. Triplet carbene are stabilized by steric protection with bromo and

⁹² Li, Y.; Schuster, G. B. *J. Org. Chem.* **1988**, *53*, 1273-1277.

⁹³ Tomioka, H. *Acc. Chem. Res.* **1997**, *30*, 315-321.

⁹⁴ Jean, Y., *Molecular orbitals of transition metal complexes*. OUP Oxford: 2005.

⁹⁵ Nemirowski, A.; Schreiner, P. R. *J. Org. Chem.* **2007**, *72*, 9533-9540.

⁹⁶ Hermann, W.; Weskamp, T.; Bohm, V. P. *Adv. Organomet. Chem.* **2001**, *48*, 1-71.

⁹⁷ Scaiano, J.; McGimpsey, W.; Casal, H. *J. Org. Chem.* **1989**, *54*, 1612-1616.

⁹⁸ a) Doyle, M. P.; Forbes, D. C. *Chem. Rev.* **1998**, *98*, 911-936. b) Ye, T.; McKervey, M. A. *Chem. Rev.* **1994**, *94*, 1091-1160. c) Herrmann, W. A.; Plank, J.; Ziegler, M. L.; Weidenhammer, K. *J. Am. Chem. Soc.* **1979**, *101*, 3133-3135. d) Maier, T. C.; Fu, G. C. *J. Am. Chem. Soc.* **2006**, *128*, 4594-4595. e) Lee, E. C.; Fu, G. C. *J. Am. Chem. Soc.* **2007**, *129*, 12066-12067. f) For C-H activation review: Davies, H. M.; Beckwith, R. E. *Chem. Rev.* **2003**, *103*, 2861-2904.

trifluoromethyl groups placed in their vicinity.⁹⁹ In contrast to singlet carbene, triplet carbenes do not react with carbon-halogen bond.¹⁰⁰

1.4.1 Fisher and Schrock carbenes.

Fisher carbene complexes have a large difference in energy between their σ - and π -orbitals and thus the singlet state is the ground state.¹⁰¹ The bond between metal and carbon are constituted⁹⁸ by mutual donor-acceptor interactions (carbene to metal by σ bond donation and metal to carbene through π back donation, see Figure 1.7). The carbon-metal bond has a partial double bond character as the π back donation can be weakened by the stabilization of the carbene by its donor substituents. Fisher carbenes act as L-type σ donors and the corresponding metal complex are usually¹⁰² possess low oxidation states. Furthermore, the late transition metals typical feature electrophilic carbene center are prone to nucleophilic attack (Figure 1.8).

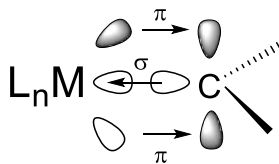


Figure 1.7. Bonding orbitals of the electrophilic Fisher metal carbenoid. There is a σ -bond donation from the carbene carbon to the metal center and a π -bond back donation from the filled metal d-orbitals to the carbene carbon that possesses a vacant 2p-orbital.

Schrock carbene complexes are formed by poorly stabilized “triplet” carbene that has a near-degeneracy of the σ - and π -orbitals.¹⁰³ Here, the metal carbon covalent bond formed is seen as a true double bond (the carbene acts as an X_2 ligand).⁹⁷ The Schrock carbene complexes are nucleophilic at the carbon-metal bond and they are formed typically among early transition metals with the higher oxidation state (see Figure 1.8).⁹³

⁹⁹ a) Roth, H. D. *Acc. Chem. Res.* **1977**, *10*, 85-91. b) Itoh, T.; Nakata, Y.; Hirai, K.; Tomioka, H. *J. Am. Chem. Soc.* **2006**, *128*, 957-967. c) Tomioka, H.; Watanabe, T.; Hattori, M.; Nomura, N.; Hirai, K. *J. Am. Chem. Soc.* **2002**, *124*, 474-482.

¹⁰⁰ Iwamoto, E.; Hirai, K.; Tomioka, H. *J. Am. Chem. Soc.* **2003**, *125*, 14664-14665.

¹⁰¹ a) Bourissou, D.; Guerret, O.; Gabbai, F. P.; Bertrand, G. *Chem. Rev.* **2000**, *100*, 39-92. b) Taylor, T.; Hall, M. *J. Am. Chem. Soc.* **1984**, *106*, 1576-1584. c) Bertrand, G., *Carbene chemistry: from fleeting intermediates to powerful reagents*. CRC Press: **2002**.

¹⁰² Cardin, D.; Cetinkaya, B.; Lappert, M. *Chem. Rev.* **1972**, *72*, 545-574.

¹⁰³ Montgomery, C. D. *J. Chem. Educ.* **2015**, *92*, 1653-1660.

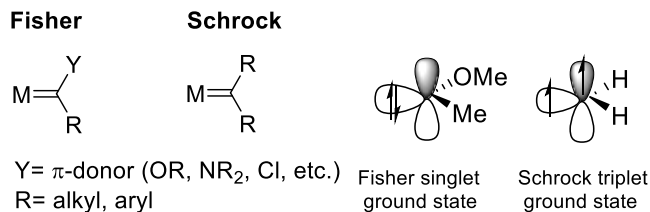
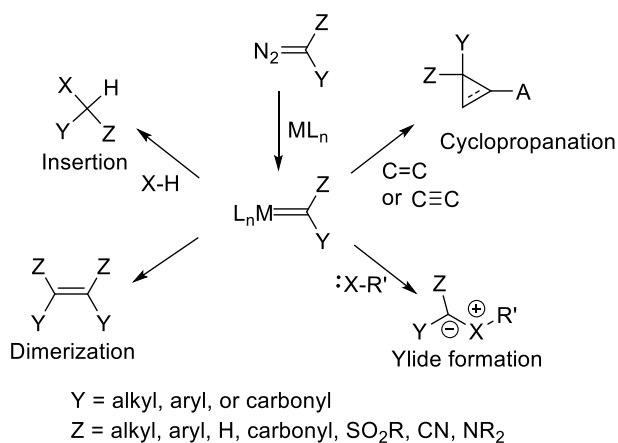


Figure 1.8. Fisher and Schrock-type carbenes

Metal carbenoid can be prepared by metal-catalyzed extrusion of nitrogen from diazo compounds (Scheme 1.24).^{97,104} Metal carbenoid intermediates are capable of a wide range of unusual reactions that can lead to novel strategies for synthesis. Metal carbenes are known for undergoing cyclopropanation reaction to unsaturated carbon-carbon bonds both intermolecularly and intramolecularly.^{101c} Electrophilic metal carbenes also have a great potential in ylide generation with amine, ether or sulfide (acting as Lewis base) and subsequent transformations including [2,3]-sigmatropic rearrangement, Stevens rearrangement, and dipolar cycloadditions.^{101d} Metal carbenes also have been broadly applied for insertion reactions for C–H or Si–H bond and more polar O–H, N–H and S–H bonds (Scheme 1.22).¹⁰⁵

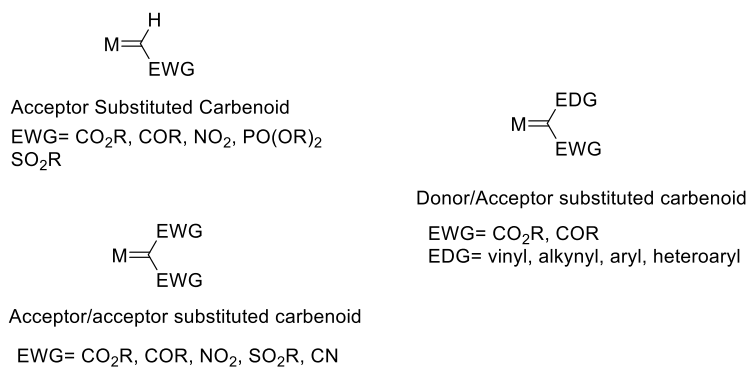


Scheme 1.22. Metal carbenoid intermediates as powerful reagents.

¹⁰⁴ a) Doyle, M. P.; Forbes, D. C. *Chem. Rev.* **1998**, *98*, 911-936. b) Doyle, M. P. *Chem. Rev.* **1986**, *86*, 919-939. c) Maas, G., Transition-metal catalyzed decomposition of aliphatic diazo compounds—new results and applications in organic synthesis. *Organic Synthesis, Reactions and Mechanisms*, Springer: 1987; pp 75-253. d) Ye, T.; McKervey, M. A. *Chem. Rev.* **1994**, *94*, 1091-1160. e) Padwa, A.; Austin, D. J. *Angew Chem Int. Ed. Engl.* **1994**, *33*, 1797-1815. f) Padwa, A.; Hornbuckle, S. F. *Chem. Rev.* **1991**, *91*, 263-309. g) Abel, E. W.; Stone, F. G. A.; Wilkinson, G. *Comprehensive Organometallic Chemistry II: A Review of the Literature 1982-1994*, 1st ed.; Pergamon: Oxford, **1995**.

¹⁰⁵ Buckley, A. M.; Brouder, T. A.; Ford, A.; Maguire, A. R. *C-H Activation for Asymmetric Synthesis*, **2019**, 1-49.

The substituent on the carbene¹⁰⁶ can affect the reactivity of the metal carbenoid. Huw Davies classified carbenoid intermediates into three major groups: acceptor, acceptor/acceptor and donor/acceptor (Scheme 1.23).¹⁰⁷ The activity profile of the metal carbenoid is dependent on the carbenoid structure and substituent, the acceptor substituents can make the carbenoid center more electrophilic and conversely the donor substituents on the metal center reduce the reactivity of the carbenoid. Donor/acceptor carbenoids have a greater chemoselectivity based on the substrates' electronic character, since compared to conventional acceptor carbenoids, the activation energies for the product determining steps are greater for donor/acceptor carbenoids.¹⁰⁸ Thus, donor/acceptor carbenoid are found to be highly efficient in terms of the intermolecular C-H insertion¹⁰⁹ and C-C bond formation.¹¹⁰ The donor/acceptor carbenoids also has enhanced stability than the acceptor carbenoids imparted by the donor group and allowed them to be efficiently applied to solid phase synthesis.¹¹¹



Scheme 1.23. Classification of Carbenoid intermediates.

1.4.2 Ru-catalyzed carbonyl olefination

¹⁰⁶ Davies, H. M. L. *Mol. Catal. A* **2002**, *189*, 125-135.

¹⁰⁷ a) Davies, H. M.; Antoulinakis, E. G. *Org. React.* **2004**, *57*, 1-326. b) Davies, H. M.; Beckwith, R. E. *Chem. Rev.* **2003**, *103*, 2861-2904.

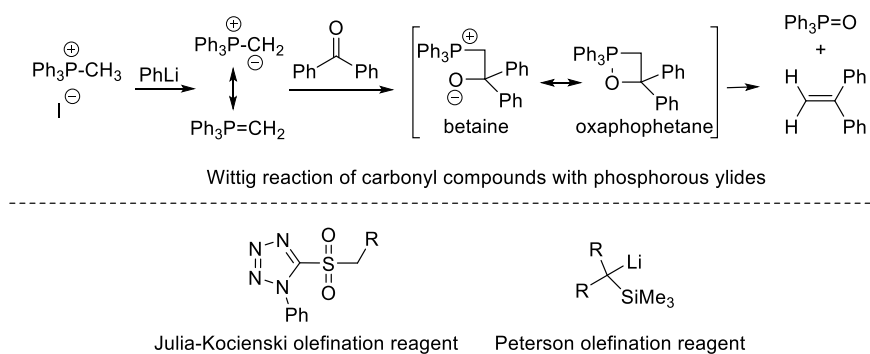
¹⁰⁸ Hansen, J.; Autschbach, J.; Davies, H. M. *J. Am. Chem. Soc.* **2009**, *74*, 6555-6563.

¹⁰⁹ Bergman, R. G. *Nature* **2007**, *446*, 391-393. b) Davies, H. M. L.; Hansen, T.; Churchill, M. R. *J. Am. Chem. Soc.* **2000**, *122*, 3063-3070. c) Godula, K.; Sames, D. *Science* **2006**, *312*, 67-72

¹¹⁰ Thompson, J. L.; Davies, H. M. L. *J. Am. Chem. Soc.* **2007**, *129*, 6090-6091.

¹¹¹ Nagashima, T.; Davies, H. M. L. *J. Am. Chem. Soc.* **2001**, *123*, 2695-2696.

Carbonyl-olefination was pioneered by Georg Wittig¹¹² in 1953, where a phosphorus ylide was utilized for the olefination of an aldehyde or ketone to afford the corresponding alkene and phosphine oxide (Scheme 1.24, top). The starting phosphonium ylides are readily generated from a phosphonium salt in the presence of a base. Betaine and oxaphosphetane intermediates are proposed intermediates for the Wittig olefination.^{112b} Other ylide reagents such as sulfur ylides¹¹³ (Julia-Kochiensi Olefination) and silicon ylides¹¹⁴ (Peterson reaction) have also been developed (Scheme 1.24, bottom).



Scheme 1.24. Commonly used olefination reagents.

In addition, transition metal carbene complexes have been reported for carbonyl olefinations. In 1976, Schrock demonstrated that high-valent early transition carbene complexes such as tantalum and niobium neopentylidene complexes show ylide-like reactivity towards carbonyl compounds.¹¹⁵ A few years later, Tebbe and coworkers¹¹⁶ synthesized the methylene-bridged metallacycle **1.48** (Scheme 1.25, eq 1) Tebbe reagent. The nucleophilic carbene complex titanocene-methylidene **1.49** can achieve methylenation of carbonyl compounds including carboxylic acid derivatives such as esters. Molybdenum-methylidene

¹¹² a) Wittig, G.; Geissler, G. *Liebigs Ann. Chem.* **1953**, 580, 44-57. b) Wittig, G.; Schölkopf, U. *Chem. Ber.* **1954**, 87, 1318-1330.

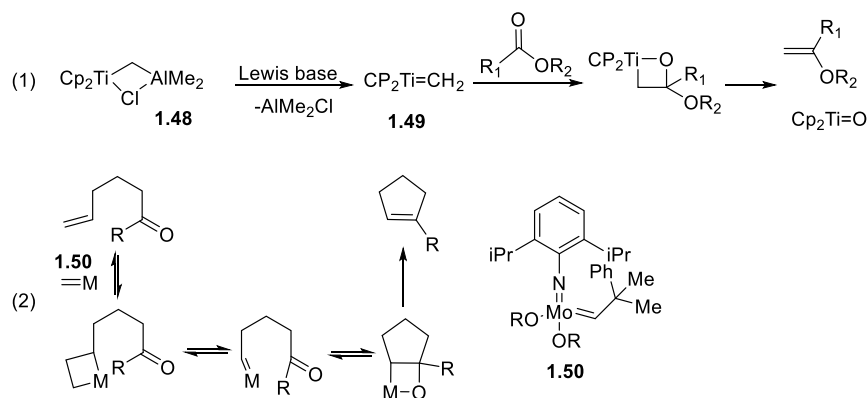
¹¹³ a) Johnson, C. R. *Acc. Chem. Res.* **1973**, 6, 341. b) Kocienski, P. J. *Phosphorus, Sulfur Silicon Relat. Elem.* **1985**, 24, 97-127.

¹¹⁴ a) J. Peterson, *J. Org. Chem.* **1968**, 33, 780-784. b) D. J. Peterson, *Organomet. Chem. Rev. A* **1972**, 7, 295-358. c) T. H. Chan, *Acc. Chem. Res.* **1977**, 10, 442-448.

¹¹⁵ R. R. Schrock, *J. Am. Chem. Soc.* **1976**, 98, 5399.

¹¹⁶ a) F. N. Tebbe, G. W. Parshall, G. S. Reddy, *J. Am. Chem. Soc.* **1978**, 100, 3611. b) K. C. Ott, E. J. M. de Boer, R. H. Grubbs, *Organometallics* **1984**, 3, 223. c) M. M. Francl, W. J. Hehre, *Organometallics* **1983**, 2, 457. R. H. Grubbs, S. H. Pine, in *Comprehensive Organic Synthesis* (Ed.: B. M. Trost), Pergamon Press, New York, **1991**.

complexes¹¹⁷ were also employed as olefination reagents. The molybdenum alkylidene complex **1.50** (shown in Scheme 1.25, eq 2) promoted a tandem olefin metathesis-carbonyl olefination and produced cycloalkenes in a stoichiometric fashion.

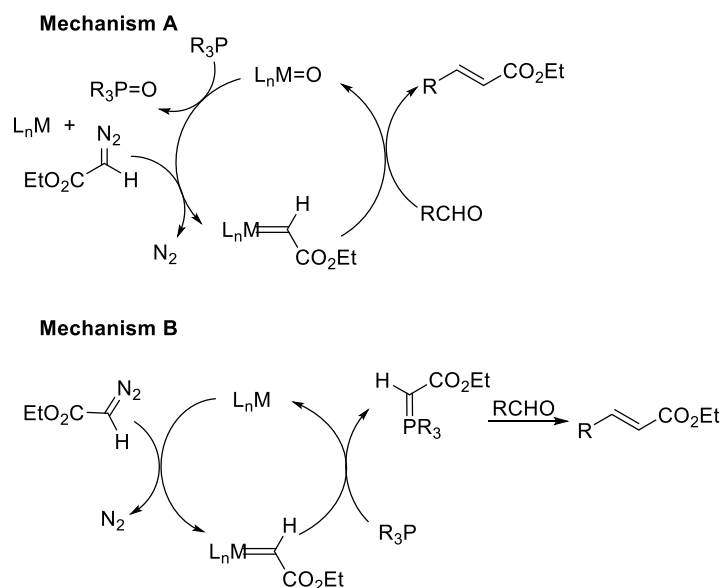


Scheme 1.25. Mechanisms for carbonyl olefination with metal-carbene complexes.

With regard to catalytic carbonyl olefination, two plausible mechanistic pathways¹¹⁸ that rely on the formation of the metal carbene have been proposed in the presence of triphenylphosphine or triethyl phosphite as the stoichiometric reductant (Scheme 1.26). In the first mechanism, the carbene undergoes [2+2] cycloaddition and retro [2+2] cycloaddition with carbonyl and generates the alkene and metal-oxo species, which then can be reduced by the PR_3 (Scheme 1.26, Mechanism A). The second mechanism involves the formation of phosphorus ylide from metal carbene and PR_3 , then the phosphorus ylide adds to the carbonyl to yield the olefin and phosphine oxide species (Scheme 1.26, Mechanism B).

¹¹⁷ a) T. Kauffmann, P. Fiegenbaum, M. Papenberg, R. Wieschollek, J. Sander, *Chem. Ber.* **1992**, *125*, 143. b) T. Kauffmann, P. Fiegenbaum, M. Papenberg, R. Wieschollek, D. Wingbermu"hle, *Chem. Ber.* **1993**, *126*, 79. c) R. R. Schrock, J. S. Murdzek, G. C. Bazan, J. Robbins, M. DiMare, M. O'Regan, *J. Am. Chem. Soc.* **1990**, *112*, 3875.

¹¹⁸ a) Lu, X.; Fang, H.; Ni, Z. *J. Organomet. Chem.* **1989**, *373*, 77–84. b) Cheng, G. L.; Mirafzal, G. A.; Woo, L. K. *Organometallics* **2003**, *22*, 1468–1474. c) Lebel, H.; Paquet, V. *J. Am. Chem. Soc.* **2004**, *126*, 320–328.



Scheme 1.26. Two different mechanisms proposed for transition metals in the presence of PR_3 .

1.4.3 C–H bond activation of diazo compounds

Metal carbene insertion reactions into carbon-hydrogen bonds can proceed in both intramolecular and intermolecular fashion. Intramolecular metal carbene insertion into C–H bonds was first discovered¹¹⁹ by Meerwein, Rathjen and Werner. Initially, few examples were reported for the copper catalyzed intramolecular reactions in geometrically rigid systems (Scheme 1.27, eq 1 and eq 2). Later on, intermolecular C–H bond insertion reactions with dirhodium (II) tetraacetate and ethyl diazoacetate were developed.¹²⁰ Wenkert¹²¹ and Taber¹²² demonstrated the synthetic advantages of dirhodium tetraacetate for the intramolecular C–H bond insertion. The regioselectivity for a tertiary C–H bond over a secondary C–H bond was observed together with the preference for the formation of five-membered cyclopentanone rings (Scheme 1.27, eq 3) and more importantly, C–H bond insertion took place with the retention of configuration at the reacting carbon center.

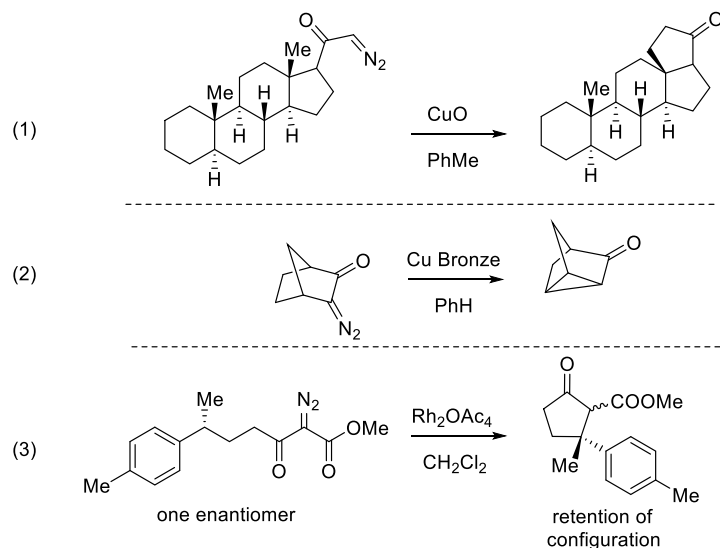
¹¹⁹ Meerwein, H.; Rathjen, H.; Werner, H. *Dtsch. Chem. Ges.* **1942**, 75, 1610-1622.

¹²⁰ a) Demonceau, A.; Noels, A. F.; Hubert, A. J.; Teyssié, P. *J. Chem. Soc., Chem. Commun.* **1981**, 14, 688-689.

b) Demonceau, A.; Noels, A.; Hubert, A. J.; Teyssié, P. *Bull. Soc. Chim. Belg.* **1984**, 93, 945-948.

¹²¹ Wenkert, E.; Davis, L. L.; Mylari, B. L.; Solomon, M. F.; Da Silva, R. R.; Shulman, S.; Warnet, R. J.; Ceccherelli, P.; Curini, M.; Pellicciari, R. *J. Org. Chem.* **1982**, 47, 3242-3247.

¹²² a) Taber, D. F.; Petty, E. H. *J. Org. Chem.* **1982**, 47, 4808-4809. b) DeAngelis, A.; Panish, R.; Fox, J. M. *Acc. Chem. Res.* **2016**, 49, 115-127. c) Candeias, N. R.; Paterna, R.; Gois, P. M. P. *Chem. Rev.* **2016**, 116, 2937-2981.



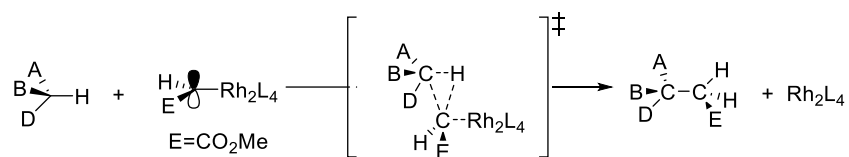
Scheme 1.27. Intramolecular carbene insertion into C–H bond examples.

1.4.4 Metal carbene C–H insertion mechanism

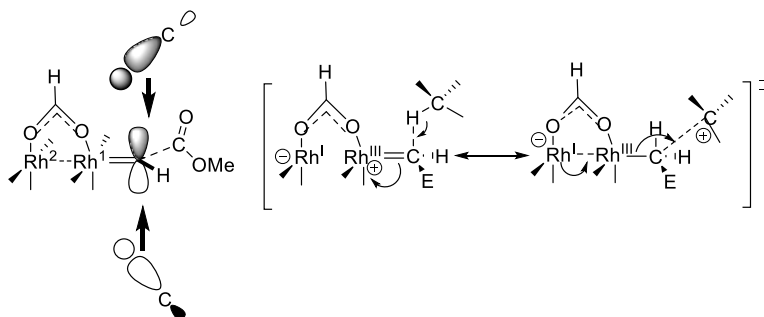
Doyle originally proposed¹²³ the mechanism of metal carbenoid insertion reaction (Scheme 1.28). The C–H bond and C–C bond formation with carbene carbon occurs at the same time as the dissociation of ligated metal. The recent DFT calculation by Nakamura and coworkers¹²⁴ further advanced this mechanism, C–H insertion was computed to occur in an asynchronous single step through a three-centered transition state with low activation energy. The empty p-orbital on the metal carbene overlaps with the σ orbital of the C–H bond of the alkane to initiate the process of C–C and C–H bond formation (Scheme 1.29). The rhodium atoms do not interact directly with the C–H bond. Rh^1 serves as the binding site for the carbene moiety. While the reaction is a concerted process, it can be envisioned as a hydride transferring from alkane to the carbene carbon that is quickly followed by the formation of the new C–C bond. The Rh^2 act as a ligand to enhance the electrophilicity of the carbene center and facilitate the cleavage of the Rh^1 –C bond in the transition state. As shown in Scheme 1.29, the two faces of the carbene moiety are not equivalent. A C–H bond can attack the carbene center from two approaches. Bulky substituents that are attached to the ester group of carbene will make the difference of these two pathways become more significant.

¹²³ Doyle, M. P.; Westrum, L. J.; Wolthuis, W. N.; Sec, M. M.; Boone, W. P.; Bagheri, V.; Pearson, M. M. *J. Am. Chem. Soc.* **1993**, *115*, 958-964.

¹²⁴ Nakamura, E.; Yoshikai, N.; Yamanaka, M. *J. Am. Chem. Soc.* **2002**, *124*, 7181-7192.



Scheme 1.28. Mechanism proposed by Doyle (1993).



Scheme 1.29. C–H bond activation proceed via an asynchronous concerted transition state.

Besides the conformational preference,¹²⁵ the electronic effects¹²⁶ also influence the preferential insertion sites and regioselectivity, as increase in electron-density of C–H bond can make it more susceptible to the attack by the electrophilic carbene species. Adjacent electron donating group of the C–H bond will enhance the insertion, whereas the adjacent electron-withdrawing¹²⁷ group usually inhibits the C–H bond insertion. For insertion tertiary C–H bond is more preferred¹²⁸ than a secondary C–H bond, and secondary C–H bond is better than primary C–H bond.

Copper and rhodium catalyst are often used for selective C–H insertion reactions.¹²⁹ Perez and coworkers extensively investigated the ligated copper complex catalyzed reactions with diazoacetates.¹³⁰

¹²⁵ Doyle, M. P.; Taunton, J.; Pho, H. Q. *Tetrahedron Lett.* **1989**, *30*, 5397-5400.

¹²⁶ a) Wang, P.; Adams, J. *J. Am. Chem. Soc.* **1994**, *116*, 3296-3305. b) Doyle, M. P.; Dyatkin, A. B. *J. Org. Chem.* **1995**, *60*, 3035-3038. c) Díaz-Requejo, M. M.; Belderráin, T. R.; Nicasio, M. C.; Trofimenko, S.; Pérez, P. J. *J. Am. Chem. Soc.* **2002**, *124*, 896-897. d) Davies, H. M.; Hansen, T.; Hopper, D. W.; Panaro, S. A. *J. Am. Chem. Soc.* **1999**, *121*, 6509-6510.

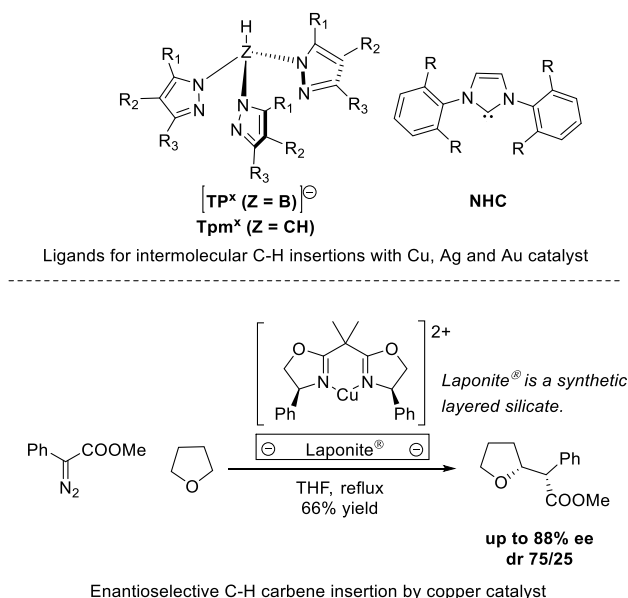
¹²⁷ a) Stork, G.; Kazuhiko, N., Regiocontrol by electron withdrawing groups in the Rh-catalyzed CH insertion of α -diazoketones. *Tetrahedron Lett.* **1988**, *29*, 2283-2286. b) Taber, D. F.; Ruckle, R. E. *J. Am. Chem. Soc.* **1986**, *108*, 7686-7693.

¹²⁸ a) Doyle, M. P.; Westrum, L. J.; Wolthuis, W. N.; See, M. M.; Boone, W. P.; Bagheri, V.; Pearson, M. M. *J. Am. Chem. Soc.* **1993**, *115*, 958-964. b) Davies, H. M.; Hansen, T.; Churchill, M. R. *J. Am. Chem. Soc.* **2000**, *122*, 3063-3070.

¹²⁹ Doyle, M. P.; Duffy, R.; Ratnikov, M.; Zhou, L. *Chem. Rev.* **2010**, *110*, 704-724.

¹³⁰ Díaz-Requejo, M. M.; Perez, P. J. *Chem. Rev.* **2008**, *108*, 3379.

Ligands have been employed for intermolecular C–H insertions with copper, silver, and gold-based catalysts that include¹³¹ trispyrazolylborate (TP^X), Trispyrozoymethane (Tpm^X), N-heterocyclic carbenes¹³² (NHC), and β-diketimidate (Scheme 1.30, top). Copper complexes with chiral bisoxazoline ligands (Scheme 1.30, bottom) was also reported to catalyze intermolecular carbene insertion reactions with high enantioselectivity.¹³³



Scheme 1.30. Selective C–H insertions with Cu catalysts and frequently employed ligands. And enantioselective C–H carbene insertion by copper catalyst.

Dirhodium (II) compounds are the most utilized and versatile catalysts for C–H insertion reactions. Doyle developed chiral dirhodium (II) carboxamide catalysts¹³⁴ based on lactams derived from amino acid. These catalysts¹³⁵ have a paddlewheel structure with four bridging carboxamidate ligands around the dirhodium core (Figure 1.9). A total of four different geometries based on the positioning of nitrogen and

¹³¹ a) Gomez-Emeterio, B. P.; Urbano, J.; Díaz-Requejo, M. M.; Perez, P. J. *Organometallics* **2008**, *27*, 4126-4130. b) Despagnet-Ayoub, E.; Jacob, K.; Vendier, L.; Etienne, M.; Alvarez, E.; Caballero, A.; Díaz-Requejo, M. M.; Perez, P. J. *Organometallics* **2008**, *27*, 4779-4787. c) Li, Z.; He, C. *Eur. J. Org. Chem.* **2006**, 4313. d) Diaz-Requejo, M. M.; Belderrain, T. R.; Nicasio, M. C.; Perez, P. J. *Dalton Trans.* **2006**, 5559.

¹³² Fructos, M. R.; de Frémont, P.; Nolan, S. P.; Díaz-Requejo, M. M.; Pérez, P. J. *Organometallics* **2006**, *25*, 2237-2241.

¹³³ Fraile, J. M.; García, J. I.; Mayoral, J. A.; Roldán, M. *Org. Lett.* **2007**, *9*, 731-733.

¹³⁴ Doyle, M. P.; McKervey, M. A.; Ye, T. *Modern Catalytic Methods for Organic Synthesis with Diazo Compounds: From Cyclopropanes to Ylides*; Wiley-Interscience: New York, **1998**.

¹³⁵ Chifotides, H. T.; Dunbar, K. R. In *Multiple Bonds between Metal Atoms*, 3rd ed.; Cotton, F. A., Murillo, C. A., Walton, R. A., Eds.; Springer: New York, **2005**; Chapter 12.

oxygen on each rhodium are possible. And examples of each geometry except for the (2,2-trans) isomer have been isolated and characterized.¹³⁶ The (2,2-cis) isomer is the dominant isomer produced by ligand replacement on rhodium acetate (A representative examples is shown as Rh₂(5S-MEPY)₄ in Figure 1.9).

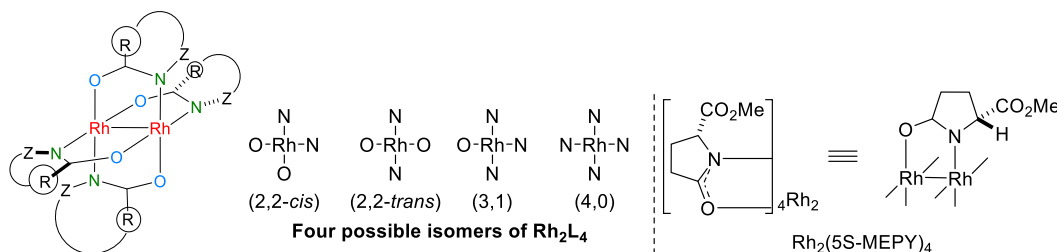
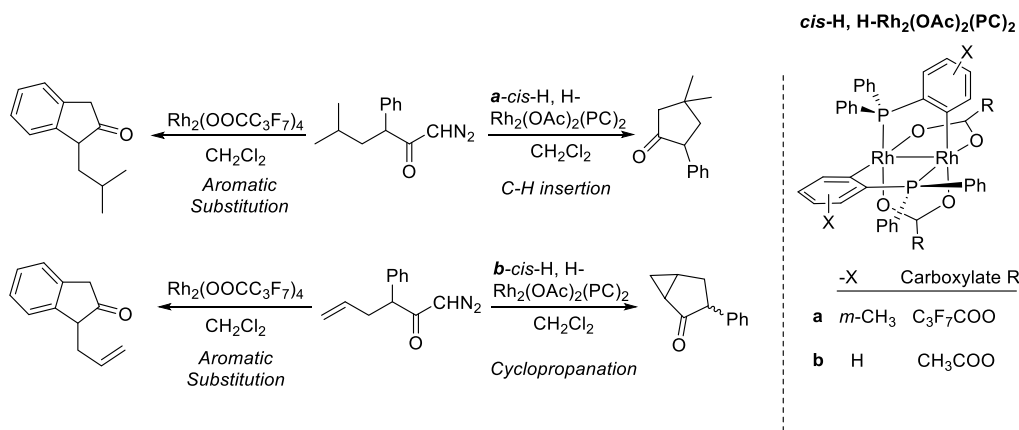


Figure 1.9. Common representations of chiral dirhodium (II) complex and Rh₂(5S-MEPY)₄.

Ortho-Metalated Rhodium (II) complexes¹³⁷ with two cisoid bridging carboxylates (R-C(O)O⁻) and two orthometalated aryl phosphines (PC) was developed by Lahuerta and coworkers. The *cis-H*, *H*-Rh₂(OAc)₂(PC)₂ isomer can undergo high reactivity and selectivity in competitive C–H insertion reactions with diazo esters and diazo ketones.¹³⁸ Variations of the carboxylate ligands can influence chemoselectivity, and cyclopropanation product can be observed instead (Scheme 1.31).



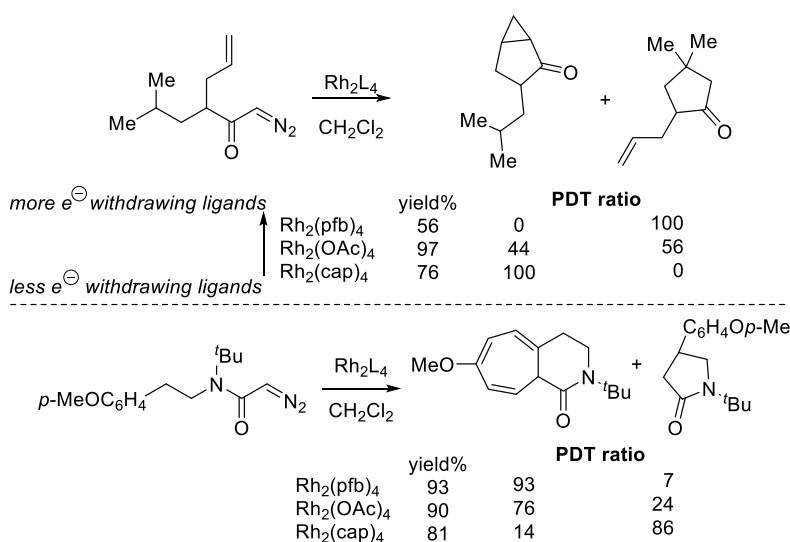
Scheme 1.31. Ligand effects on the chemoselectivity of Rh (II) catalyzed α -diazo ketone transformations.

¹³⁶ Doyle, M. P.; Raab, C. E.; Roos, G. H. P.; Lynch, V.; Simonsen, S. H. *Inorg. Chim. Acta* **1997**, 266, 13.

¹³⁷ a) Estevan, F.; Lahuerta, P.; Perez-Prieto, J.; Sanau, M.; Stiriba, S.-E.; Ubeda, M. A. *Organometallics* **1997**, 16, 880. b) Barberis, M.; Estevan, F.; Lahuerta, P.; Perez-Prieto, J.; Sanau, M. *Inorg. Chem.* **2001**, 40, 4226.

¹³⁸ Estevan, F.; Lahuerta, P.; Perez-Prieto, J.; Pereira, I.; Stiriba, S.-E. *Organometallics* **1998**, 17, 3442.

In general, electrophilic aromatic C–H activation is favored over cyclopropanation and cyclopropanation is more favored than aliphatic C–H insertion when considering the selectivity for carbene-based transformations.¹³⁹ Chemo-selectivity of C–H insertion over other carbene-based transformations (such as cyclopropanation) are affected by ligands' electron-withdrawing ability.¹⁴⁰ An increase in the electrophilic character of the metal carbene leads to higher selectivity towards C–H activation (Scheme 1.32). Diazo compounds' steric and electronic factors can also affect the distribution of C–H insertion and cyclopropanation product.¹⁴¹ Disubstituted diazo compounds tend to undergo C–H insertion compared to their monosubstituted analogues, and diazoacetate ester that have an electron-donating group exhibit a stronger selectivity in favor of insertion than those with an electron-withdrawing group (Scheme 1.33, entry 1 and 3 vs. entry 2).

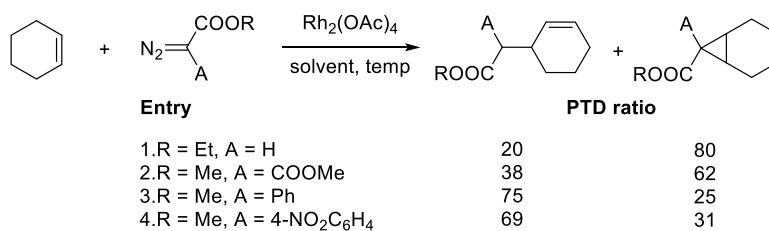


Scheme 1.32. Chemoselectivity based on the electrophilicity of metal carbenes.

¹³⁹ Doyle, M. P.; Westrum, L. J.; Wolthuis, W. N. E.; See, M. M.; Boone, W. P.; Bagheri, V.; Pearson, M. M. *J. Am. Chem. Soc.* **1993**, *115*, 958–964.

¹⁴⁰ a) Muller, P.; Tohill, S. *Tetrahedron* **2000**, *56*, 1725-1731. b) Padwa, A.; Austin, D. J.; Price, A. T.; Semones, M. A.; Doyle, M. P.; Protopopova, M. N.; Winchester, W. R. *J. Am. Chem. Soc.* **1993**, *115*, 8669-8680.

¹⁴¹ Ye, T.; McKervey, M. A. *Chem. Rev.* **1994**, *94*, 1091-1160.



Scheme 1.33. Intermolecular C-H insertion in competition with cyclopropanation reaction.

1.4.5 Diazo X-H insertion reactions.

Sensitivity towards acids was recognized as one of the characteristic properties of diazo compounds since the discovery of diazoalkanes. Along with C-H bond insertion reaction, the insertion into polar X-H bonds was also one of the characteristic reactions of carbenes. In contrast to metal-catalyzed carbene insertions into C-H or Si-H bonds, which are concerted, insertion into polar X-H (X = O, S) bonds has been proposed to occur via a stepwise process which begins with attack of the heteroatom on the electrophilic carbene, subsequent ylide formation, and then proton transfer.¹⁴²

Diazo esterification reaction was first discovered by Staudinger and Gaule¹⁴³ in 1917, who used diphenyldiazomethane to react with benzoic acid to form an ester. Roberts and coworkers proposed a mechanism¹⁴⁴ of this reaction in 1951. Benzoic acid was proposed to act as a general acid catalyst and underwent a direct reaction with the diazo compound via a three-center mechanism (Scheme 1.34, pathway a). Although the concerted pathway cannot be completely excluded, there is no direct experiment data so far to support it.

Another alternative stepwise mechanism (Scheme 1.34, pathway b) that was proposed involves an initial slow transfer of a proton to diazocarbon to give a diazonium ion, which then combines with the anion with concomitant loss of nitrogen to give the final product. This mechanism is consistent with the second-order kinetics¹⁴⁵ and a kinetic isotope effect $k_H/k_D=3.5$ (benzoic-H acid in ethanol-H and benzoic-

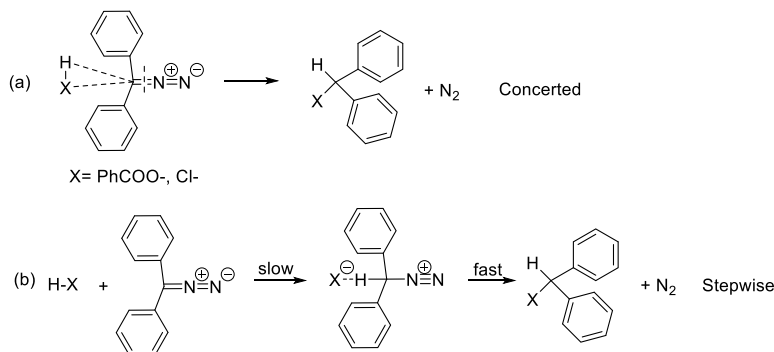
¹⁴² Miller, D. J.; Moody, C. J. *Tetrahedron* **1995**, *51*, 10811-10843.

¹⁴³ Staudinger, H.; Gaule, A. *Ber. Dtsch. Chem. Ges.* **1916**, *49*, 1951-1960.

¹⁴⁴ Roberts, J. D.; Watanabe, W. *J. Am. Chem. Soc.* **1951**, *73*, 2521-2523.

¹⁴⁵ O'Ferrall, R. M.; Kwok, W. *J. Am. Chem. Soc.* **1964**, *86*, 5553-5561.

D acid in ethanol-D).¹⁴⁶ This mechanism is currently accepted as the working mechanism for the X–H insertion reaction into diazo compounds.¹⁴⁷



Scheme 1.34. Proposed H-X insertion reaction mechanism pathways.

Yate reported the first systematic¹⁴⁸ transition metal catalyzed H–X insertion reaction using copper metal as a catalyst and proposed a metal-carbenoid intermediate (Scheme 1.35, eq 1). Nozaki, Noyori and coworkers¹⁴⁹ reported the copper catalyzed H–X insertion reactions. In 1973, Teyssie reported the first¹⁵⁰ Rh (II) catalyzed insertion of diazo compounds into hydroxylic bonds (Scheme 1.35, eq 2). An application of this methods is the Merck synthesis of antibiotic thienamycin¹⁵¹ that employed insertion of N–H bond of β -lactam motif as a key step in 1980 (Scheme 1.35, eq 3). There are two possible insertion X–H mechanisms into a metal carbenoid generated by decomposition of diazo compounds (Scheme 1.36). While the concerted mechanism is generally accepted for non-polar bonds (i.e. C–H, Si–H insertion), polar X–H bonds seem to prefer the stepwise ylide mechanism.¹⁵² The stepwise mechanism (Scheme 1.36, pathway b)¹⁵³ is initiated by the attack of nucleophile on the electrophilic carbene to give an ylide which is then followed by proton transfer.

¹⁴⁶ Kirmse, W.; Kund, K. *J. Org. Chem.* **1990**, *55*, 2325-2332.

¹⁴⁷ Kuhnle, E.; Laffan, D. D.; Lloyd-Jones, G. C.; Martinez Del Campo, T.; Shepperson, I. R.; Slaughter, J. L. *Angew. Chem., Int. Ed.* **2007**, *46*, 7075–7078.

¹⁴⁸ Yates, P., *J. Am. Chem. Soc.* **1952**, *74*, 5376-5381.

¹⁴⁹ Nozaki, H.; Takaya, H.; Moriuti, S.; Noyori, R. *Tetrahedron* **1968**, *24*, 3655-3669.

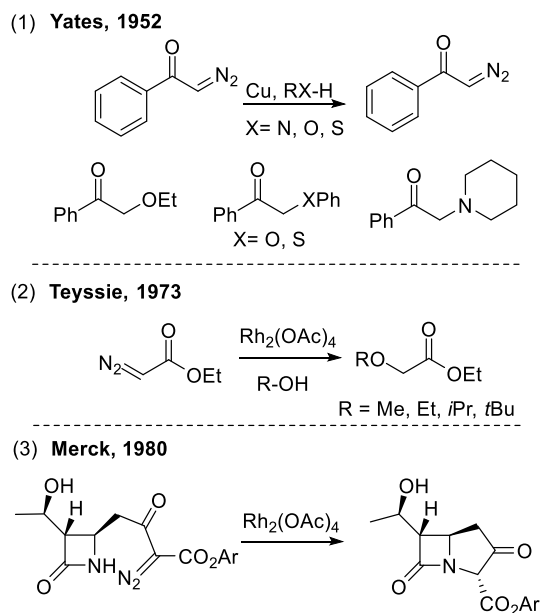
¹⁵⁰ a) Paulissen, R.; Reimlinger, H.; Hayez, E.; Hubert, A. J.; Teyssié, P. *Tetrahedron Lett.* **1973**, *14*, 2233-2236.

b) Doyle, M. P.; McKervey, M. A.; Ye, T., *Modern catalytic methods for organic synthesis with diazo compounds*. Wiley: **1998**.

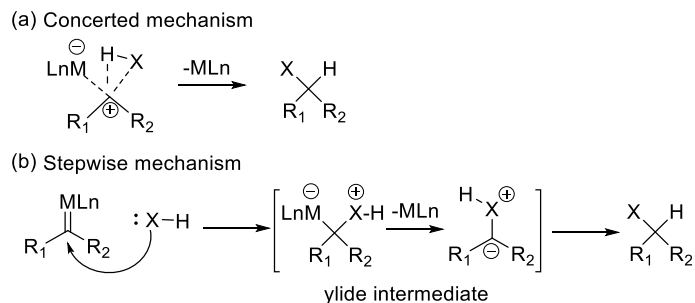
¹⁵¹ Salzmann, T. N.; Ratcliffe, R. W.; Christensen, B. G.; Bouffard, F. A. *J. Am. Chem. Soc.* **1980**, *102*, 6161–6163.

¹⁵² a) Gillingham, D.; Fei, N. *Chem. Soc. Rev.* **2013**, *42*, 4918-4931. b) Liang, Y.; Zhou, H.; Yu, Z.-X. *J. Am. Chem. Soc.* **2009**, *131*, 17783-17785.

¹⁵³ a) Kirmse, W.; Brinker, U., *Advances in Carbene Chemistry*. by U. Brinker, JAI Press, Stamford **1994**, *1*, 1-57.



Scheme 1.35. Catalyzed X-H insertion reactions with diazo compounds.



Scheme 1.36. Transition-Metal-Catalyzed X-H insertion reaction mechanisms.

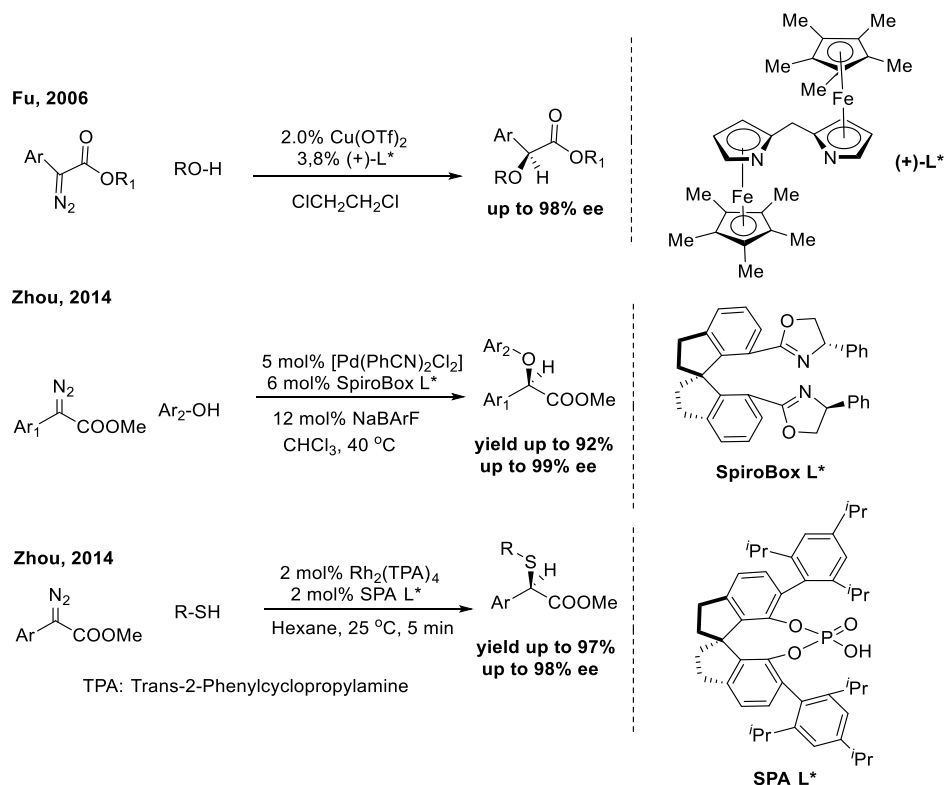
Initial transition-metal-catalyzed asymmetric X-H insertion reactions are reported with moderate to low enantioselectivity.¹⁵⁴ To date, some highly enantioselective X-H insertion reaction have been reported by chiral copper, rhodium, and iron complexes (Scheme 1.40). Fu and coworkers¹⁵⁵ developed an effective copper/bisazaferrocene-catalyzed enantioselective insertion of α -aryl- α -diazoacetates into O-H

b) Helson, H. E.; Jorgensen, W. L. *J. Org. Chem.* **1994**, *59*, 3841-3856.

¹⁵⁴ a) García, C. F.; McKervey, M. A.; Ye, T. *Chem. Commun.* **1996**, 1465-1466. b) Buck, R. T.; Moody, C. J.; Pepper, A. G. *ARKIVOC* **2002**, *viii*, 16-33. c) Bachmann, S.; Fielenbach, D.; Jørgensen, K. A. *Org. Biomol. Chem.* **2004**, *2*, 3044-3049. d) Bulugahapitiya, P.; Landais, Y.; Parra-Rapado, L.; Planchenault, D.; Weber, V. *J. Org. Chem.* **1997**, *62*, 1630-1641.

¹⁵⁵ Maier, T. C.; Fu, G. C. *J. Am. Chem. Soc.* **2006**, *128*, 4594-4595.

bonds of alcohols. Chiral spiro bisoxazoline ligands SpiroBOXs developed by Zhou group¹⁵⁶ was found to have advantages for asymmetric carbene insertions of various X–H bonds such as N–H, O–H, and S–H bonds with high yields and excellent enantioselectivities. Zhou group also reported the highly enantioselective S–H bond insertion¹⁵⁷ using cooperative catalysis of dirhodium (II) carboxylates and chiral SPAs (spiro phosphoric acids).



Scheme 1.37. Enantioselective H–X bond insertion examples.

For select applications in chemical biology field, Riehm and Scheraga¹²⁷ used a diazo acetoglycinamide¹⁵⁸ to selectively esterify the aspartic acid residues in the solvent-accessible area of ribonuclease A. Shortly after, Delpierre and Fruton used¹⁵⁹ an α -diazoketone to label a single residue in the active site of pepsin that led to the inhibition of the enzyme activity (Figure 1.10). Protein carboxylation

¹⁵⁶ a) Zhu, S.-F.; Zhou, Q.-L. *Acc. Chem. Res.* **2012**, *45*, 1365-1377. b) Xie, X. L.; Zhu, S. F.; Guo, J. X.; Cai, Y.; Zhou, Q. L. *Angew. Chem.* **2014**, *126*, 3022-3025.

¹⁵⁷ Xu, B.; Zhu, S.-F.; Zhang, Z.-C.; Yu, Z.-X.; Ma, Y.; Zhou, Q.-L. *Chem. Sci.* **2014**, *5*, 1442-1448.

¹⁵⁸ Riehm, J. P.; Scheraga, H. A. *Biochemistry* **1965**, *4*, 772-782.

¹⁵⁹ Delpierre, G. R.; Fruton, J. S. *Proc. Natl. Acad. Sci. U.S.A.* **1966**, *56*, 1817-1822.

reactions also shown can be performed in an aqueous medium.¹⁶⁰ Chibnall¹⁶¹ employed diazomethane in an 85% ethanol solution to achieve a partial methylation of the Carboxyls in β -lactoglobulin. Diazoacetamide and methyl diazoacetate were utilized to esterify carboxyl groups in human serum albumin by Wilcox¹⁶² in the Aqueous medium.

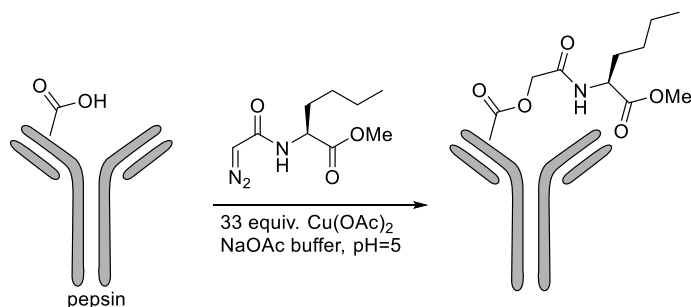


Figure 1.10. Active-site carboxyl residue of pepsin is modified with diazo compounds in the presence of large excess of copper (II) salts.

1.4.6 Halo functionalization of diazo compounds

Diazo compounds were applied as a step-economic approach to construct carbon-halogen bonds. Halogenation of diazo compound can proceed in the presence of transition metal catalyst via the formation of carbene or via a non-carbene pathway.¹⁶³ Acyl halides, benzyl halides and alkyl halides have polarized carbon-halogen bonds which render the halogen atom nucleophilic for an attack to a carbene. Lee group¹⁶⁴ developed several Rhodium (II)-catalyzed halogenation reactions with cyclic diazocarbonyl compounds using various halides (Scheme 1.38). Recently, Lee group also developed a $\text{Rh}_2(\text{OPiv})_4$ catalyzed

¹⁶⁰ Doscher, M. S.; Wilcox, P. E. *J. Biol. Chem.* **1961**, *236*, 1328-1337.

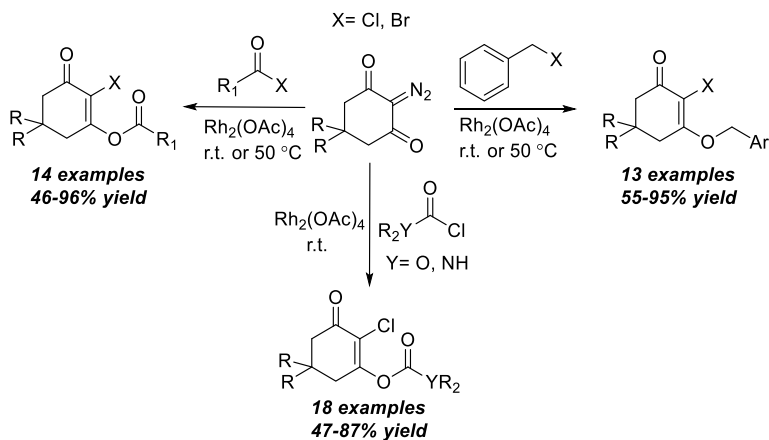
¹⁶¹ Chibnall, A.; Rees, M. *Biochem. J.* **1958**, *68*, 105-111.

¹⁶² Doscher, M. S.; Wilcox, P. E. *J. Biol. Chem.* **1961**, *236*, 1328-1337.

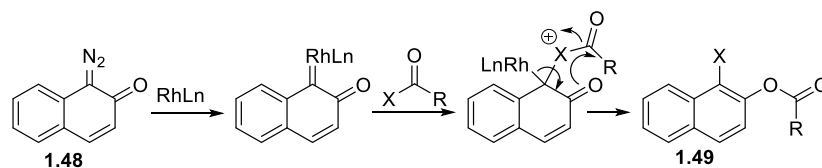
¹⁶³ Khanal, H. D.; Thombal, R. S.; Maezono, S. M. B.; Lee, Y. R. *Adv. Synth. Catal.* **2018**, *360*, 3185– 3212.

¹⁶⁴ a) Y. R. Lee, J. Y. Suk, *Chem. Commun.* **1998**, *23*, 2621-2622. b) Y. R. Lee, D. H. Kim, *Tetrahedron Lett.* **2001**, *42*, 6561-6563. c) Y. R. Lee, B. S. Cho, H. J. Kwon, *Tetrahedron* **2003**, *59*, 9333-9347. d) K. B. Somai Magar, Y. R. Lee, *Bull. Korean Chem. Soc.* **2012**, *33*, 4150-4154.

halogenation reaction of diazo **1.48** coupled to halonaphthalenyl ether and form esters **1.49** along with a proposed mechanism (see Scheme 1.39).¹⁶⁵



Scheme 1.38. Rh (II) catalyzed reactions of diazo compounds with various halides.

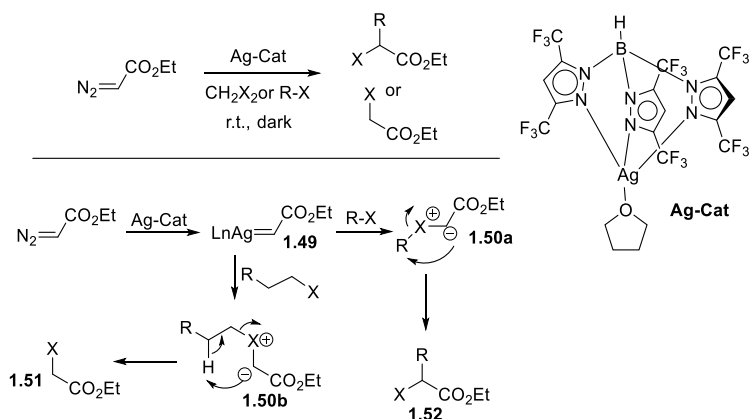


Scheme 1.39. Proposed mechanism for formation of halonaphthalenyl esters.

Silver-catalyzed halogenation of α -diazo ester with dichloromethane and other chlorinated solvents to generate α -chloro- or bromo esters was reported by Dias et al.¹⁶⁶ A tris(pyrazolyl)borate ligand was used to support the metal, and the reaction was proposed to undergo a carbene insertion into the C–X bond of dihalomethanes (Scheme 1.40). A silver carbene **1.49** is initially formed, and subsequently reacts with the halide to form ylide **1.50**. If a β -H is present, it undergoes a deprotonation to give **1.51**. Alternatively, a 1,2-shift of alkyl moiety can occur in the absence of β -H to give the rearranged product **1.52**.

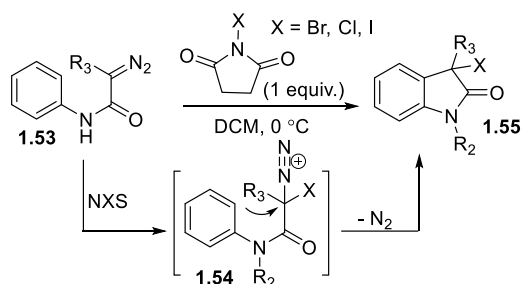
¹⁶⁵ E. R. Baral, Y. R. Lee, S. H. Kim, Y.-J. Wee, *Synthesis* **2016**, 48, 579-587.

¹⁶⁶ H. V. R. Dias, R. G. Browning, S. A. Polach, H. V. K. Diyabalanage, C. J. Lovely, *J. Am. Chem. Soc.* **2003**, 125, 9270-9271.



Scheme 1.40. Synthesis of α -halo ester by C–X insertion.

Halogenating reagents such as *N*-halosuccinimides¹⁶⁷ (NXS, X=Br, I or Cl), *N*-fluorobenzenesulfonimide¹⁶⁸ (NFSI) and Selectfluor¹⁶⁹ can also be employed to convert carbon diazo bond to C–X bonds. In 2016, Hu et al. developed a halogenative cyclization of *N*-aryl diazoamides **1.53** using *N*-halosuccinimides under catalyst-free conditions. The carbene-free pathway starts with the electrophilic NXS reacting with **1.53** at the diazo carbon atom and generating diazonium ion **1.54**, which further undergoes intramolecular Friedel-Crafts alkylation with extrusion of N₂ gas to give product **1.55** (Scheme 1.41).



Scheme 1.41. Carbene-free halogenation of α -diazo carbonyl compounds using *N*-halosuccinimide.

¹⁶⁷ a) F.-N. Ng, Y.-F. Lau, Z. Zhou, W. Y. Yu, *Org. Lett.* **2015**, *17*, 1676-1679. b) C. Ma, D. Xing, W. Hu, *Org. Lett.* **2016**, *18*, 3134-3137. c) X. Wang, K. Dong, B. Yan, C. Zhang, L. Qiu, X. Xu, *RSC Adv.* **2016**, *6*, 70221-70225.

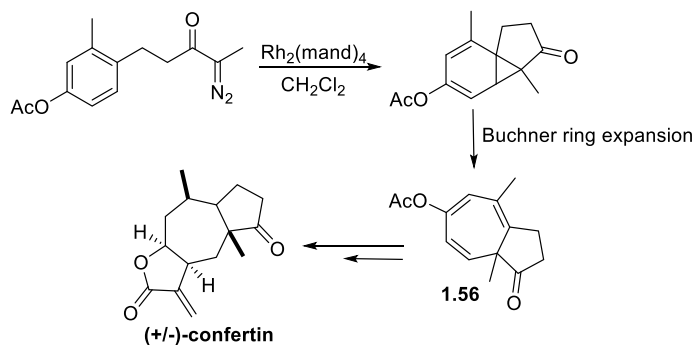
¹⁶⁸ a) W. Yuan, K. J. Szabo, *ACS Catal.* **2016**, *6*, 6687. b) J. Huang, L. Li, H. Chen, T. Xiao, Y. He, L. Zhou, *Org. Chem. Front.* **2017**, *4*, 529-533. c) K. Zhang, G. Zhao, W. Cao, *Tetrahedron* **2014**, *70*, 5659-5665. d) K. Dong, B. Yan, S. Chang, Y. Chi, L. Qiu, X. Xu, *J. Org. Chem.* **2016**, *81*, 6887-6892.

¹⁶⁹ a) R. E. Banks, *J. Fluorine Chem.* **1998**, *87*, 1-17. b) M. Brunavs, C. P. Dell, M. W. Owton, *J. Fluorine Chem.* **1994**, *68*, 201-203. c) R. E. Banks, N. J. Lawrence, A. L. Popplewell, *Synlett* **1994**, 831-832. d) A. K. Forrest, P. J. O'Hanlon, *Tetrahedron Lett.* **1995**, *36*, 2117-2118.

1.4.7 Diazo compounds utility in total synthesis

Diazo compounds are exceptionally useful reagent in synthetic organic chemistry as nearly every class of organic compounds can be prepared using diazo compounds.¹⁷⁰ They are versatile building blocks for creating carbon-carbon and carbon-heteroatom bonds that would be arduous to obtain otherwise.¹⁷¹

Below are select synthesis of biologically active molecules involving diazo chemistry as a key step. Rhodium(II)-catalyzed cycloaddition of aryl diazoketones provided direct access to the pseudo-guaianolide tricyclic framework.¹⁷² Subsequent Buchner ring expansion step provided a key intermediate **1.56** in the formal synthesis of (+/-)-Confertin (Scheme 1.42).¹⁷³



Scheme 1.42. The synthesis of (+/-)-confertin.

Asymmetric C–H bond insertion of diazo compound have been widely employed in natural product synthesis. Doyle’s chiral rhodium (II) carboxamidate catalysts such as $\text{Rh}_2(\text{S-MPPIM})_4$ has shown great success, and this highly enantioselective C–H insertion is a key step in the total synthesis of the platelet-aggregation inhibitor (S)-(+)-Imperanene (Scheme 1.43).¹⁷⁴ The enantioselective synthesis of β -lactam antibiotic also employed the asymmetric intramolecular C–H insertion chemistry of diazo substrates.

¹⁷⁰ a) Ford, A.; Miel, H.; Ring, A.; Slattery, C. N.; Maguire, A. R.; McKerverey, M. A., *Chem. Rev.* **2015**, *115*, 9981-10080. b) Medvedev, J.; Nikolaev, V. *Russ. Chem. Rev.* **2015**, *84*, 737-757.

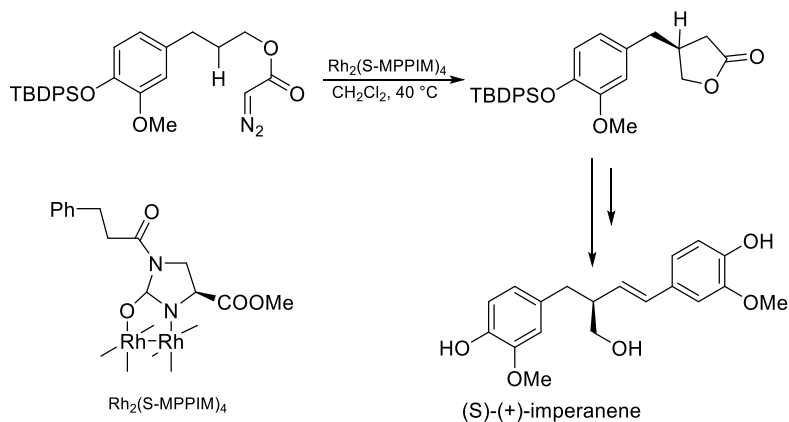
¹⁷¹ Budev, A.; Kantin, G.; Dar'in, D.; Krasavin, M. *Molecules* **2021**, *26*, 2530-2600. b) Ford, A.; Miel, H.; Ring, A.; Slattery, C. N.; Maguire, A. R.; McKerverey, M. A. *Chem. Rev.* **2015**, *115*, 9981-10080.

¹⁷² Foley, D. A.; O'Leary, P.; Buckley, N. R.; Lawrence, S. E.; Maguire, A. R. *Tetrahedron* **2013**, *69*, 1778-1794.

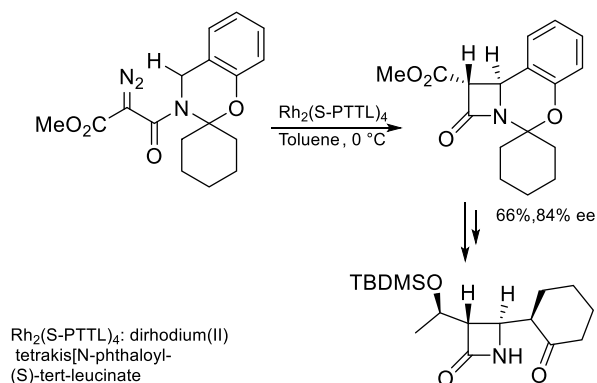
¹⁷³ Kennedy, M.; McKerverey, M. A. *J. Chem. Soc., Perkin Trans. 1* **1991**, 2565-2574.

¹⁷⁴ Doyle, M. P.; Hu, W.; Valenzuela, M. V. *J. Org. Chem.* **2002**, *67*, 2954-2959.

Hashimoto and coworkers reported the synthesis of trinem,¹⁷⁵ a new family of synthetic β -lactam antibiotics that shows excellent activity against bacteria strains producing β -lactamase (Scheme 1.44).



Scheme 1.43. Synthesis of (S)-(+)-imperanene.



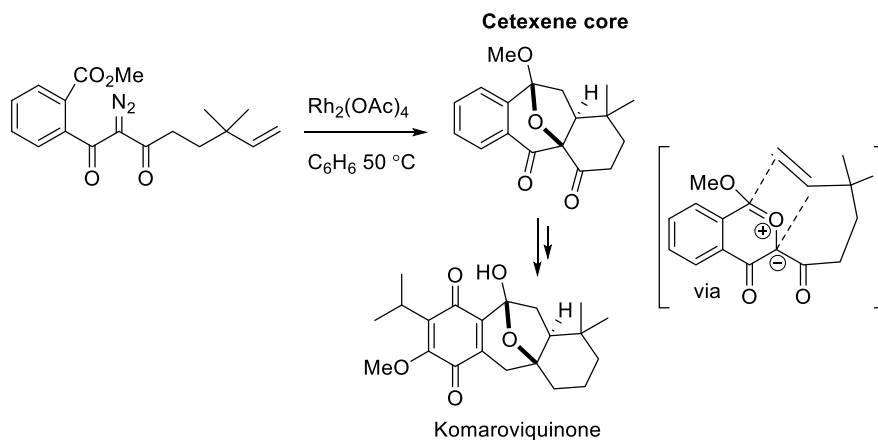
Scheme 1.44. Synthesis of trinem antibiotics.

Diazo compounds are also frequently reported to undergo tandem reactions to efficiently construct the skeleton of complex molecules. Padwa published the total synthesis of komaroviquinone¹⁷⁶ that employed Rh-catalyzed cyclization/1,3-dipolar cycloaddition across the tethered π -bond of carbonyl ylide intermediate and allowed the access to the icetexane core of komaroviquinone (Scheme 1.45). A similar example is the formal synthesis of vallesamidine¹⁷⁷ via the cycloaddition of diazoimide **1.56** to give the desired cycloadduct **1.57** in 85% yield as a single diastereomer (Scheme 1.46).

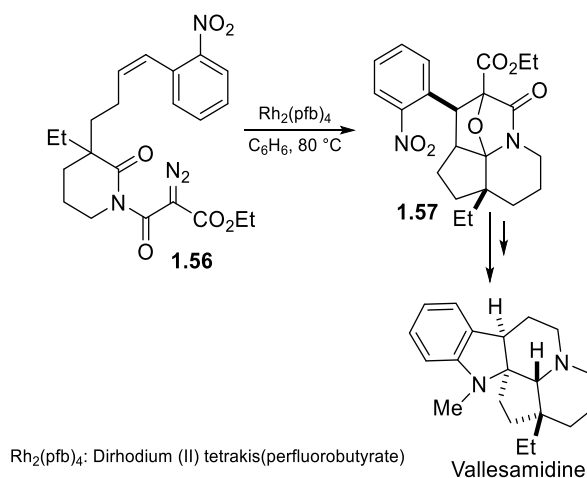
¹⁷⁵ Anada, M.; Hashimoto, S.-i. *Tetrahedron Lett.* **1998**, *39*, 9063-9066.

¹⁷⁶ Padwa, A.; Boonsombat, J.; Rashatasakhon, P.; Willis, J. *Org. Chem.* **2005**, *7*, 3725-3727.

¹⁷⁷ Padwa, A.; Haring, S. R.; Semones, M. A. *J. Org. Chem.* **1998**, *63*, 44-54.



Scheme 1.45. Synthetic key step of komaroviquinone.

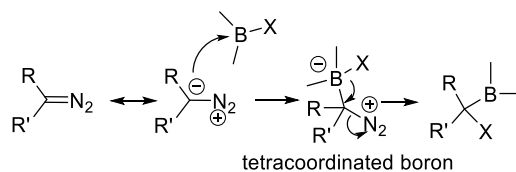


Scheme 1.46. Synthetic key step of vallesamidine.

1.4.8 Reaction of diazo compounds with organoboron compounds

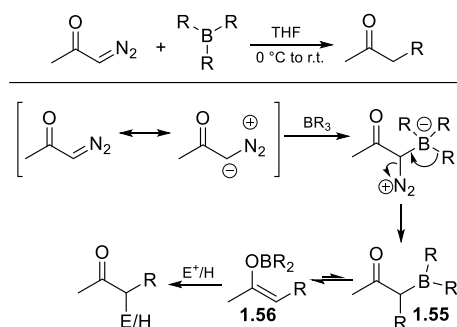
Reaction between nucleophilic diazo and electro-deficient boron compounds is an alternative way to achieve C–C bond coupling.¹⁷⁸ The general reaction mechanism for diazo compound reaction with boron reagents are shown in Scheme 1.47. The diazo carbon can serve as a nucleophile to react with an electron-deficient boron center to form a tetra-coordinated boron intermediate, and one of the boron substituents on boron will shift to carbon center with the release of dinitrogen gas.

¹⁷⁸ Li, H.; Zhang, Y.; Wang, J. B. *Synthesis* **2013**, 45, 3090–3098.



Scheme 1.47. General reaction mechanism for the addition of an organoboron reagent to diazo compounds.

Reaction of diazo compounds with organoboranes was reported back in 1968 by Hooz,¹⁷⁹ where treatment of diazo acetone with trialkylboranes led to the transfer of one of the R groups from boron to diazo carbon. The reaction mechanism is shown in scheme 1.48. After extrusion of N₂, the C–boron enolate **1.55** is in equilibrium with O–boron enolate **1.56**. Experimental evidence shows that adduct formation, migration and the equilibrium favor the O–boron enolate **1.56**. Final hydrolysis or reaction with electrophile E⁺ yields the final product (Scheme 1.48).

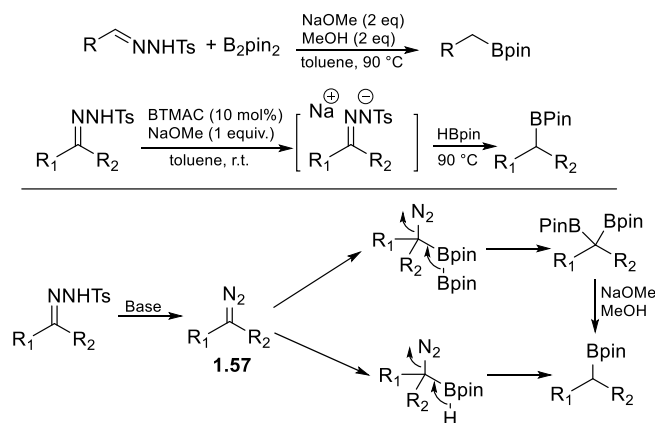


Scheme 1.48. Reaction of diazo with carbonyl diazo compound.

Wang and co-workers¹⁸⁰ reported the borylation of tosylhydrazones with B₂Pin₂ or pinacolborane (HBpin). The diazo compound **1.57** is formed in situ, which then reacts with B₂Pin₂ or HBpin followed by 1,2-B migration or 1,2-H shift to afford the final products (Scheme 1.49).

¹⁷⁹ Hooz, J.; Linke, S. *J. Am. Chem. Soc.* **1968**, *90*, 5936-5937.

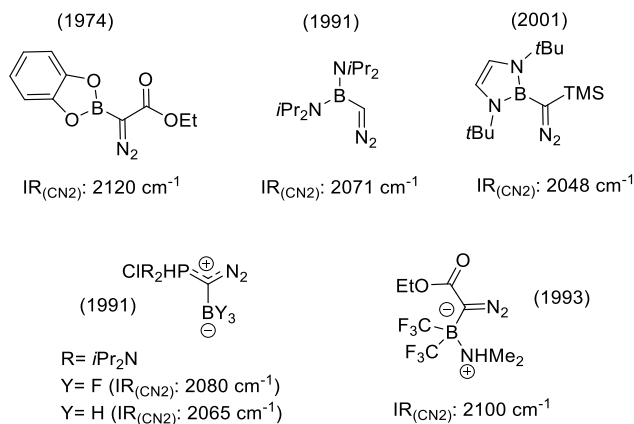
¹⁸⁰ Li, H.; Wang, L.; Zhang, Y.; Wang, J. *Angew. Chem. Int. Ed.* **2012**, *51*, 2943-2946.



Scheme 1.49. Proposed mechanism for borylation of tosylhydrazones.

1.5 Diazomethyl-1,2-azaborine compounds as a new class of α -boryl diazo compounds.

As we discussed in the background session, α -boryl diazo compounds are rare, with only about a handful of examples reported to date (Scheme 1.50).¹⁸¹ Lewis acidic boranes have been demonstrated to decompose diazo compounds;¹⁸² thus all the reported α -boryl diazo compounds either contain quaternized boron or involve trigonal planar boron atoms attached to two π -donating heteroatoms (O, N) to minimize boron's Lewis acidity (Scheme 1.50). Despite the broad applicability of diazo compounds as versatile reagents in synthetic organic applications,¹⁸³ no instances of organic reaction chemistry have been described for α -boryl diazo compounds, presumably due to their perceived highly sensitive nature toward reaction conditions for organic synthesis.



¹⁸¹ Schollkopf, U.; Banhidai, B.; Frasnelli, H.; Meyer, R.; Beckhaus, H. *Liebigs Ann. Chem.* **1974**, *11*, 1767–1783.

¹⁸² Hooz, J.; Gunn, D. M. *J. Am. Chem. Soc.* **1969**, *91*, 6195–6198.

¹⁸³ Maas, G. New syntheses of diazo compounds. *Angew. Chem., Int. Ed.* **2009**, *48*, 8186–95.

Scheme 1.50. Previously reported α -boryl diazo compounds.

We envisioned that when the boron atom of an α -boryl diazo species is embedded in an aromatic scaffold¹⁸⁴ such as in diazomethyl-1,2-azaborine **1** (Figure 1.11), sufficient stability could still be achieved to enable diverse reaction chemistry of the diazo functional group. Diazomethyl-1,2-azaborine **1** turned out to be an exceptional example of the α -boryl diazo family of compounds that is remarkably stable and capable of engaging in a wide range of diazo activation modes, in some cases with distinct reaction selectivities, thus rendering **1** a powerful synthetic building block for 1,2-azaborine chemistry.¹⁸⁵ In view of emerging applications of BN heterocycles in materials chemistry,¹⁸⁶ biomedical research,¹⁸⁷ and organic synthesis,¹⁸⁸ the development of new versatile 1,2-azaborine building blocks is a significant objective.

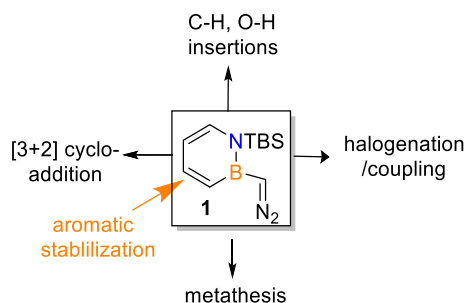


Figure 1.11. New α -boryl diazo family.

1.5.1 Synthesis of Diazomethyl-1,2-azaborine

Diazomethyl-1,2-azaborine **1** can be prepared in a two-step procedure from commercially available starting materials. Treatment of *N*-TBS-*B*-Cl-1,2-azaborine with AgOTf furnishes the *B*-OTf

¹⁸⁴ Campbell, P. G.; Abbey, E. R.; Neiner, D.; Grant, D. J.; Dixon, D. A.; Liu, S.-Y. *J. Am. Chem. Soc.* **2010**, *132*, 18048–50.

¹⁸⁵ a) Liu, Z.; Marder, T. B. *Angew. Chem., Int. Ed.* **2008**, *47*, 242–244. b) Bosdet, M. J. D.; Piers, W. E. *Can. J. Chem.* **2009**, *87*, 8–29. c) Campbell, P. G.; Marwitz, A. J. V.; Liu, S.-Y. *Angew. Chem., Int. Ed.* **2012**, *51*, 6074–6092. d) Belanger-Chabot, G.; Braunschweig, H.; Roy, D. K. *Eur. J. Inorg. Chem.* **2017**, 38–39, 4353–4368. e) Giustra, Z. X.; Liu, S. Y. *J. Am. Chem. Soc.* **2018**, *140*, 1184–1194.

¹⁸⁶ a) Wang, X.-Y.; Wang, J.-Y.; Pei, J. *Chem. - Eur. J.* **2015**, *21*, 3528–3539. b) Morgan, M. M.; Piers, W. E. *Dalton Trans.* **2016**, 45, 5920–5924. c) Huang, J.; Li, Y. *Front. Chem.* **2018**, *6*, 341–351.

¹⁸⁷ a) Vlasceanu, A.; Jessing, M.; Kilburn, J. P. *Bioorg. Med. Chem.* **2015**, *23*, 4453–4461. b) Rombouts, F. J.; Tovar, F.; Austin, N.; Tresadern, G.; Trabanco, A. A. *J. Med. Chem.* **2015**, *58*, 9287–9295. c) Lee, H.; Fischer, M.; Shoichet, B. K.; Liu, S. Y. *J. Am. Chem. Soc.* **2016**, *138*, 12021–12024.

¹⁸⁸ a) Burford, R. J.; Li, B.; Vasiliu, M.; Dixon, D. A.; Liu, S.-Y. *Angew. Chem., Int. Ed.* **2015**, *54*, 7823–7827. b) Edel, K.; Yang, X.; Ishibashi, J. S. A.; Lamm, A. N.; Maichle-Mossmeyer, C.; Giustra, Z. X.; Liu, S.-Y.; Bettinger, H. F. *Angew. Chem., Int. Ed.* **2018**, *57*, 5296–5300. c) Giustra, Z. X.; Yang, X.; Chen, M.; Bettinger, H. F.; Liu, S.-Y. *Angew. Chem., Int. Ed.* **2019**, *58*, 18918–18922.

adduct,¹⁸⁹ which is more electrophilic toward nucleophilic attack by TMSCHN₂ to generate the target compound **1** with concomitant release of TMSOTf (Scheme 1.51, top). It is worth noting that the outcome of this process contrasts with the reaction observed between TMSCHN₂ and other B–X-containing compounds, where insertion chemistry with elimination of N₂ and retention of the TMS group is typically observed.¹⁹⁰ I would like to acknowledge Dr. Raimon Puig de la Bellacosa for the discovery of compound **1**.

Diazomethyl-1,2-azaborine **1** is the BN isosteric analogue of phenyldiazomethane; thus comparisons (Scheme 1.51, bottom) are warranted: (1) Stability: We determined that diazomethyl-1,2-azaborine **1** is a stable oil. When stored at room temperature as a neat compound, no decomposition of **1** has been observed for over a month. In stark contrast, phenyldiazomethane is an unstable and potentially explosive liquid that decomposes readily at room temperature.¹⁹¹ (2) IR: The presence of the diazo functional group in **1** is indicated by an intense band at $\nu=2062\text{ cm}^{-1}$ for the asymmetric CN₂ stretching vibration. In comparison, the CN₂ vibration for phenyldiazomethane¹⁹² is at 2053 cm^{-1} . The higher CN₂ vibrational frequency observed for **1** in comparison to phenyldiazomethane is consistent with some additional stabilization of the negative charge at the CN₂ carbon position¹⁹³ as three-coordinate boron has been demonstrated to stabilize anions at adjacent carbon centers.

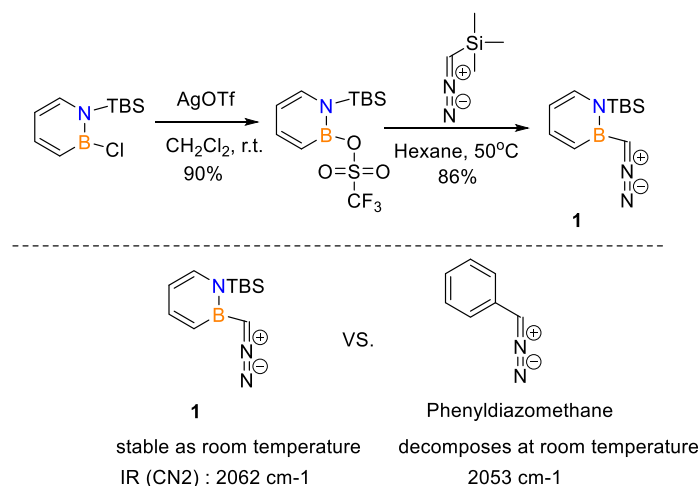
¹⁸⁹ a) Marwitz, A. J. V.; Jenkins, J. T.; Zakharov, L. N.; Liu, S.-Y. *Int. Ed.* **2010**, *49*, 7444–7447. b) Marwitz, A. J. V.; Jenkins, J. T.; Zakharov, L. N.; Liu, S.-Y. *Organometallics* **2011**, *30*, 52–54.

¹⁹⁰ a) Li, H.; Zhang, Y.; Wang, J. B. *Synthesis* **2013**, *45*, 3090–3098. b) Buynak, J. D.; Geng, B. *Organometallics* **1995**, *14*, 3112–3115. c) Burgos, C. H.; Canales, E.; Matos, K.; Soderquist, J. A. *J. Am. Chem. Soc.* **2005**, *127*, 8044–8049. d) Wommacka, A. J.; Kingsbury, J. S. *Tetrahedron Lett.* **2014**, *55*, 3163–3166. e) Cuenca, A. B.; Cid, J.; García-López, D.; Carbó, J. J.; Fernández, E. *Org. Biomol. Chem.* **2015**, *13*, 9659–9664. f) La Cascia, E.; Cuenca, A. B.; Fernandez, E. *Chem. - Eur. J.* **2016**, *22*, 18737–18741. g) Civit, M. G.; Royes, J.; Vogels, C. M.; Westcott, S. A.; Cuenca, A. B.; Fernandez, E. *Org. Lett.* **2016**, *18*, 3830–3833. h) Trofimova, A.; LaFortune, J. H. W.; Qu, Z.-W.; Westcott, S. A.; Stephan, D. W. *Chem. Commun.* **2019**, *55*, 12100–12103. Bartholome, T. A.; Bluer, K. R.; Martin, C. D. *Dalton Trans.* **2019**, *48*, 6319–6322.

¹⁹¹ a) Creary, X. Tosylhydrazone Salt Pyrolyses: Phenyldiazomethanes. *Org. Synth.* **1986**, *64*, 207. b) Sammakia, T. In *Encyclopedia of Reagents for Organic Synthesis*; Wiley, 2001. c) Green, S. P.; Wheelhouse, K. M.; Payne, A. D.; Hallett, J. P.; Miller, P. W.; Bull, J. A. *Org. Process Res. Dev.* **2020**, *24*, 67–84.

¹⁹² Yates, P.; Shapiro, B. L. *J. Am. Chem. Soc.* **1957**, *79*, 5756–5760.

¹⁹³ Hong, K.; Liu, X.; Morken, J. P. *J. Am. Chem. Soc.* **2014**, *136*, 10581–10584.



Scheme 1.51. Synthesis and comparative characterization of diazomethyl-1,2-azaborine **1**.

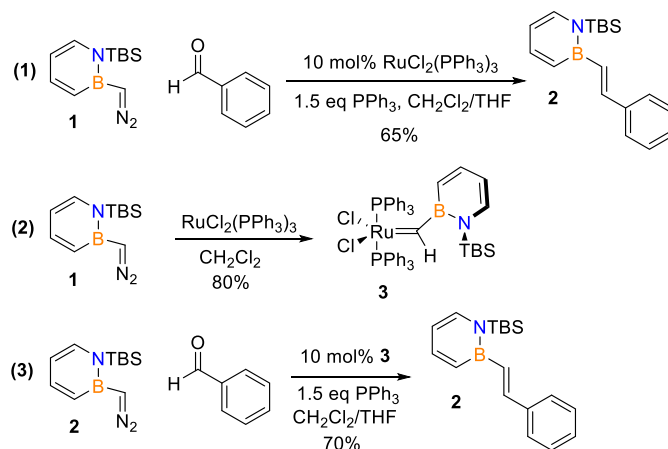
1.5.2 Diazomethyl-1,2-azaborine as a new versatile 1,2-azaborine building blocks

Undaunted by the lack of precedent of synthetic applications of α -boryl diazo compounds, we investigated the reaction chemistry of diazomethyl-1,2-azaborine **1** in the context of diversity-oriented synthesis¹⁹⁴ using **1** as a universal building block. The first reaction we examined is the catalytic cross-metathesis of a diazo compound and a carbonyl to form an alkene.¹⁹⁵ In the presence of $\text{Cl}_2\text{Ru}(\text{PPh}_3)_3$ as the catalyst, diazo compound **1** undergoes metathesis with benzaldehyde to furnish BN stilbene derivative **2** with PPh_3 as the stoichiometric reductant (Scheme 1.52, eq 1).¹⁹⁶ We were able to isolate the corresponding Ru- α -borylalkylidene complex **3** (Scheme 1.52, eq 2) and demonstrate its chemical competency as a catalyst for the transformation (Scheme 1.52, eq 3). There are two possible mechanisms for this reaction as depicted in Scheme 1.26, and further mechanistic experiments will be required to distinguish mechanism A from B for this metathesis reaction.

¹⁹⁴ McConnell, C. R.; Liu, S. Y. *Chem. Soc. Rev.* **2019**, *48*, 3436–3453.

¹⁹⁵ Fujimura, O.; Honma, T. *Tetrahedron Lett.* **1998**, *39*, 625–626.

¹⁹⁶ a) Lu, X.; Fang, H.; Ni, Z. *J. Organomet. Chem.* **1989**, *373*, 77–84. b) Cheng, G. L.; Mirafzal, G. A.; Woo, L. K. *Organometallics* **2003**, *22*, 1468–1474. c) Lebel, H.; Paquet, V. *J. Am. Chem. Soc.* **2004**, *126*, 320–328.



Scheme 1.52. Ru-Catalyzed carbonyl olefination with diazomethyl-1,2-azaborine.

Gratifyingly, we were able to grow single crystals of complex **3** from a pentane/dichloromethane solution that are suitable for X-ray diffraction analysis. To the best of our knowledge, complex **3** is the first isolated Ru- α -borylalkylidene complex.^{197, 198} Not many *trans*-bistriphenylphosphine dichlororuthenium alkylidene complexes have been crystallographically characterized, and we were unfortunately unable to obtain the structure of the corresponding carbonaceous Ru-benzylidene complex for direct comparison due to its facile decomposition in solution¹⁹⁹. Instead, we used the reported Cl₂(PPh₃)₂Ru-vinylcarbene **4** as the reference compound.²⁰⁰ While most structural parameters are quite similar between **3** and **4**, we note a few features for the Ru- α -borylalkylidene **3** that are distinct from the reference complex **4** (Figure 1.13, table): (1) The two Ru–P bonds in **3** (2.484 Å, 2.326 Å; $\Delta = 0.158$ Å) are significantly more nonsymmetrical than the ones observed in **4** (2.400 Å, 2.372 Å; $\Delta = 0.028$ Å). (2) The \angle Ru–C1–B angle (124.1°) in **3** is smaller than the corresponding angle in **4** (131.2°). (3) The Ru–C1–B plane in **3** is somewhat perpendicular to the plane of the BN-heterocyclic ring (\angle Ru–C1–B–N = 135.8(9)°). This is in contrast to compound **4**, where the alkenyl group is more aligned to conjugate with the Ru alkylidene (\angle Ru–C1–C–C = –158.6(4)°).

¹⁹⁷ an example of a Ru-methylidene complex: Batsanov, A. S.; Cabeza, J. A.; Crestani, M. G.; Fructos, M. R.; Garcia-Alvarez, P.; Gille, M.; Lin, Z.; Marder, T. B. *Angew. Chem., Int. Ed.* **2016**, *55*, 4707–4710.

¹⁹⁸ select examples of metal- α -borylalkylidene complexes: a) Townsend, E. M.; Kilyanek, S. M.; Schrock, R. R.; Muller, P.; Smith, S. J.; Hoveyda, A. H. *Organometallics* **2013**, *32*, 4612–4617. b) Bailey, B. C.; Fout, A. R.; Fan, H.; Tomaszewski, J.; Huffman, J. C.; Mindiola, D. J. *Angew. Chem., Int. Ed.* **2007**, *46*, 8246–8249. c) Braunschweig, H.; Celik, M. A.; Dewhurst, R. D.; Kachel, S.; Wennemann, B. *Angew. Chem., Int. Ed.* **2016**, *55*, 5076–5080.

¹⁹⁹ Schwab, P.; France, M. B.; Ziller, J. W.; Grubbs, R. H. *Angew. Chem., Int. Ed. Engl.* **1995**, *34*, 2039–2041.

²⁰⁰ Volland, M. A. O.; Rominger, F.; Eisentrager, F.; Hofmann, P. *J. Organomet. Chem.* **2002**, *641*, 220–226.

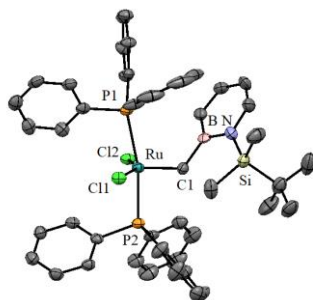


Figure 1.12. X-ray structure of Ru- α -borylalkylidene complex **3**.

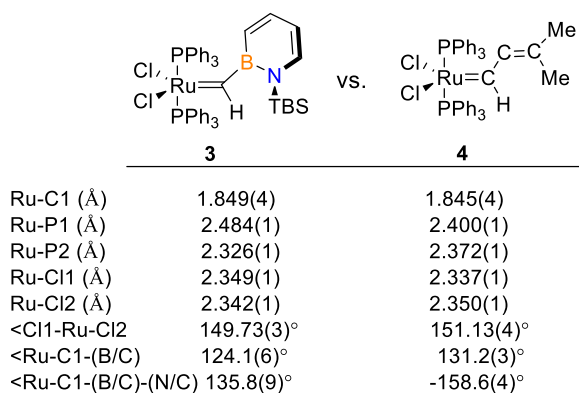
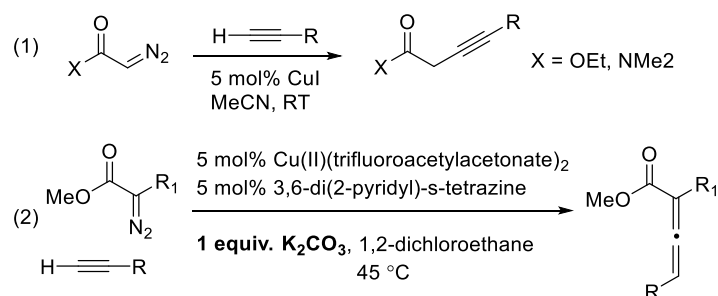


Figure 1.13. Ru- α -borylalkylidene intermediate comparison.

Next, we investigated the Cu-catalyzed C–H activation of terminal alkynes in the presence of the α -boryl diazo compound **1**. Fu et al. reported a simple CuI-catalyzed procedure that couples terminal alkynes with diazoesters and diazoamides to furnish 3-alkynoates (Scheme 1.53, eq 1).²⁰¹ In a number of cases, the corresponding allene isomer was observed as a minor byproduct. Fox and co-workers subsequently optimized the conditions for allene formation for α -alkyl- α -diazoesters with terminal alkynes and determined that the initially formed alkynoate intermediates isomerize to the allenoate products in the presence of the stoichiometrically employed K_2CO_3 base (Scheme 1.53, eq 2).²⁰² Thus, it appears that the alkynoate species is the kinetically preferred product under Cu catalysis that subsequently can isomerize to the allenoates in the presence of a base.

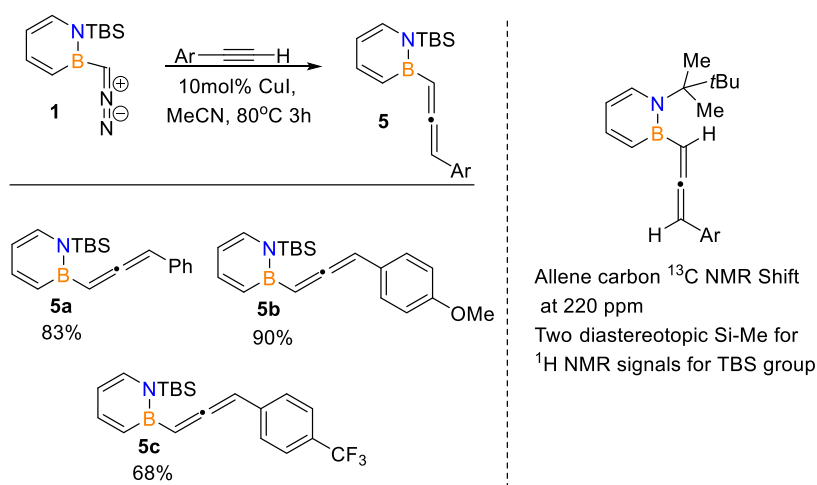
²⁰¹ Suarez, A.; Fu, G. C. *Angew. Chem., Int. Ed.* **2004**, *43*, 3580–3582

²⁰² Hassink, M.; Liu, X.; Fox, J. M. *Org. Lett.* **2011**, *13*, 2388–91.



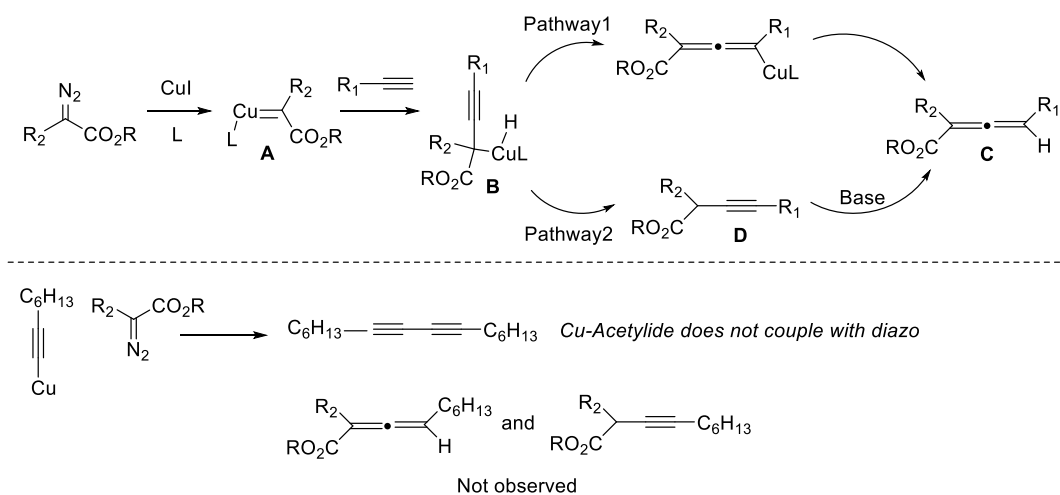
Scheme 1.53. CuI-catalyzed C-H insertion with terminal alkynes reported by Fu and Fox.

Surprisingly, when we adapted the protocol developed by Fu and treated diazomethyl-1,2-azaborine **1** with terminal alkynes in the presence of catalytic amounts of CuI in MeCN, and in the *absence* of any base, the corresponding allene **5** is formed exclusively instead of the expected internal alkyne (Scheme 1.54). The formation of allene **5** is indicated by the two diastereotopic Si–Me signals of the *N-tert*-butyldimethylsilyl (TBS) group in the ¹H NMR, which is consistent with the existence of an axially chiral stereogenic unit. The distinct product selectivity of CuI-catalyzed alkyne–diazo coupling for α -boryl diazo compound **1** again highlights its unique electronic structure that is likely underlying the observed selectivity. The detailed reaction mechanism of the formation of allene **5** is presently unknown. We speculate that the anion-stabilizing effect of boron might increase the acidity of the propargylic C–H protons to potentially allow for a spontaneous isomerization to the allene structure.



Scheme 1.54. Cu-catalyzed C-H activation of terminal alkynes with diazomethyl-1,2-azaborine.

In the literature, there are two possible pathways for CuI-catalyzed coupling of terminal alkynes with diazo compounds to generate the corresponding allenoate product (Scheme 1.55, top).²⁰³ The mechanism starts with the low valent Cu that reacts with an α -diazoester to give carbenoid **A**. The carbenoid then undergoes C–H activation to generate organocopper intermediate **B**. Pathway 1 involves an isomerization of the organocopper intermediate and a protonation process to give allenoates **C**. In Pathway 2, the intermediate **B** will undergo reductive elimination to form the alkynoate precursor **D** which then isomerizes to the allenoate product **C**.²⁰⁴ A mechanistic experiment by Fox group^{203a} suggests that this reaction may not involve initial formation of a Cu(I)-acetylide intermediate (see Scheme 1.55, bottom). Copper acetylide failed to undergo coupling reaction with diazo ester and instead the alkyne was converted to hexadeca-7,9-diyne. In the case of diazomethyl-1,2-azaborine with terminal alkyne, the allene was generated without any external base, thus it may indicate the reaction undergoes by Pathway 1, however, further mechanistic experiments should be conducted.

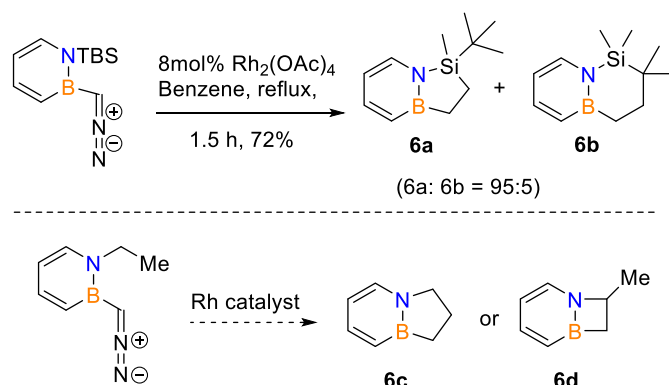


Scheme 1.55. Plausible mechanisms for C–H bond insertion of diazo compounds into terminal alkynes.

²⁰³ a) Hassink, M.; Liu, X.; Fox, J. M. *Org. Lett.* **2011**, *13*, 2388-2391. b) Tang, Y.; Chen, Q.; Liu, X.; Wang, G.; Lin, L.; Feng, X. *Angew. Chem.* **2015**, *127*, 9648-9652.

²⁰⁴ Wadsworth, W. S.; Emmons, W. D. *J. Am. Chem. Soc.* **1961**, *83*, 1733-1738.

We also note that in the absence of a viable external C–H source and in the presence of the $\text{Rh}_2(\text{OAc})_4$ catalyst an intramolecular C–H insertion occurs at the methyl or *t*-Bu group (on the *N*-TBS moiety), respectively, yielding the corresponding bicyclic 1,2-azaborine compounds **6a** and **6b** with a strong preference for the formation of the five-membered **6a** (Scheme 1.56, top).²⁰⁵ This reaction can be further explored for different substituents on the N of the azaborine ring, for instance, as shown in Scheme 1.56 (bottom). Ethyl-substituted nitrogen diazo azaborine can potentially serve as a precursor for different-sized ring-fused product **6c** and **6d**.



Scheme 1.56. Intramolecular C–H insertion with $\text{Rh}_2(\text{OAc})_4$.

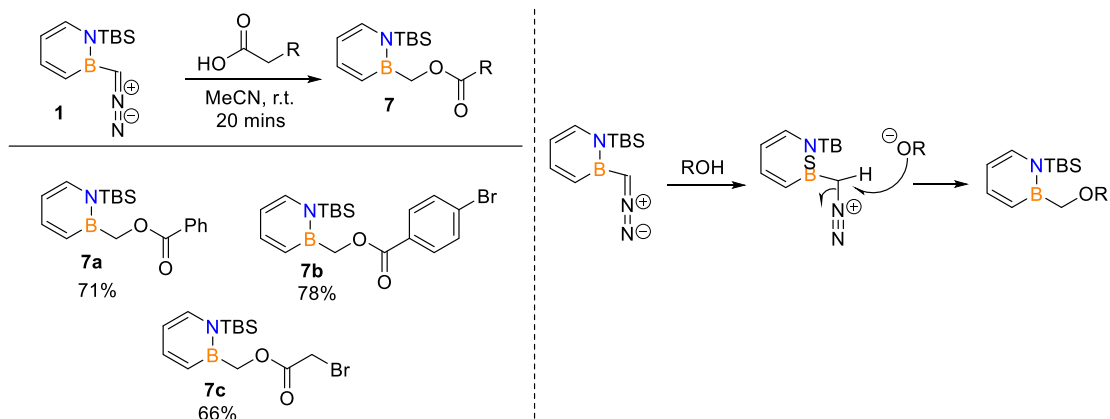
In addition to C–H activation chemistry, diazo compounds are known to engage in uncatalyzed O–H insertion chemistry.²⁰⁶ This reactivity feature has been utilized in chemical biology applications, where stabilized diazo compounds have been developed to label proteins and nucleic acids via *O*-alkylation.²⁰⁷ For an α -boryl diazo compound the high oxophilicity of boron may present an additional challenge to successfully *O*-alkylate suitable oxygen-based nucleophiles such as carboxylic acids. Gratifyingly, we determined that diazomethyl-1,2-azaborine **1** reacts quite rapidly at room temperature with carboxylic acids to form esters in acetonitrile in the absence of a catalyst. As can be seen from Scheme 1.56, aryl and alkyl carboxylic acids are suitable substrates. An electrophilic alkyl bromide functional group is also tolerated (Scheme 1.57, entry **7c**). The reaction mechanism (Scheme 1.57, right) was

²⁰⁵ Doyle, M. P.; Westrum, L. J.; Wolthuis, W. N. E.; See, M. M.; Boone, W. P.; Bagheri, V.; Pearson, M. M. *J. Am. Chem. Soc.* **1993**, *115*, 958–964.

²⁰⁶ Kuhnle, E.; Laffan, D. D.; Lloyd-Jones, G. C.; Martinez Del Campo, T.; Shepperson, I. R.; Slaughter, J. L. *Angew. Chem., Int. Ed.* **2007**, *46*, 7075–7078.

²⁰⁷ a) Mix, K. A.; Aronoff, M. R.; Raines, R. T. *ACS Chem. Biol.* **2016**, *11*, 3233–3244. b) Mix, K. A.; Raines, R. T. *Org. Lett.* **2015**, *17*, 2359–2361.

considered to follow the proposed stepwise H-X insertion mechanism as proposed in Scheme 1.34. The first step is the protonation of diazo carbon to form a diazonium species then followed by subsequent nucleophilic attack by alkoxide to kick off the nitrogen gas and yield the final product.



Scheme 1.57. O-Alkylation of carboxylic acids with diazomethyl-1,2-azaborine.

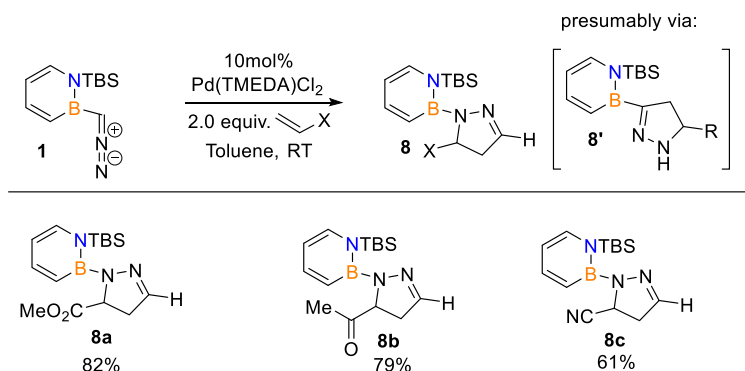
To explore additional reactivity types that diazo compounds can engage in, we investigated the [3+2] cycloaddition of diazomethyl-1,2-azaborine **1** with alkenes. A diazo compound is typically considered electron-rich and thus reacts as a nucleophile in normal-electron-demand cycloadditions with electron-deficient dipolarophiles.²⁰⁸ We are pleased to find that diazomethyl-1,2-azaborine **1** undergoes regioselective [3+2] cycloaddition reactions with α,β -unsaturated esters, ketones, and nitriles in the presence of a Pd catalyst to presumably initially form intermediates **8'**, which then subsequently undergoes a formal 1,3-boryl shift to furnish adducts **8** (Scheme 1.58). This reaction mechanism is assumed to be a concerted 1,3-dipolar cycloaddition as described in Section 1.3.2, and it also seems to follow the frontier orbital interaction rules proposed by Sustmann.⁷¹⁻⁷³

In contrast, phenyldiazomethane preferentially forms cyclopropane compounds with elimination of N_2 . As an additional comparison, while phenyldiazomethane reacts relatively cleanly with styrene to furnish 1,2-diphenylcyclopropane in the presence of cobalt(II) tetraphenylporphyrin,²⁰⁹ diazomethyl-1,2-

²⁰⁸ a) Jangra, H.; Chen, Q.; Fuks, E.; Zenz, I.; Mayer, P.; Ofial, A. R.; Zipse, H.; Mayr, H. *J. Am. Chem. Soc.* **2018**, *140*, 16758–16772. b) Gold, B.; Aronoff, M. R.; Raines, R. T. *Org. Lett.* **2016**, *18*, 4466–4469.

²⁰⁹ Wang, Y.; Wen, X.; Cui, X.; Wojtas, L.; Zhang, X. P. *J. Am. Chem. Soc.* **2017**, *139*, 1049–1052.

azaborine **1** remains mostly unreactive, producing minor amounts of the intramolecular C–H activation product **6a**.



Scheme 1.58. [3+2] Cycloaddition reaction with diazomethyl-1,2-azaborine.

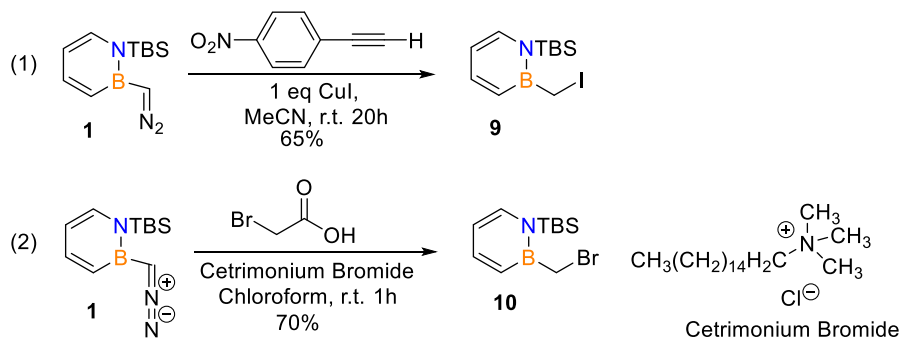
Finally, we envisioned that diazomethyl-1,2-azaborine **1** can serve as a precursor to the halomethyl building blocks **9** and **10** (Scheme 1.59). Benzyl halides are versatile intermediates in diversity-oriented synthesis in medicinal chemistry,²¹⁰ and compounds **9** and **10** represent the direct BN isosteres of benzylic halides. While examples of halomethyl BN naphthalenes have been reported, to the best of our knowledge, such a building block for the monocyclic 1,2-azaborine heterocycle has not been prepared. Importantly, the annulation method involving potassium chloromethyltrifluoroborate and 2-aminostyrene to yield the chloromethyl BN naphthalene²¹¹ is not applicable to the monocyclic benzene-type BN heterocycle. We envisioned that similar to how *O*-alkylation proceeds (See Scheme 1.57) with protonation of the α -boryl carbon followed by nucleophilic attack of the oxygen nucleophile, treatment of **1** with a suitably matched proton/halide source should yield the corresponding halomethyl 1,2-azaborines **9** and **10**.²¹² After screening a number of conditions (Table 1.1 and 1.2), we determined that 1-ethynyl-4-nitrobenzene as the proton source in combination with CuI as the iodide nucleophile works well for the iodination of diazomethyl-1,2-azaborine **1** (Scheme 1.59, eq 1). Similarly, the combination of

²¹⁰ a) Davies, K. A.; Abel, R. C.; Wulff, J. E. *J. Org. Chem.* **2009**, *74*, 3997–4000. b) Chen, X.; Zhou, L.; Li, Y.; Xie, T.; Zhou, S. *J. Org. Chem.* **2014**, *79*, 230–239

²¹¹ Molander, G. A.; Wisniewski, S. R.; Amani, J. *Org. Lett.* **2014**, *16*, 5636–5639.

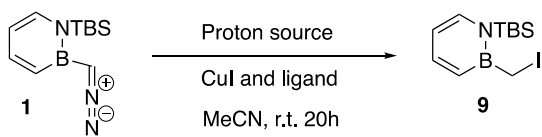
²¹² For an overview of halo-functionalization of diazo compounds, see: Khanal, H. D.; Thombal, R. S.; Maezono, S. M. B.; Lee, Y. R. *Adv. Synth. Catal.* **2018**, *360*, 3185–3212.

bromoacetic acid as the proton source and cetrimonium (hexadecyltrimethylammonium) bromide is suitable for converting **1** to the bromomethyl 1,2-azaborine **10** (Scheme 1.59, eq 2).²¹³



Scheme 1.59. Synthesis of halomethyl 1,2-azaborine building blocks.

Tables 1.1 Survey of reaction conditions for formation of **9**



Entry	Reagent	9 Yield (NMR)
Proton source (with CuI) ^a		
1	Binol	N/A
2	Taddol	N/A
3	HDMS	N/A
4	HCl	N/A
Ligand screening (with CuI) ^b		
1	BINAP	N/A
2	tBuXphos	N/A
3	tris(pentafluorophenyl) phosphine	50%
Alkyne screening (as additional proton source) ^c		
1	4-ethynylbenzonitrile	N/A
2	1-ethynyl-4-nitrobenzene	66-80%
3	1-ethynyl-4-methoxy-benzene	<10%
4	4-ethynyl-a,a,a-trifluorotoluene	56%
5	methyl 4-ethylbenzoate	39%

^a CuI, no ligand, MeCN, RT, 20 h

^b CuI, ethynylbenzene, ligand, MeCN, RT, 20 h

^c CuI, MeCN, RT, 20 h

²¹³ Treatment of diazomethyl-1,2-azaborine **1** with anhydrous HCl (as an HX model) in CHCl₃ did not produce the halogenated products in substantial amounts.

Table 1.2 Survey of reaction conditions for formation of **10**

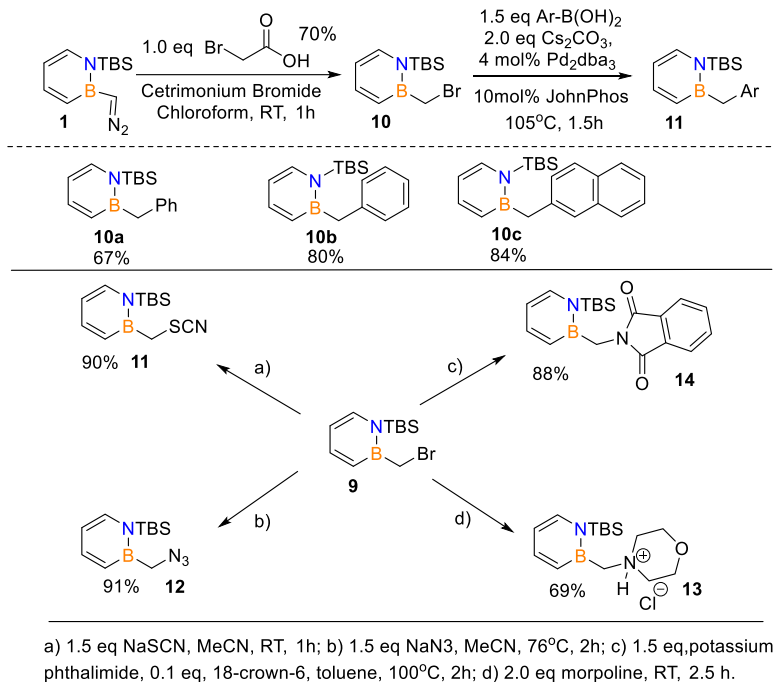
Entry	Reagents	10 Yield (isolated yield)
Bromide source (with bromoacetic acid)		
1	CuBr	N/A
2	CuBr ₂	N/A
3	NaBr	N/A
4	Cetrimonium bromide	70%
Proton source (with cetrimonium bromide)		
1	acetic acid	50%
2	HCl	N/A

N/A: no desired product was observed.

We chose bromomethyl 1,2-azaborine **10** to demonstrate the ability of halomethyl 1,2-azaborines to serve as an electrophilic building block in a variety of coupling and substitution reactions²¹⁴. As can be seen from Scheme 1.62, compound **10** can engage in Suzuki–Miyaura cross-coupling reaction to produce BN diarylmethanes **11**. The cross-coupling reaction conditions we screened (See Experimental Section) includes ligands for Pd(0) catalyst and different reaction temperature and solvents. The optimized condition we found is 4 mol% Pd₂dba₃ catalysts with 10 mol% JohnPhos ligands in the presence of Cs₂CO₃ as base at 105 °C for 1.5 hours.

Compound **10** also reacts with a number of nucleophiles such as thiocyanate, azide, amine, and phthalimide anion to furnish the corresponding adducts **11–14** in moderate to good yields, further demonstrating the diversity of compounds that can be accessed with diazomethyl-1,2-azaborine **1** as the universal precursor (Scheme 1.60).

²¹⁴ Molander, G. A.; Amani, J.; Wisniewski, S. R. *Org. Lett.* **2014**, *16*, 6024–6027.



Scheme 1.60. Bromomethyl 1,2-azaborine as a versatile electrophilic building block.

Conclusion

We synthesized the first α -boryl diazo compound that is capable of engaging in classic synthetic organic diazo reaction chemistry, including C–H activation, O–H activation, [3+2] cycloaddition, halogenation, and Ru-catalyzed carbonyl olefination. Furthermore, we showed that diazomethyl-1,2-azaborine **1**, a BN isostere of phenyldiazomethane, is a stable compound and that its corresponding Ru carbene complex **3** exhibits bonding features that are distinct from an analogous Ru-alkylidene complex. Overall, we believe that diazomethyl-1,2-azaborine **1** as a new member of the α -boryldiazo compound family and as a remarkably versatile 1,2-azaborine building block will advance both the basic science of diazo chemistry and the multifaceted chemistry of 1,2-azaborine heterocycles.

1.5.3 Experimental section

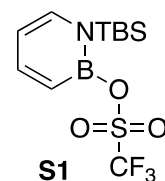
General

^1H , ^{13}C , and ^{19}F spectra were recorded on Varian 400, 500 or 600 MHz spectrometers, and 11 B spectra were on an Inova 500 MHz spectrometer at ambient temperature. ^1H NMR spectra were reported with the

solvent resonance as internal standard. ^{13}C NMR spectra were reported with the solvent resonance as internal standard. ^{11}B NMR spectra were reported with $\text{BF}_3 \cdot \text{Et}_2\text{O}$ (δ 0 ppm) as the external reference. ^{31}P NMR spectra were reported with H_3PO_4 (δ 0 ppm) as the external reference. IR spectra were recorded on a Bruker FTIP Alpha (ATR mode) spectrometer. High-resolution mass spectroscopy data were obtained at the Mass Spectroscopy Facilities at Chemistry Department of Boston College with DART ion source in positive ion mode. All oxygen- and moisture-sensitive manipulations were carried out under N_2 atmosphere with standard Schlenk techniques or in N_2 glovebox. Hexanes were purified by distillation prior to use as the eluent in column chromatography. Solvents used under N_2 atmosphere (pentane, THF, Et_2O , toluene, and CH_2Cl_2) were purified by passing through a neutral alumina column under nitrogen. N-TBS-B-Cl-1,2-azaborine was prepared according to literature procedures.²¹⁵ AgOTf was purchased from Strem and used as received. All other chemicals and solvents were purchased and used as received.

Synthesis of Diazomethyl-1,2-Azaborine 1

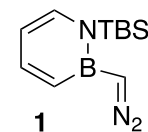
Compound S1. In a nitrogen glovebox, AgOTf (4.52 g, 17.5 mmol) was added in portions to a stirring solution of N-TBS-B-Cl-1,2-azaborine¹ (4.00 g, 17.5 mmol) in CH_2Cl_2 (150 mL). The reaction mixture was then allowed to stir at room temperature for 4h. At the conclusion of the reaction, the mixture was passed through an acrodisc. The filtrate was concentrated under reduced pressure, and the resulting oil was taken up in pentane to further remove insoluble AgCl impurities. The mixture was passed through an acrodisc with copious washing with pentane. The combined filtrates were concentrated *in vacuo* and the resulting crude material was purified by distillation (bp: 55-60 °C at 220 mTorr) to furnish **S1** as a colorless liquid in an average of 90% yield (run 1: 92%, run 2: 87%).



^1H NMR (400 MHz, CDCl_3): δ 7.81 (dd, $J = 11.8, 6.4$, 1H), 7.26 (d, $J = 6.7$ Hz, 1H), 6.71 (d, $J = 11.6$ Hz, 1H), 6.42 (dd, $J = 6.7, 6.4$ Hz, 1H), 0.93 (s, 9H), 0.51 (s, 6H). ^{13}C NMR (100 MHz, CDCl_3): δ 149.3, 137.7, 119 (br), 118.5 (q, $^1J_{\text{CF}} = 479$ Hz), 111.9, 25.8, 18.5, -3.13; ^{19}F NMR (376MHz, CD_2Cl_2): δ -77.5; ^{11}B NMR (128 MHz, CDCl_3): δ 30.3; FTIR (thin film): $\tilde{\nu} = 2954\text{-}2862, 1604, 1515, 1393, 1200, 1151, 1131, 1077, 937, 922, 808, 792$; HRMS (DART) calcd. for $\text{C}_{11}\text{H}_{19}\text{BF}_3\text{NO}_3\text{Si}$ $[\text{M}+\text{H}^+]$: 341.23859, found 341.23647.

Procedure for synthesis of diazomethyl-1,2-azaborine 1.

In a nitrogen glovebox, a 10mL round bottom flask was charged with diazomethyl(trimethyl)silane (5.86ml, 2M in hexane) and compound **S1** (2.00g, 5.86 mmol). The reaction mixture was allowed to stir at room temperature for 5 minutes. Then the flask was transferred to a Schlenk line, and the mixture was heated at 50°C for 3 hours. At the conclusion of the reaction, the reaction mixture was concentrated *in vacuo*, and the reaction crude material was purified by distillation (bp: 85°C at 250mTorr) to furnish **1** as a pale



²¹⁵ Marwitz, A. J. V.; Matus, M. H.; Zakharov, L. N.; Dixon, D. A.; Liu, S.-Y. *Angew. Chem. Int. Ed.* **2009**, *48*, 973-977.

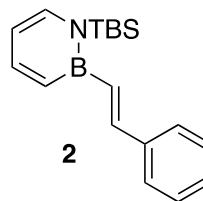
yellow oil in an average yield of 86% (run1: 83%, run2: 89%).

^1H NMR (600 MHz, CDCl_3): δ 7.40 (dd, $J = 11.2, 6.1$, Hz, 1H), 7.18 (d, $J = 6.9$ Hz, 1H), 6.51 (d, $J = 11.3$ Hz, 1H), 6.08 (dd, $J = 6.9, 6.2$ Hz, 1H), 3.70 (s, 1H), 0.92 (s, 9H), 0.43 (s, 6H). ^{13}C NMR (151 MHz, CDCl_3): δ 142.0, 138.6, 126 (br), 109.7, 34(br), 26.6, 19.4, -2.1; ^{11}B NMR (160 MHz, CDCl_3): δ 34.2; FTIR (thin film): $\tilde{\nu} = 2955, 2930, 2858, 2062, 1608, 1505, 1471, 1456, 1394, 1363, 1325, 1271, 1262, 1143, 1060, 982$; HRMS (DART) calcd. for $\text{C}_{11}\text{H}_{21}\text{BN}_3\text{Si}$ [$\text{M}+\text{H}^+$]: 234.15923, 234.15920 found.

Procedure for synthesis of compound 2

In a nitrogen glovebox, a 10 ml vial containing a stir bar was charged with benzaldehyde (20.0 mg, 188 μmol), $[\text{RuCl}_2(\text{PPh}_3)_3]$ (18.0 mg, 18.8 μmol) and PPh_3 (74.1 mg, 283 μmol) in THF (600 μL). The vial was transferred to the Schlenk line, and a solution of compound **1** (43.9 mg, 188 μmol) in CH_2Cl_2 (0.6 mL) was added dropwise to the reaction mixture at 50 $^\circ\text{C}$ using a syringe pump over a period of 4 hours. At the conclusion of the dropwise addition, the reaction mixture was allowed to stir for another 2 hours at 50 $^\circ\text{C}$.

At the conclusion of the reaction, the solvent was removed *in vacuo*. The resulting crude material was purified by silica gel chromatography using a mixture of CH_2Cl_2 : pentane (2:100) as the eluent to furnish **2** as a white solid in 64% average yield (run1: 68%, run2: 61%).



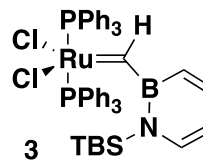
^1H NMR (400 MHz, CD_2Cl_2): δ 7.60 (dd, $J = 11.2, 6.3$ Hz, 1H), 7.55-7.48 (m, 2H), 7.36 (ddd, $J = 8.0, 6.5, 1.2$ Hz, 3H), 7.31-7.21 (m, 2H), 7.10-6.94 (m, 2H), 6.32 (dd, $J = 7.3, 5.8$ Hz, 1H), 0.98 (s, 9H), 0.54 (s, 6H). ^{13}C NMR (101 MHz, CD_2Cl_2): δ 143.1, 142.5, 139.1, 138.5, 128.5, 127.6, 126.4, 111.5, 26.2, 18.9, -1.73 (signal for two carbons next to boron not observed); ^{11}B NMR (160 MHz, CD_2Cl_2): δ 37.3; FTIR (thin film): $\tilde{\nu} = 3064, 3023, 2955, 2929, 2885, 2857, 1604, 1504, 1393, 1256, 1150, 1067, 987, 809$; HRMS (DART) calcd. for $\text{C}_{18}\text{H}_{27}\text{BNSi}$ [$\text{M}+\text{H}^+$]: 296.20003, 296.19987 found.

Procedure for Scheme 1.52, eq 3

In a nitrogen atmosphere glovebox, benzaldehyde (20.0 mg, 188 μmol), complex **3** (17.0 mg, 18.8 μmol) and PPh_3 (74.1 mg, 283 μmol) in THF (600 μL) was added to a 10ml vial, after mixing the vial was taken out of the glovebox and connected to the nitrogen line. A solution of compound **1** (43.9 mg, 188 μmol) in CH_2Cl_2 (0.6 mL) was added drop wise at 50 $^\circ\text{C}$ using a syringe pump over a period of 4hrs. The reaction mixture was stirred for another 2 hours at 50 $^\circ\text{C}$ and then cooled to 25 $^\circ\text{C}$. At the conclusion of the reaction, the solvent was removed *in vacuo* and crude material was purified on silica gel chromatography using a mixture of CH_2Cl_2 : pentane (ratio=2:100) as the eluent inside a dry box. Isolated as white solid in 70% yield.

Procedure for the synthesis of Ru- α -borylalkylidene complex 3.

In a nitrogen glovebox, a 20mL vial containing a stir bar was charged with $\text{RuCl}_2[\text{PPh}_3]_3$ (822 mg, 0.858mmol) in 8.0ml CH_2Cl_2 . The vial was transferred to a Schlenk line, and the solution was allowed to cool to -78C for 5mins. A solution of compound **1** (240mg, 1.03mmol) in 2.0 ml CH_2Cl_2 was added in a dropwise fashion at -78C. After the cool-bath had been removed, the mixture was allowed to stirred for 5 mins. At the conclusion of the reaction, the brown-red solution was concentrated under reduced pressure to yield a crude sticky solid. Upon the addition of 1ml of CH_2Cl_2 and 8ml pentane, a brown solid was precipitated, which was separated from the brown-red mother liquor. This procedure was repeated until the mother liquor was almost colorless. After drying in vacuo, a brown reddish solid **3** was recovered in a yield range from 40-80% (run1: 87%, run2: 48%).



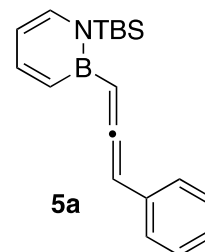
^1H NMR (500 MHz, CDCl_3): δ 22.08 (s, 1H), 7.58 (s, 12H), 7.46-7.33 (m, 6H), 7.28 (m, 13H), 7.13 (d, $J = 6.6$ Hz, 1H), 6.79 (m, 1H), 6.21 (dd, $J = 6.6, 5.1$ Hz, 1H), 0.66 (s, 9H), -0.13 (s, 6H). ^{13}C NMR (126 MHz,

CDCl₃): δ 142.1, 136.3, 134.7, 131.2, 129.6, 127.8, 112.8, 26.1, 18.8, -4.41 (signal for two carbons next to boron not observed); ¹¹B NMR (160 MHz, CDCl₃): δ 38.8; ³¹P NMR (202 MHz, CDCl₃): δ = 23.4 (s, PPh₃). FTIR (thin film): $\tilde{\nu}$ = 3056, 2954, 2928, 2883, 2856, 1596, 1499, 1434, 1362, 1253, 1067, 821-789, 741, 692, 512; HRMS (DART) calcd. for C₄₇H₅₀NBSiRuCl₂P₂: 901.72, not found.

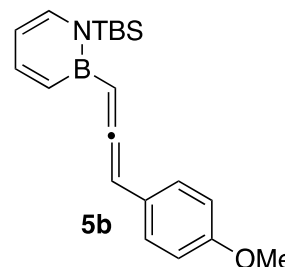
General Procedure for Synthesis of Allenes 5a-5c (Scheme 1.54)

The following procedure for the synthesis of allene **5b** is representative for the products Shown in Scheme 4, eq 6): In a nitrogen glove box, CuI (3.27 mg, 0.017 mmol) was added to a mixture of 4-methoxy-ethynylbenzene (48.9 μ l, 0.377 mmol) and compound 1 (80.0 mg, 0.343 mmol) in 1ml MeCN. The mixture was then allowed to stir at 80°C for 3h. At the conclusion of the reaction, the solvent was removed under reduced pressure. The resulting crude material was purified by silica gel column chromatography with ether:pentane (1:10) as the eluent inside a dry box.

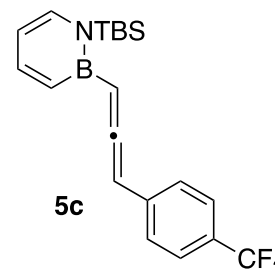
Allene **5a** was Isolated as colorless oil in an average of 83% yield (run1: 90%, run2: 76%). ¹H NMR (600 MHz, CD₂Cl₂): δ 7.52 (dd, J = 11.1, 6.3 Hz, 1H), 7.36 (d, J = 6.9 Hz, 1H), 7.33 (m, 4H), 7.18 (td, J = 6.5, 3.1 Hz, 1H), 6.90 (d, J = 11.0 Hz, 1H), 6.32 (dd, J = 6.4, 6.9 Hz, 1H), 6.15 (app. s, 2H), 1.01 (s, 9H), 0.60 (s, 3H), 0.58 (s, 3H). ¹³C NMR (151 MHz, CD₂Cl₂): δ 215.7, 143.4, 138.8, 135.4, 131(br), 128.9, 126.6, 126.5, 112.0, 92.0(br), 89.8, 26.6, 19.3, -1.44, -1.47; ¹¹B NMR (192 MHz, CD₂Cl₂): δ 36.1; FTIR (thin film): $\tilde{\nu}$ = 2954-2857, 1921, 1748, 1606, 1506, 1457, 1392, 1268, 1144, 986, 821, 811; HRMS (DART) calcd. for C₁₉H₂₇BNSi [M+H⁺]: 308.20003, found 308.20034.



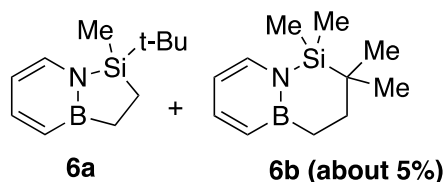
Allene **5b** was isolated as light yellow oil in 90% average yield. (run1: 90%, run2: 89%). ¹H NMR (500 MHz, CDCl₃): δ 7.49 (dd, J = 11.1, 6.3 Hz, 1H), 7.29 (d, J = 6.8 Hz, 1H), 7.22 (d, J = 8.5 Hz, 2H), 6.90 (d, J = 11.0, 1H), 6.85 (d, J = 8.7 Hz, 2H), 6.28 (dd, J = 6.8, 6.3 Hz, 1H), 6.10 (d, J = 6.5 Hz, 1H), 6.07 (d, J = 6.5 Hz, 1H), 3.80 (s, 3H), 0.99 (s, 9H), 0.56 (s, 3H), 0.54 (s, 3H). ¹³C NMR (125 MHz, CDCl₃): δ 215.4, 158.2, 142.9, 138.2, 130.5, 127.3, 127.1, 114.2, 111.7, 92.5, 89.0, 55.3, 26.5, 19.1, -1.59, -1.64; ¹¹B NMR (160 MHz, CDCl₃): δ 36.1; FTIR (thin film): $\tilde{\nu}$ = 2954-2931, 1921, 1739, 1718, 1607, 1507, 1456, 1393, 1248, 1144, 986, 833, 822; HRMS (DART) calcd. for C₂₀H₂₉BNOSi [M+H⁺]: 338.21060, found 338.21045.



Allene **5c** was isolated as an oil compound in 67% average yield (run1: 66%, run 2: 68%). ¹H NMR (600 MHz, CDCl₃): δ 7.54-7.51 (m, 3H), 7.39 (d, J = 8.0 Hz, 2H), 7.33 (d, J = 6.8 Hz, 1H), 6.88 (d, J = 11.1 Hz, 1H), 6.32 (dd, J = 6.8, 6.6 Hz, 1H), 6.17 (d, J = 6.7 Hz, 1H), 6.15 (d, J = 6.6 Hz, 1H), 1.00 (s, 9H), 0.58 (s, 3H), 0.56 (s, 3H). ¹³C NMR (125.8MHz, CDCl₃): δ 215.6, 143.3, 139.2, 138.4, 130.0(br), 127.7 (q, J = 32.3 Hz), 126.3, 125.5 (q, J = 3.9Hz), 124.5 (q, J = 271.7Hz), 112.0, 92.5(br), 89.0, 26.5, 19.1, -1.56, -1.62; ¹¹B NMR (160 MHz, CDCl₃): δ 36.0; FTIR (thin film): $\tilde{\nu}$ = 2955-2859, 1921, 1608, 1507, 1393, 1323, 1123, 1109, 1067, 842, 821, 810; HRMS (DART) calcd. for C₂₀H₂₆BNF₃Si [M+H⁺]: 376.18742, found 376.18770.



Synthesis of 6a (Scheme 1.55). In a nitrogen box, a 20ml vial containing a stir bar was charged with $\text{Rh}_2(\text{OAc})_4$ (9.10 mg, 0.021 mmol) and **1** (60.0 mg, 0.257 mmol) in 1.5ml MeCN. The vessel was transferred to the Schlenk line, and the reaction mixture was allowed to stir at 80°C for 90 minutes. At the conclusion of the reaction, volatiles were removed under reduced pressure. The resulting crude material was purified by silica gel chromatography using ether: pentane (1:100) as the eluent to yield the product as a colorless oil in an average of 72% yield (run1: 66%, run2: 76%).

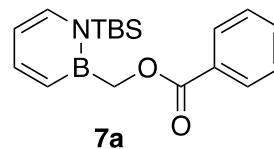


^1H NMR (600 MHz, CDCl_3): δ 7.55 (dd, $J = 11.2, 6.4$ Hz, 1H), 7.33 (d, $J = 6.2$ Hz, 1H), 6.68 (d, $J = 11.2$ Hz, 1H), 6.30 (dd, $J = 6.4, 6.1$ Hz, 1H), 1.58 (ddd, $J = 17.4, 10.5, 2.8$ Hz, 1H), 1.38 (ddd, $J = 17.6, 10.0, 7.8$ Hz, 1H), 1.06 (ddd, $J = 15.3, 10.0, 2.8$, 1H), 0.94 (s, 9H), 0.76 (ddd, $J = 15.3, 10.6, 7.9$ Hz, 1H), 0.37 (s, 3H). ^{13}C NMR (125 MHz, CDCl_3): δ 143.3, 136.0, 112.2, 25.9, 18.6, 5.40, -5.53 (signal for two carbons next to boron not observed); ^{11}B NMR (160 MHz, CDCl_3): δ 42.8; FTIR (thin film): $\tilde{\nu} = 2953, 2927, 2857, 1739, 1718, 1601, 1499, 1418, 1363, 1278, 1083, 1004, 825, 738$; HRMS (DART) calcd. for $\text{C}_{11}\text{H}_{20}\text{BNSi}$ [$\text{M}+\text{H}^+$]: 206.15308, found 206.15283.

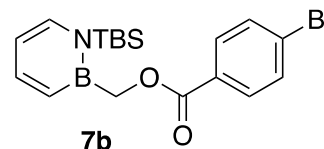
General Procedure for Synthesis of O-alkylation Product 7a-7c (Scheme 1.56)

The following procedure for the synthesis of **7b** is representative for the products Shown in Scheme 5): In a nitrogen glove box, 4-bromobenzoic acid (43.1mg, 0.214mmol) was added into compound **1** (50.0 mg, 0.214 mmol) dropwise in 1.5 mL MeCN. The reaction was allowed to stir at room temperature for 30 minutes. At the conclusion of the reaction, the reaction mixture was concentrated *in vacuo*. The resulting crude material was purified by silica gel chromatography with ether:pentane (0.5:10) as the eluent inside the glovebox.

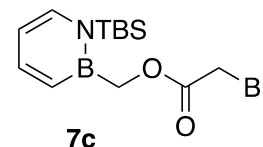
Ester **7a** was isolated as a white solid in 71% average yield (run1: 69%, run2: 72%). ^1H NMR (500 MHz, CDCl_3): δ 8.16 (d, $J = 8.3$ Hz, 2H), 7.61 (dd, $J = 11.1, 6.5$ Hz, 1H), 7.56 (t, $J = 7.1$ Hz, 1H), 7.47 (m, 2H), 7.32 (d, $J = 6.7$ Hz, 1H), 6.96 (d, $J = 11.1$ Hz, 1H), 6.37 (dd, $J = 6.6, 6.5$ Hz, 1H), 4.60 (s, 2H), 0.97 (s, 9H), 0.52 (s, 6H). ^{13}C NMR (100 MHz, CDCl_3): δ 167.6, 143.7, 138.0, 132.5, 131.0, 129.6, 128.3, 111.9, 61(br), 26.3, 19.1, -2.38 (signal for one of the carbon next to boron not observed); ^{11}B NMR (160 MHz, CDCl_3): δ 39.6; FTIR (thin film): $\tilde{\nu} = 2954-2858, 1735, 1717, 1609, 1509, 1395, 1364, 1283, 1265, 1023, 823, 811$; HRMS (DART) calcd. for $\text{C}_{18}\text{H}_{27}\text{BNO}_2\text{Si}$ [$\text{M}+\text{H}^+$]: 328.18986, found 328.18903.



Ester **7b** was isolated as a white solid in a 78% average yield (run1: 79%, run2: 76%). ^1H NMR (600 MHz, CDCl_3): δ 8.00 (d, $J = 8.2$ Hz, 2H), 7.59 (m, 3H), 7.31 (d, $J = 6.7$ Hz, 1H), 6.89 (d, $J = 11.1$ Hz, 1H), 6.36 (dd, $J = 6.6, 6.0$ Hz, 1H), 4.58 (s, 2H), 0.96 (s, 9H), 0.50 (s, 6H). ^{13}C NMR (125.8MHz, CDCl_3): δ 166.8, 143.8, 138.1, 131.6, 131.1, 130.0, 127.6, 111.9, 26.3, 19.1, -2.37 (signal for two carbons next to boron not observed); ^{11}B NMR (160 MHz, CDCl_3): δ 39.5; FTIR (thin film): $\tilde{\nu} = 2969-2858, 1737, 1716, 1509, 1395, 1364, 1266, 1229, 1217, 1114, 810$; HRMS (DART) calcd. for $\text{C}_{18}\text{H}_{26}\text{BNO}_2\text{SiBr}$ [$\text{M}+\text{H}^+$]: 406.10038, found 406.10057.



Ester **7c** was isolated as light yellow oily compound in 66% average yield (run1: 68%, run2: 64%). ^1H NMR (600 MHz, CDCl_3): δ 7.61 (dd, $J = 11.1, 6.3$

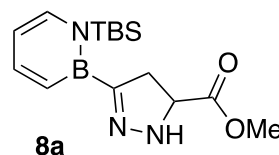


Hz, 1H), 7.29 (d, $J = 6.7$ Hz, 1H), 6.87 (d, $J = 11.0$ Hz, 1H), 6.36 (dd, $J = 6.7, 6.3$ Hz, 1H), 4.45 (s, 2H), 3.93 (s, 2H), 0.93 (s, 9H), 0.47 (s, 6H). ^{13}C NMR (150 MHz, CDCl_3): δ 168.2, 144.1, 138.2, 128(br), 112.2, 62(br), 26.5, 26.4, 19.2, -2.24; ^{11}B NMR (160 MHz, CDCl_3): δ 39.0; FTIR (thin film): $\tilde{\nu} = 2955\text{--}2858$, 1728, 1608, 1509, 1395, 1284, 1265, 1146, 978, 822, 810; HRMS (DART) calcd. for $\text{C}_{13}\text{H}_{24}\text{BNO}_2\text{SiBr}$ $[\text{M}+\text{H}^+]$: 344.08473, found 344.08568.

General Procedure for Synthesis of Pyrazoline 8a-8c (Scheme 1.57)

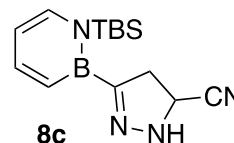
The following procedure for the synthesis of **8b** is representative for the products Shown in Scheme 6): In a nitrogen glove box, $[(\text{C}_6\text{H}_{11})_3\text{P}]_2\text{PdCl}_2$ (4.00 mg, 0.025 mmol) was added to a mixture of but-3-en-2-one (42.0 μl , 0.515 mmol) and compound **1** (60.0mg, 0.257 mmol) in 2.5ml toluene. The mixture was then allowed to stir at room temperature for 13 hours. At the conclusion of the reaction, the solvent was removed under reduced pressure. The resulting crude material was purified by silica gel chromatography with ether: pentane (1:4) as the eluent inside a glove box.

Pyrazoline **8a** was isolated as colorless oily compound in 82% average yield (run1: 83%, run2: 81%). ^1H NMR (400 MHz, CD_2Cl_2): δ 7.30 (dd, $J = 11.6, 6.0$ Hz, 1H), 7.18 (d, $J = 6.8$ Hz, 1H), 6.53 (s, 1H), 6.05 (d, $J = 11.6, 1\text{H}$), 5.88 (dd, $J = 7.2, 6.0$ Hz, 1H), 4.70 (dd, $J = 13.1, 6.3$ Hz, 1H), 3.71 (s, 3H), 3.12 (dd, $J = 17.8, 13.1$ Hz, 1H), 2.94 (dd, $J = 17.8, 6.3$ Hz, 1H), 1.04 (s, 9H), 0.39 (s, 3H), 0.31 (s, 3H). ^{13}C NMR (100 MHz, CD_2Cl_2): δ 173.8, 143.1, 139.7, 137.3, 120.0 (br), 107.5, 59.0, 52.5, 39.0, 28.6, 19.6, 1.34, 0.23; ^{11}B NMR (160 MHz, CD_2Cl_2): δ 27.7; FTIR (thin film): $\tilde{\nu} = 2952\text{--}2856$, 1738, 1609, 1510, 1403, 1358, 1265, 1199, 1118, 971, 823, 811, 731, 706; HRMS (DART) calcd. for $\text{C}_{15}\text{H}_{27}\text{BN}_3\text{O}_2\text{Si}$ $[\text{M}+\text{H}^+]$: 320.20003, found 320.19714.

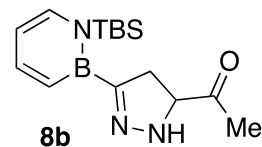


Pyrazoline **8c** was isolated as light brown oil in 79% average yield (run1: 77%, run2: 81%).

^1H NMR (500 MHz, CDCl_3): δ 7.45 (dd, $J = 11.6, 6.0$ Hz, 1H), 7.19 (d, $J = 7.0$ Hz, 1H), 6.68 (s, 1H), 6.27 (d, $J = 11.6$ Hz, 1H), 6.00 (dd, $J = 7.3, 6.2$ Hz, 1H), 4.85 (dd, $J = 10.4, 8.2$ Hz, 1H), 3.24-3.10 (m, 2H), 1.03 (s, 9H), 0.38 (s, 3H), 0.33 (s, 3H). ^{13}C NMR (150 MHz, CDCl_3): δ 144.1, 139.7, 136.8, 119.5, 108.2, 46.9, 39.4, 28.3, 19.5, 0.92, 0.29 (signal for a carbon next to boron not observed); ^{11}B NMR (160 MHz, CDCl_3): δ 29.5; FTIR (thin film): $\tilde{\nu} = 3070\text{--}2858$, 2358, 2340, 1739, 1610, 1511, 1398, 1289, 1261, 842, 824, 811; HRMS (DART) calcd. for $\text{C}_{14}\text{H}_{24}\text{BN}_4\text{Si}$ $[\text{M}+\text{H}^+]$: 287.18578, found 287.18592.

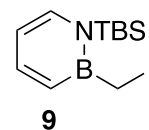


Pyrazoline **8b** was isolated as colorless oil in 61% average yield (run 1: 58%, run 2: 65%). ^1H NMR (600 MHz, CDCl_3): δ 7.31 (dd, $J = 11.6, 6.0$ Hz, 1H), 7.15 (d, $J = 7.0$ Hz, 1H), 6.58 (s, 1H), 5.94 (d, $J = 11.6$ Hz, 1H), 5.90 (dd, $J = 6.9, 6.0$ Hz, 1H), 4.55 (dd, $J = 13.4, 6.7$ Hz, 1H), 3.12 (dd, $J = 18.1, 13.4$ Hz, 1H), 2.79 (dd, $J = 18.2, 6.7$ Hz, 1H), 2.09 (s, 3H), 1.04 (s, 9H), 0.40 (s, 3H), 0.34 (s, 3H). ^{13}C NMR (150 MHz, CDCl_3): δ 209.6, 143.6, 139.7, 137.3, 120(br), 107.5, 66.5, 38.0, 28.5, 24.9, 19.5, 1.44, 0.71; ^{11}B NMR (160 MHz, CDCl_3): δ 30.5; FTIR (thin film): $\tilde{\nu} = 2953\text{--}2857$, 1715, 1609, 1511, 1400, 1356, 1302, 1260, 1249, 842, 823, 810; HRMS (DART) calcd. for $\text{C}_{15}\text{H}_{27}\text{BN}_3\text{OSi}$ $[\text{M}+\text{H}^+]$: 304.20110, found 304.20062.



Synthesis of halomethyl 1,2-azaborine building blocks from 1 (Scheme 1.58)

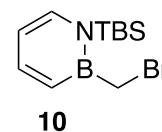
Compound 9. In a nitrogen glove box, a 5 mL vial containing a stir bar was charged with **1** (100 mg, 0.428 mmol), CuI (100 mg, 0.514mmol), the 1-ethynyl-4-nitrobenzene (63.1 mg, 0.428 mmol) in 1.7mL MeCN. The reaction mixture was



allowed to stir at room temperature for 12 hours. At the conclusion of the reaction, the reaction mixture was concentrated under reduced pressure. And the resulting crude material was purified by silica gel chromatography with 8% CH₂Cl₂ in as eluent to yield the product as a colorless oil in an average of 65% yield (run1: 66%, run 2: 65%).

¹H NMR (500 MHz, CDCl₃): δ 7.53 (dd, *J* = 11.1, 6.3 Hz, 1H), 7.17 (d, *J* = 6.8 Hz, 1H), 6.82 (d, *J* = 11.0 Hz, 1H), 6.25 (dd, *J* = 6.8, 6.3 Hz, 1H), 2.89 (s, 2H), 0.91 (s, 9H), 0.52 (s, 6H). ¹³C NMR (125.8MHz, CDCl₃): δ 143.9, 137.1, 132(br), 112.0, 26.3, 19.1, -2.24 (signal for one of carbon next to boron not observed); ¹¹B NMR (160 MHz, CDCl₃): δ 38.9; FTIR (thin film): $\tilde{\nu}$ = 2955-2859, 1924, 1607, 1507, 1392, 1277, 1173, 1135, 986, 821, 810; HRMS (DART) calcd. for C₁₁H₂₂BNSi [M+H⁺]: 334.06428, found 334.06538.

Compound 10. In a nitrogen glove box, a 20 mL vial containing a stir bar was charged with **1** (750 mg, 3.22 mmol), cetrimonium bromide (1.17 g, 3.22 mmol), 2-bromoacetic acid (447 mg, 3.22 mmol) in 2mL anhydrous CHCl₃. The reaction mixture was allowed to stir at room temperature for 30 minutes. At the conclusion of the reaction, volatiles were removed under reduced pressure. And the resulting crude material was purified by silica gel chromatography with 10% ether in pentane as eluent to yield the product as a colorless oil in an average of 70% yield (run1: 71%, run2: 69%).



¹H NMR (500 MHz, CDCl₃): δ 7.62 (dd, *J* = 11.1, 6.3 Hz, 1H), 7.24 (d, *J* = 6.8 Hz, 1H), 6.95 (d, *J* = 11.0 Hz, 1H), 6.34 (dd, *J* = 6.9, 6.3 Hz, 1H), 3.24 (s, 2H), 0.93 (s, 9H), 0.53 (s, 6H). ¹³C NMR (125.8MHz, CDCl₃): δ 144.1, 137.4, 131(br), 112.3, 26.3, 22(br), 18.9, -2.03; ¹¹B NMR (160 MHz, CDCl₃): δ 37.1; FTIR (thin film): $\tilde{\nu}$ = 2954-2858, 1607, 1508, 1393, 1266, 986, 821, 810; HRMS (DART) calcd. for C₁₁H₂₂BNSiBr [M+H⁺]: 286.08007, found 286.07925.

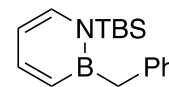
General Procedure for Synthesis of Suzuki-coupling Product 11a-11c (Scheme 1.59)

Optimization table for Suzuki-Miyaura cross-coupling reaction.

Entry	Conditions	Yield% (NMR)
Ligand screening		
1	Xphos	10%
2	Sphos	trace
3	RuPhos	N/A
4	MePhos	19%
5	JohnPhos	70%
6	(tBu) ₃ P	trace
7	DavePhos	9%
Deviations from standard condition		
8	80 °C, 3 h	34%
9	120 °C, 1 h	50%
10	Microwave, 100 °C	55%
11	1,4-Dioxane	38%
12	K ₂ CO ₃	trace

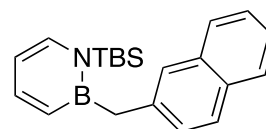
The following procedure for the synthesis of **11a** is representative for the products Shown in Scheme 8, 11a-11c): In a nitrogen box, a 20ml vial containing a stir bar was charged with **10** (100 mg, 0.350 mmol) Pd₂dba₃ (12.8 mg, 14.0 μmol), Cs₂CO₃ (228 mg, 699 μmol), JohnPhos (10.4 mg, 35.0 μmol), phenylboronic acid (63.9 mg, 525 μmol) in 3.5ml toluene. The reaction mixture was allowed to stir at 105°C for 1.5 hours. At the conclusion of the reaction, the volatiles were removed under reduce pressure. The resulting crude mixture was purified by silica gel chromatography using 1~3% ether in pentane as the eluent inside a glovebox.

Compound **11a** was isolated as white solid in 67% average yield (run1: 65%, run 2: 68%). ¹H NMR (400 MHz, CDCl₃): δ 7.38 (dd, *J* = 11.2, 6.2 Hz, 1H), 7.29 (d, *J* = 6.8 Hz, 1H), 7.28-7.21 (m, 2H), 7.14-7.07 (m, 3H), 6.29 (d, *J* = 11.1 Hz, 1H), 6.22 (dd, *J* = 6.8, 6.3 Hz, 1H), 2.77 (s, 2H), 0.99 (s, 9H), 0.53 (s, 6H). ¹³C NMR (125.8MHz, CDCl₃): δ 144.3, 142.7, 138.1, 131(br), 129.3, 128.2, 124.1, 111.0, 31(br), 26.6, 19.3, -1.36; ¹¹B NMR (160 MHz, CDCl₃): δ 41.7; FTIR (thin film): $\tilde{\nu}$ = 3063-2858, 1607, 1508, 1391, 1264, 1141, 1059, 984, 890, 760; HRMS (DART) calcd. for C₁₇H₂₇BNSi [M+H⁺]: 284.19974, found 284.20003.



11a

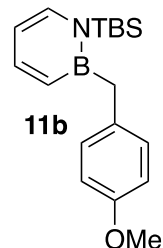
Compound **11c** was isolate as white solid in 84% average yield (run1: 87%, run2: 82%). ¹H NMR (500 MHz, Benzene-d₆): δ 7.66 (m, 4H), 7.34 (m, 2H), 7.26(m, 2H), 7.13(s, 1H), 6.63 (d, *J* = 11.1 Hz, 1H), 6.14 (dd, *J* = 6.8, 6.4 Hz, 1H), 2.95 (s, 2H), 0.83 (s, 9H), 0.23 (s, 6H). ¹³C NMR (125.8MHz, Benzene-d₆): δ 143.2, 138.0, 134.8, 132.1, 129.4, 127.7, 127.3, 126.1, 124.8, 111.6, 26.7, 19.3, -1.51 (signal for two carbons next to



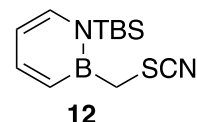
11c

boron not observed); ^{11}B NMR (160 MHz, *Benzene-d*₆): δ 42.1; FTIR (thin film): $\tilde{\nu}$ = 3051-2857, 2359, 2340, 1738, 1727, 1391, 1366, 1264, 1229, 1216, 811; HRMS (DART) calcd. for C₂₁H₂₉BN₂Si [M+H⁺]: 334.21587, found 334.21568.

Compound **11b** was isolate as light yellow solid in an 80% average yield (run1: 89%, run2: 71%). ^1H NMR (600 MHz, *CDCl*₃): δ 7.40 (dd, J = 11.2, 6.2 Hz, 1H), 7.30 (d, J = 6.8 Hz, 1H), 7.03 (d, J = 8.6 Hz, 2H), 6.82 (d, J = 8.6 Hz, 2H), 6.34 (d, J = 11.1 Hz, 1H), 6.23 (dd, J = 6.8, 6.2 Hz, 1H), 3.80 (s, 3H), 2.71 (s, 2H), 0.99 (s, 9H), 0.53 (s, 6H). ^{13}C NMR (150 MHz, *CDCl*₃): δ 156.8, 142.8, 138.2, 135.9, 131(br), 130.2, 113.8, 111.1, 55.4, 29(br), 26.8, 19.4, -1.23; ^{11}B NMR (160 MHz, *CDCl*₃): δ 39.2; FTIR (thin film): $\tilde{\nu}$ = 3000-2857, 2359, 2340, 1738, 1609, 1509, 1398, 1391, 1244, 1217, 842, 823; HRMS (DART) calcd. for C₁₈H₂₉BNOSi [M+H⁺]: 314.21125, found 314.21060.

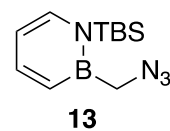


Synthesis of 12 (Scheme 1.59). In a nitrogen glovebox, a 20ml vial containing a stir bar was charged with **10** (100 mg, 349 μmol), NaSCN (43.1 mg, 532 μmol) in 3.5ml anhydrous MeCN. The reaction mixture was allowed to stir at room temperature for 1hour. At the conclusion of the reaction, the reaction crude mixture was filtered over celite and rinsed with cold pentane. The combined filtrates were concentrated *in vacuo*. Then the resulting crude material was purified by silica gel chromatography with 5% ether in pentane as eluent to yield the product as a white solid in 90% average yield (run1: 91%, run2: 88%).



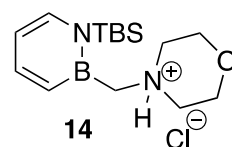
^1H NMR (500 MHz, *CDCl*₃): δ 7.66 (dd, J = 11.1, 6.4 Hz, 1H), 7.34 (d, J = 6.7 Hz, 1H), 6.85 (d, J = 11.1 Hz, 1H), 6.43 (dd, J = 6.6, 6.4 Hz, 1H), 3.13 (s, 2H), 0.94 (s, 9H), 0.54 (s, 6H). ^{13}C NMR (125.8MHz, *CDCl*₃): δ 144.9, 138.6, 129(br), 115.0, 112.9, 26.2, 24(br), 18.9, -1.78; ^{11}B NMR (160 MHz, *CDCl*₃): δ 37.5; FTIR (thin film): $\tilde{\nu}$ = 2954-2858, 2158, 2070, 1608, 1510, 1397, 1280, 1010, 814.2, 822, 810; HRMS (DART) calcd. for C₁₂H₂₂BN₂SiS [M+H⁺]: 265.13682, found 265.13605.

Synthesis of 13 (Scheme 1.59). In a nitrogen glovebox, a 20ml vial containing a stir bar was charged with **10** (100 mg, 0.349 mmol), NaN₃ (27.3 mg, 0.419 mmol) in 3.5 mL dry MeCN. The reaction mixture heated to reflux at 76°C for 2 hours. At the conclusion of the reaction, the solvent was removed in vacuo. The resulting crude mixture was purified by silica gel chromatography with pure pentane as eluent to yield the product as light brown oil in 91% average yield (run1: 90%, run2: 91%).



^1H NMR (500 MHz, *CDCl*₃): δ 7.66 (dd, J = 11.1, 6.3 Hz 1H), 7.31 (d, J = 6.8 Hz, 1H), 6.98 (d, J = 11.1 Hz, 1H), 6.39 (dd, J = 6.8, 6.4 Hz, 1H), 3.46 (s, 2H), 0.93 (s, 9H), 0.48 (s, 6H). ^{13}C NMR (125.8MHz, *CDCl*₃): δ 144.2, 138.3, 129(br), 112.2, 45(br), 26.3, 19.0, -2.02; ^{11}B NMR (160 MHz, *CDCl*₃): δ 38.9; FTIR (thin film): $\tilde{\nu}$ = 3028-2859, 2359, 2340, 2087, 1738, 1608, 1509, 1394, 1263, 822, 811; HRMS (DART) calcd. for C₁₁H₂₂BN₄Si [M+H⁺]: 249.17080, found 249.17013.

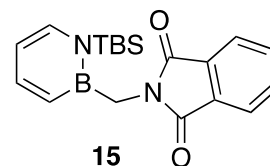
Synthesis of 14 (Scheme 1.59). In a nitrogen glove box, a 20ml vial containing a stir bar was charged with the secondary amine (60.9 mg, 0.699 mmol) was added dropwise to **10** (100 mg, 0.349 mmol) in dry 1ml THF. Then the reaction mixture was allowed to stir at room temperature for 2.5 hours inside the glove box. Upon the completion of the reaction, and after the



removal of the reaction solvent under reduced pressure. 1M HCl in ether was added to the reaction crude material. The morpholine salt product was precipitated out as white solid. Then the white solid was washed by cold pentane and dried *in vacuo* to furnish the **14** as white solid with an average of 69% yield (run1: 65%, run2: 72%).

^1H NMR (600 MHz, *DMSO*): δ 9.96 (s, 1H), 7.65 (dd, J = 11.2, 6.3 Hz, 1H), 7.51 (d, J = 6.7 Hz, 1H), 7.04 (d, J = 11.1 Hz, 1H), 6.49 (dd, J = 6.7, 6.3 Hz, 1H), 3.99-3.82 (m, 4H), 3.45-3.42 (m, 2H), 3.26 (d, J = 5.7 Hz, 2H), 3.15-3.10 (m, 2H), 0.87 (s, 9H), 0.50 (s, 6H). ^{13}C NMR (125.8MHz, *DMSO*): δ 144.3, 139.9, 128(br), 112.2, 63.3, 54.1, 52(br), 26.1, 18.6, -2.05; ^{11}B NMR (160 MHz, *DMSO*): δ 39.7(br); FTIR (thin film): $\tilde{\nu}$ = 2546, 2478, 1607, 1510, 1466, 1398, 1267, 1150, 1120, 988; HRMS (DART) calcd. for $\text{C}_{15}\text{H}_{30}\text{BN}_2\text{OSi}$ [$\text{M}+\text{H}^+$]: 293.22150, found 293.22098.

Synthesis of 15 (Scheme 1.59). In a nitrogen dry box, a 20ml vial containing a stir bar was charged with compound **10** (100 mg, 0.349 mmol), potassium phthalimide (77.7 mg, 0.419 mmol) and 18-crown-6 (10.0 mg, 0.035 mmol) in 2ml toluene. The reaction mixture was allowed to stir at 100°C for 2 hours under nitrogen flow. At the conclusion of the reaction, the volatiles in crude were removed under reduced pressure. The crude mixture was purified by silica gel chromatography with 20% ether in pentane as eluent to yield the product as a white solid in 88% average yield (run1: 89%, run2: 87%).



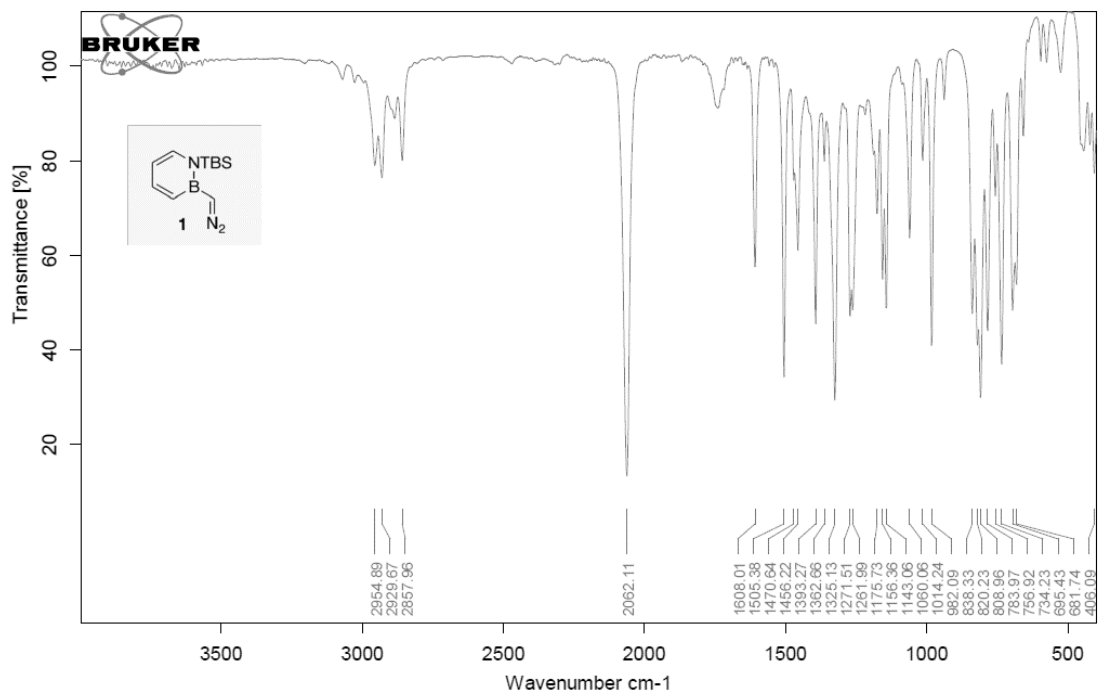
^1H NMR (500 MHz, CDCl_3): δ 7.84 (dd, J = 5.4, 3.0 Hz, 2H), 7.70 (dd, J = 5.4, 3.0 Hz, 2H), 7.45 (dd, J = 11.2, 6.3 Hz, 1H), 7.32 (d, J = 6.9 Hz, 1H), 6.36 (d, J = 11.1 Hz, 1H), 6.30 (dd, J = 6.8, 6.3 Hz, 1H), 3.79 (s, 2H), 1.03 (s, 9H), 0.56 (s, 6H). ^{13}C NMR (125.8MHz, CDCl_3): δ 167.0, 143.8, 138.3, 133.5, 132.6, 122.9, 111.6, 26.3, 19.2, -1.97 (signal for two carbons next to boron not observed); ^{11}B NMR (160 MHz, CDCl_3): δ 39.3; FTIR (thin film): $\tilde{\nu}$ = 2952-2858, 2358, 2334, 1728, 1709, 1399-1352, 986, 822, 812; HRMS (DART) calcd. for $\text{C}_{19}\text{H}_{26}\text{BN}_2\text{O}_2\text{Si}$ [$\text{M}+\text{H}^+$]: 353.18573, found 353.18511.

Crystallographic Data for Ru- α -borylalkylidene complex 3

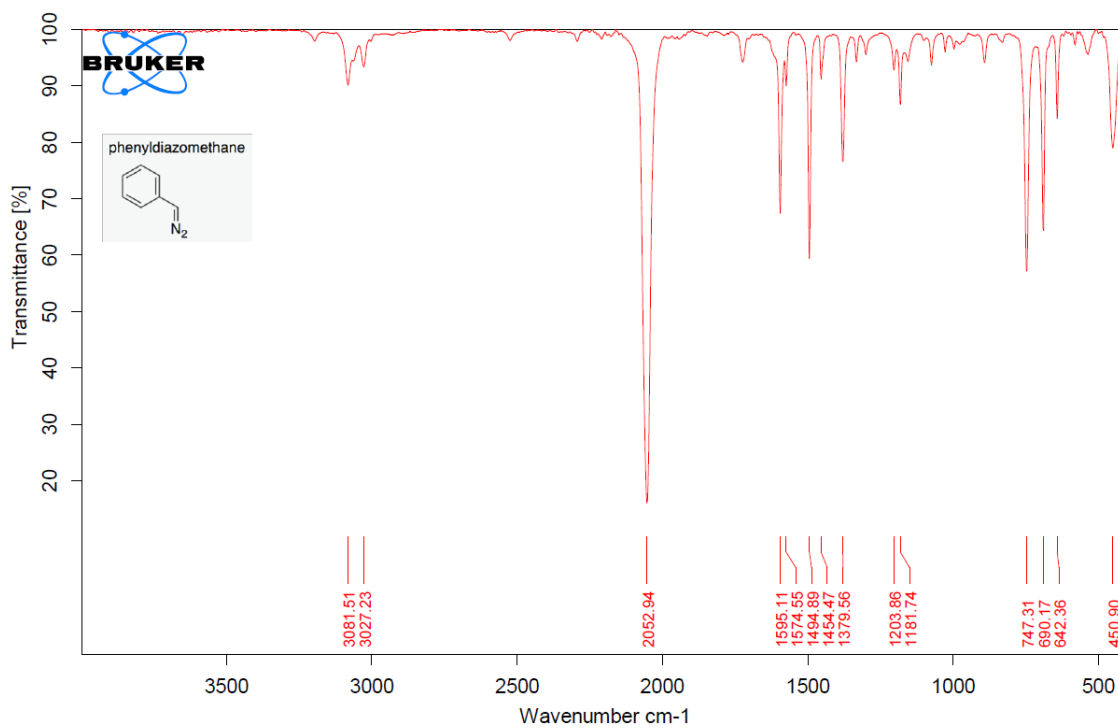
Crystal data and structure refinement for C₄₇H₅₀BCl₂NP₂RuSi.

Identification code	C ₄₇ H ₅₀ BCl ₂ NP ₂ RuSi	
Empirical formula	C ₄₇ H ₅₀ B Cl ₂ N P ₂ Ru Si	
Formula weight	901.69	
Temperature	100(2) K	
Wavelength	1.54178 Å	
Crystal system	Monoclinic	
Space group	P2 ₁ /c	
Unit cell dimensions	a = 20.0645(4) Å	$\alpha = 90^\circ$.
	b = 11.7459(2) Å	$\beta = 92.6720(10)^\circ$.
	c = 19.5025(4) Å	$\gamma = 90^\circ$.
Volume	4591.27(15) Å ³	
Z	4	
Density (calculated)	1.304 Mg/m ³	
Absorption coefficient	4.982 mm ⁻¹	
F(000)	1864	
Crystal size	0.280 x 0.120 x 0.100 mm ³	
Theta range for data collection	2.204 to 66.661°.	
Index ranges	-23 ≤ h ≤ 23, -13 ≤ k ≤ 13, -20 ≤ l ≤ 23	
Reflections collected	36081	
Independent reflections	8068 [R(int) = 0.0658]	
Completeness to theta = 66.661°	99.6 %	
Absorption correction	Semi-empirical from equivalents	
Max. and min. transmission	0.7528 and 0.5231	
Refinement method	Full-matrix least-squares on F ²	
Data / restraints / parameters	8068 / 478 / 615	
Goodness-of-fit on F ²	1.031	
Final R indices [I > 2σ(I)]	R ₁ = 0.0391, wR ₂ = 0.0824	
R indices (all data)	R ₁ = 0.0601, wR ₂ = 0.0928	
Extinction coefficient	n/a	
Largest diff. peak and hole	0.655 and -0.561 e.Å ⁻³	

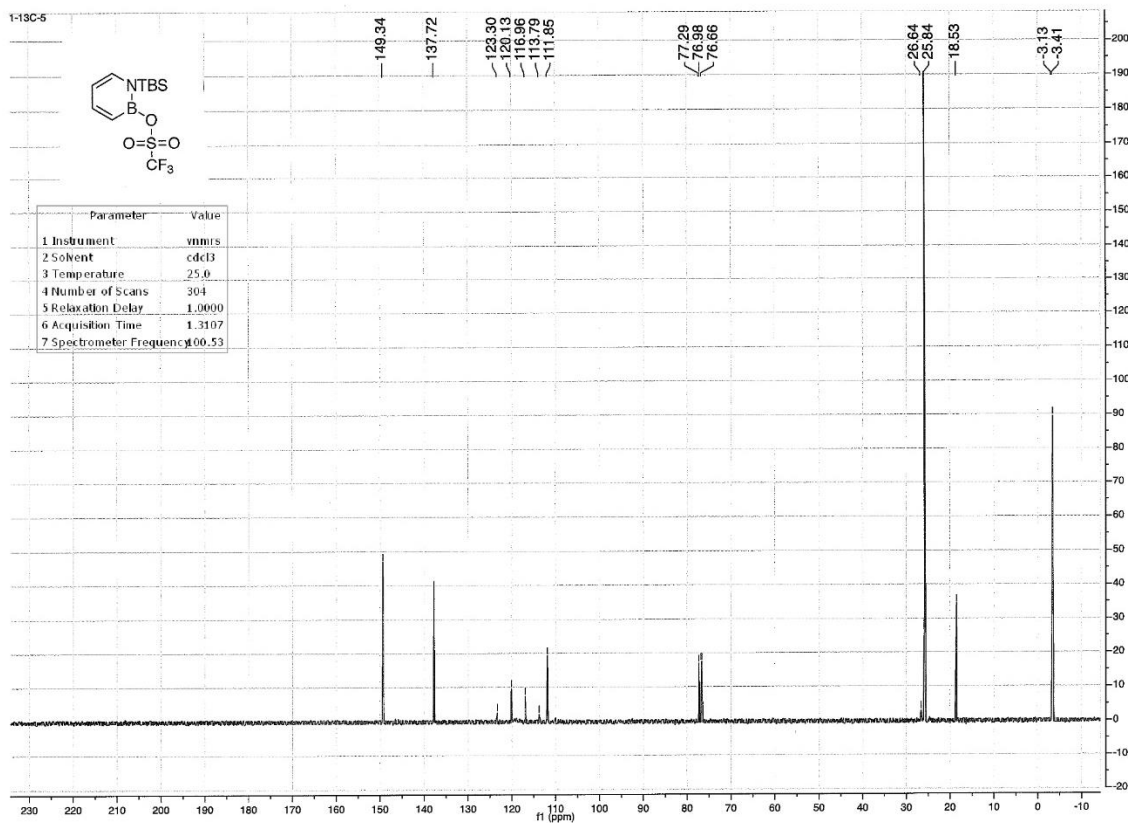
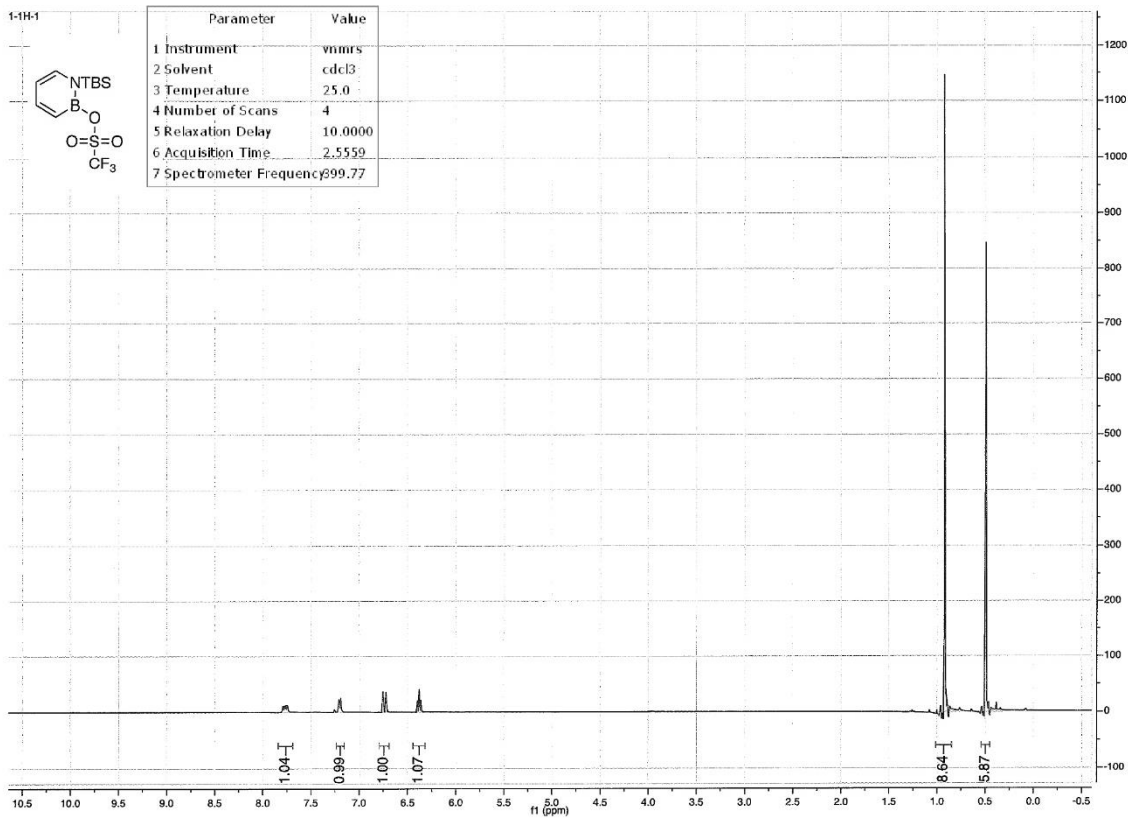
IR spectrum for compound 1



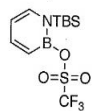
IR spectrum for phenyldiazomethane



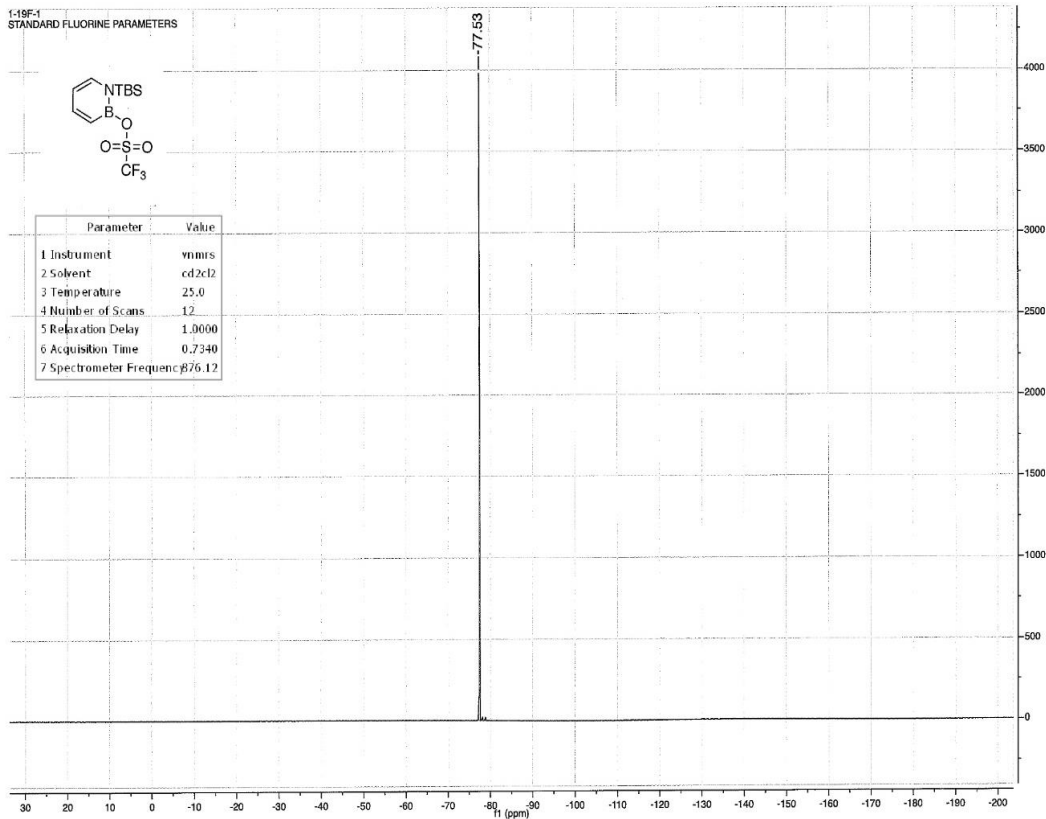
NMR spectrums



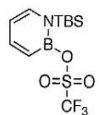
1-19F-1
STANDARD FLUORINE PARAMETERS



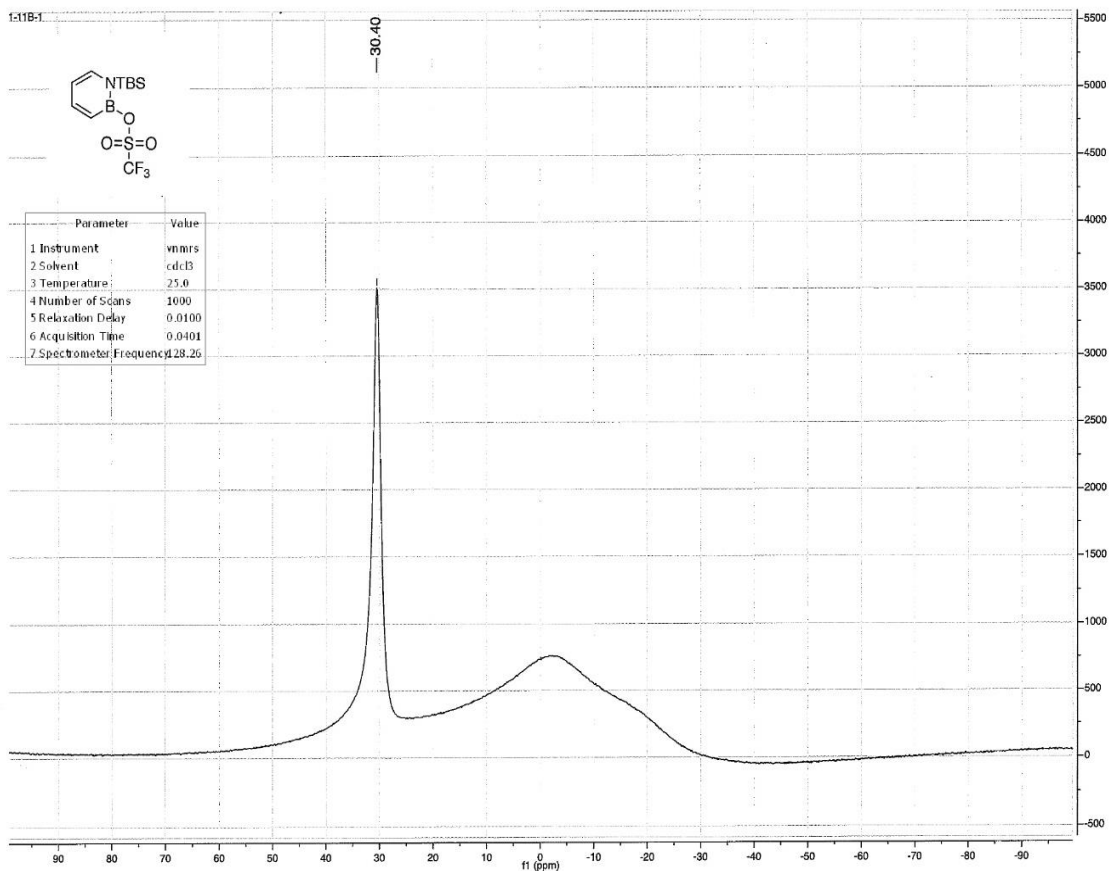
Parameter	Value
1 Instrument	nmr5
2 Solvent	cd2cl2
3 Temperature	25.0
4 Number of Scans	12
5 Relaxation Delay	1.0000
6 Acquisition Time	0.7340
7 Spectrometer Frequency	376.12



1-11B-1



Parameter	Value
1 Instrument	nmr5
2 Solvent	cdcl3
3 Temperature	25.0
4 Number of Scans	1000
5 Relaxation Delay	0.0100
6 Acquisition Time	0.0401
7 Spectrometer Frequency	128.26

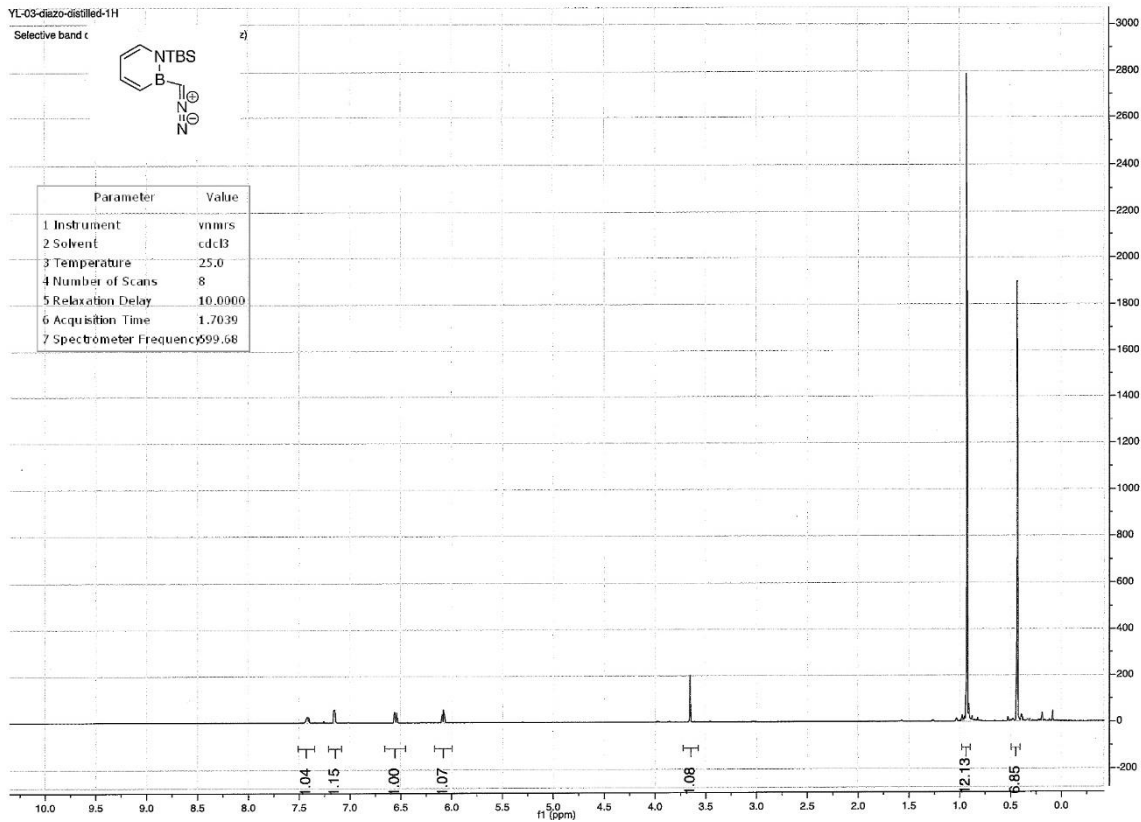


YL-03-diazo-distilled-1H

Selective band c



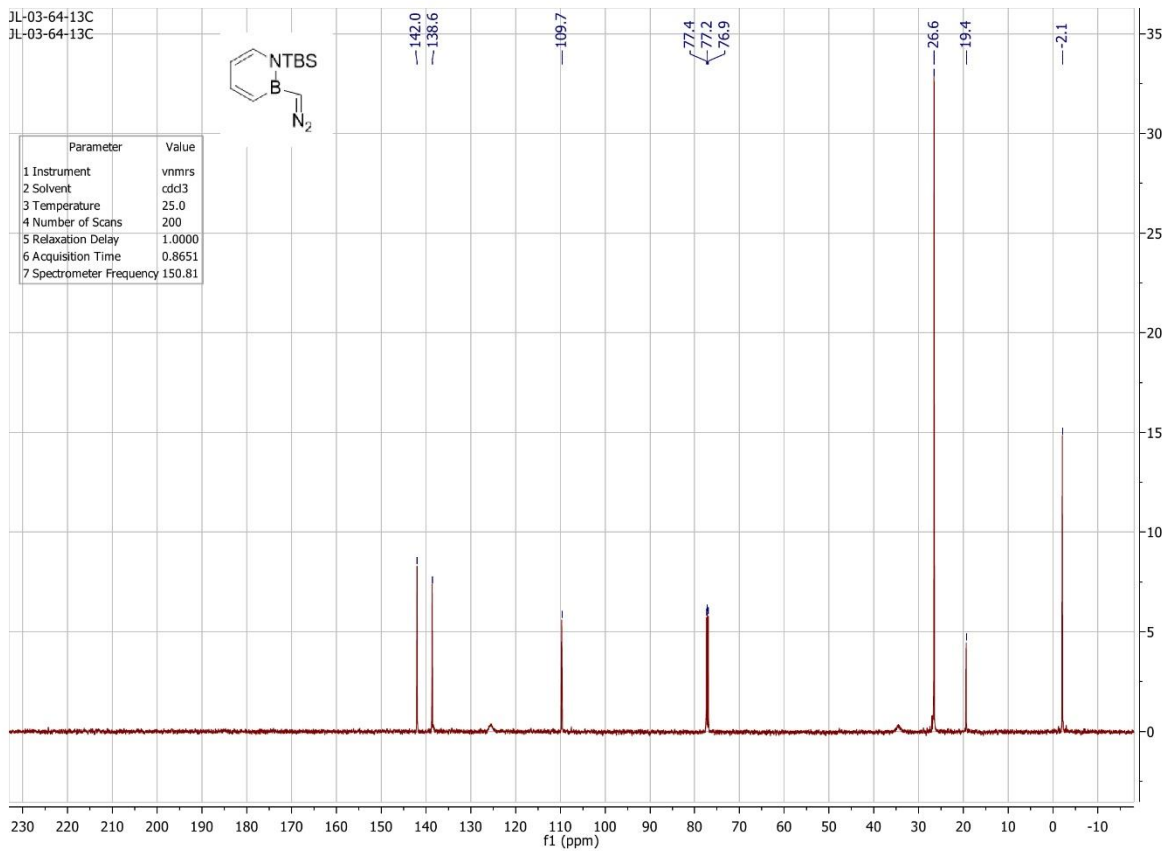
Parameter	Value
1 Instrument	nmr5
2 Solvent	cdcl3
3 Temperature	25.0
4 Number of Scans	8
5 Relaxation Delay	10.0000
6 Acquisition Time	1.7039
7 Spectrometer Frequency	599.68



JL-03-64-13C
JL-03-64-13C



Parameter	Value
1 Instrument	nmr5
2 Solvent	cdcl3
3 Temperature	25.0
4 Number of Scans	200
5 Relaxation Delay	1.0000
6 Acquisition Time	0.8651
7 Spectrometer Frequency	150.81



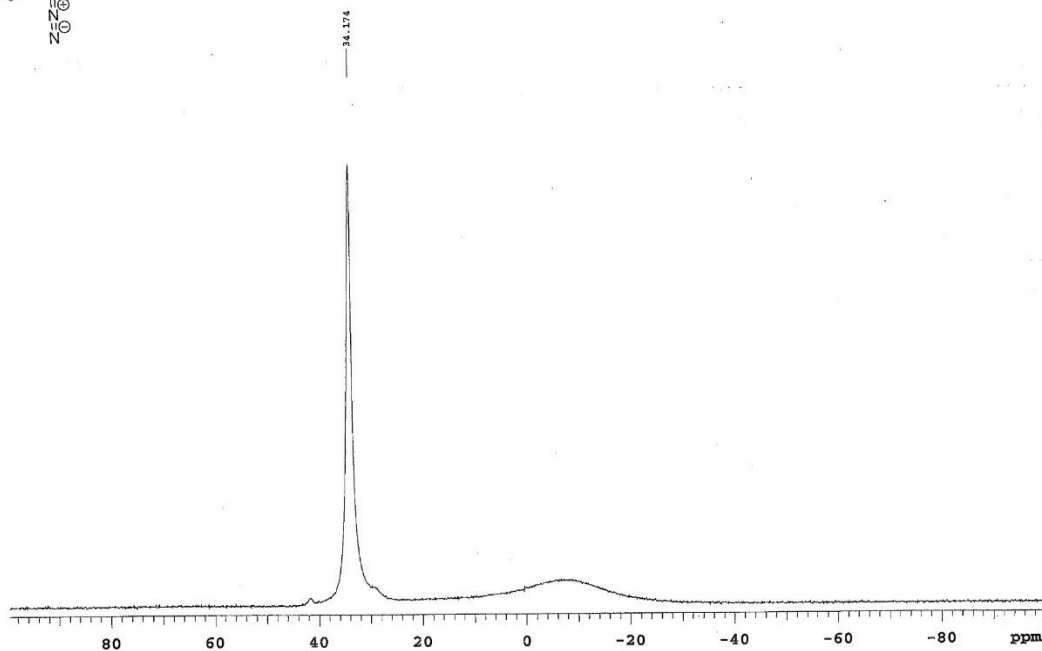
YL-03-diazo-11B-crude

Sample Name: YL-03-diazo-11B-crude
 Date Collected: 2019-07-15

Pulse sequence: s2pul
 Solvent: cdcl3

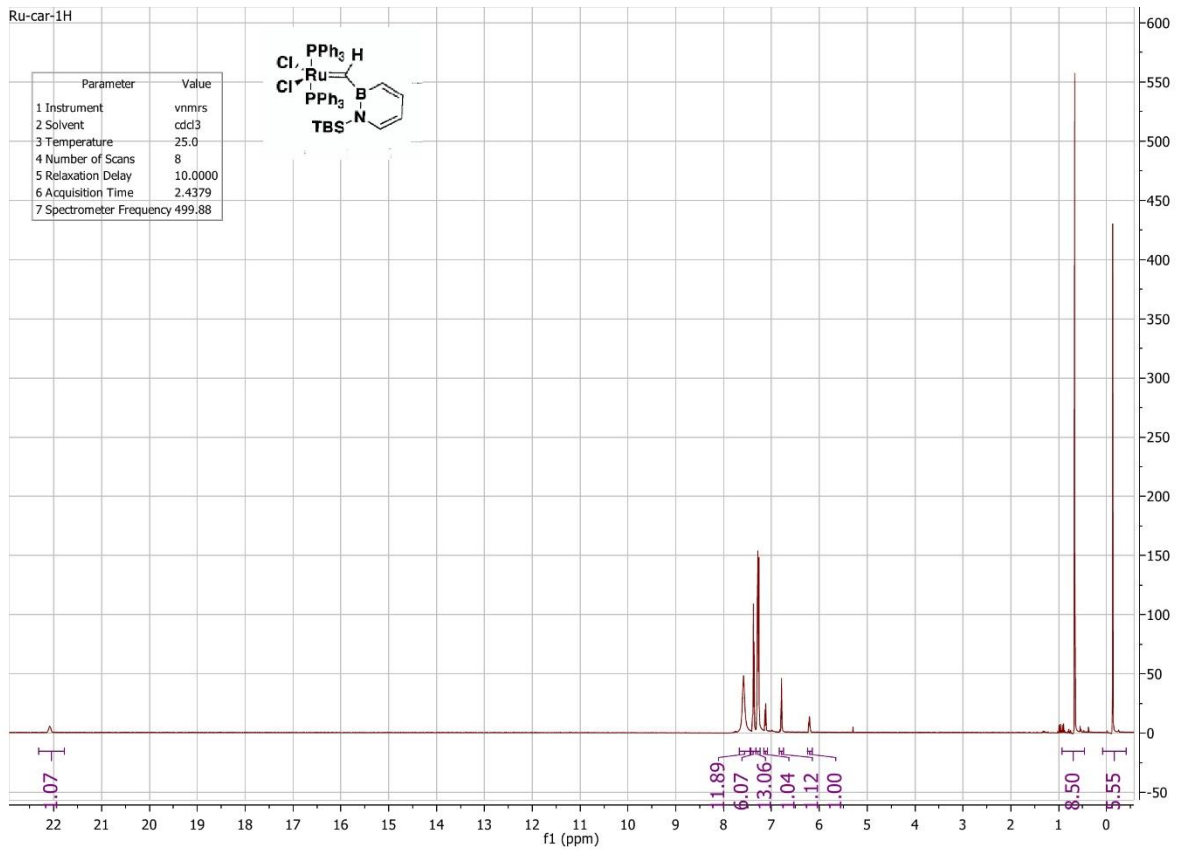
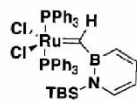
Temperature: 25
 Spectrometer: nmr11-inova500

Study Name: Liu
 Operator: Liu

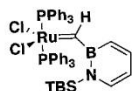


Ru-car-1H

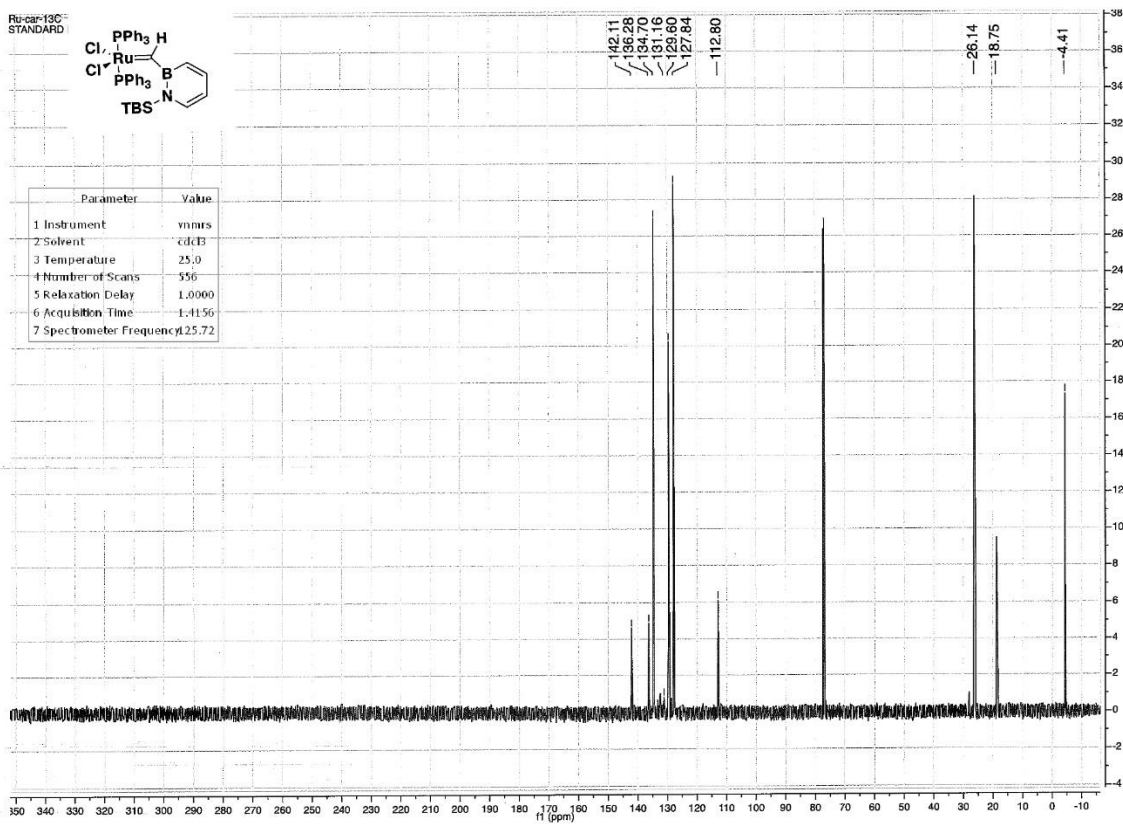
Parameter	Value
1 Instrument	nmr11
2 Solvent	cdcl3
3 Temperature	25.0
4 Number of Scans	8
5 Relaxation Delay	10.0000
6 Acquisition Time	2.4379
7 Spectrometer Frequency	499.88



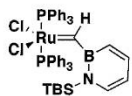
Ru-car-13C
STANDARD



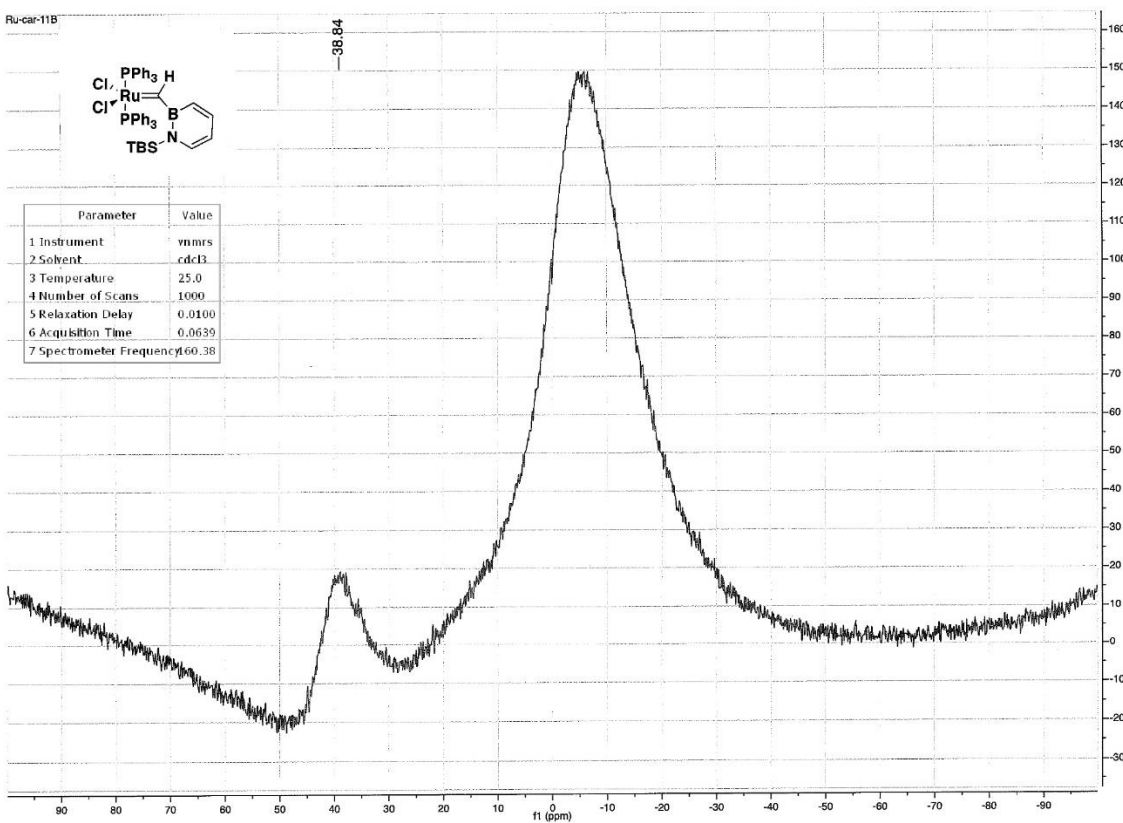
Parameter	Value
1 Instrument	nmrs
2 Solvent	cdcl3
3 Temperature	25.0
4 Number of Scans	556
5 Relaxation Delay	1.0000
6 Acquisition Time	1.4156
7 Spectrometer Frequency	125.72



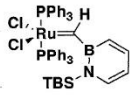
Ru-car-11B



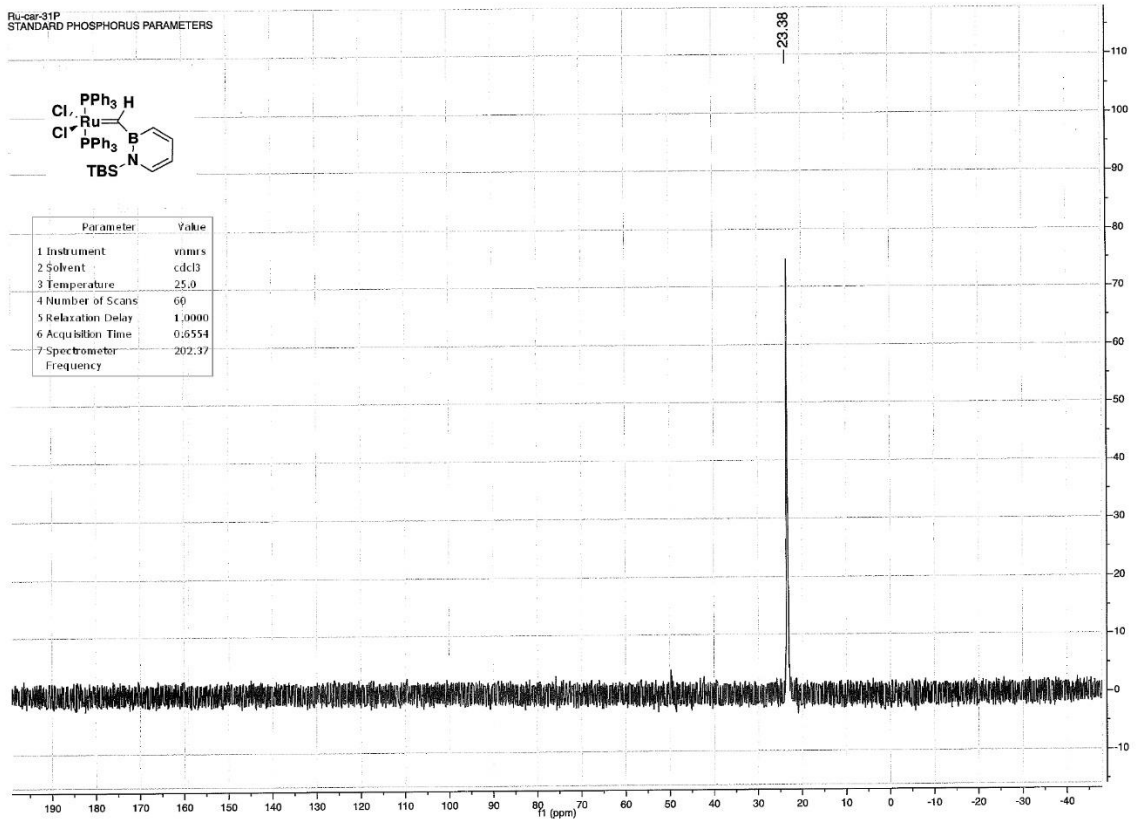
Parameter	Value
1 Instrument	nmrs
2 Solvent	cdcl3
3 Temperature	25.0
4 Number of Scans	1000
5 Relaxation Delay	0.0100
6 Acquisition Time	0.0639
7 Spectrometer Frequency	60.38



Ru-car-31P
STANDARD PHOSPHORUS PARAMETERS

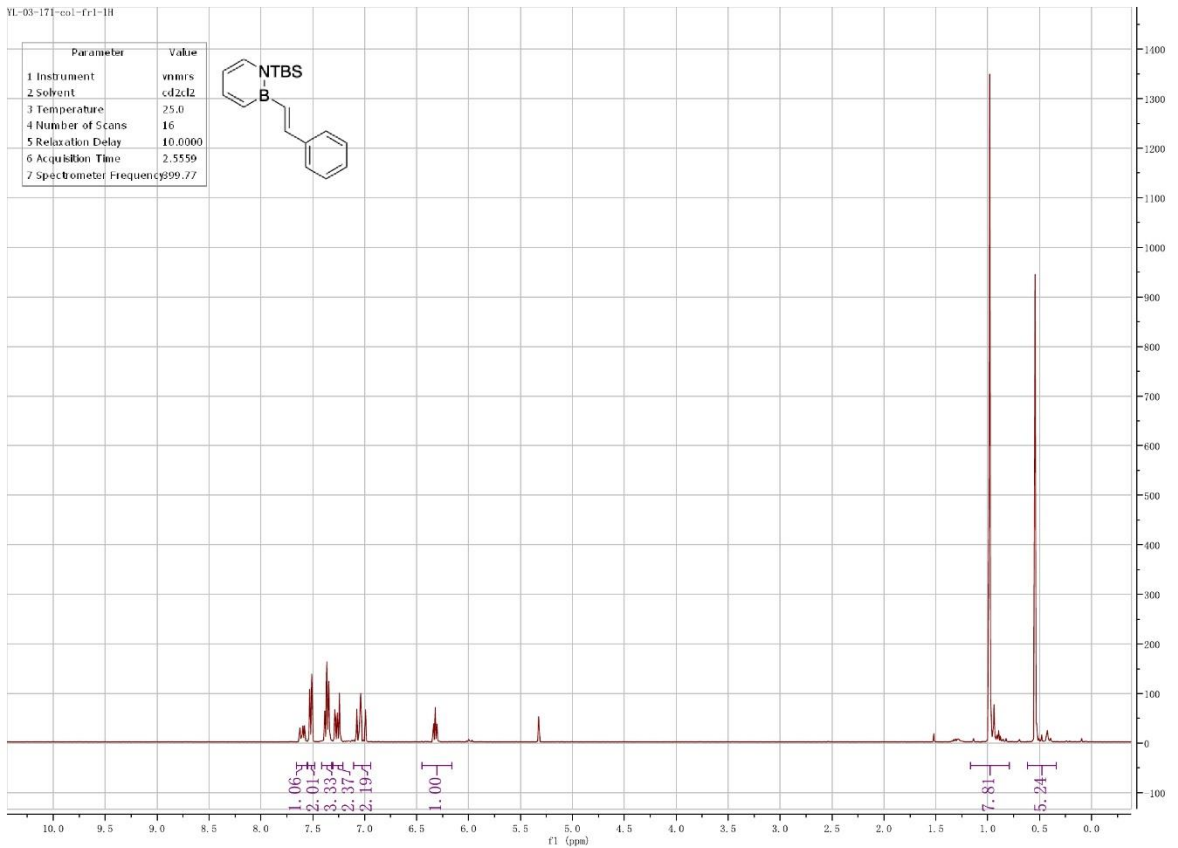
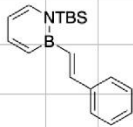


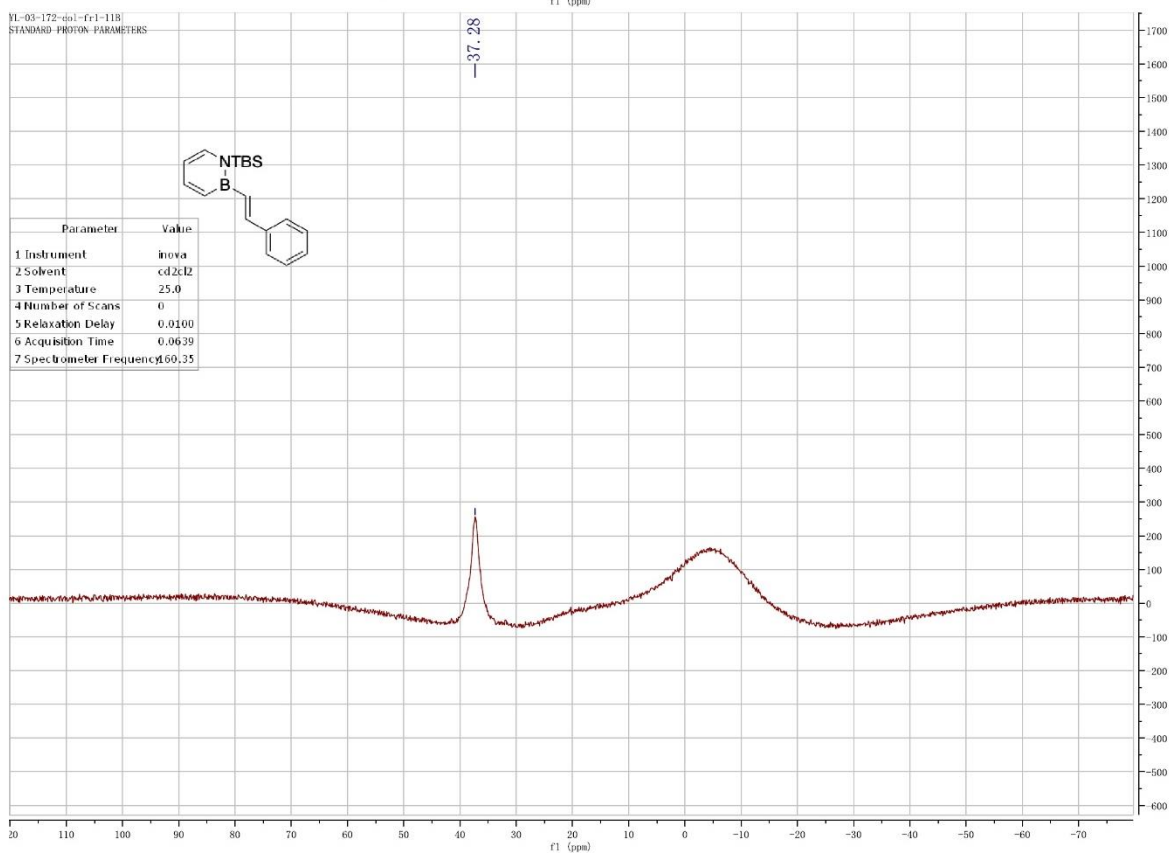
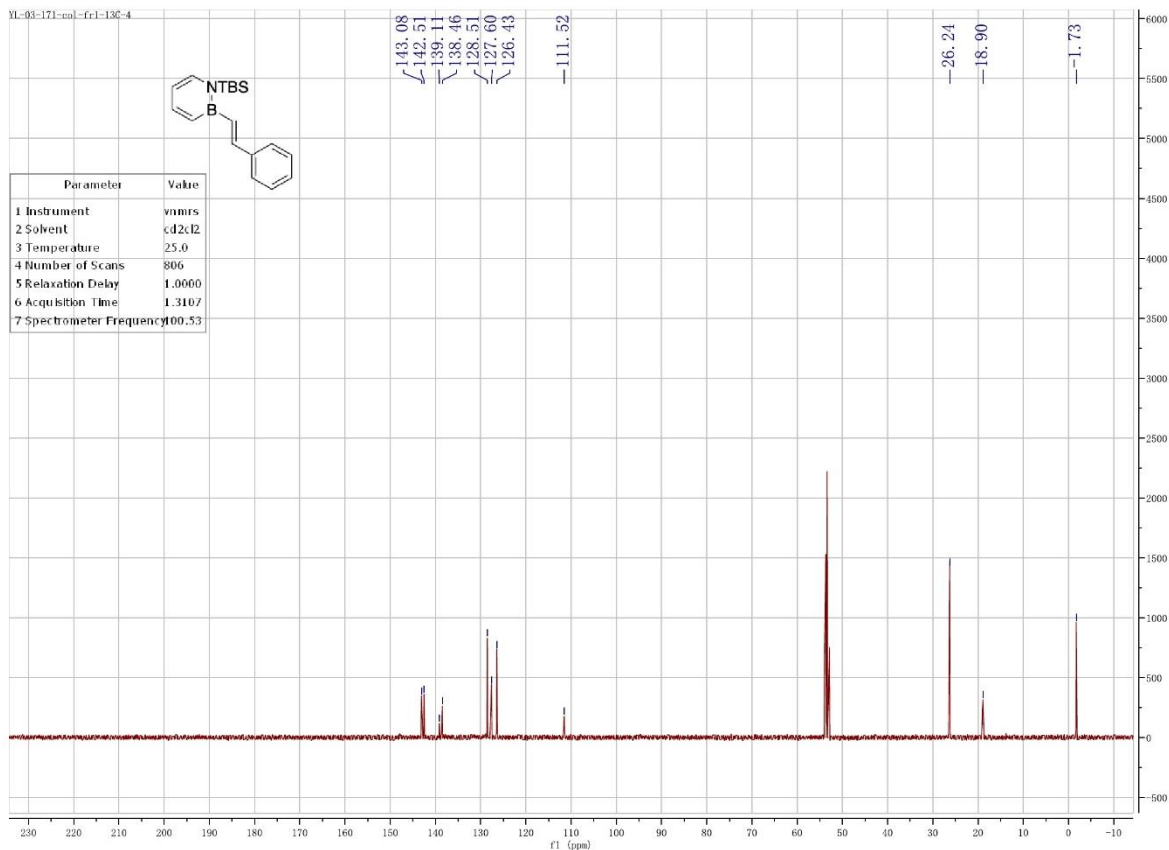
Parameter	Value
1 Instrument	vnmr5
2 Solvent	cdcl3
3 Temperature	25.0
4 Number of Scans	60
5 Relaxation Delay	1.9990
6 Acquisition Time	0.6554
7 Spectrometer Frequency	202.37

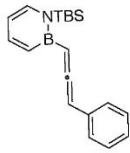


VL-03-171-col-tri-H

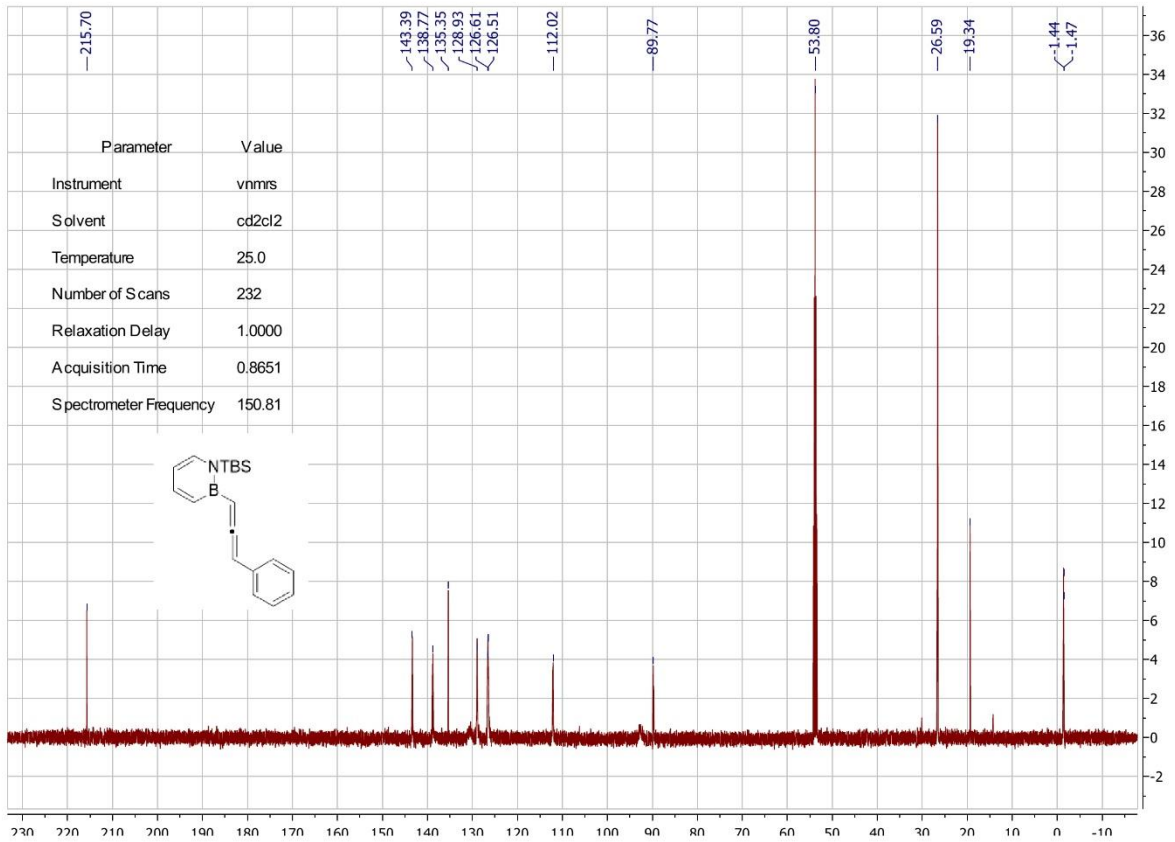
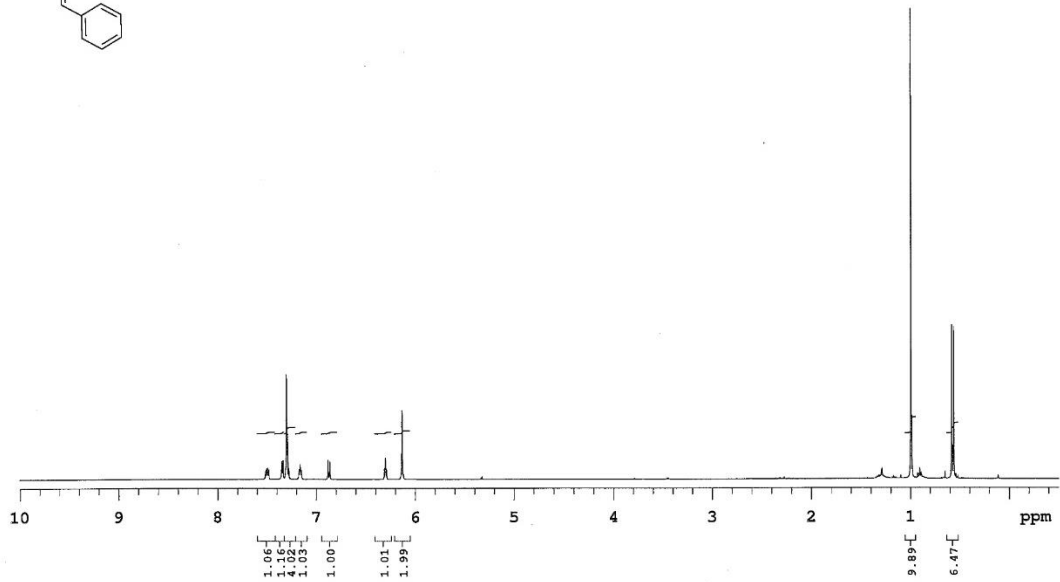
Parameter	Value
1 Instrument	vnmr5
2 Solvent	cd2cl2
3 Temperature	25.0
4 Number of Scans	16
5 Relaxation Delay	10.0000
6 Acquisition Time	2.5559
7 Spectrometer Frequency	399.77







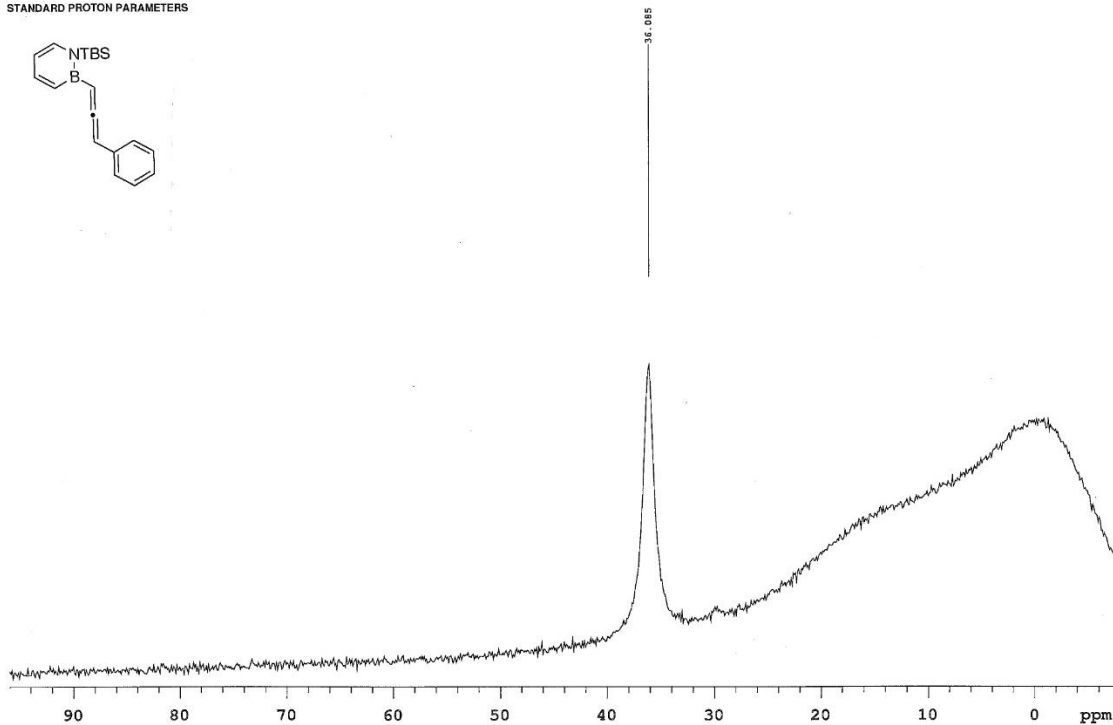
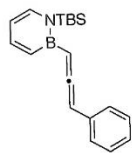
Sample Name:
 Date collected: 2019-01-09
 Pulse sequence: PROTON
 Solvent: cd2cl2
 Temperature: 25
 Spectrometer: nmr19-vnmrs600
 Study owner: Liu
 Operator: Liu



YL-03-phenylacetylenesub-11B

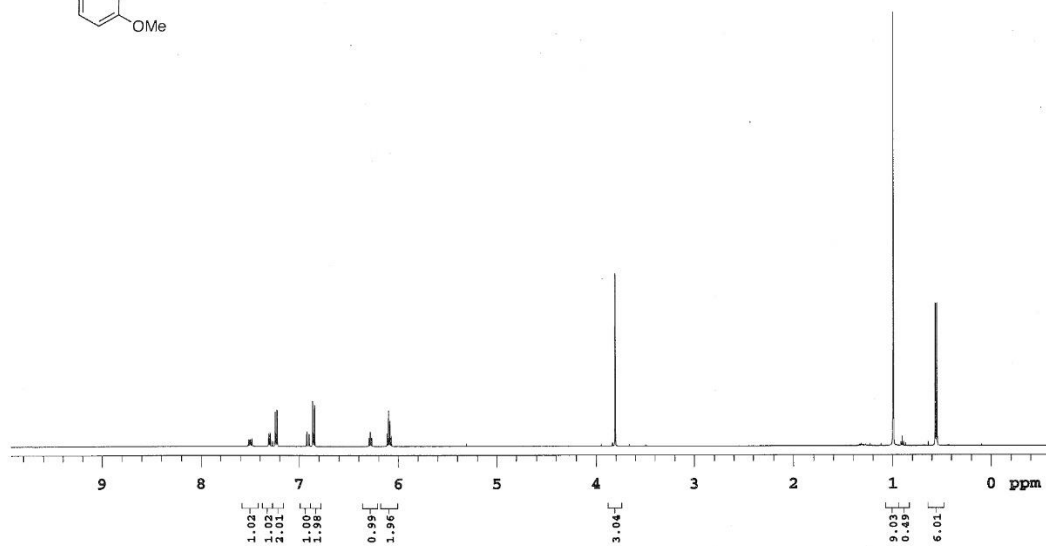
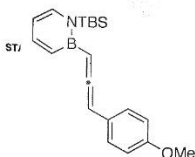
Sample Name YL-03-phenylacetylenesub-11B sequence s2pul Temperature 25
 Date collected 2019-01-09 Solvent cd2cl2 Spectrometer nmr18-vnmrs600 Study owner Liu
 Operator Liu

STANDARD PROTON PARAMETERS



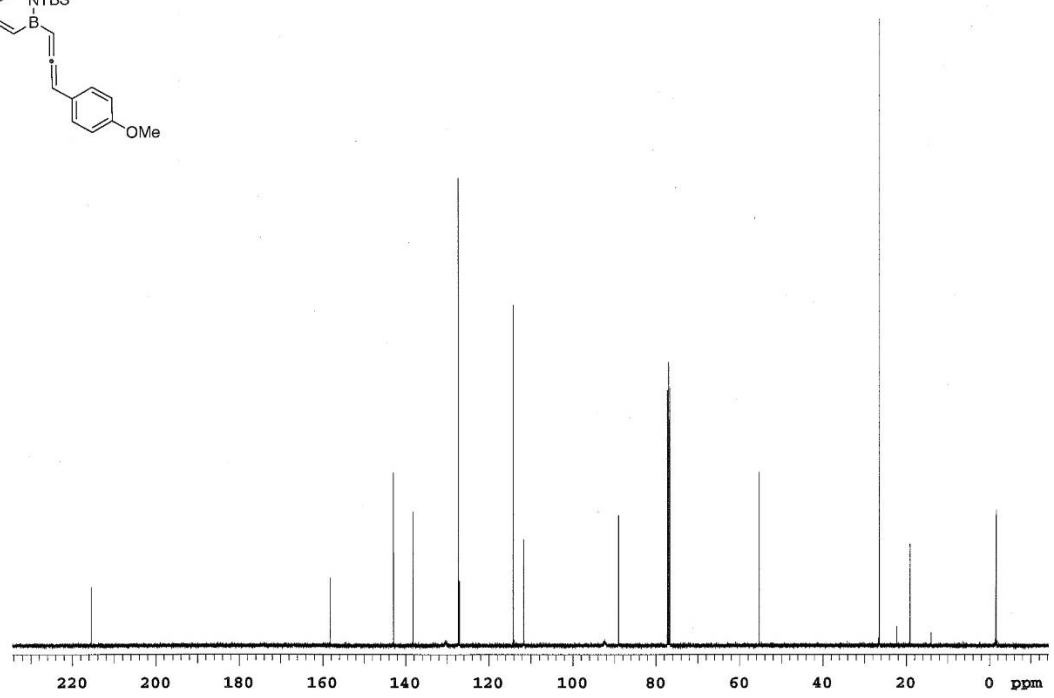
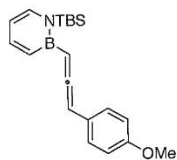
YL-03-OMe-col3-fr2-2

Sample Name YL-03-OMe-col3-fr2-2 Pulse sequence PROTON Temperature 25
 Date collected 2019-09-07 Solvent cdcl3 Spectrometer nmr18-vnmrs500 Study owner Liu
 Operator Liu



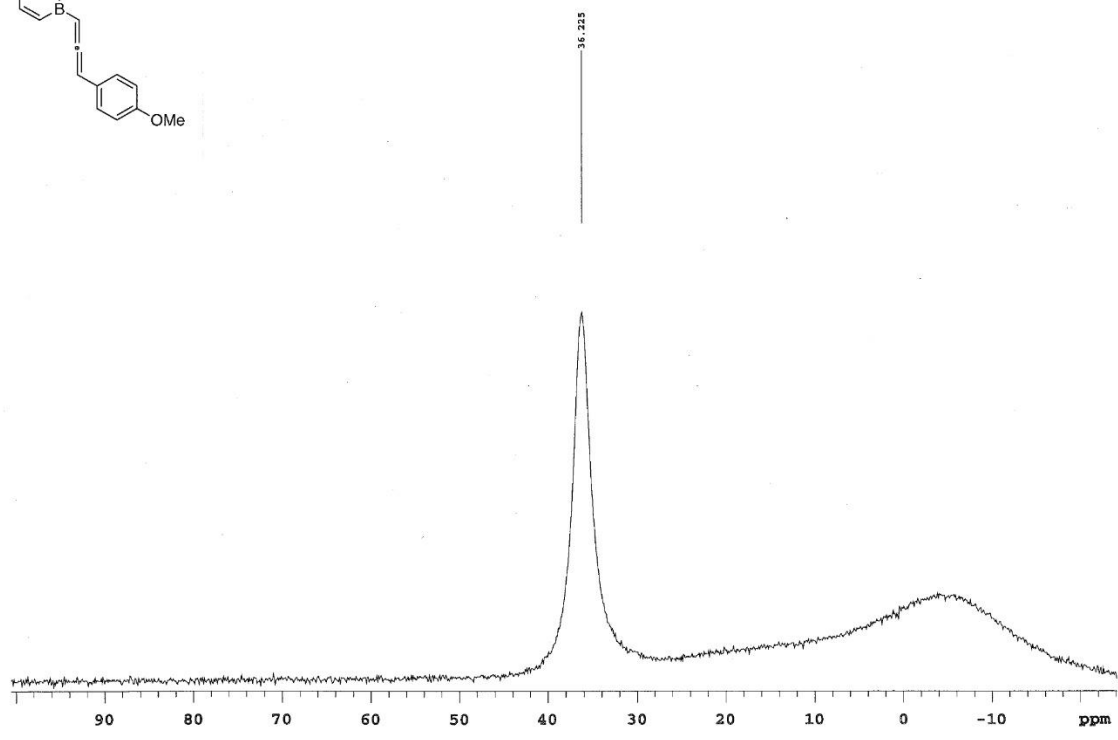
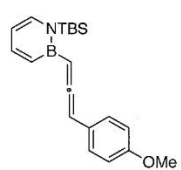
YL-03-allene-OMe-13C-pure

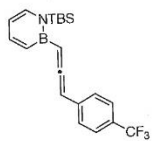
Sample Name YL-03-allene-OMe-13C-pure Pulse sequence CARBON Temperature 25
Date collected 2019-09-07 Solvent cdcl3 Spectrometer nmr16-vnmrs500 Study owner Liu
Operator Liu



YL-03-alleneOMe-pure-11B

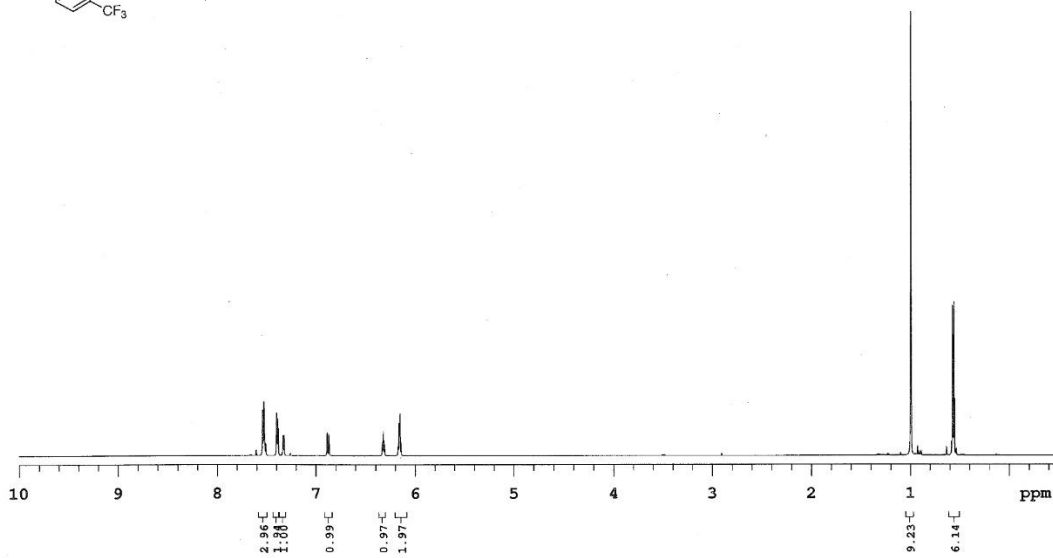
Sample Name YL-03-alleneOMe-pure-11B Pulse sequence s2pul Temperature 25
Date collected 2019-09-07 Solvent cdcl3 Spectrometer nmr11-inova500 Study owner Liu
Operator Liu





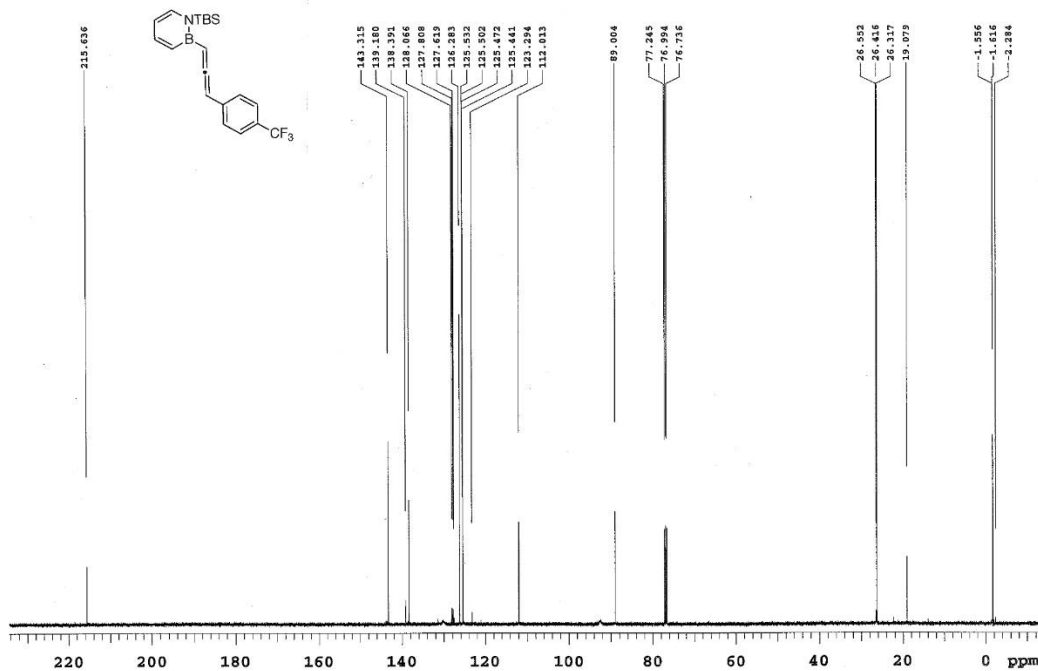
YL-03-CF3-co1-fr2-1H

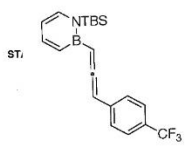
Sample Name: YL-03-CF3-co1-fr2-1H Pulse sequence: PROTON Temperature: 25 Study owner: Liu
 Date collected: 2019-09-12 Solvent: cdcl3 Spectrometer: nmr19-vnmrs600 Operator: Liu



YL-03-CF3-13C

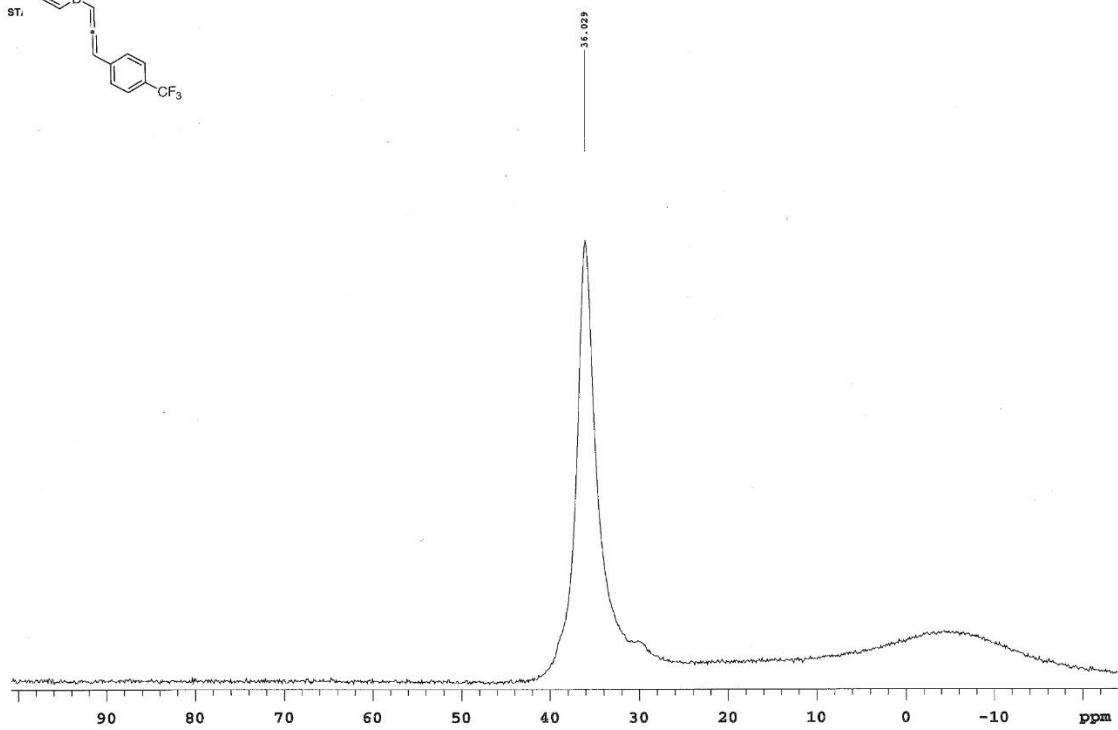
Sample Name: YL-03-CF3-13C Pulse sequence: CARBON Temperature: 25 Study owner: Liu
 Date collected: 2019-09-12 Solvent: cdcl3 Spectrometer: nmr19-vnmrs500 Operator: Liu





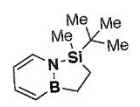
YL-03-CF3-11B

Sample Name: **YL-03-CF3-11B** Pulse sequence: **s2pul** Temperature: **25** Study owner: **Liu**
 Date collected: **2019-09-12** Solvent: **cdcl3** Spectrometer: **nmr11-inova500** Operator: **Liu**

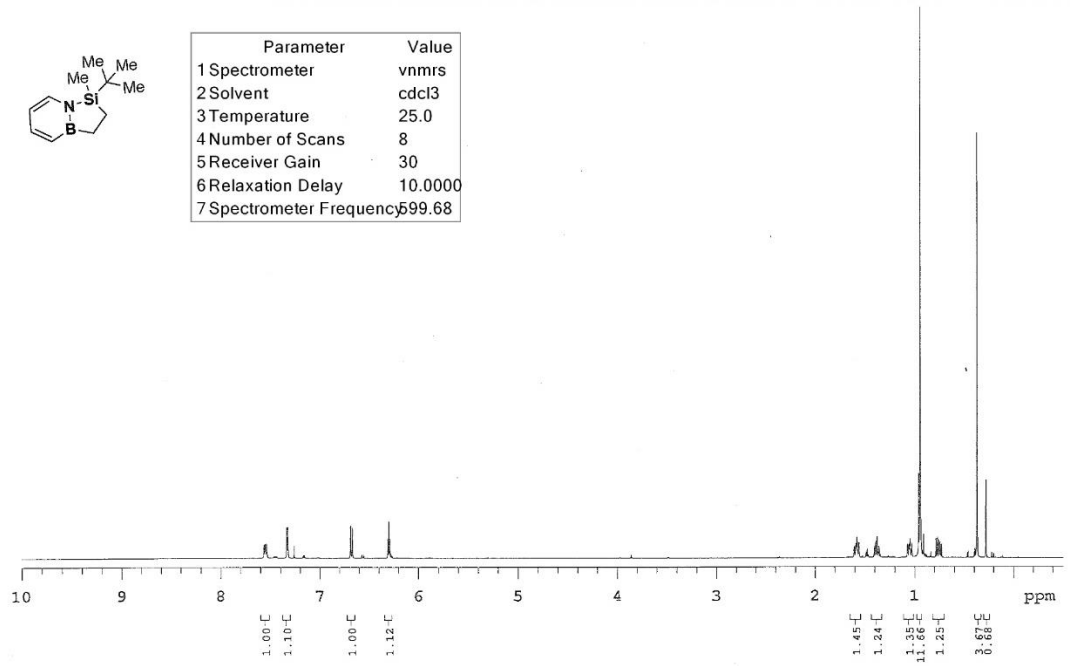


YL-03-internal-H-col2-fr2-1H

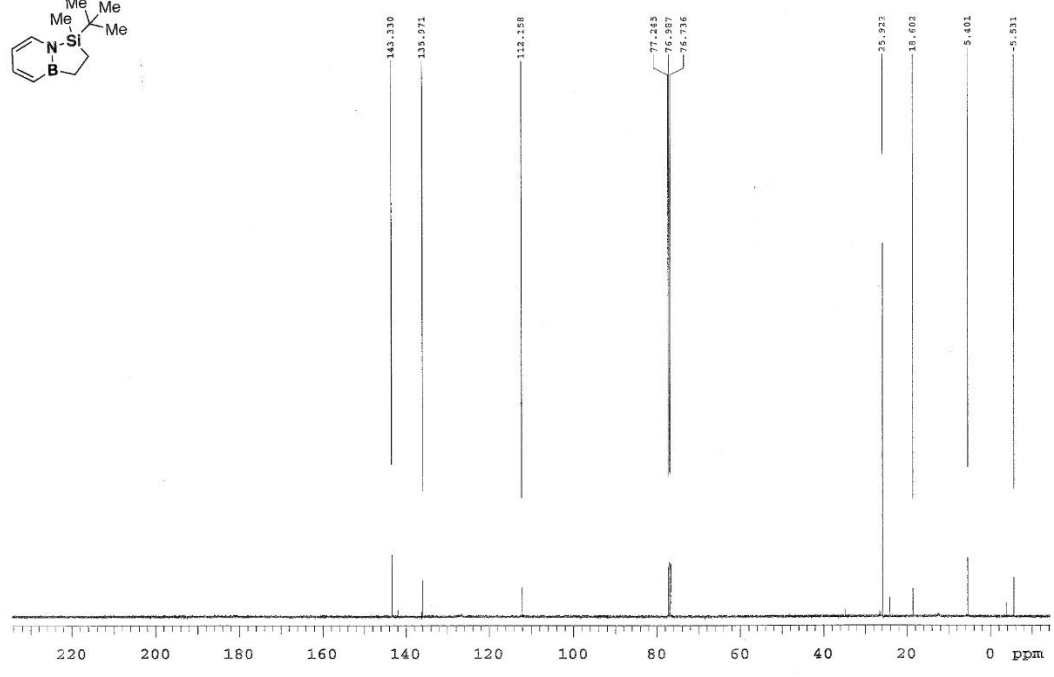
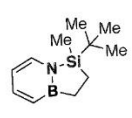
Sample Name: **YL-03-internal-H-col2-fr2-1H** Pulse sequence: **PROTON** Temperature: **25** Study owner: **Liu**
 Date collected: **2020-02-06** Solvent: **cdcl3** Spectrometer: **nmr19-vnmrs600** Operator: **Liu**



Parameter	Value
1 Spectrometer	vnmrs
2 Solvent	cdcl3
3 Temperature	25.0
4 Number of Scans	8
5 Receiver Gain	30
6 Relaxation Delay	10.0000
7 Spectrometer Frequency	599.68

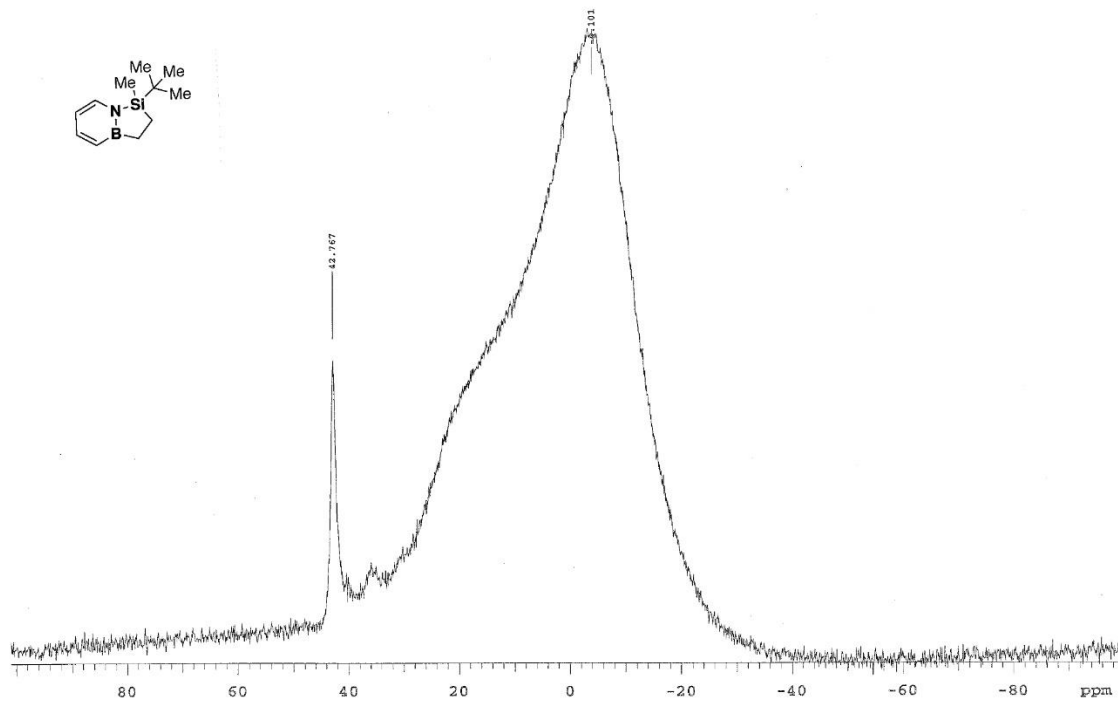
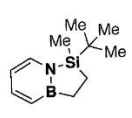


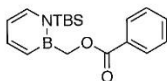
Sample Name: YL-03-internalCH-11B-pure
 Date Collected: 2020-02-06
 NMR Reference: CDCl3
 Temperature: 25
 Experiment: nmr18-vnmrs500
 Study Code: Liu
 Operator: Liu



YL-03-internalCH-11B-pure
 Sample Name: YL-03-internalCH-11B-pure
 Date Collected: 2020-02-06
 NMR Reference: CDCl3
 Temperature: 25
 Experiment: nmr11-inova500
 Study Code: Liu
 Operator: Liu

STANDARD PROTON PARAMETERS





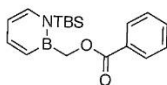
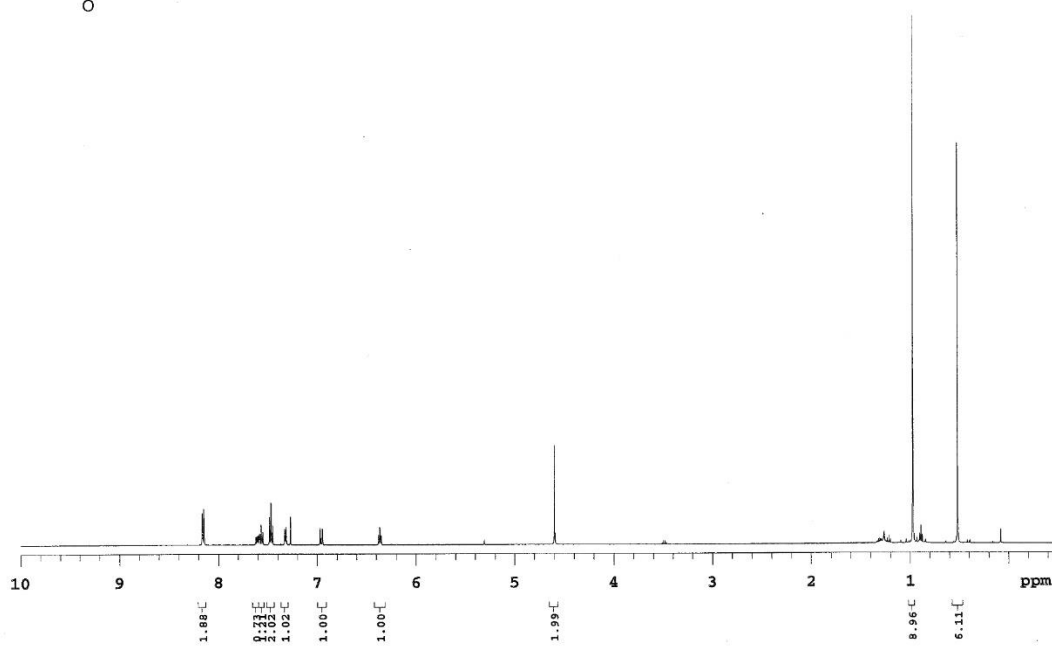
YL-03-benzoic ester-1H

Sample Name: YL-03-benzoic ester-1H
Date collected: 2019-08-08

Sample Acquired: PROTON
Solvent: cdcl3

Temperature: 25
Spectrometer: nmr18-vnmrs500

Study owner: Liu
Operator: Liu



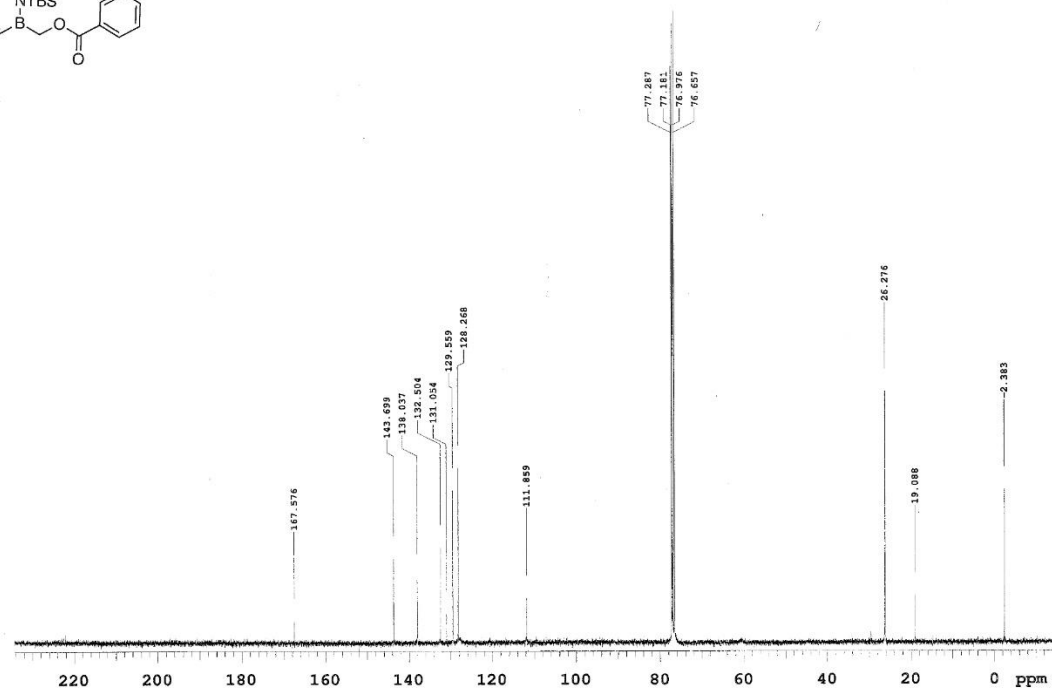
YL-03-benzoic acid-13C-pure

Sample Name: YL-03-benzoic acid-13C-pure
Date collected: 2019-08-09

Sample Acquired: CARBON
Solvent: cdcl3

Temperature: 25
Spectrometer: nmr14-vnmrs400

Study owner: Liu
Operator: Liu



YL-03-bezoicacidester-11B

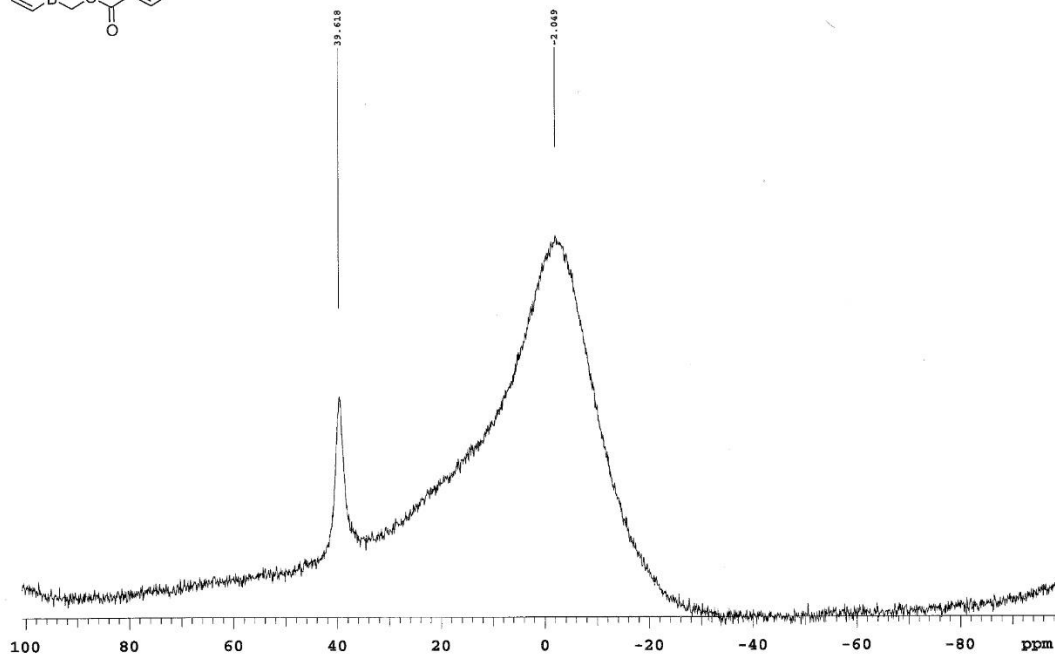
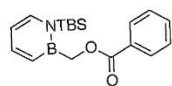
Sample Name YL-03-bezoicacidester-11B
Date collected 2019-08-08

7.000 sequence
Solvent cdc13

szpul

Temperature 25
Spectrometer nmr18-vnmrs500

Study owner Liu
Operator Liu



YL-03-brbenzoicacid-1H-col2-fr1

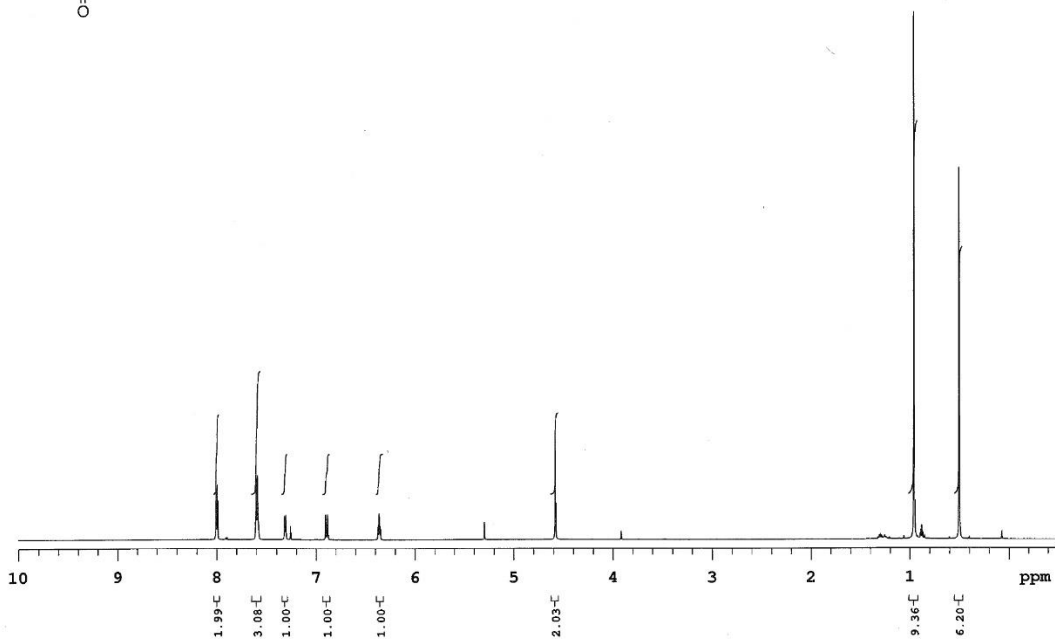
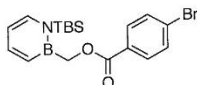
Sample Name YL-03-brbenzoicacid-1H-col2-fr1 sequence
Date collected 2019-08-24

7.000 sequence
Solvent cdc13

PROTON

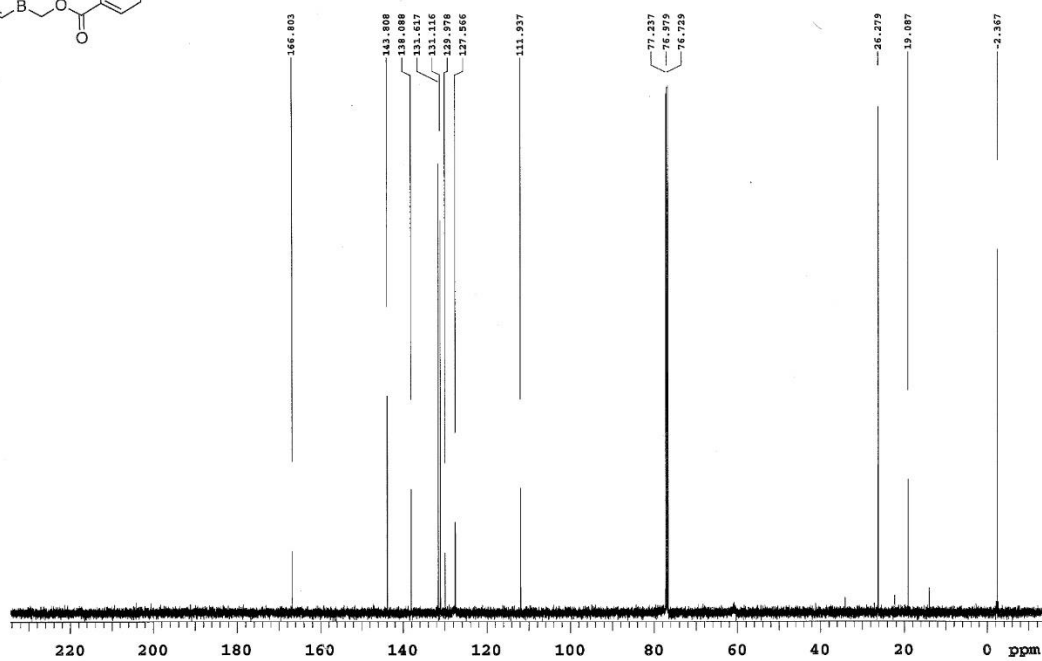
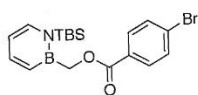
Temperature 25
Spectrometer nmr19-vnmrs500

Study owner Liu
Operator Liu



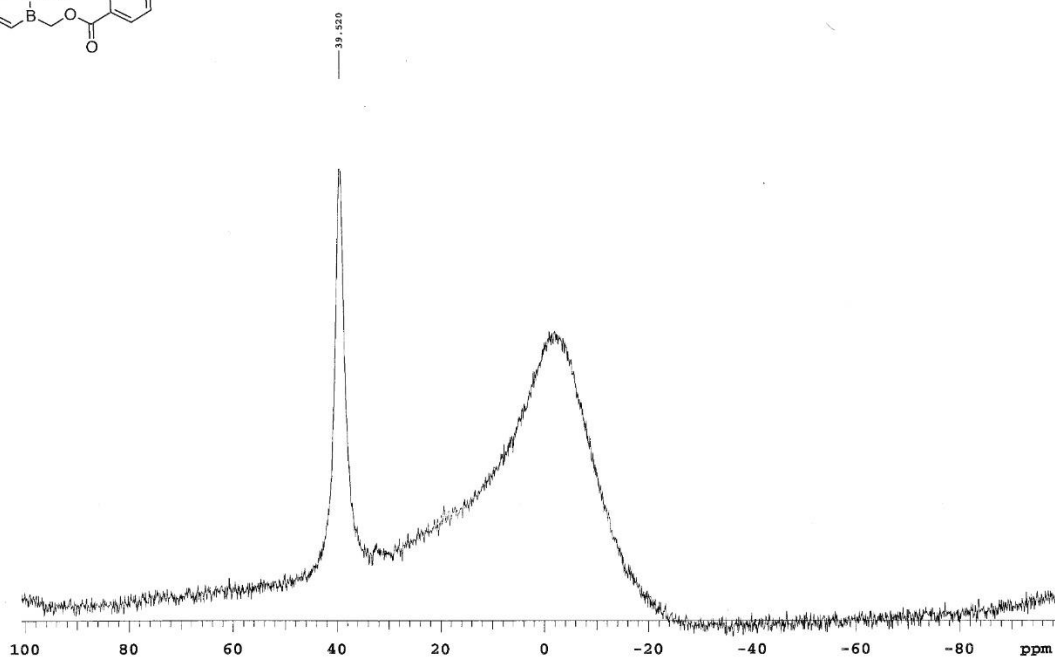
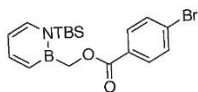
YL-03-brbenzoicacid-13C-pure

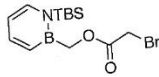
Sample Name: YL-03-brbenzoicacid-13C-pure
Date collected: 2019-08-24
Solvent: cdcl3
Temperature: 25
Spectrometer: nmr18-vnmrs500
Study owner: Liu
Operator: Liu



YL-03-Br-benzoicacid-fr2-coi-11B

Sample Name: YL-03-Br-benzoicacid-fr2-coi-11B
Date collected: 2019-08-17
Solvent: cdcl3
Temperature: 25
Spectrometer: nmr18-vnmrs500
Study owner: Liu
Operator: Liu





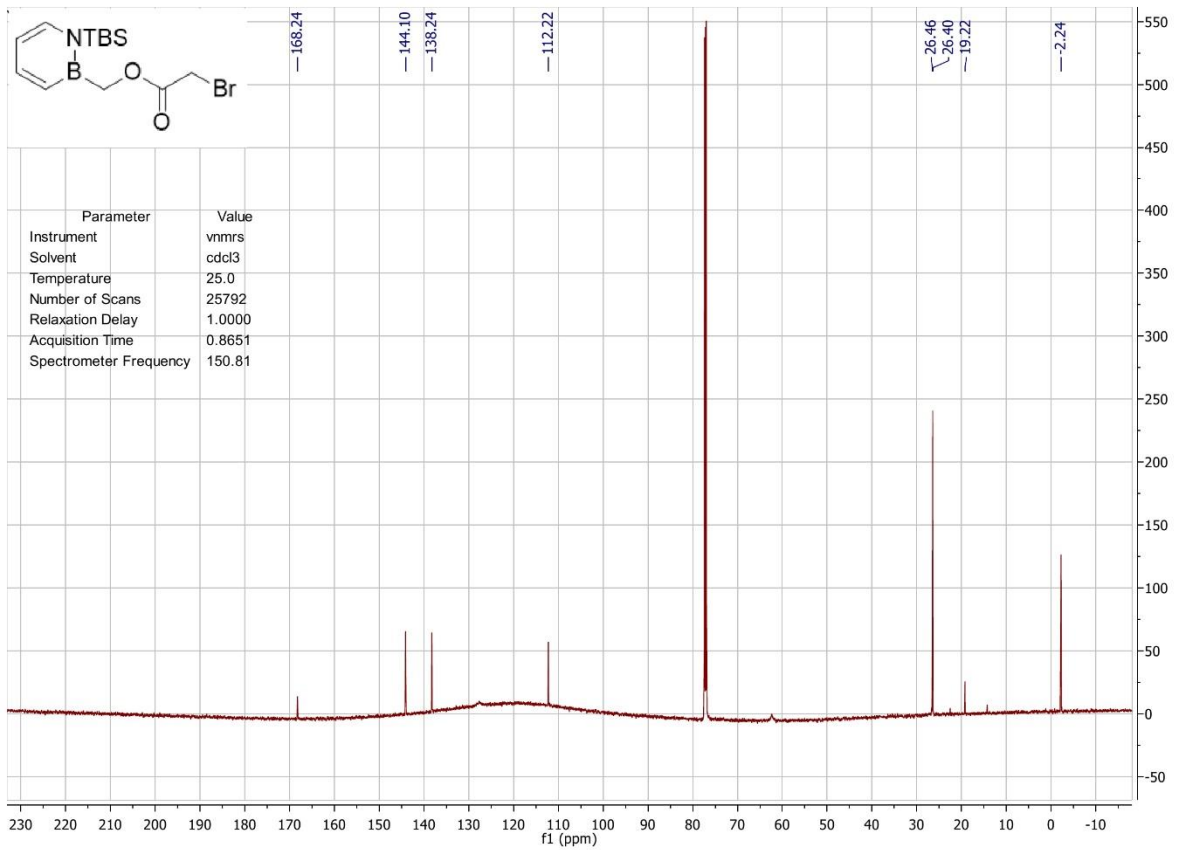
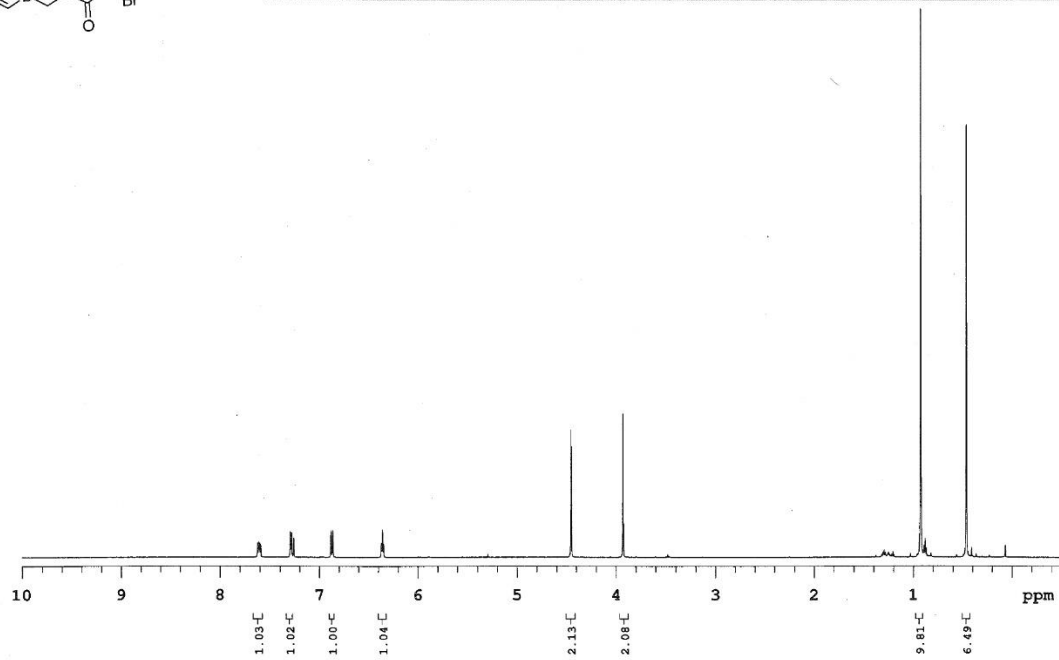
YL-03-BrAceticacid-1H-pure

Sample Name YL-03-BrAceticacid-1H-pure
Date collected 2019-09-10
Solvent cdcl3

PROTON

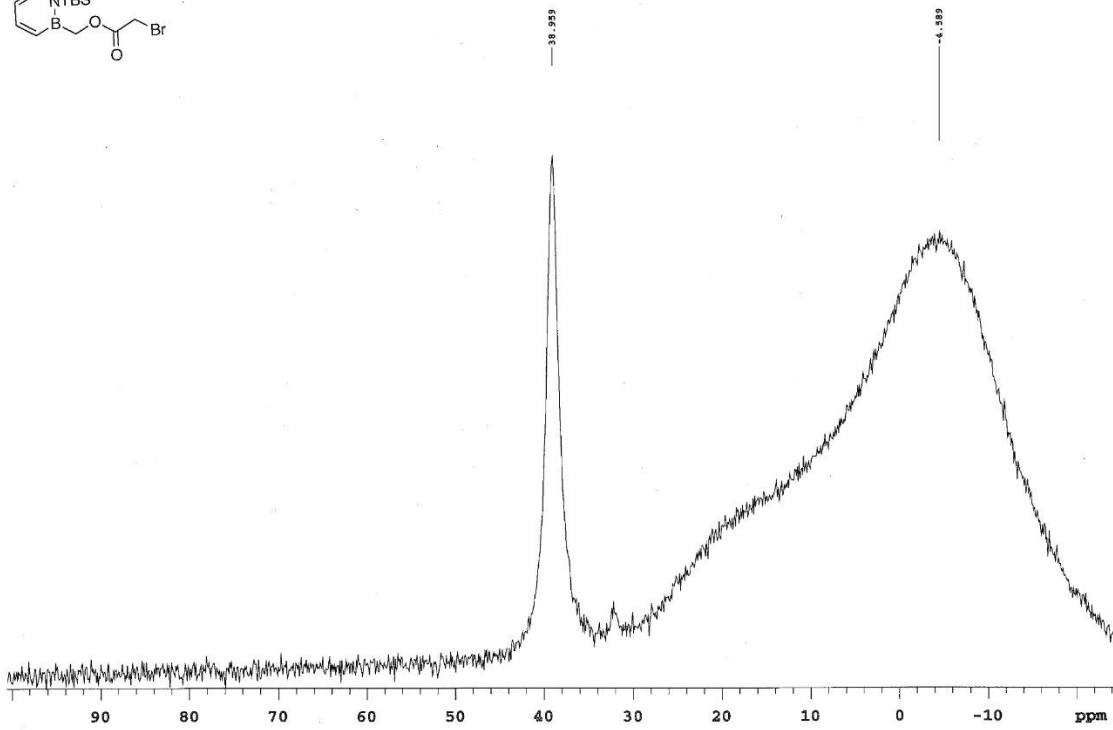
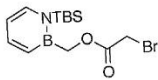
Temperature 25
Spectrometer nmr19-vnmrs600

Study owner Liu
Operator Liu



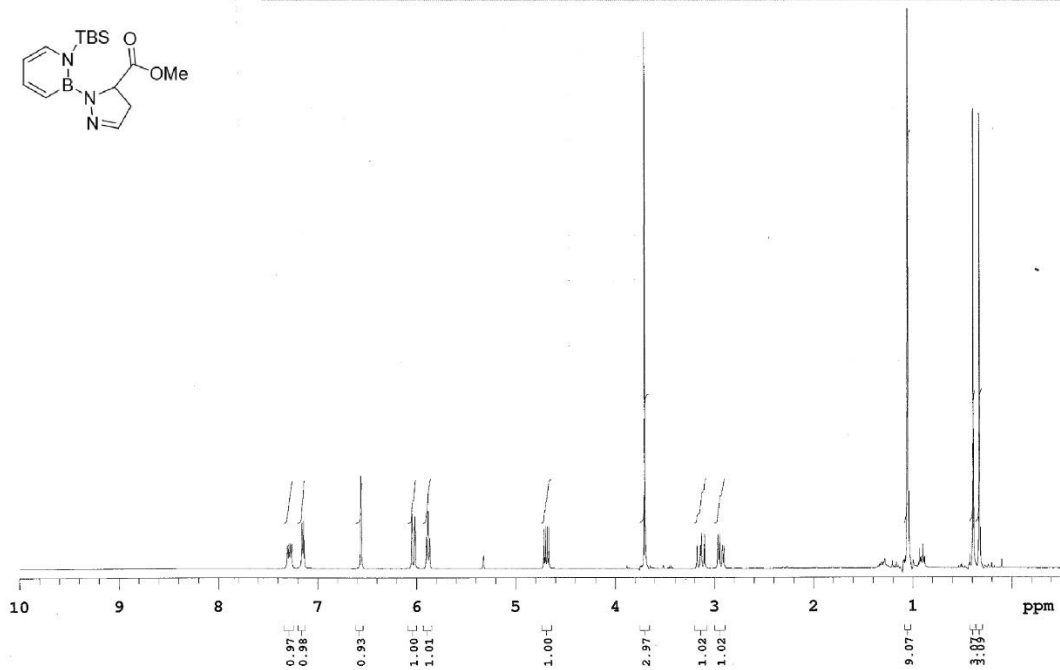
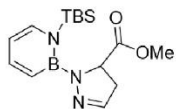
YL-03-braa-0_5hrs-col1-fr2-11B

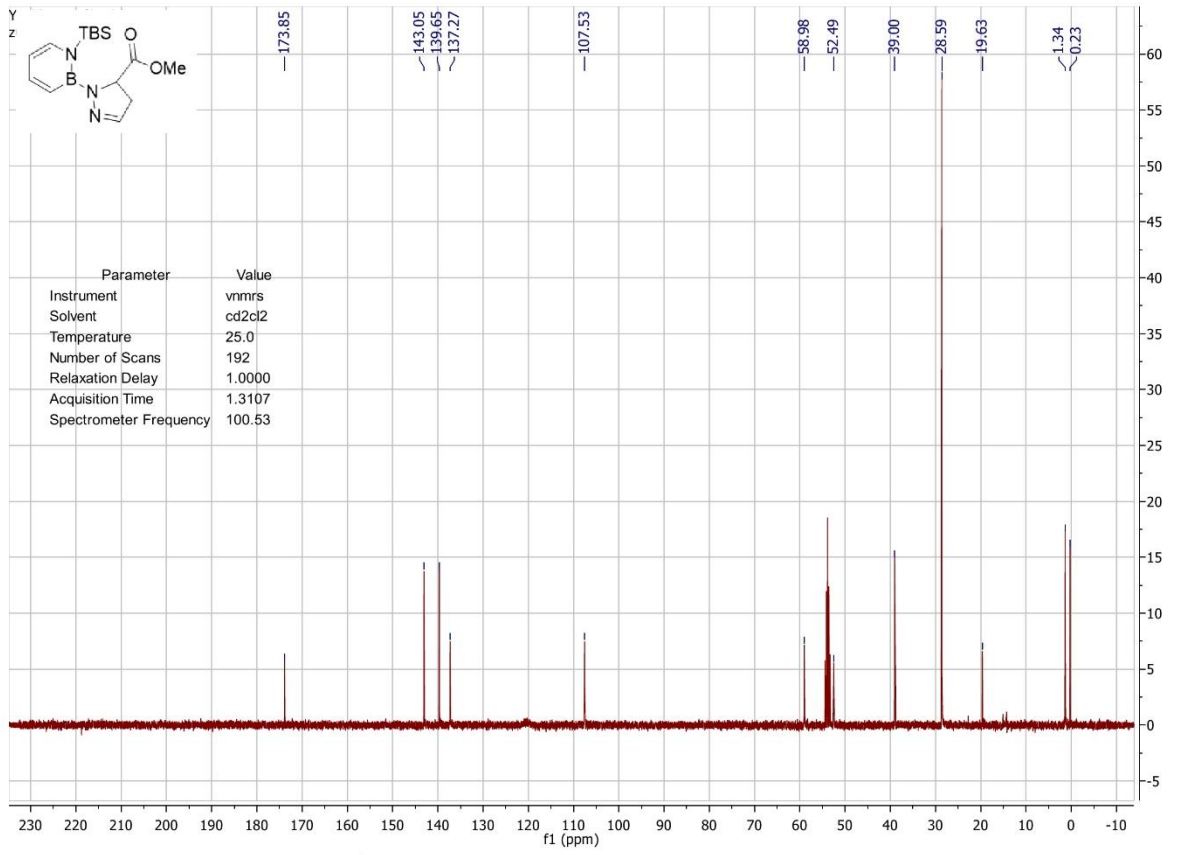
Sample Name YL-03-braa-0_5hrs-col1-fr2-11B; pulse sequence s2pul
Date collected 2019-09-09 Solvent cdcl3 Temperature 25 Spectrometer nmr11-inova500
Study owner Liu Operator Liu



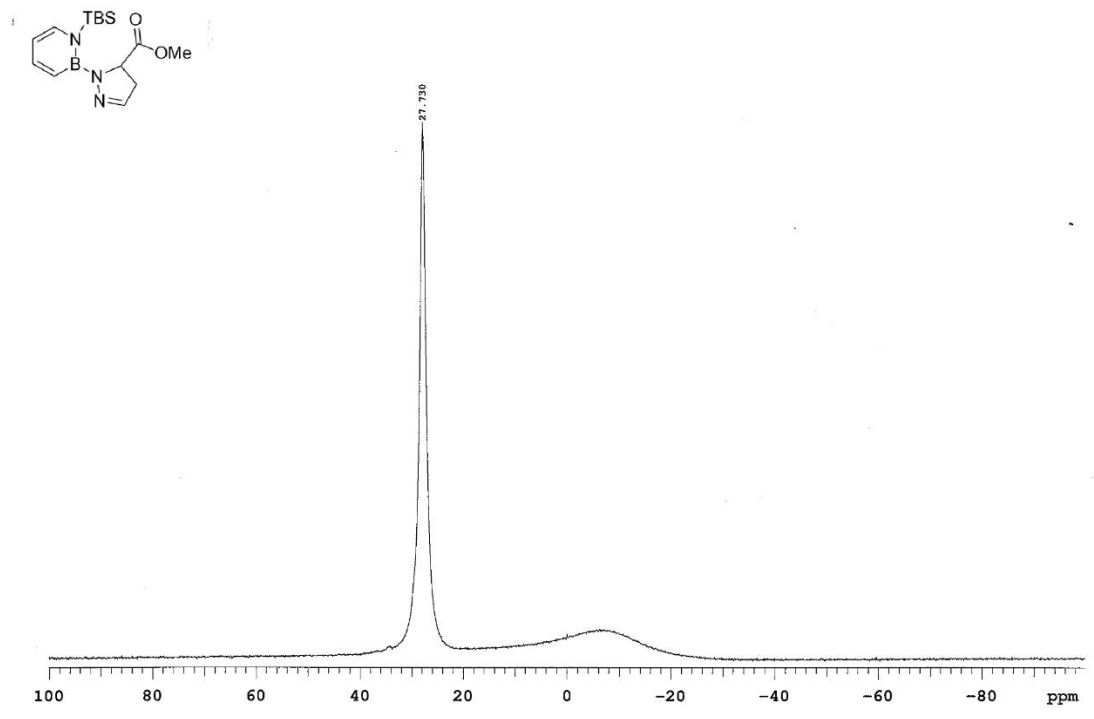
YL-03-11-col2-1H

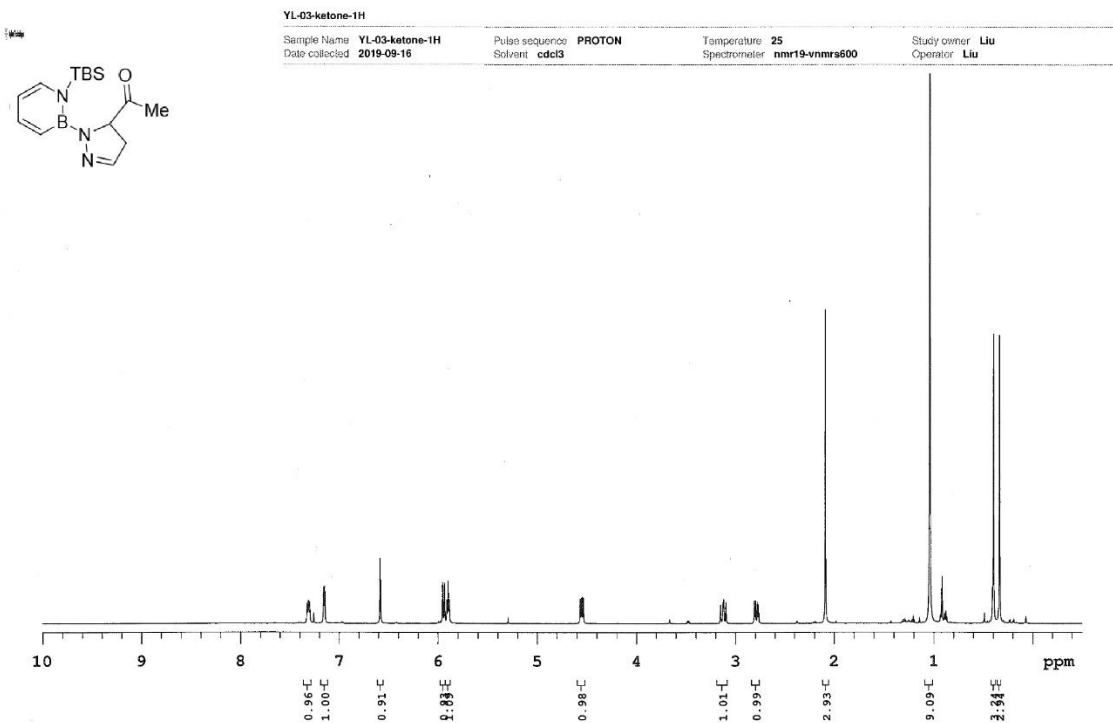
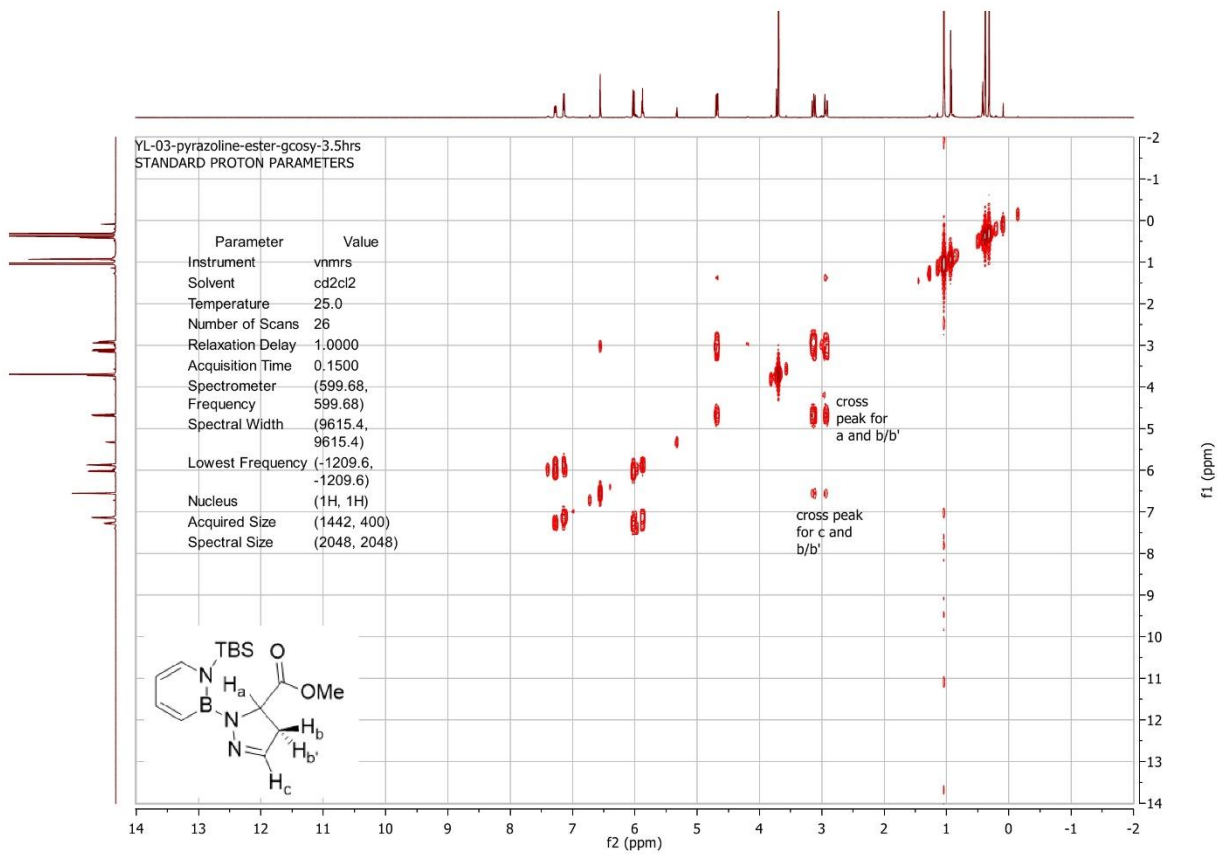
Sample Name YL-03-11-col2-1H Pulse sequence PROTON
Date collected 2019-01-23 Solvent cd2cl2 Temperature 25 Spectrometer nmr14-vnmrs400
Study owner Liu Operator Liu

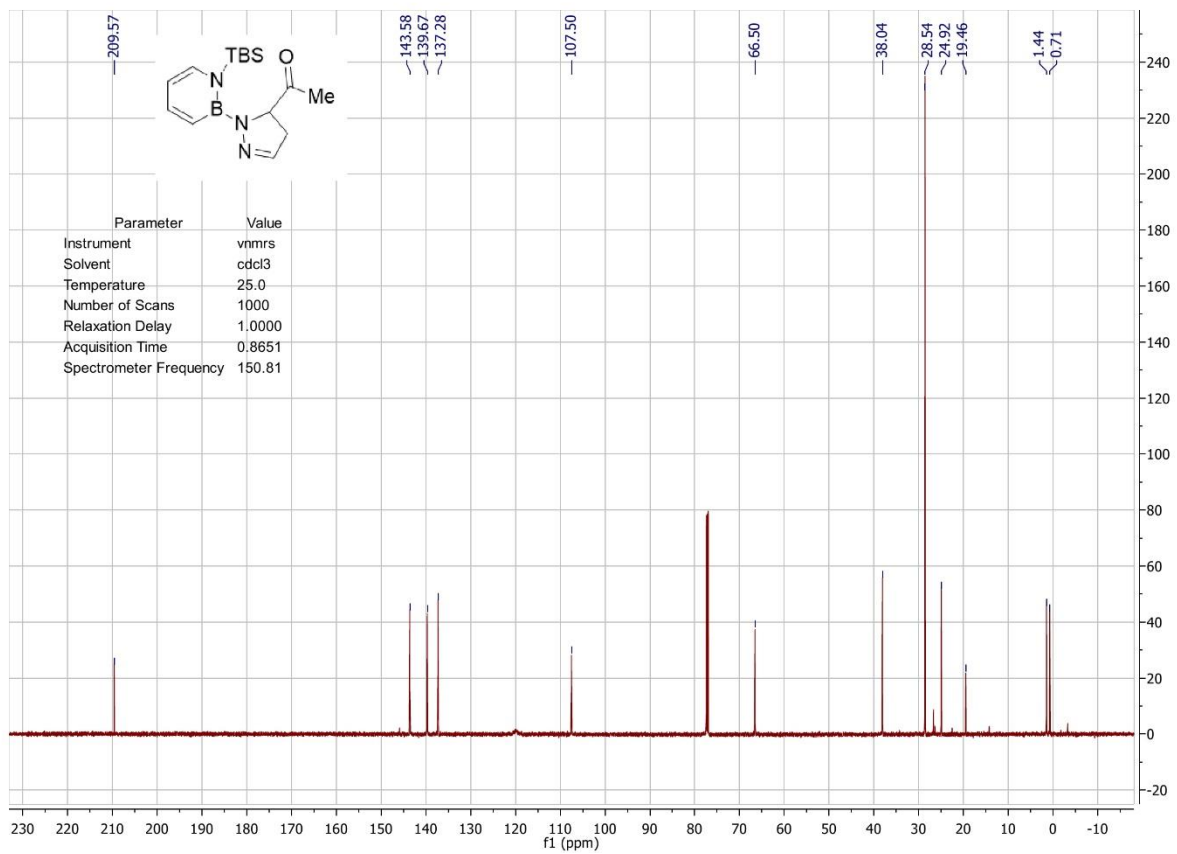




YL-03-11-11B
 Sample Name: YL-03-11-11B Pulse sequence: s2pul Temperature: 25 Study owner: Liu
 Date collected: 2019-01-23 Solvent: cd2cl2 Spectrometer: nmr11-nova500 Operator: Liu

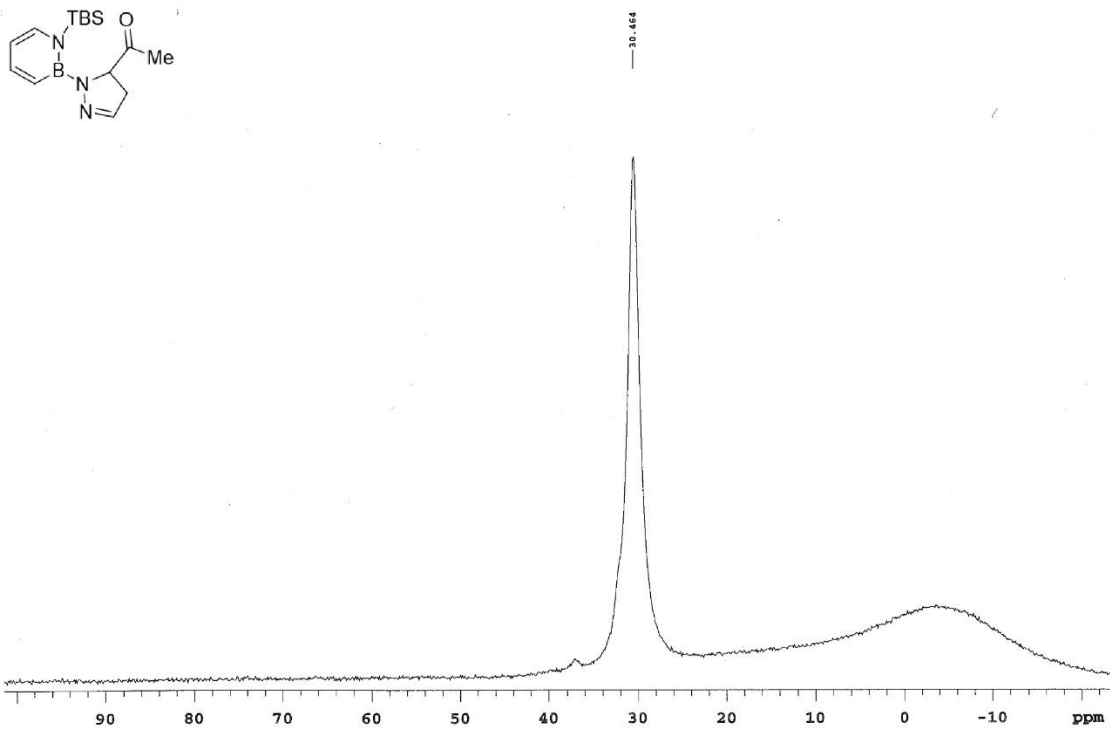






YL-03-ketone-col1-fr2-11B

Sample Name: YL-03-ketone-col1-fr2-11B Pulse sequence: s2pul Temperature: 25 Study owner: Liu
 Date collected: 2019-09-14 Solvent: cdcl3 Spectrometer: nmr11-inova500 Operator: Liu



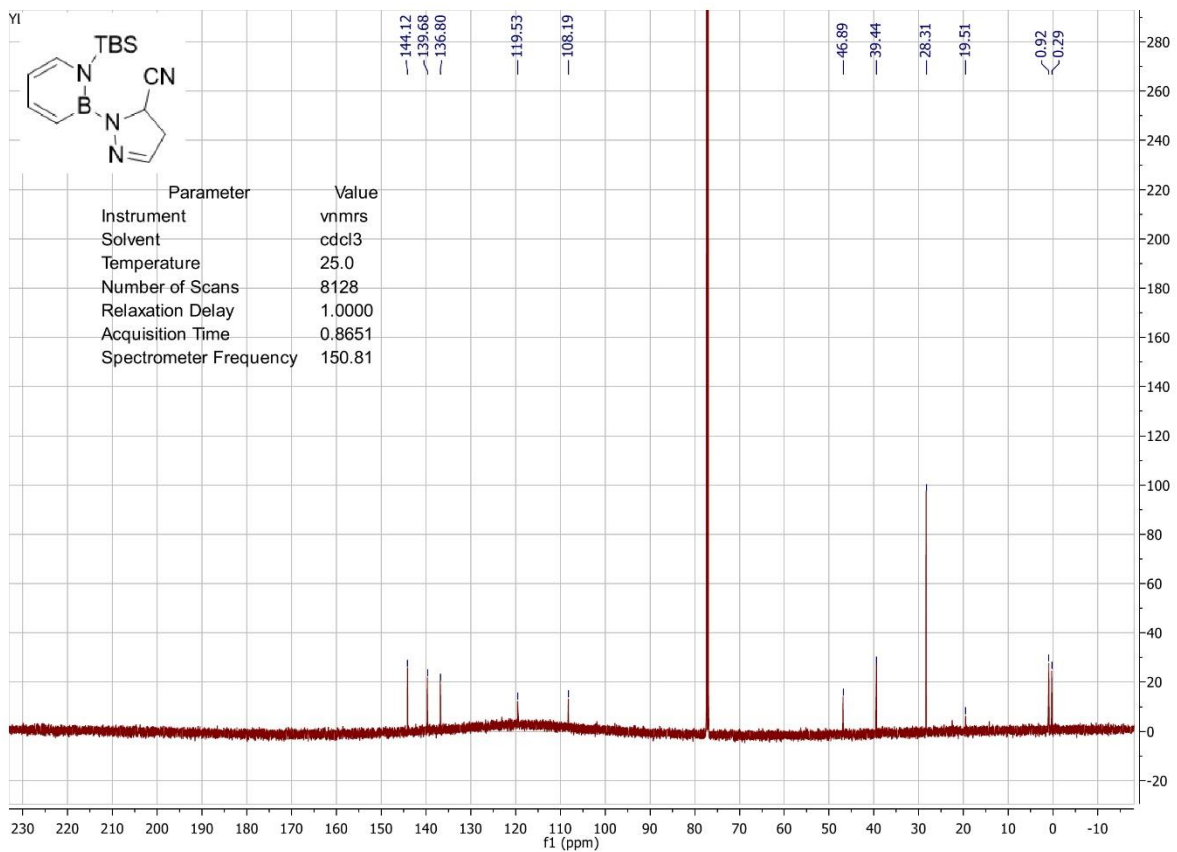
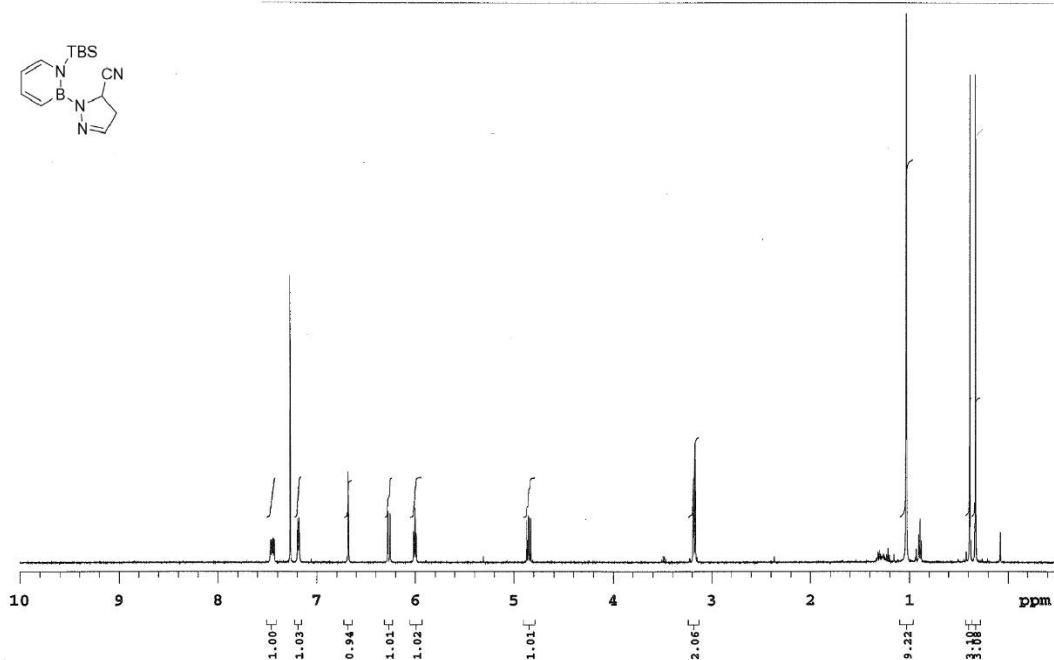
YL-03-CN-co3-fr2-1H

Sample Name YL-03-CN-co3-fr2-1H
Date collected 2019-06-22

Pulse sequence PROTON
Solvent cdcl3

Temperature 25
Spectrometer nmr18-vnmrs500

Study owner Liu
Operator Liu



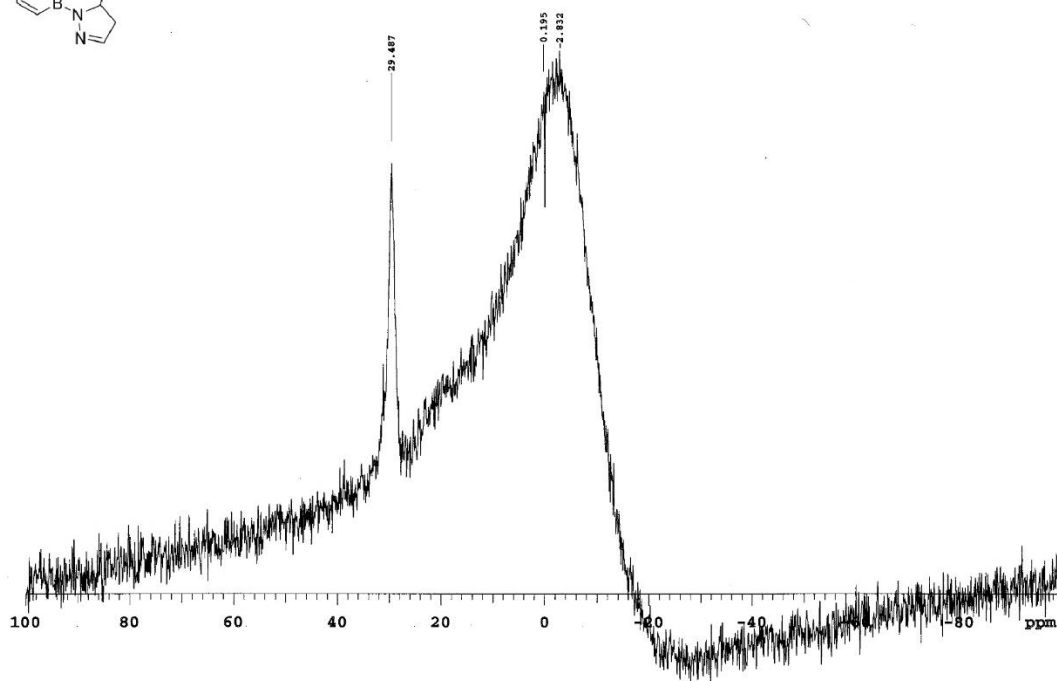
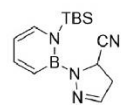
YL-03-CN-col2-fr1-11B

Sample Name YL-03-CN-col2-fr1-11B
Date collected 2019-09-22

Pulse sequence s2pul
Solvent cdcl3

Temperature 25
Spectrometer nmr11-inova500

Study owner Liu
Operator Liu



YL-03-33-col-spot1-1H

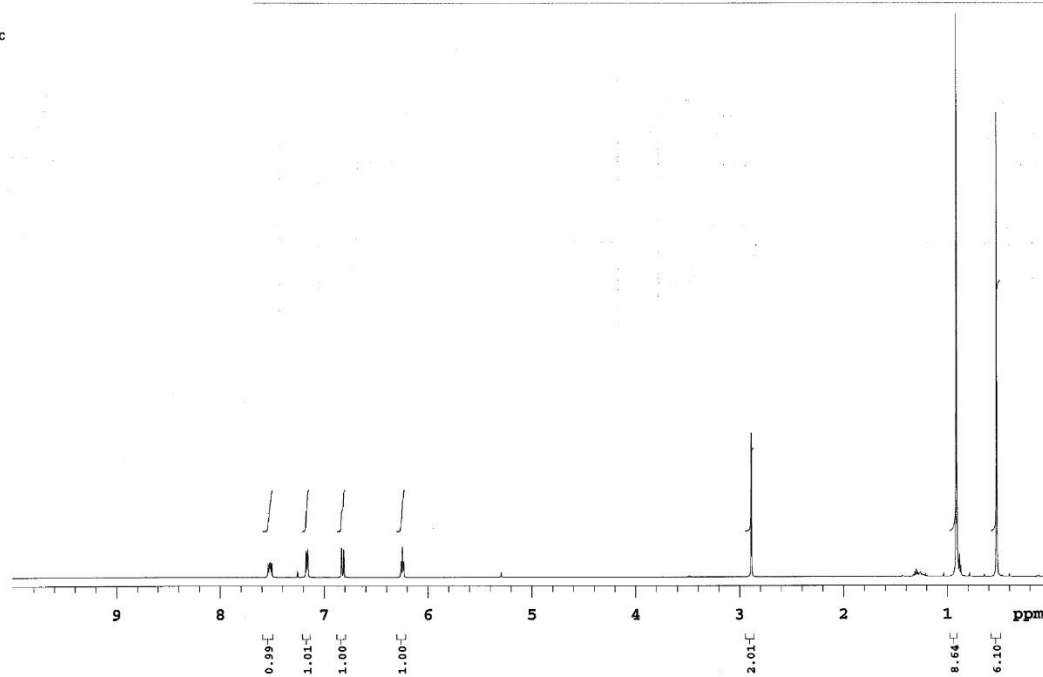
Sample Name YL-03-33-col-spot1-1H
Date collected 2019-03-29

Pulse sequence PROTON
Solvent cdcl3

Temperature 25
Spectrometer nmr16-vnmrs500

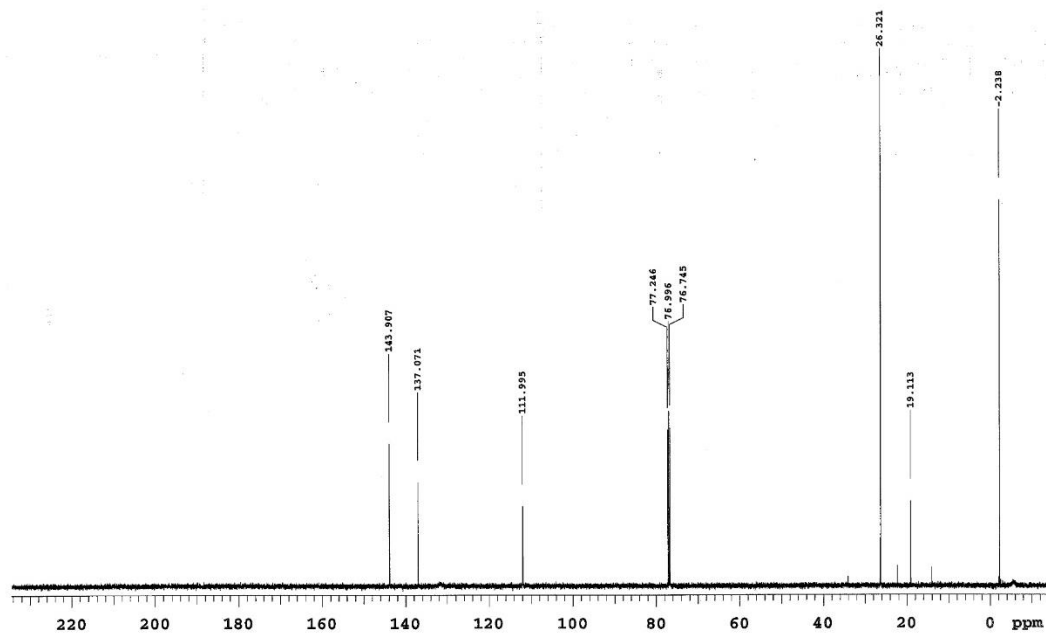
Study owner Liu
Operator Liu

125oC



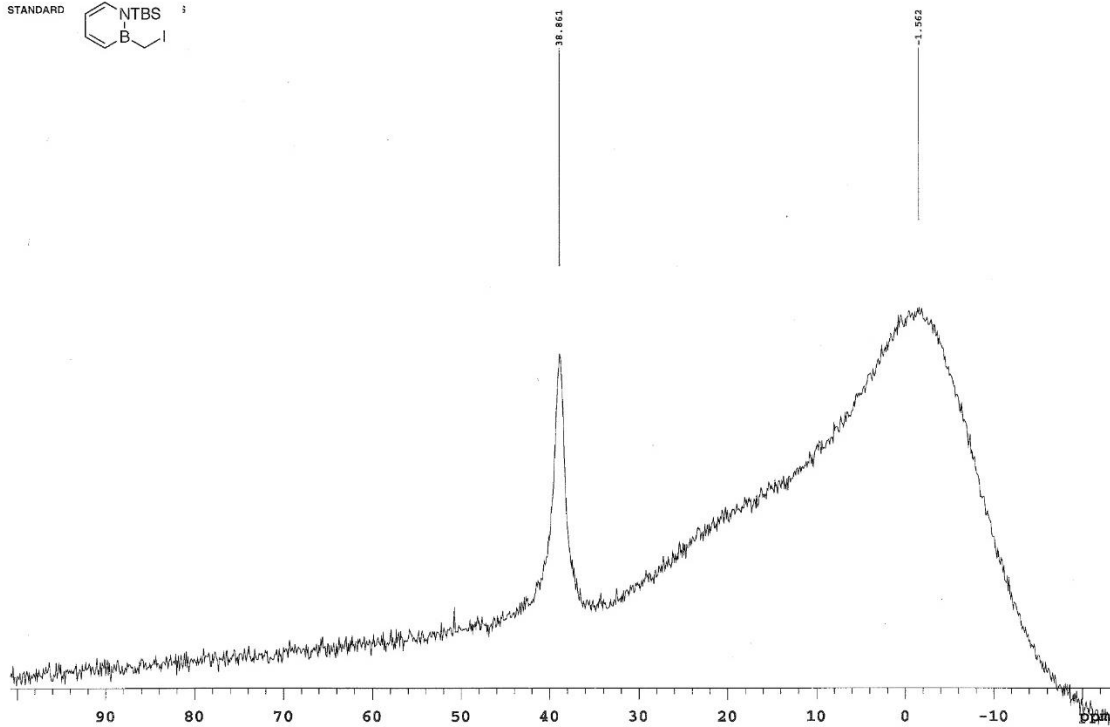
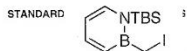
YL-03-33-col-spot1-13C

Sample Name YL-03-33-col-spot1-13C Pulse sequence CARBON Temperature 25
Date collected 2019-03-29 Solvent cdcl3 Spectrometer nmr18-vnmr500 Study owner Liu
Operator Liu



YL-03-iodo-11B-col

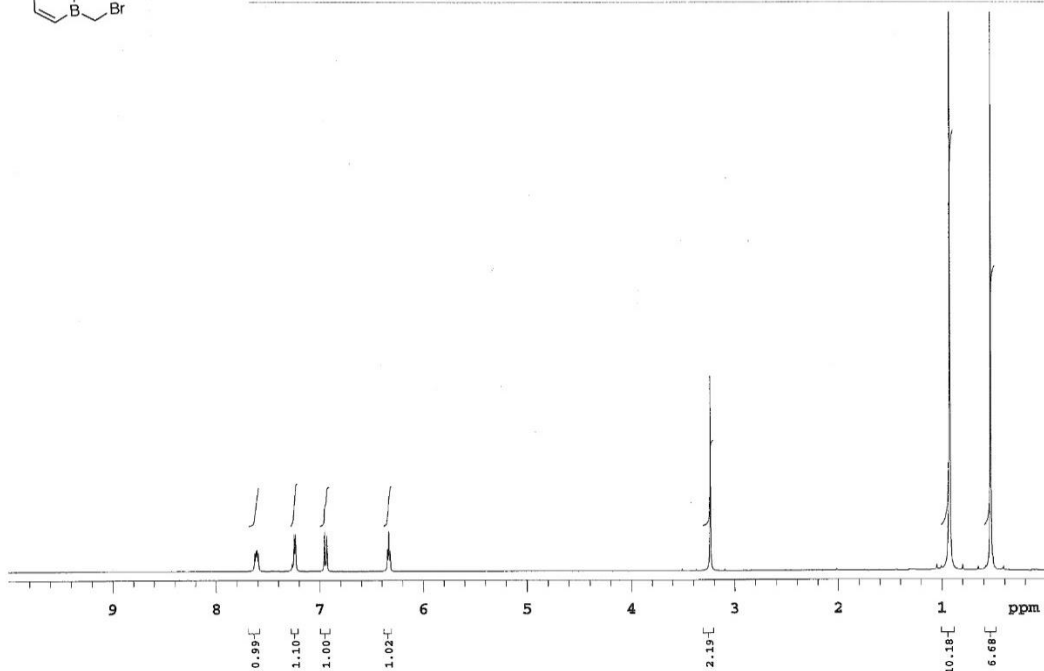
Sample Name YL-03-iodo-11B-col Pulse sequence s2pul Temperature 25
Date collected 2019-07-19 Solvent cdcl3 Spectrometer nmr11-inova500 Study owner Liu
Operator Liu





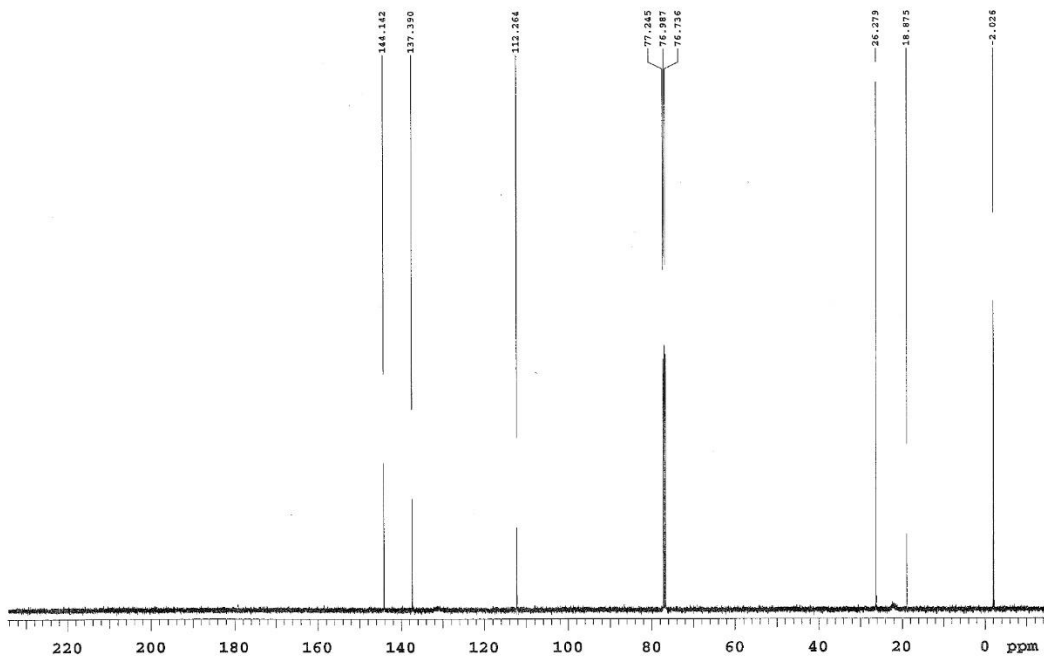
YL-03-BmethyleneBr-1H-charact

Sample Name YL-03-BmethyleneBr-1H-charact Sequence PROTON Temperature 25
Date collected 2019-10-31 Solvent cdcl3 Spectrometer nmr18-vnmrs500 Study owner Liu
Operator Liu



YL-03-BmethyleneBr-13C-charact

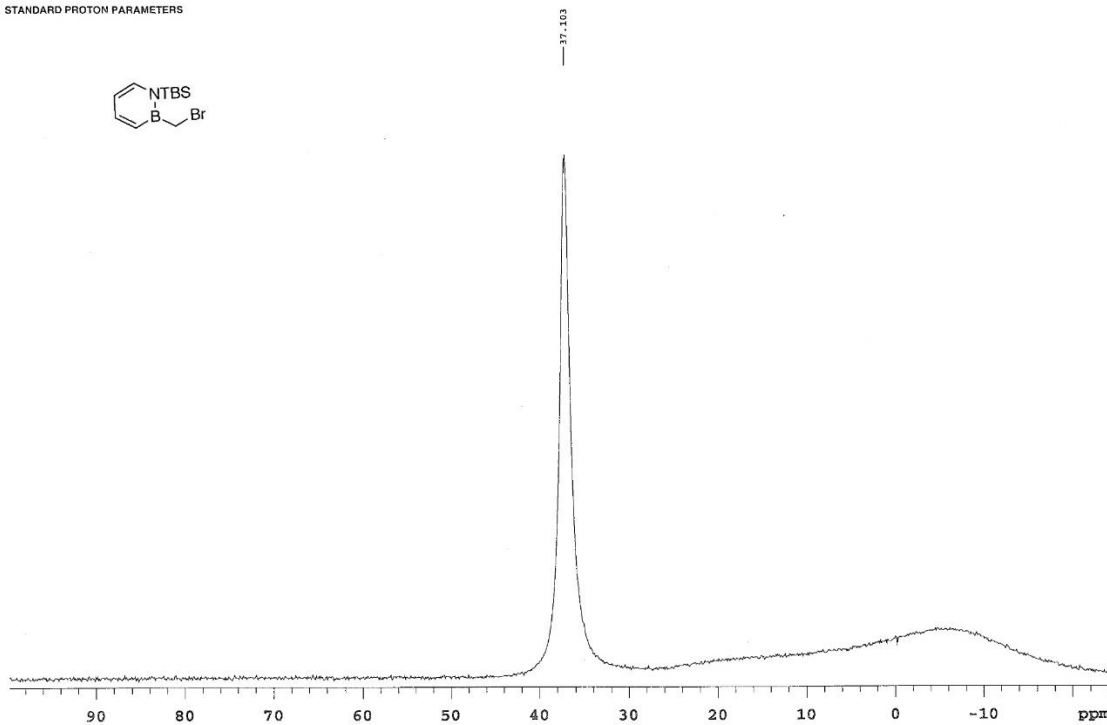
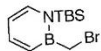
Sample Name YL-03-BmethyleneBr-13C-charact Sequence CARBON Temperature 25
Date collected 2019-10-31 Solvent cdcl3 Spectrometer nmr18-vnmrs500 Study owner Liu
Operator Liu



YL-03-Bmethylene-11B-charact

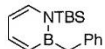
Sample Name: YL-03-Bmethylene-11B-character sequence s2pul Temperature: 25
 Date collected: 2019-10-31 Solvent: cdcl3 Spectrometer: nmr11-inova500 Operator: Liu

STANDARD PROTON PARAMETERS

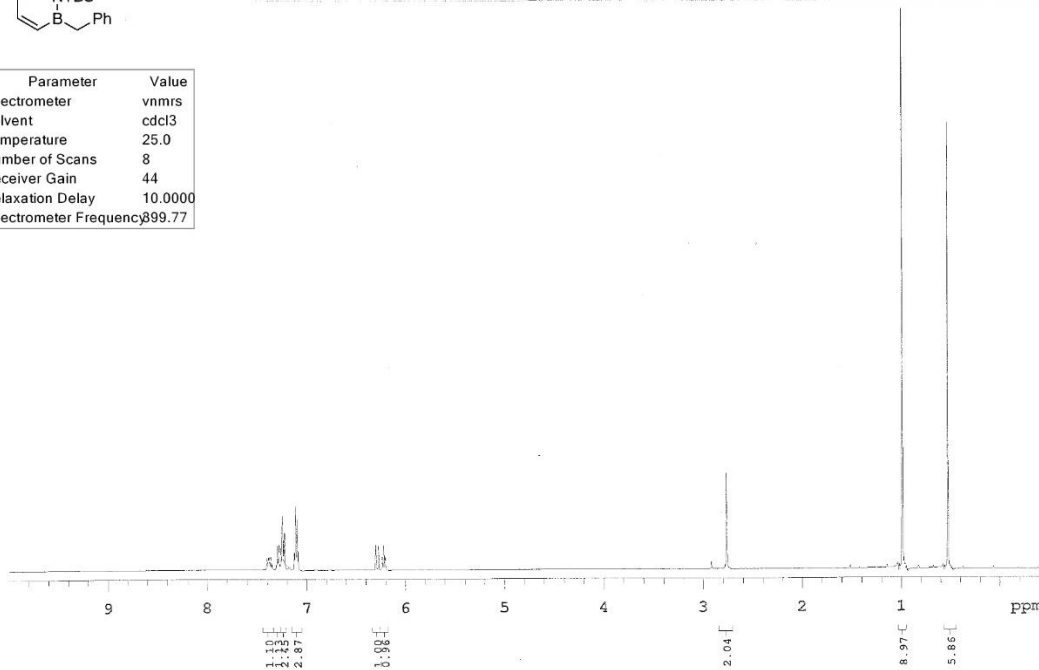


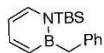
YL-03-suzuki-Ph-1H-pure

Sample Name: YL-03-suzuki-Ph-1H-pure Pulse sequence: PROTON Temperature: 25
 Date collected: 2020-02-06 Solvent: cdcl3 Spectrometer: nmr14-vnmrs400 Operator: Liu



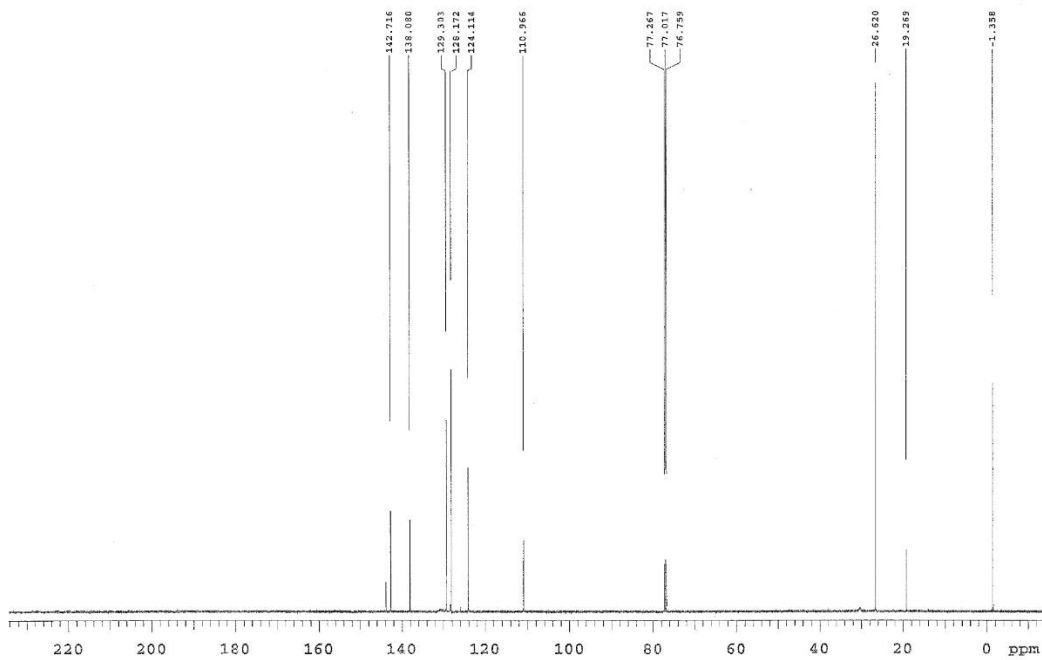
Parameter	Value
1 Spectrometer	vnmrs
2 Solvent	cdcl3
3 Temperature	25.0
4 Number of Scans	8
5 Receiver Gain	44
6 Relaxation Delay	10.0000
7 Spectrometer Frequency	399.77





YL-03-phenyl-suzuki-1H-pure

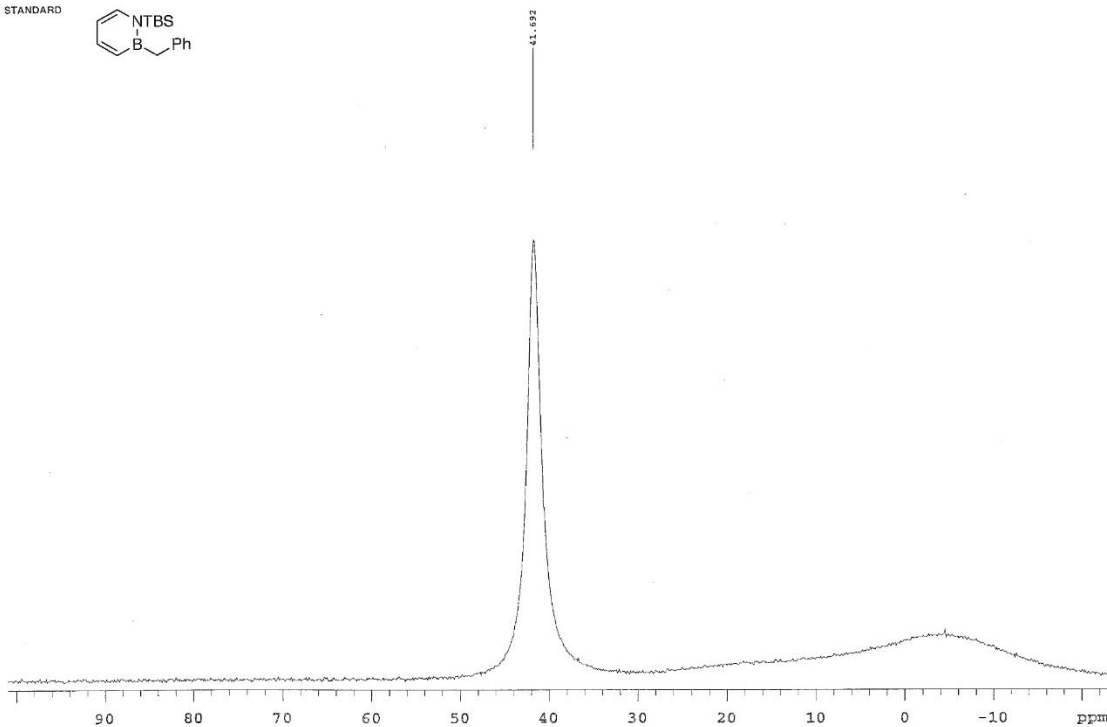
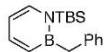
Sample Name: YL-03-phenyl-suzuki-1H-pure
 Date Collected: 2020-01-07
 Solvent: cdcl3
 Temperature: 25
 Spectrometer: nmr18-vnmrs500
 Study: Liu
 Operator: Liu

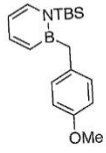


YL-03-phenyl-suzuki-11B-pure

Sample Name: YL-03-phenyl-suzuki-11B-pure
 Date Collected: 2020-01-07
 Solvent: cdcl3
 Temperature: 25
 Spectrometer: nmr11-inova500
 Study: Liu
 Operator: Liu

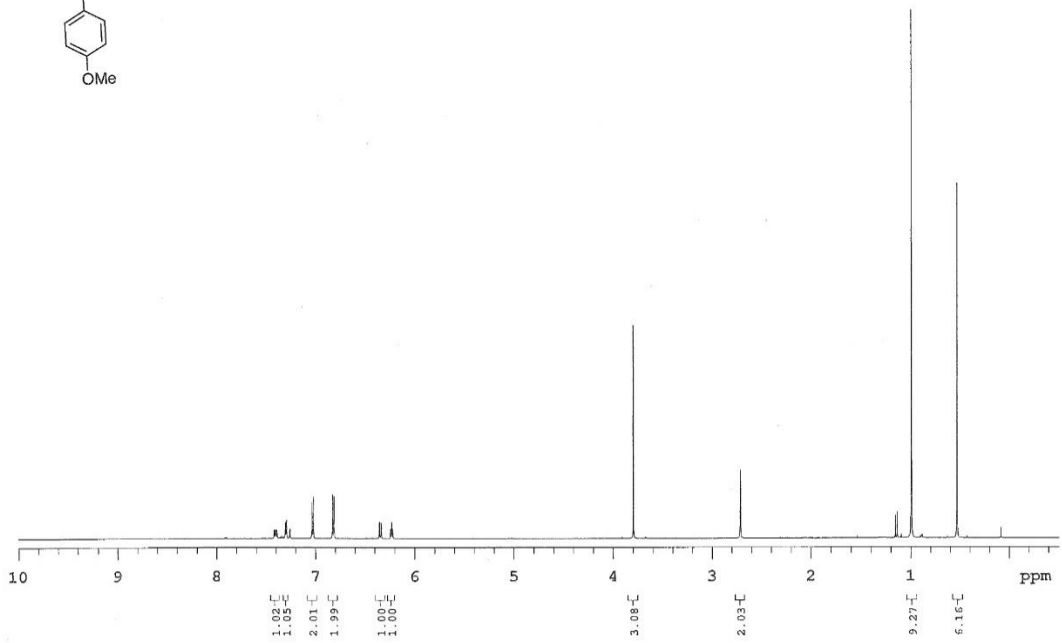
STANDARD



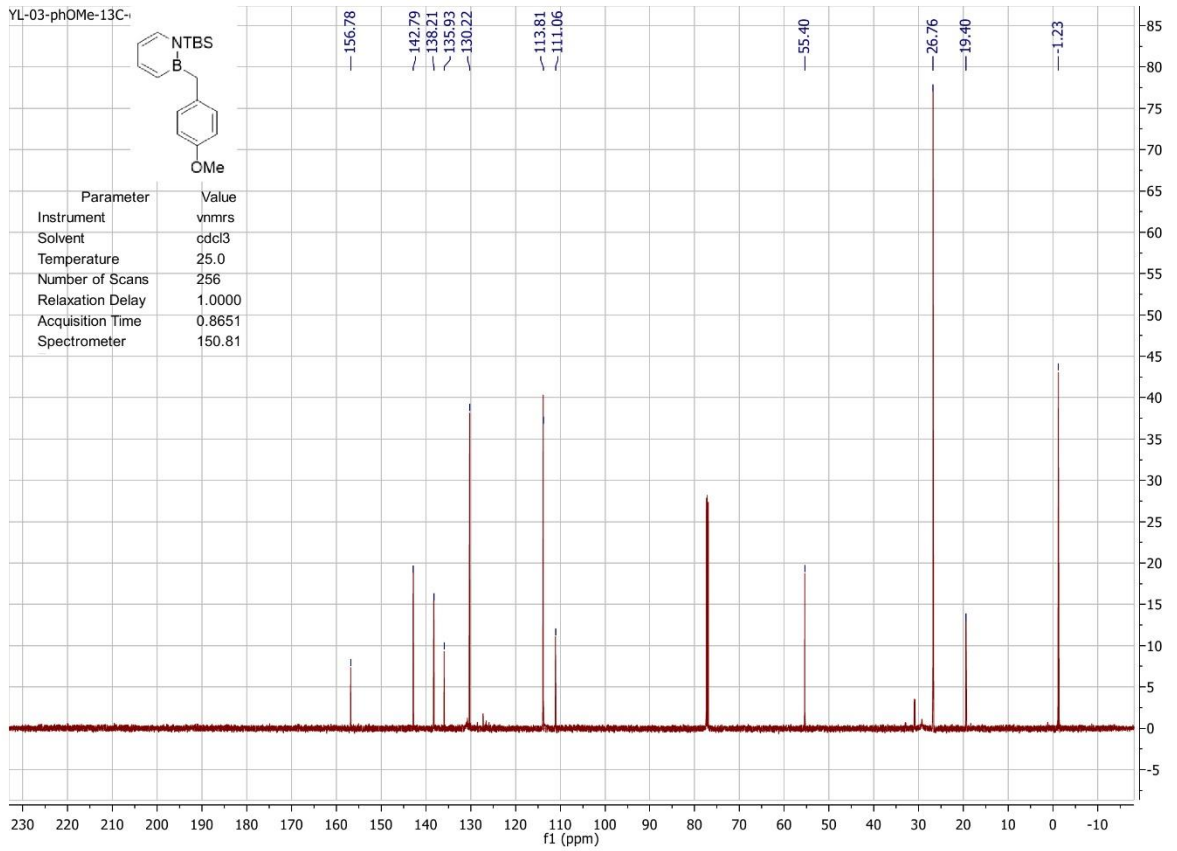
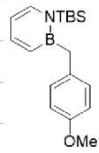


YL-03-phOMe-1H-co2

Sample Name: YL-03-phOMe-1H-co2
 Date collected: 2020-01-13
 Pulse sequence: PROTON
 Solvent: cdcl3
 Temperature: 25
 Spectrometer: nmr19-vnmrs600
 Study owner: Liu
 Operator: Liu

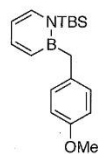


YL-03-phOMe-13C-



Parameter	Value
Instrument	vnmrs
Solvent	cdcl3
Temperature	25.0
Number of Scans	256
Relaxation Delay	1.0000
Acquisition Time	0.8651
Spectrometer	150.81

STAT



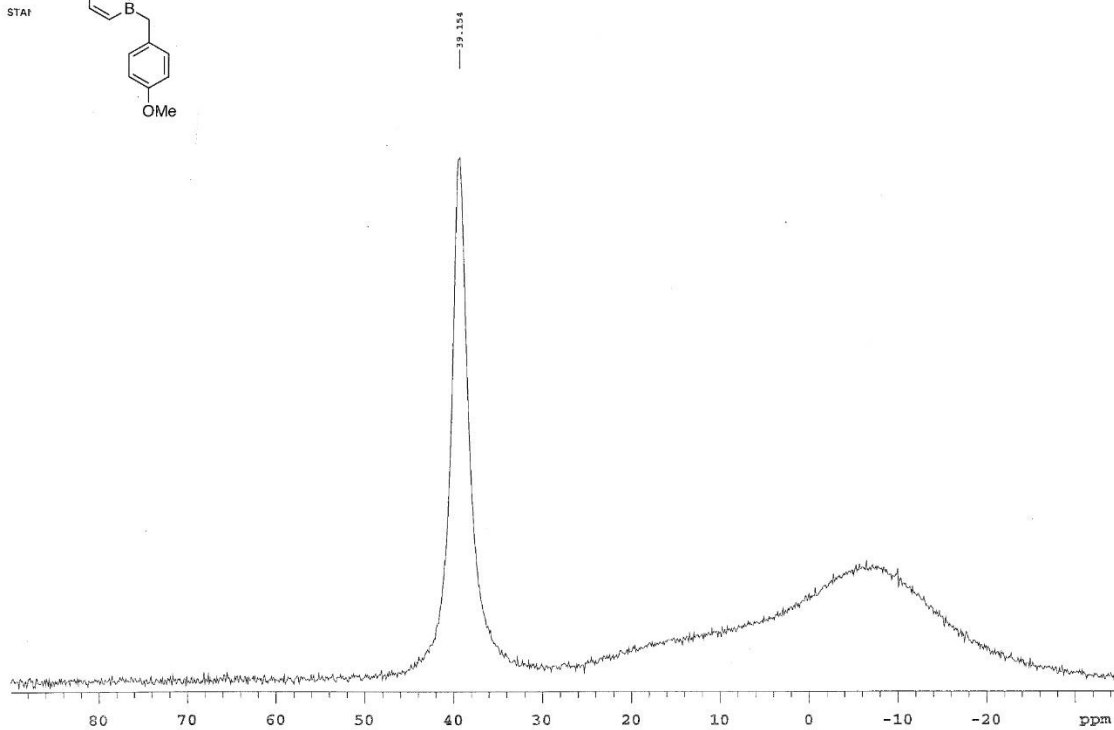
YL-03-PHOMe-11B-pure

Sample Name: YL-03-PHOMe-11B-pure
Date collected: 2020-01-13

Probe Name: s2pul
Solvent: cdcl3

Temperature: 25
Spectrometer: nmr11-inova500

Study Name: Liu
Operator: Liu



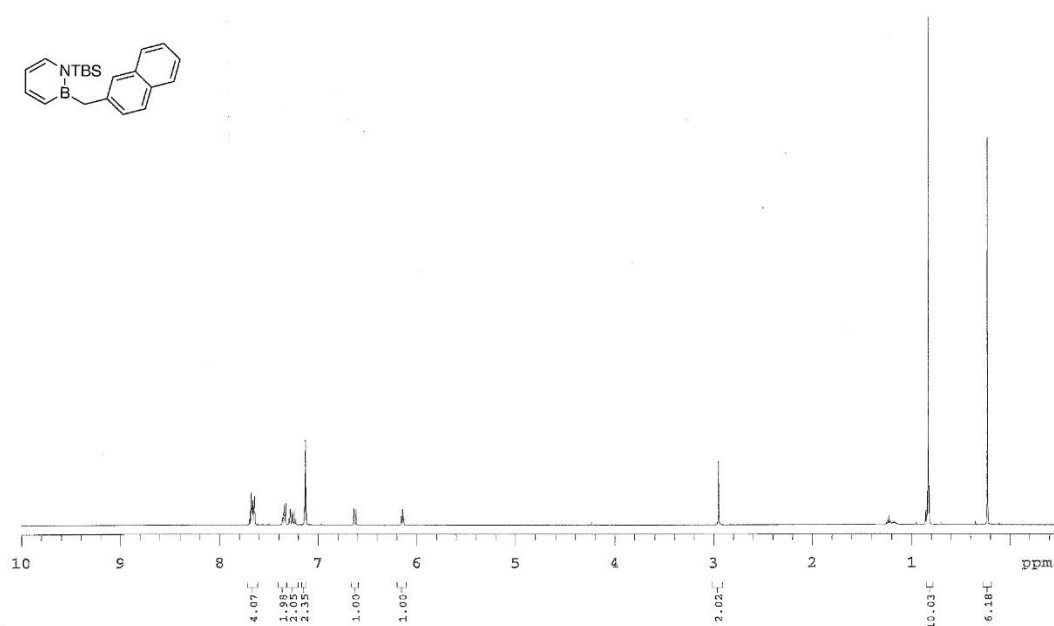
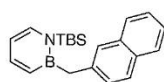
YL-03-naphthalene-1H

Sample Name: YL-03-naphthalene-1H
Date collected: 2020-01-16

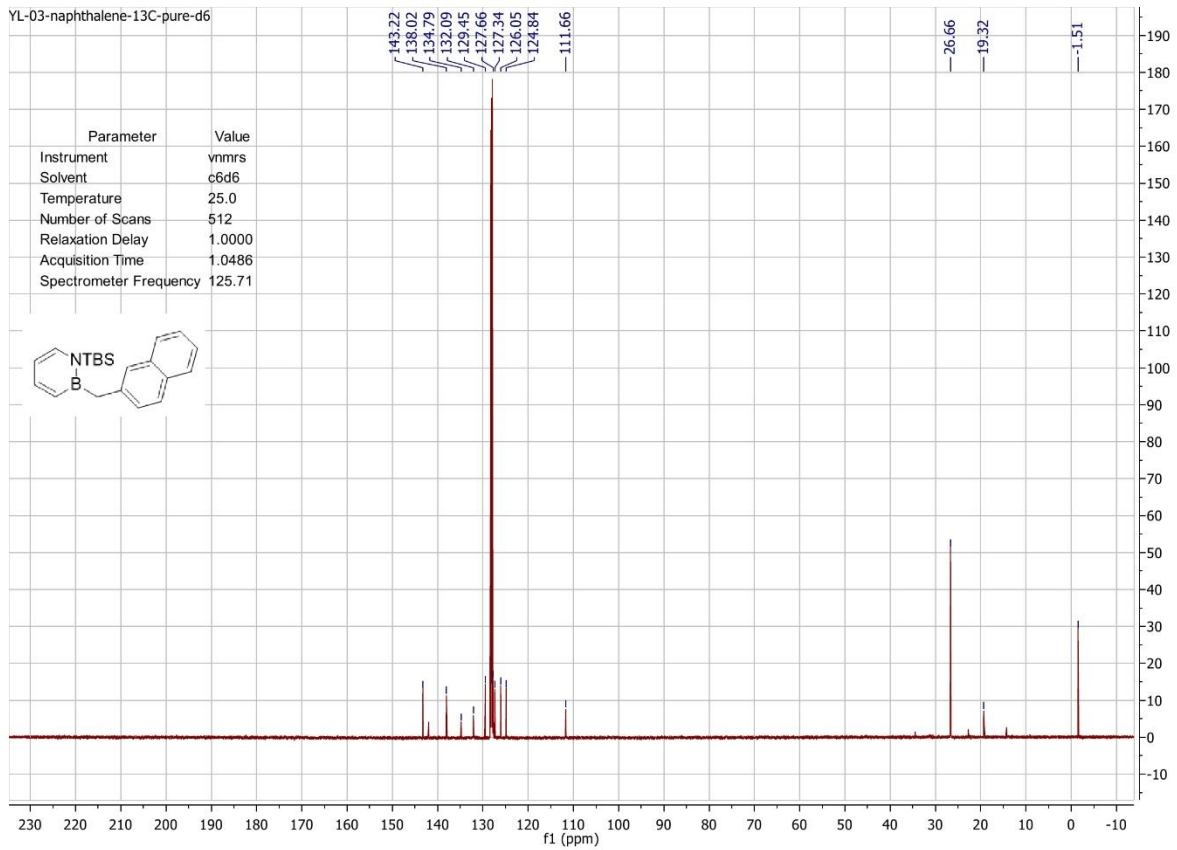
Probe Name: PROTON
Solvent: c5d6

Temperature: 25
Spectrometer: nmr18-vnmr500

Study Name: Liu
Operator: Liu

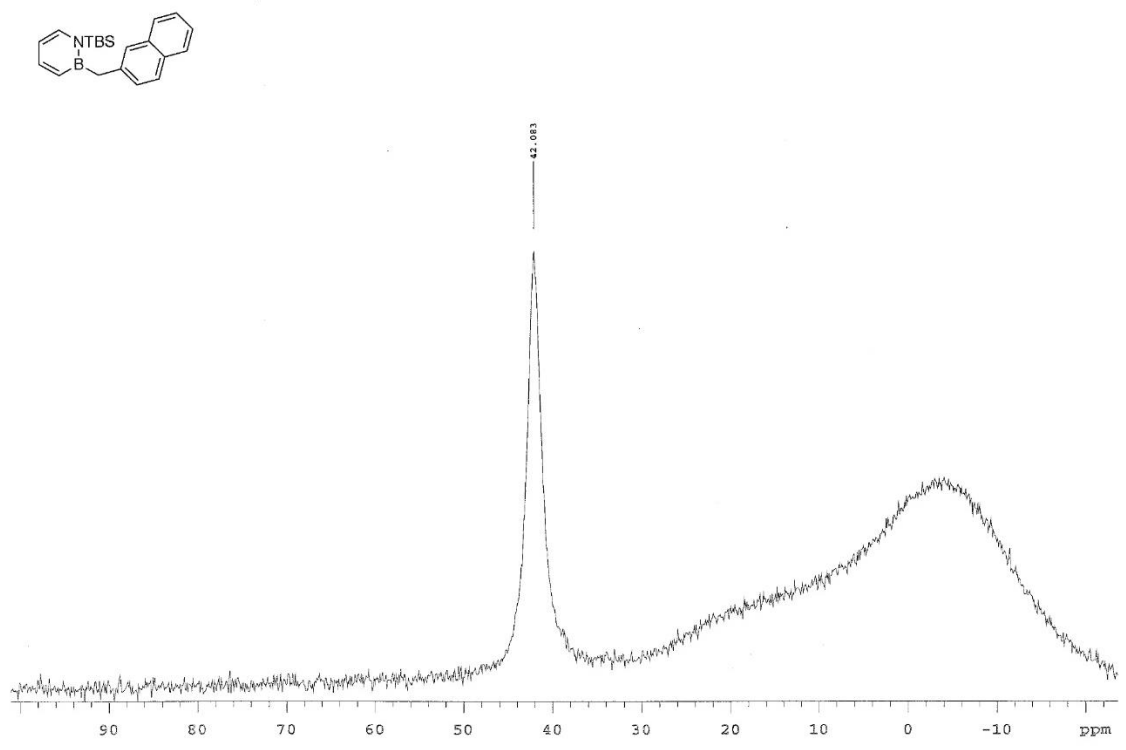


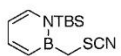
YL-03-naphthalene-13C-pure-d6



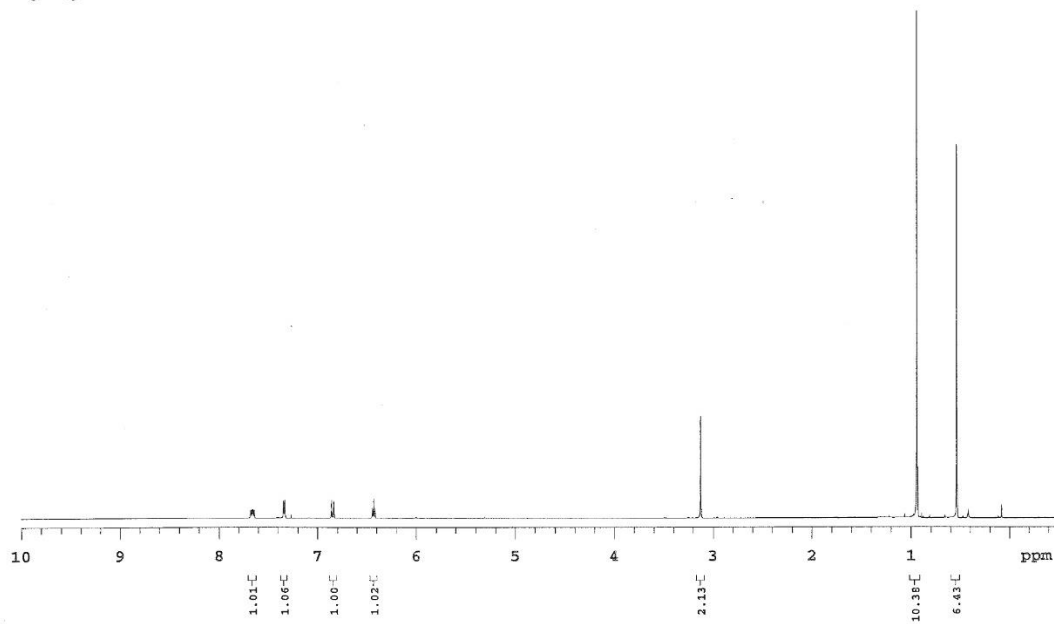
YL-03-naph-11B-pure

Sample Name: YL-03-naph-11B-pure Pulse program: s2pul Temperature: 25
Date collected: 2020-01-16 Solvent: c6d6 Spectrometer: nmr11-inova500 Study name: Liu
Operator: Liu

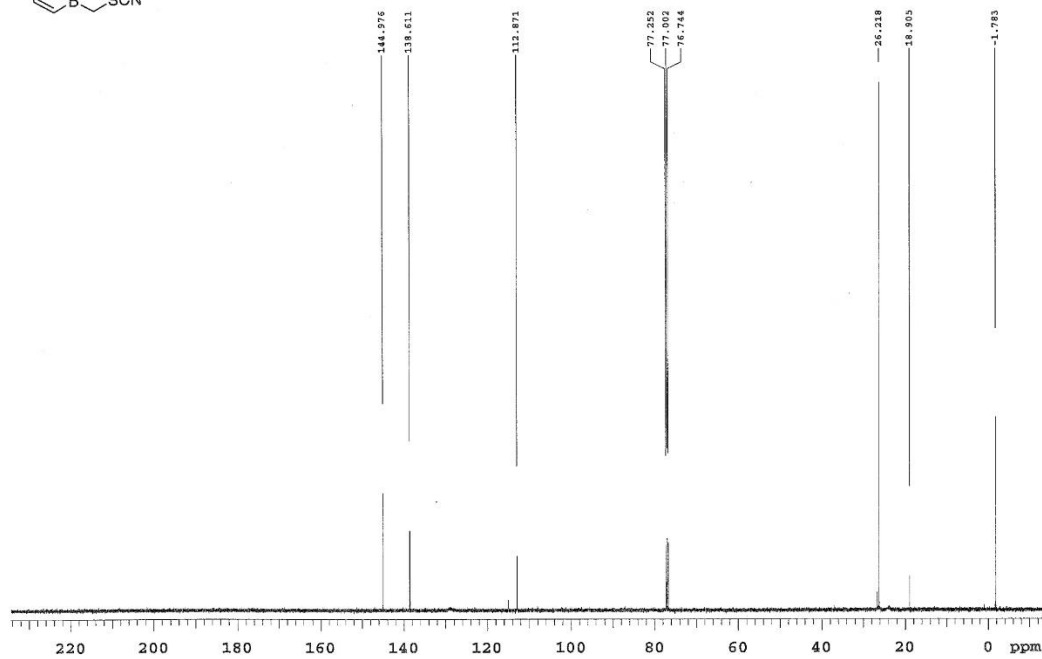
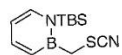


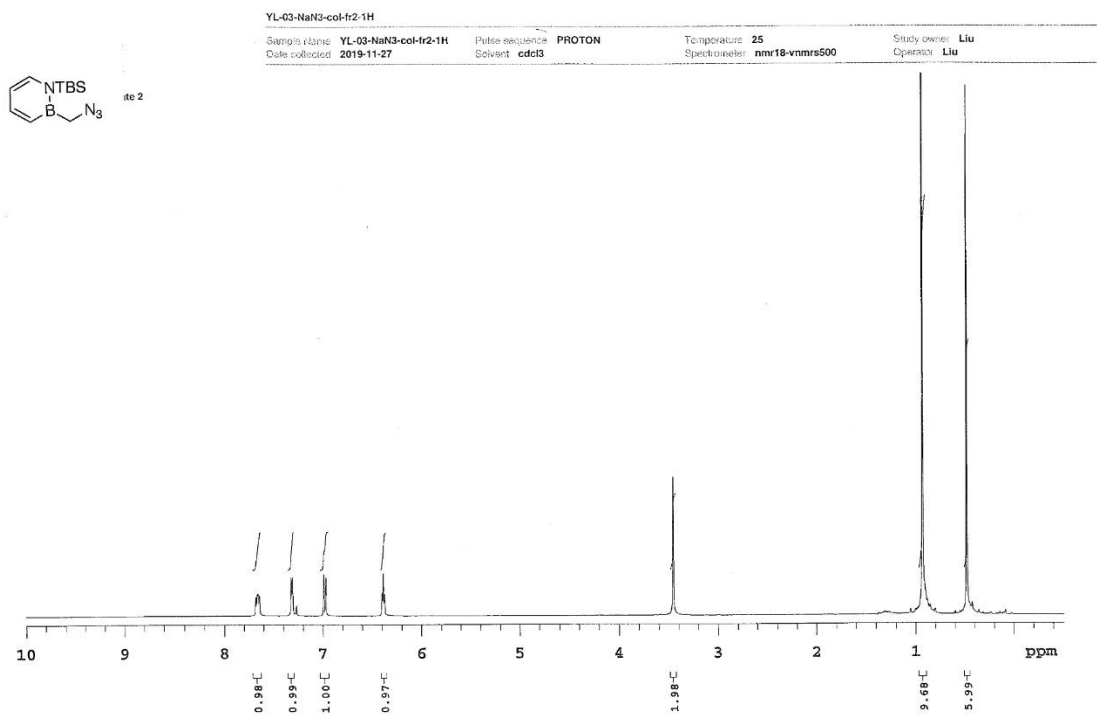
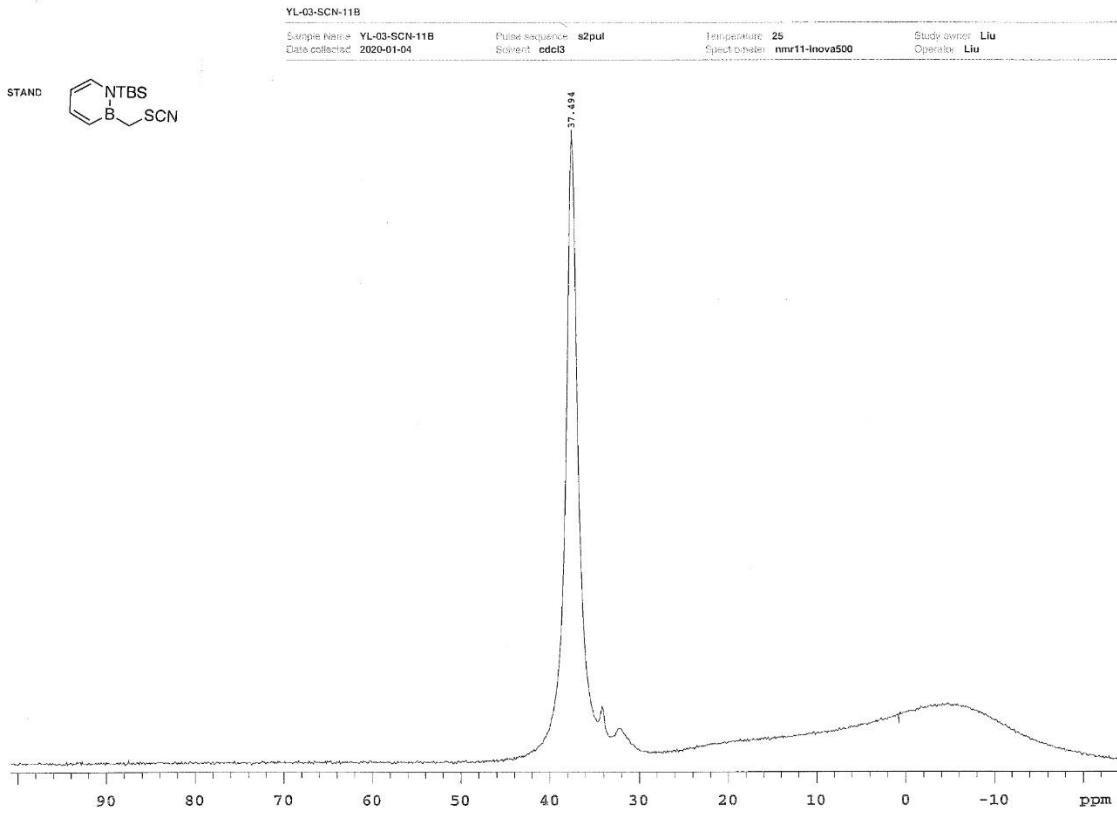


YL-03-SCN-1H
 Sample Name: YL-03-SCN-1H Pulse sequence: PROTON Temperature: 25 Study owner: Liu
 Date collected: 2020-01-04 Solvent: cdcl3 Spectrometer: nmr16-vnmrs500 Operator: Liu



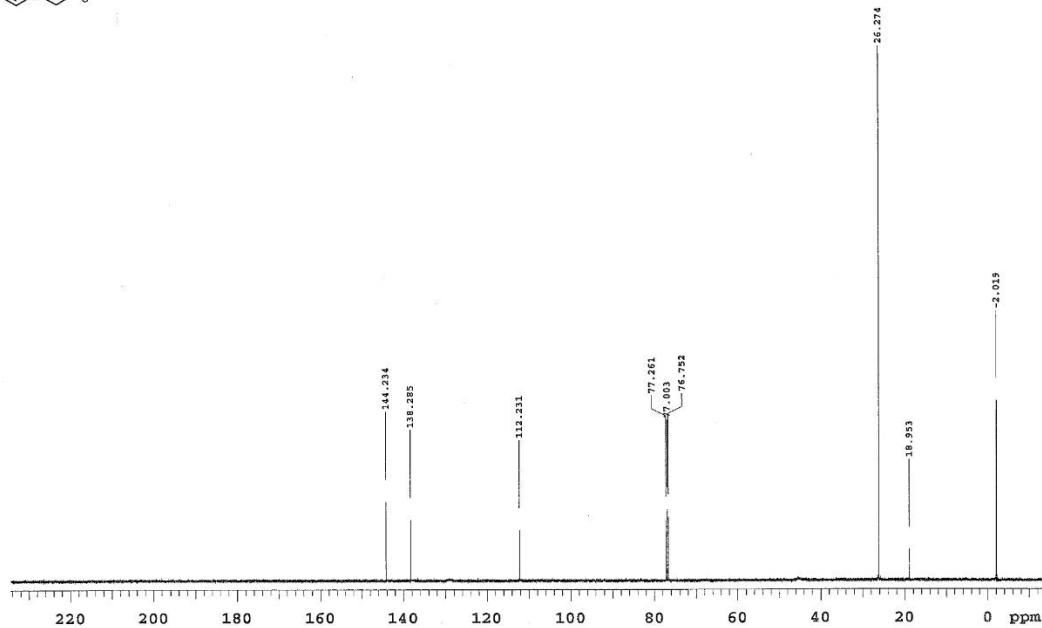
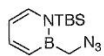
Sample Name: YL-03-SCN-1H Pulse sequence: CARBON Temperature: 25 Study owner: Liu
 Date collected: 2020-01-04 Solvent: cdcl3 Spectrometer: nmr16-vnmrs500 Operator: Liu





YL-03-NaN3-13C-pure

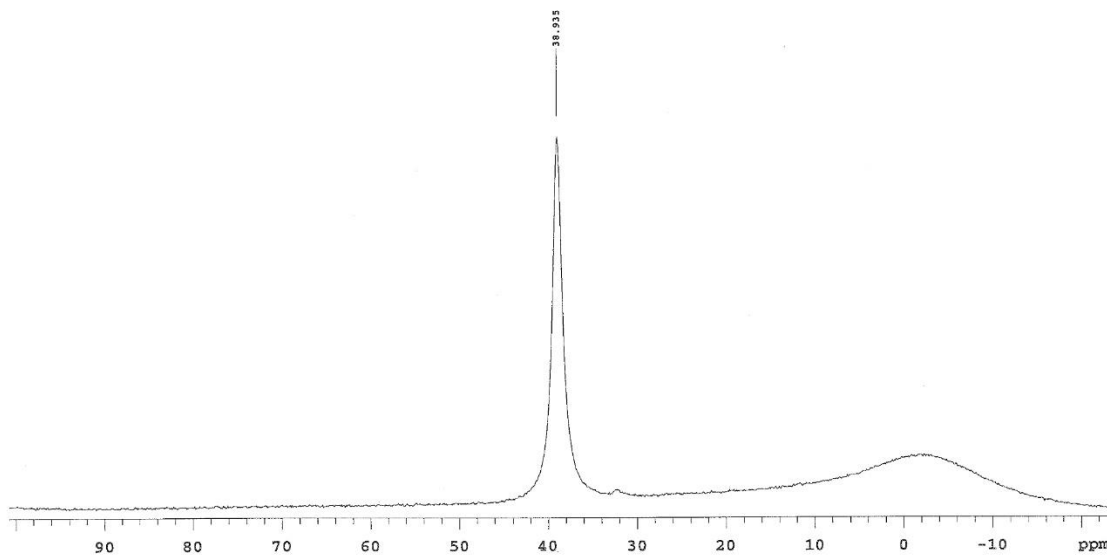
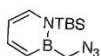
Sample Name: YL-03-NaN3-13C-pure Pulse sequence: CARBON Temperature: 25 Study owner: Liu
Date collected: 2019-11-27 Solvent: cdcl3 Spectrometer: nmr18-vnmrs500 Operator: Liu



YL-03-NaN3-11B-pure

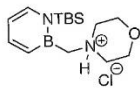
Sample Name: YL-03-NaN3-11B-pure Pulse sequence: s2pul Temperature: 25 Study owner: Liu
Date collected: 2019-11-27 Solvent: cdcl3 Spectrometer: nmr18-vnmrs500 Operator: Liu

STANDA

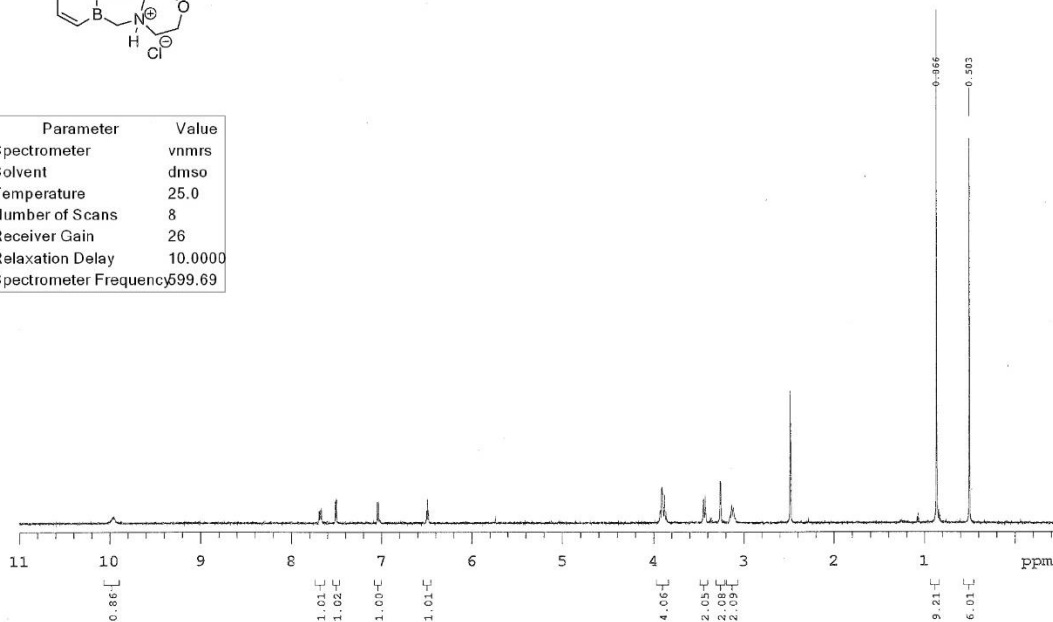


YL-03-morphine-pure-DMSO

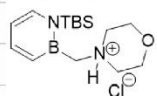
Sample Name YL-03-morphine-pure-DMSO Date collected 2020-03-12
Sequence PROTON Solvent dms0 Temperature 25 Spectrometer nmr19-vnmrs600
Study owner Liu Operator Liu



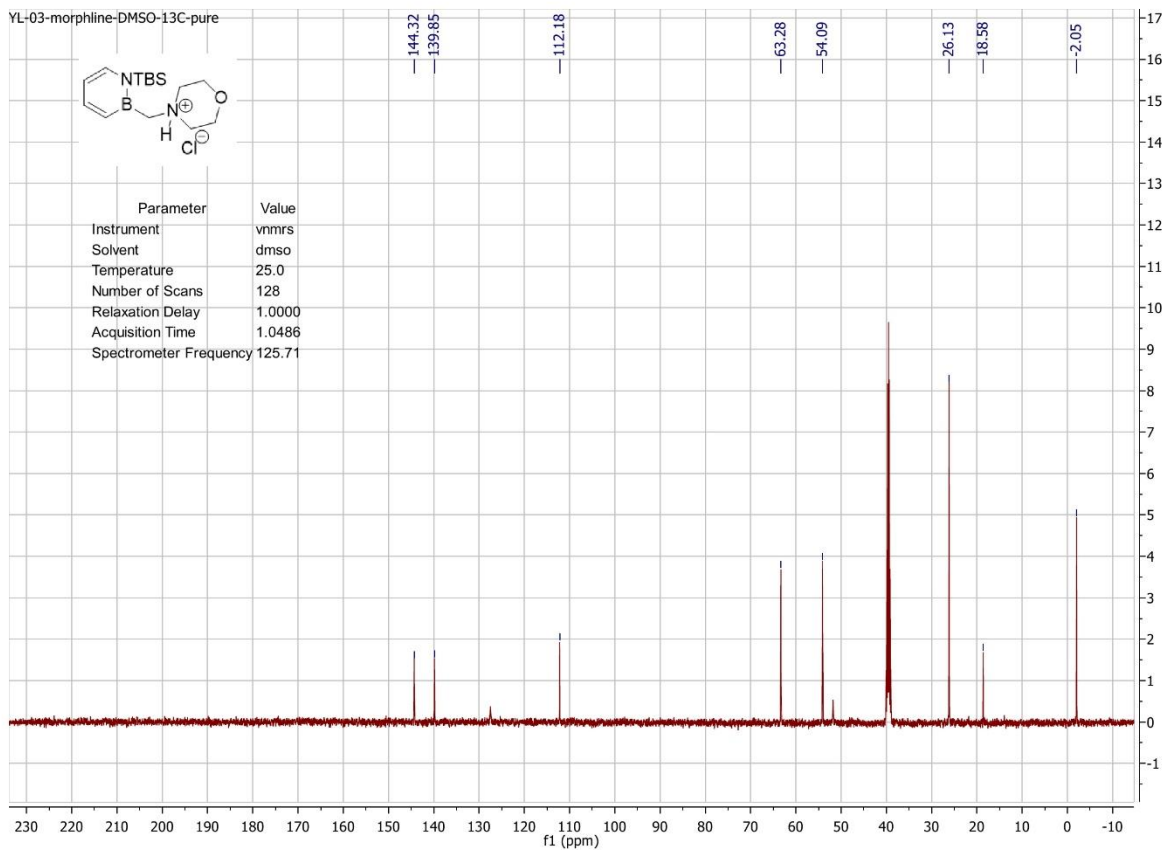
Parameter	Value
1 Spectrometer	vnmrs
2 Solvent	dms0
3 Temperature	25.0
4 Number of Scans	8
5 Receiver Gain	26
6 Relaxation Delay	10.0000
7 Spectrometer Frequency	599.69



YL-03-morphine-DMSO-13C-pure



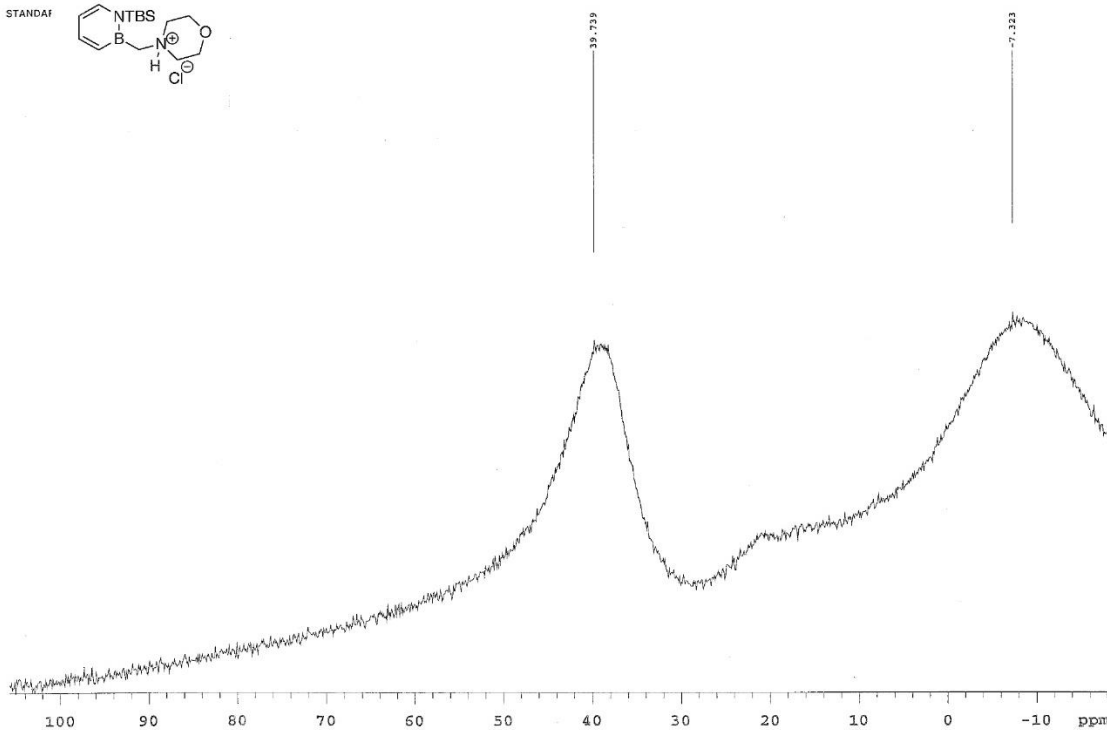
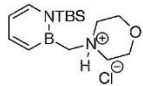
Parameter	Value
Instrument	vnmrs
Solvent	dms0
Temperature	25.0
Number of Scans	128
Relaxation Delay	1.0000
Acquisition Time	1.0486
Spectrometer Frequency	125.71



YL-03-morpholine-DMSO-11B-pure

Sample Name	YL-03-morpholine-DMSO-11B-pure	Substance	s2pul	Temperature	25	Study owner	Liu
Date collected	2020-01-18	Solvent	dmsd	Spectrometer	nmr11-inova500	Operator	Liu

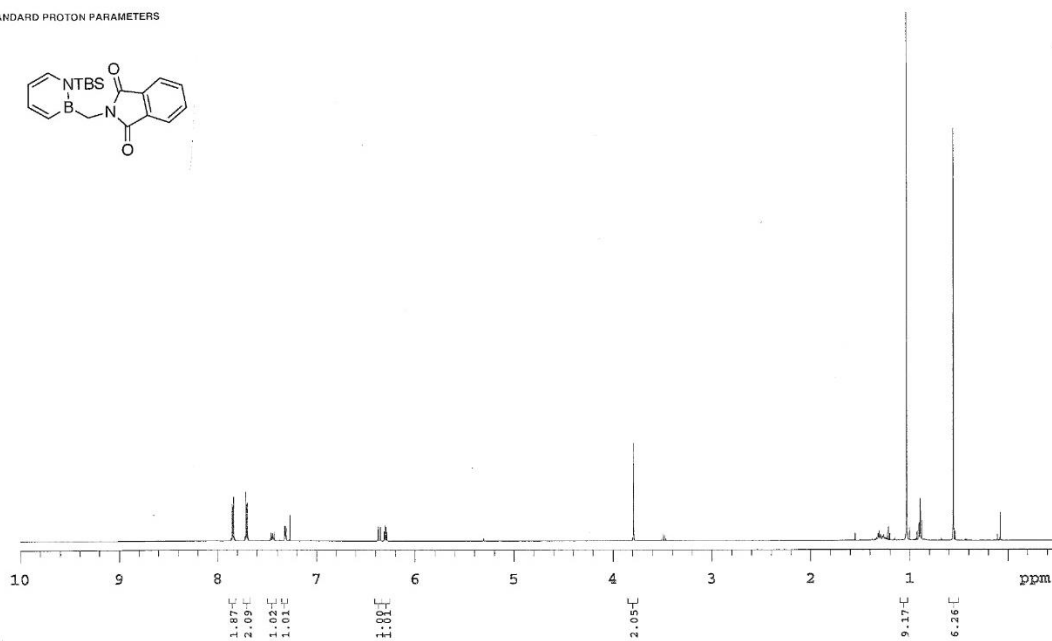
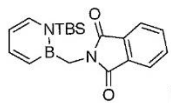
STANDAF



YL-03-kphthamide-1H

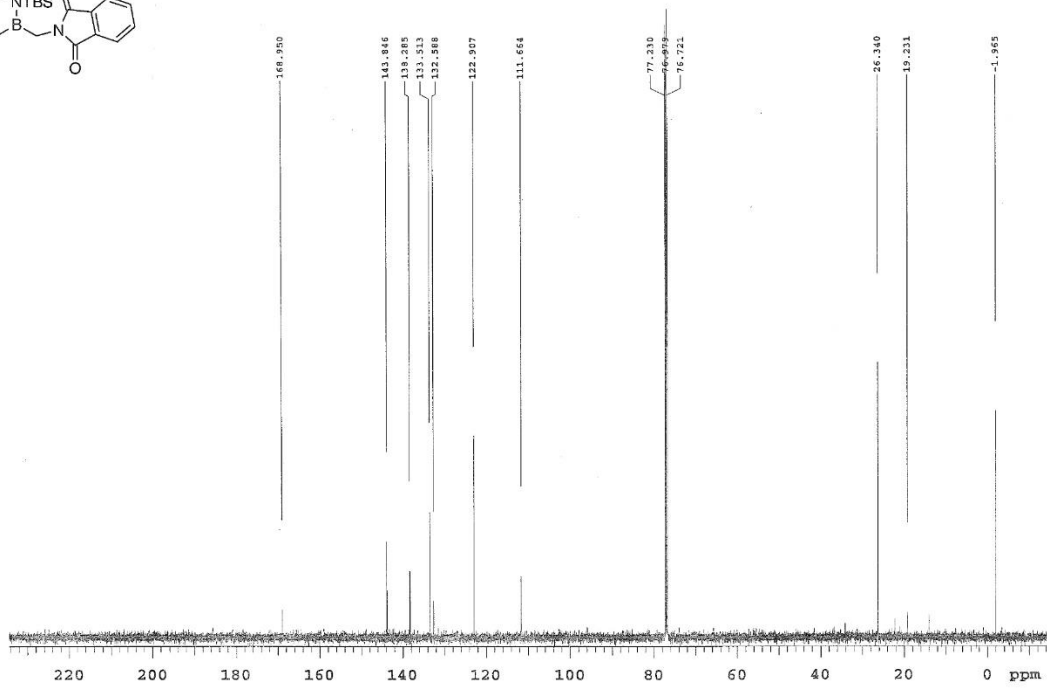
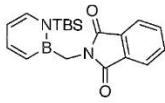
Sample Name	YL-03-kphthamide-1H	Pulse Sequence	PROTON	Temperature	25	Study owner	Liu
Date collected	2019-12-01	Solvent	cdcl3	Spectrometer	nmr18-vnmr500	Operator	Liu

STANDARD PROTON PARAMETERS



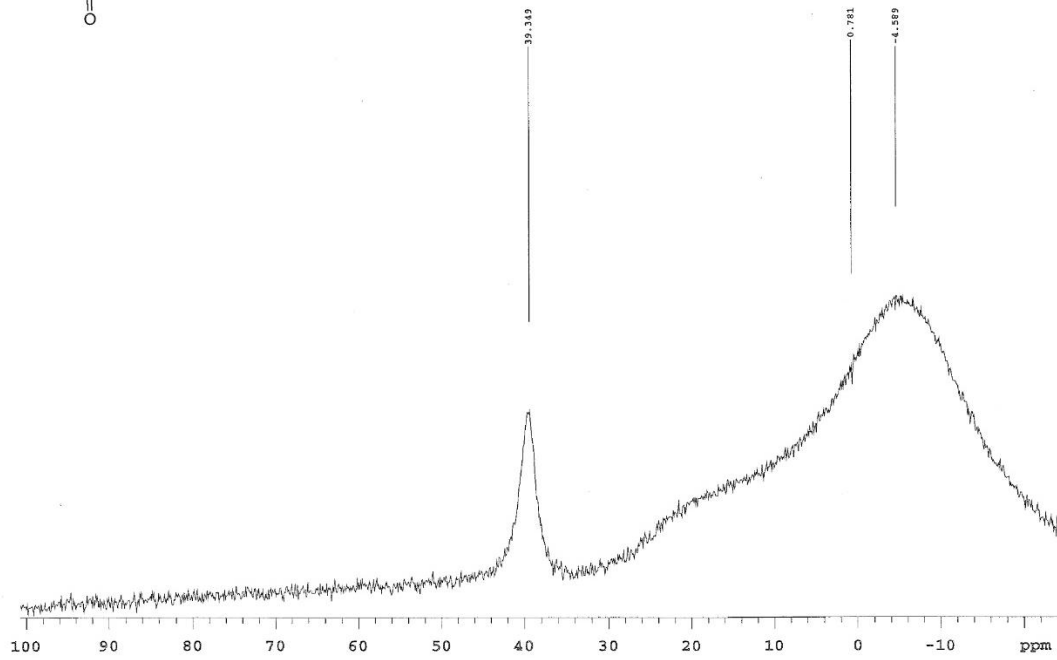
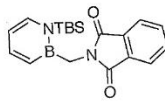
YL-03-kphthamide-13C

Sample Name: YL-03-kphthamide-13C Pulse sequence: CARBON Temperature: 25
Date collected: 2019-12-01 Solvent: cdcl3 Spectrometer: nmr18-vnmrs500 Study owner: Liu
Operator: Liu



YL-03-Kphthamide-11B

Sample Name: YL-03-Kphthamide-11B Pulse sequence: s2pul Temperature: 25
Date collected: 2019-11-30 Solvent: cdcl3 Spectrometer: nmr11-inova500 Study owner: Liu
Operator: Liu



Chapter 2 Understanding the hydrogen bond donor capability of 1,2-azaborines

This chapter begins with a brief introduction to 1,2-azaborine chemistry and the application of 1,2-azaborine in biomedical research (Chapter 2.1). It is then followed by a review of hydrogen bonding interaction in biological setting, and a review on T4 double mutant lysozymes as an arene recognition platform (Chapter 2.3). There are two parts of my research, first, we studied how the hydrogen bonding strength was affected by the ligand steric environment in the cavity of L99A/M102Q T4 lysozyme binding site (Chapter 2.7). Second, we revealed the existence of a water bridge as a new binding mode of 1,2-azaborine ligand in the L99A/M102H T4 lysozyme double mutant cavity (Chapter 2.9).

2.1 Introduction to 1,2-azaborine chemistry

2.1.1 Basic electronic structure of 1,2-azaborines

The generation of chemical space beyond what can be achieved by nature is one of the main goals of synthetic chemistry and an important tenet in drug discovery research. The BN/CC isosterism¹ (i.e., replacement of a carbon-carbon bond with a boron-nitrogen bond) has emerged as a viable strategy to increase the chemical space of compounds relevant to biomedical research (see Figure 2.1). 1,2-azaborine **2.1** represents a BN isostere of the ubiquitous benzene motif.² Even though it has the same number of valence electrons as benzene, exhibits unique electronic structure due to the presence of the polar BN unit. Based on a previous DFT calculation study,³ 1,2-dihydro-1,2-azaborine has a calculated molecular dipole moment of 2.15 Debye whereas benzene is a relatively non-polar molecule.

¹ Campbell, P. G.; Marwitz, A. J. V.; Liu, S.-Y. *Angew. Chem. Int. Ed.* 2012, 51, 6074-6092.

² Giustra, Z. X.; Liu, S.-Y. *J. Am. Chem. Soc.* **2018**, 140, 1184-1194.

³ Chrostowska, A.; Xu, S.; Lamm, A. N.; Mazière, A.; Weber, C. D.; Dargelos, A.; Baylère, P.; Graciaa, A.; Liu, S.-Y. *J. Am. Chem. Soc.* **2012**, 134, 10279-10285.

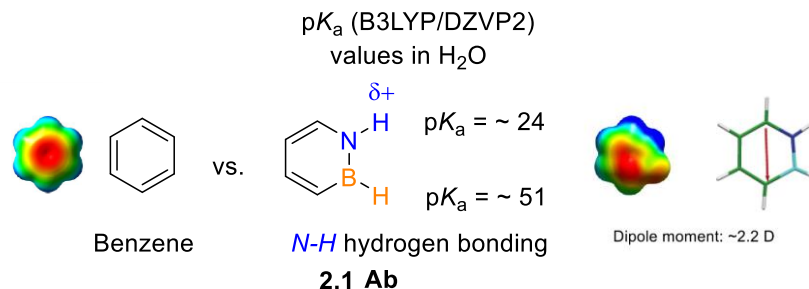


Figure 2.1. Electronic structure comparison between benzene and 1,2-azaborine.

1,2-Dihydro-1,2-azaborine **2.1** has substantial amount of aromaticity, which is revealed by the ¹H NMR chemical shifts consistent with the presence of aromatic ring current effects.⁴ Liu group and co-workers sought to utilize the technique employed by Kistiakowsky⁵ in 1936 to experimentally measure resonance stabilization energy (RSE) of 1,2-azaborine by reaction calorimetry. A series of reference BN-cyclohexene analogues are synthesized, and the heats of hydrogenation for the 1,2-azaborine and the reference “N-vinyl” and “B-vinyl” BN heterocycle compounds are compared and the RSE of 1,2-azaborine was determined to be 16.6 kcal/mol.⁶ While benzene’s RSE is two folds higher (36 kcal/mol), the RSE of 1,2-azaborine is comparable to other heterocycles⁷ such as pyrrole (~21 kcal/mol) and furan (~15 kcal/mol). Similar to furan and thiophene (~20 kcal/mol), lower RSE value enables 1,2-azaborine undergo Diels-alder reactions with highly activated dienophiles.^{7, 8}

2.1.2 Synthesis of 1,2-azaborine: A brief historical perspective

Dewar and White first described the early synthesis of polycyclic fused 1,2-azaborine and monocyclic azaborines during 1950-1960s (Figure 2.2).⁹ The interests in this research field waned until early 2000s, when Ashe revisited and improved the synthetic access to monocyclic 1,2-azaborine **2.3** in a

⁴ Ashe, A. J., III; Fang, X.; Fang, X.; Kampf, J. W. *Organometallics* **2001**, *20*, 5413–5418.

⁵ Kistiakowsky, G. B.; Ruhoff, J. R.; Smith, H. A.; Vaughan, W. E. *J. Am. Chem. Soc.* **1936**, *58*, 146–153.

⁶ a) Campbell, P. G.; Abbey, E. R.; Neiner, D.; Grant, D. J.; Dixon, D. A.; Liu, S.-Y. *J. Am. Chem. Soc.* **2010**, *132*, 18048–18050. b) Turner, D. W.; Baker, C.; Baker, A. D.; Brundle, C. R. *Molecular Photoelectron Spectroscopy*; Wiley-Interscience: New York, 1970.

⁷ Burford, R. J.; Li, B.; Vasiliu, M.; Dixon, D. A.; Liu, S.-Y. *Angew. Chem. Int. Ed.* **2015**, *54*, 7823–7827.

⁸ M. Manoharan, F. De Proft, P. Geerlings, *J. Chem. Soc. Perkin Trans.* **2000**, *2*, 1767–1773.

⁹ a) White, D. G. *J. Am. Chem. Soc.* **1963**, *85*, 3634–3636. b) Dewar, M. J. S.; Kubba, V. P.; Pettit, R. *J. Chem. Soc.* **1958**, 3073–3076. c) Dewar, M. J. S.; Dietz, R. *J. Chem. Soc.* **1959**, 2728–2730. d) Dewar, M. J. S.; Kaneko, C.; Bhattacharjee, M. K. *J. Am. Chem. Soc.* **1962**, *84*, 4884–4887. e) Dewar, M. J. S.; Poesche, W. H. *J. Am. Chem. Soc.* **1963**, *85*, 2253–2256.

mild and efficient synthetic route based on a ring closing metathesis, a methodology rendered feasible only after 1990, to facilitate the dehydrogenation step (Scheme 2.1).¹⁰

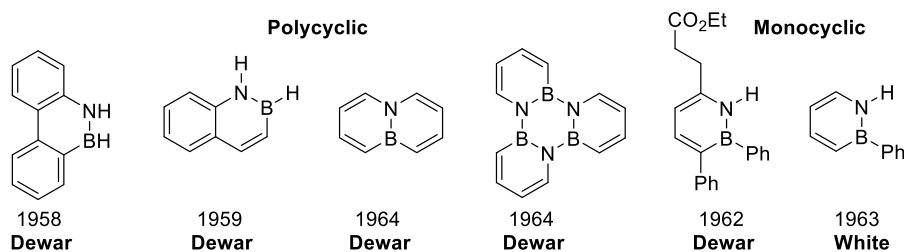
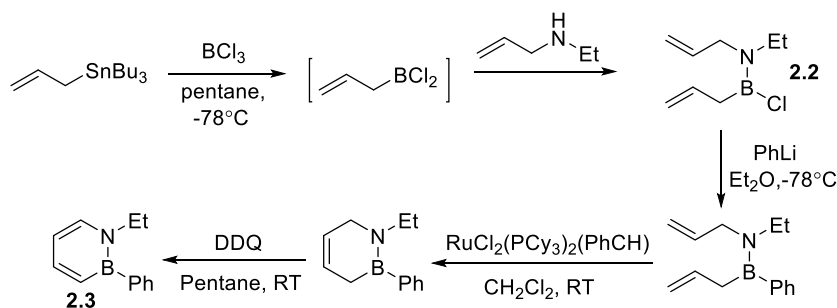


Figure 2.2. 1,2-azaborine derivatives developed by Dewar and White.



Scheme 2.1. Synthetic routes to 1,2-azaborine involving ring-closing metathesis.

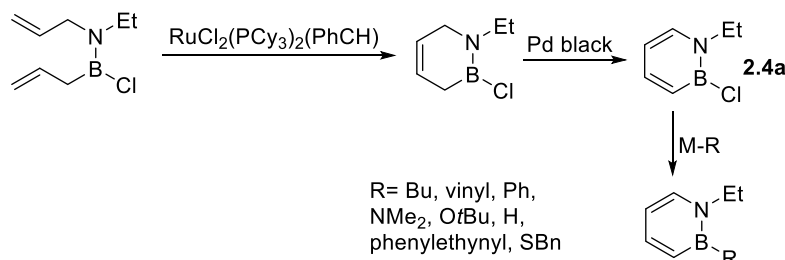
Liu group made a contribution to the synthesis of 1,2-azaborine **2.4a** by preserving the flexible B-Cl bond, and this enabled the convenient installation of a variety of boron substituents via simple substitution chemistry (Scheme 2.2).¹¹ Liu and coworkers also developed the versatile 1,2-azaborine synthon N-TBS-BCl-1,2-azaborine **2.4b** (Scheme 2.3),¹² which features a removable TBS group on nitrogen and a chloride leaving-group on boron. The first successful synthesis of parent 1,2-dihydro-1,2-azaborine was reported by Liu group in 2009 (Scheme 2.3).¹¹ The TBS nitrogen protecting group was removed by treating **2.5** with $[\text{Cr}(\text{CO})_3(\text{MeCN})_3]$ to form complex **2.6** and subsequent treatment with HF-pyridine. Decomplexation was accomplished by ligand exchange with PPh_3 to furnish 1,2-dihydro-1,2-

¹⁰ Ashe, A. J., III; Fang, X. *Org. Lett.* **2000**, 2, 2089–2091.

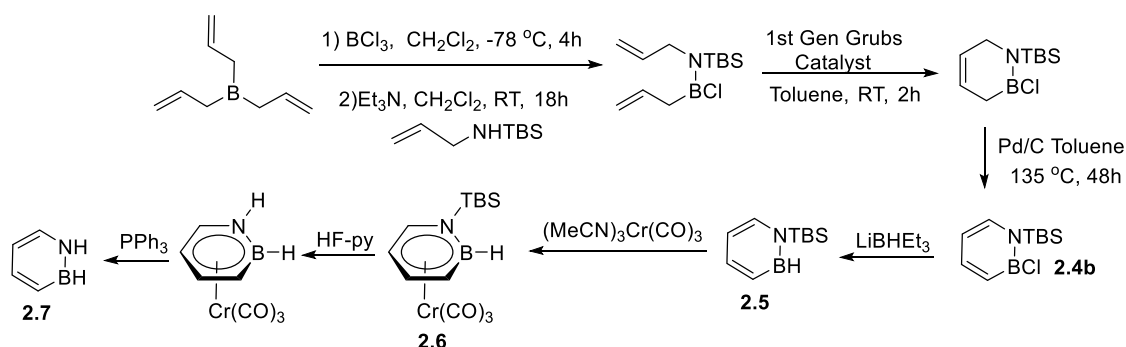
¹¹ a) Marwitz, A. J. V.; Matus, M. H.; Zakharov, L. N.; Dixon, D. A.; Liu, S.-Y. *Angew. Chem. Int. Ed.* **2009**, 48, 973–977. b) Abbey, E. R.; Lamm, A. N.; Baggett, A. W.; Zakharov, L. N.; Liu, S.-Y. *J. Am. Chem. Soc.* **2013**, 135, 12908–12913.

¹² Marwitz, A. J. V.; Abbey, E. R.; Jenkins, J. T.; Zakharov, L. N.; Liu, S.-Y. *Org. Lett.* **2007**, 9, 4905–4908.

azaborine **2.7**. Compound **2.7** represents the first isolated and characterized hybrid organic/inorganic benzene.



Scheme 2.2. Synthetic routes developed by Liu.



Scheme 2.3. Synthesis of parental 1,2-dihydro-1,2-azaborine.

2.1.3 Late-stage functionalization of 1,2-azaborine

Late-stage functionalization of 1,2-azaborine in this context means the installation of various functional group after the assembly of the 1,2-azaborine ring (Figure 2.3).¹³ The late-stage functionalization of 1,2-azaborine has enabled the burgeoning applications of BN-containing arenes in different fields such as material chemistry,¹⁴ biomedical chemistry¹⁵ and ligand design in homogeneous catalysis.¹⁶

¹³ McConnell, C. R.; Liu, S.-Y. *Chem. Soc. Rev.* **2019**, *48*, 3436-3453.

¹⁴ a) Wang, X.-Y.; Wang, J.-Y.; Pei, J. B.N. *Chem.-Eur. J.* **2015**, *21*, 3528-3539. b) Morgan, M. M.; Piers, W. E. *Dalton Trans.* **2016**, *45*, 5920-5924. c) Huang, J.; Li, Y. *Front. Chem.* **2018**, *6*, 341-350.

¹⁵ a) Vlasceanu, A.; Jessing, M.; Kilburn, J. P. *Bioorg. Med. Chem.* **2015**, *23*, 4453-4461. b) Rombouts, F. J.; Tovar, F.; Austin, N.; Tresadern, G.; Trabanco, A. A. *J. Med. Chem.* **2015**, *58*, 9287-9295. c) Lee, H.; Fischer, M.; Shoichet, B. K.; Liu, S.-Y. *J. Am. Chem. Soc.* **2016**, *138*, 12021-12024. d) Zhao, P.; Nettleton, D. O.; Karki, R.; Zecri, F. J.; Liu, S.-Y. *ChemMedChem* **2017**, *12*, 358-361.

¹⁶ a) Segawa, Y.; Yamashita, M.; Nozaki, K. *J. Am. Chem. Soc.* **2009**, *131*, 9201-9203. b) Bailey, J. A.; Haddow, M. F.; Pringle, P. G. *Chem. Comm.* **2014**, *50*, 1432-1434. c) Sun, F.; Huang, M.; Zhou, Z.; Fang, X. *RSC Advances* **2015**, *5*,

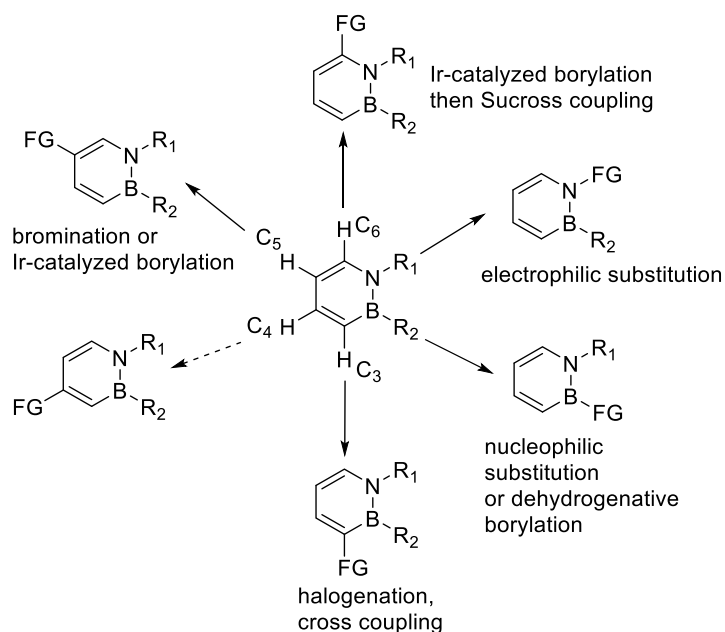


Figure 2.3. Late-stage functionalization of 1,2-azaborines.

According to calculations, the C3 and C5 positions of 1,2-azaborine are most electron-rich and thus expected to undergo attack by an electrophile. The Ashe¹⁷ group reported the halogenation of 1,2-azaborine by electrophilic aromatic substitution (EAS) at C3 position with bromine to afford C3-Br **2.8** in high yield (Scheme 2.4, eq 1). In the same year, Fang group also developed¹⁸ halogenation methods involving acetyl chloride or AlCl₃ as activating agent with CuBr₂ or N-Iodosuccinimide (NIS) as halogen source to synthesize C3 halogenated azaborines (Scheme 2.4, eq 2). The bromination of the C3 position opened the possibility of cross-coupling methods at the C3 position. Negishi cross-coupling¹⁹ was developed with good functional group tolerance. The catalyst Pd(P-*t*-Bu₃)₂ was used in combination with alkyl, alkenyl and aryl zinc halides reagents at room temperature, and the labile B-Cl bond remains intact in the resulting Negishi coupling products **2.10** (Scheme 2.4, eq 3).

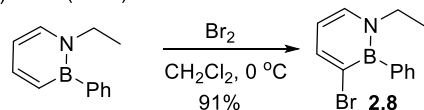
75607-75611. d) Xu, S.; Zhang, Y.; Li, B.; Liu, S.-Y. *J. Am. Chem. Soc.* **2016**, *138*, 14566-14569. e) McConnell, C. R.; Campbell, P. G.; Fristoe, C. R.; Memmel, P.; Zakharov, L. N.; Li, B.; Darrigan, C.; Chrostowska, A.; Liu, S.-Y. *Eur. J. Inorg. Chem.* **2017**, 2207-2210. f) Wang, G.; Liu, L.; Wang, H.; Ding, Y.-S.; Zhou, J.; Mao, S.; Li, P. *J. Am. Chem. Soc.* **2017**, *139*, 91-94.

¹⁷ Pan, J.; Kampf, J. W.; Ashe, A. *J. Org. Lett.* **2007**, *9*, 679-681.

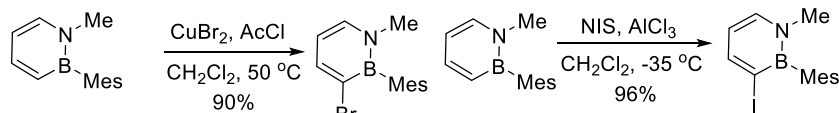
¹⁸ a) Zhang, Y.; Dan, W.; Fang, X. *Organometallics* **2017**, *36*, 1677-1680. b) Zhang, Y.; Sun, F.; Dan, W.; Fang, X. *J. Org. Chem.* **2017**, *82*, 12877-12887.

¹⁹ Brown, A. N.; Li, B.; Liu, S.-Y. *J. Am. Chem. Soc.* **2015**, *137*, 8932-8935.

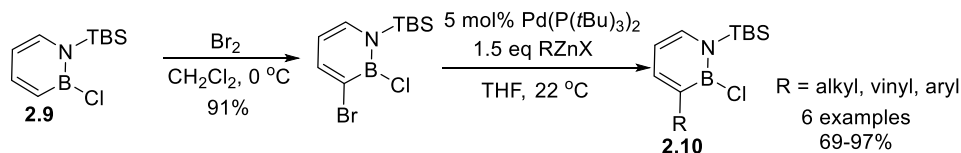
(1) Ashe (2007)



(2) Fang (2017)

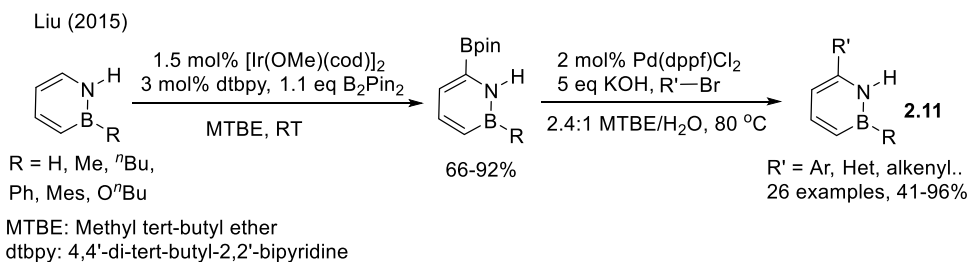


(3) Liu (2015)



Scheme 2.4. Halogenation of various 1,2-azaborine through EAS and Negishi cross-coupling.

C-H borylation²⁰ was found to proceed at room temperature with regioselectivity at the most acidic C6-H position among all the C-H positions on azaborine ring. The development of C-H borylation provided access to the Suzuki-Miyaura coupling²¹ product 1,2-azaborine **2.11** at the C6 position in the presence of $\text{Pd}(\text{dppf})\text{Cl}_2$ and KOH at 80 °C in MTBE/ H_2O solvent system with phenyl bromides, heteroaryl bromides, and alkenyl bromide.

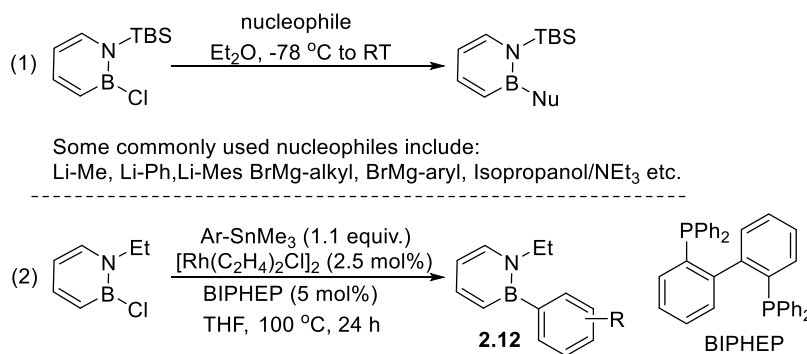


Scheme 2.5. Borylation of 1,2-azaborine followed by the Suzuki-Miyaura cross-coupling reaction at C6 position.

²⁰ Baggett, A. W.; Vasiliu, M.; Li, B.; Dixon, D. A.; Liu, S.-Y. *J. Am. Chem. Soc.* **2015**, *137*, 5536-5541.

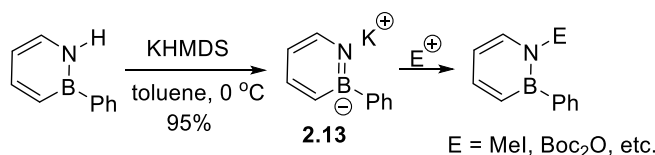
²¹ a) Baggett, A. W.; Liu, S.-Y. *J. Am. Chem. Soc.* **2017**, *139*, 15259-15264. b) Baggett, A. W.; Guo, F.; Li, B.; Liu, S.-Y.; Jäkle, F. *Angew. Chem. Int. Ed.* **2015**, *54*, 11191-11195.

The labile B-Cl bond also can be functionalized as the Lewis acidic boron atom of the 1,2-azaborine renders the boron position susceptible to nucleophilic attack.²² Suitable nucleophiles^{7, 16, 17a} include alkyl, aryl, alkenyl and alkynyl organometallic reagents and various N- or O-based nucleophiles (Scheme 2.6, eq 1). An alternative way to activate the B-Cl bond that Liu group discovered was through Rh-catalyzed²³ cross-coupling with arylstannanes which gave access to the BN biphenyls **2.12**. This method allows the aryl substituents with functional (e.g. aldehydes, ketones, esters) groups that are not compatible with organomagnesium and organolithium reagents to be installed onto the monocyclic 1,2-azaborines (Scheme 2.6, eq 2).



Scheme 2.6. Nucleophilic substitution at boron position.

Electrophilic substitution at nitrogen was observed after the deprotonation of N-H proton, which has *pK_a* of approximately.²⁴ Ashe demonstrated²⁵ that strong amide bases such as LDA or KHMDS can generate amide **2.13** which can be isolated as a solid and then subjected to electrophilic attack by various electrophiles (Scheme 2.7).



²² a) Lamm, A. N.; Garner, E. B.; Dixon, D. A.; Liu, S.-Y. *Angew. Chem. Int. Ed.* **2011**, *50*, 8157-8160. b) Baggett, A. W.; Guo, F.; Li, B.; Liu, S.-Y.; Jäkle, F. *Angew. Chem. Int. Ed.* **2015**, *54*, 11191-11195.

²³ Rudebusch, G. E.; Zakharov, L. N.; Liu, S.-Y. *Angew. Chem. Int. Ed.* **2013**, *52*, 9316-9319.

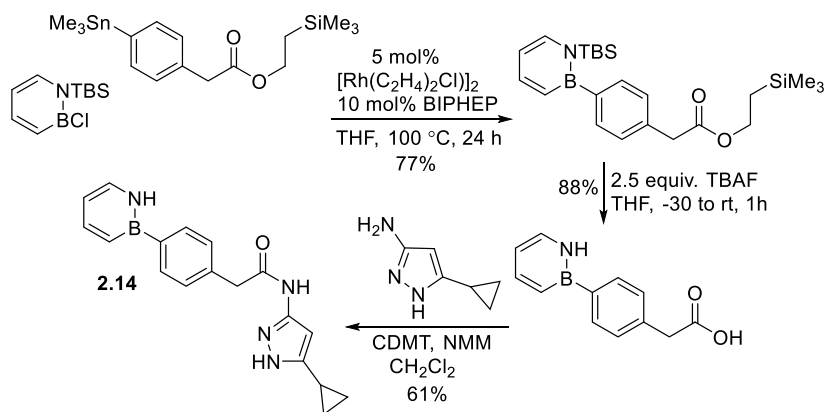
²⁴ Baggett, A. W.; Vasiliu, M.; Li, B.; Dixon, D. A.; Liu, S.-Y. *J. Am. Chem. Soc.* **2015**, *137*, 5536-5541.

²⁵ a) Pan, J.; Kampf, J. W.; Ashe, A. J. *Organometallics* **2004**, *23*, 5626-5629. b) Pan, J.; Kampf, J. W.; Ashe III, A. J. *Organometallics* **2008**, *27*, 1345-1347.

Scheme 2.7. Electrophilic substitution at nitrogen atom.

2.1.4 The application of 1,2-azaborine in biomedical research

In the medicinal chemistry context, we have shown that 1,2-azaborine represents a novel pharmacophore with higher aqueous solubility that can serve additionally as a hydrogen bond donor.²⁶ The first examples of biological active monocyclic 1,2-azaborines **2.14** were synthesized as BN biphenyl carboxamides based CDK2 inhibitor.²⁷ The synthesis involves a functional group tolerant rhodium-catalyzed coupling of aryl stannanes with boron substituted chloroazaborines that is followed by hydrolysis and amide-coupling to furnish for example the BN analog of a CDK2 inhibitor **2.14** in moderate yield (Scheme 2.8).



Scheme 2.8. Synthesis of an azaborine-containing CDK2 inhibitor.

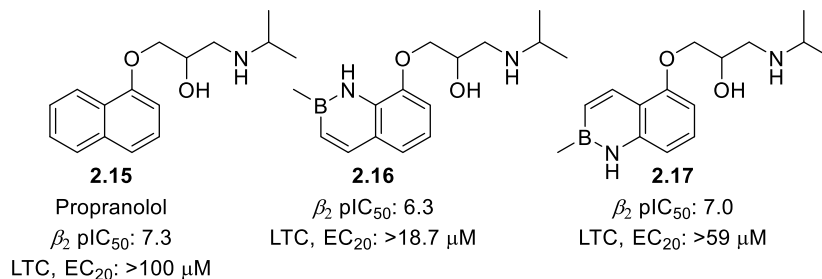
The *in vivo* ADMET (absorption, distribution, metabolism, excretion, toxicity) profile of compound **2.14** showed two trends: 1) when compared to its carbonanous compound, the BN isotere demonstrates better aqueous solubility.²⁶ 2) the greater polarity of B-N bond also induced a slightly lower membrane permeability. As a CDK2 inhibitor, compound **2.14** has an IC₅₀ four times lower than its carbon

²⁶ Zhao, P.; Nettleton, D. O.; Karki, R.; Zecri, F. J.; Liu, S.-Y. *ChemMedChem*, **2017**, *12*, 358-361.

²⁷ Pevarello, P.; Brasca, M. G.; Amici, R.; Orsini, P.; Traquandi, G.; Corti, L.; Piutti, C.; Sansonna, P.; Villa, M.; Pierce, B. S. *J. Med. Chem.* **2004**, *47*, 3367-3380.

version, and the improved biological activity were attributed to the extra hydrogen bonding interaction between the NH of azaborine and backbone carbonyl of Ile10 of the CDK2. In vivo, pharmacokinetic behavior study in male Sprague Dawley Rat models exhibited a two-fold increase in AUC_{po} (area under the curve per oral administration) resulting from a lower clearance rate and greater bioavailability.

Rombouts group also utilized BN/CC isosterism for naphthalene in drug discovery.²⁸ Two naphthalene bioisostere benzazaborine analogues (**2.16** and **2.17** in Scheme 2.9) of Propranolol **2.15**, which is well-known as β -blocker antagonist,²⁹ were synthesized and evaluated. Benzazaborine **2.17** showed a similar inhibition profile as **2.15** and **2.16** was found to be a less potent inhibitor of β_2 adrenergic receptor. The lowest toxic concentration (LTC) for hepatotoxicity was tested in human hepatocarcinoma cell line (HepG2 cells), while **2.16** was found to have some potential risks for hepatotoxicity, compound **2.17** had much higher LTC of 59 μ M and it was considered to be non-hepatotoxic.



Scheme 2.9. Benzazaborinine analogues of propranolol and pharmacokinetic profile comparison.

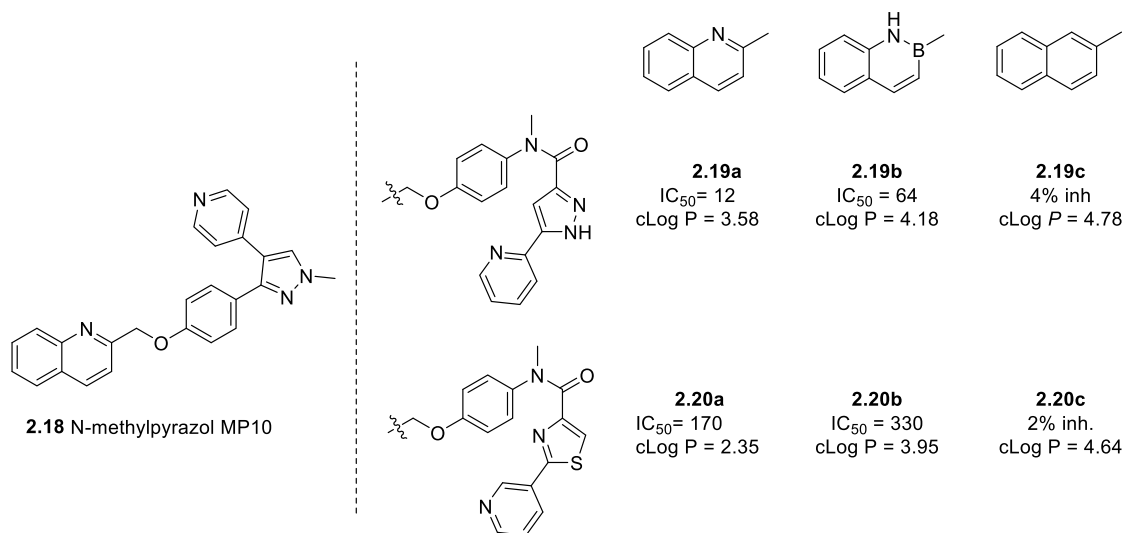
Incorporating BN-heteroaromatic moieties in naphthalene derivatives was explored in phosphodiesterase (PDE10A) inhibitors analogies as well.³⁰ Compound **2.18** (Scheme 2.10) named as MP10 is an efficient inhibitor of phosphodiesterase (PDE10A), an enzyme localized in human brain tissue and a target for treatment of various neurological diseases, and has been used as the benchmark compound regarding to PDE10A inhibition. Previous co-crystal structure analysis studies have indicated that the quinoline moiety has a strong H-bonding interaction with the nearby Tyr-693 residue. Borazaronaphthalenes

²⁸ Rombouts, F. J.; Tovar, F.; Austin, N.; Tresadern, G.; Trabanco, A. A. *J. Med. Chem.* **2015**, *58*, 9287–9295.

²⁹ Black, J. W.; Crowther, A. F.; Shanks, R. G.; Smith, L. H.; Dornhorst, A. C. *Lancet* **1964**, *283*, 1080–1081.

³⁰ Vlasceanu, A.; Jessing, M.; Kilburn, J. P. *Bioorg. Med. Chem.* **2015**, *23*, 4453–4461.

as an isosteric and isoelectronic naphthalene analogs have a partial protic character in NH moiety and a polarized BN bond. Compound **2.19b** and **2.20b** exhibit an unexpected high affinity towards PDE10A that is similar to the corresponding quinolinyl compounds (**2.19a** and **2.20a**) and significantly higher than the naphthyl analogs (**2.19c** and **2.20c**).



Scheme 2.10. Metabolic stability and potency of PDE10A inhibitors with naphthyl-, quinolinyl-, or borazanaphthyl- groups.

2.2 Hydrogen bonding in molecular binding recognition

Hydrogen bonding plays a key role in determining the shape, properties and functions of biomolecules³¹ such as proteins and nucleic acids, they also provide directionality and specificity in protein-ligand interactions, enzyme catalysis and in biological information transfer.³²

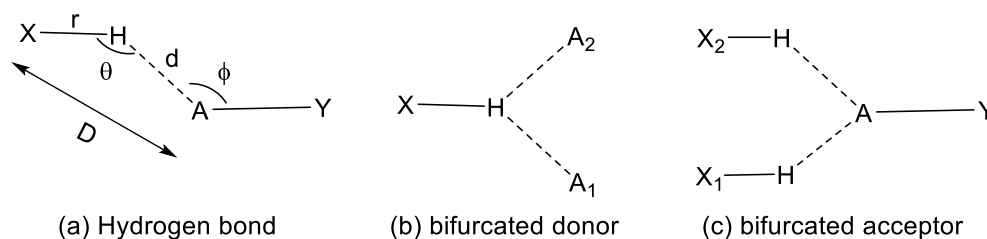
Hydrogen bond was defined by Pauling in 1939 to be a type of chemical bond and an electrostatic interaction.³³ In a configuration of X-H...A, where X and A can be any of the following elements: F, O, Cl, N, Br, and I, the hydrogen bond donor is X-H and A is the hydrogen bond acceptor the H atom is accepted as a bridging or bonding agent between the element X and A. The hydrogen bond was often described by

³¹ Hobza, P.; Havlas, Z. *Chem. Rev.* **2000**, *100*, 4253-4264.

³² Fersht, A. R.; Shi, J.-P.; Knill-Jones, J.; Lowe, D. M.; Wilkinson, A. J.; Blow, D. M.; Brick, P.; Carter, P.; Waye, M. M.; Winter, G. *Nature* **1985**, *314*, 235-238.

³³ a) Pauling, L. The nature of the chemical bond; and the structure of molecules and crystals; an introduction to modern structural chemistry; 1940. b) Pitzer, K. *J. Am. Chem. Soc.* **1960**, *82*, 4121-4121. c) Desiraju, G. R. *Acc. Chem. Res.* **2002**, *35*, 565-573.

geometrical parameters involving H atom, d , θ and r (Scheme 2.11a). Parameter D was often used in the older literature for describing the distance between two heavy atoms as the position of H atoms were hard to determine. Hydrogen bonds are long-range interactions. If there are two acceptors A_1 and A_2 (bifurcated donor), or Y-A bonded to more than one hydrogen (bifurcated acceptor), the hydrogen bonds formed is called bifurcated hydrogen bonds (Scheme 2.11, b and c).³⁴



Scheme 2.11. Geometrical parameters of hydrogen bond and definition of a bifurcated donor and acceptor.

Energy scale of hydrogen bond range from -0.5 to nearly -40 kcal/mol.³⁵ The weakest hydrogen bonds are barely distinguishable from van der Waals interactions and the strongest ones are comparable to weak covalent bonds. Hydrogen bonds are classified into three categories: weak, strong and very strong based on properties such as geometry, energy, thermodynamic and function in nature (Table 2.1). Strong hydrogen bonds are formed usually between acids and its conjugate base or between a base and its conjugate acid. One of the distinguish features is its covalent bond character with an energy range of 15-40 kcal/mol. The moderate (4-15 kcal/mol) hydrogen bonds represent a transition from quasi-covalent to electrostatic character and often occurs between molecules that contains functional groups (carboxylic acids, alcohols) capable of forming moderate hydrogen bonds. Weak hydrogen bonds with bonding energy smaller than 4 kcal/mol are electrostatic interactions, and its nature depends on the donor and acceptor group.

³⁴ Zeegers-Huyskens, T.; Huyskens, P., *Intermolecular Forces*, Springer: 1991, pp 1-3.

³⁵ Van der Lubbe, S. C.; Fonseca Guerra, C. *Asian J. Chem.* **2019**, *14*, 2760-2769.

Table 2.1. Properties of three different types of hydrogen bonds.

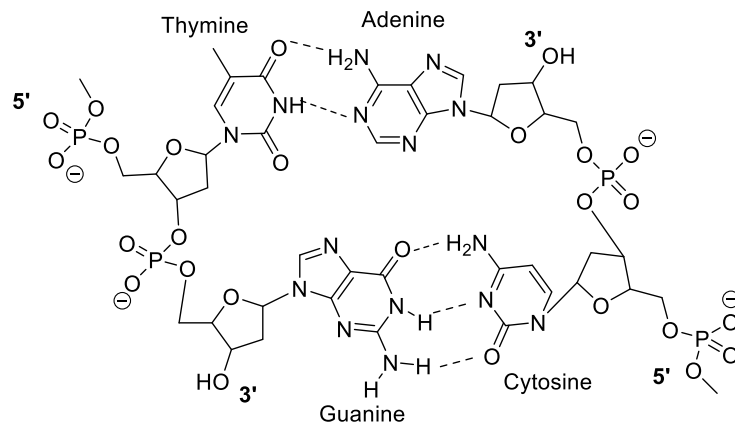
	Strong	Medium	Weak
Interaction type	Most covalent	Mostly electrostatic	Electrostatic
Bond energy (kcal/mol)	15-40	4-15	0-4
Bond lengths d (Å)	1.2-1.5	1.5-2.2	2.0-3.0
Bond angle θ , X-H...A (°)	175-180	130-180	90-150
Examples	HF complexes	carboxylic acid, alcohols, biomolecules	C-H...O/N O/N-H... π

Hydrogen bonding is one of the most important fundamental interactions for molecular associations and molecular structure maintaining in various biological and chemical systems.³⁶ One of the typical examples of hydrogen bonding is base-pairing in the DNA double-helix structure. Double-stranded DNA run antiparallel in opposite directions with 5' carbon end of one strand matched with 3' carbon end of another strand.³⁷ The double-helix structure was composed of sugar-phosphate backbone forming the outside of the helix, and the nitrogenous base pairs, joined by hydrogen bonds, are stacked in the interior of the helix similar to the steps of a staircase. Base complementary rules also determine adenine pair with thymine and guanine pairs with cytosine (Scheme 2.12).

³⁶ a) Liu, Z.; Wang, G.; Li, Z.; Wang, R. *J. Chem. Theory Comput.* **2008**, *4*, 1959-1973.

b) Minch, M. J., An introduction to hydrogen bonding (Jeffrey, George A.). ACS Publications: 1999.

³⁷ Alberts, B.; Johnson, A.; Lewis, J.; Raff, M.; Roberts, K.; Walter, P., The structure and function of DNA. In *Molecular Biology of the Cell. 4th edition*, Garland Science: 2002.



Scheme 2.12. Complementary base pairs in the DNA double helix. The hydrogen bonds are indicated by the dash line.

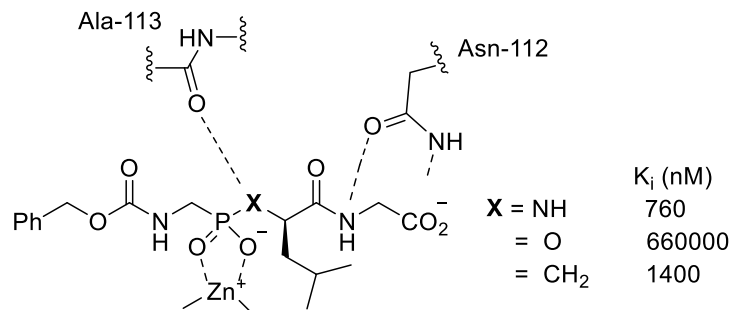
In biological conditions, hydrogen bond provides specificity and directionality.³⁸ Hydrogen bonds can form and break rapidly during the process of molecular recognition and conformational change, and due to the bond strength and directional nature of hydrogen bond interactions, a desired specificity in the binding process can be achieved.³⁹ As an example, in a series of phosphorus-containing peptide inhibitors for zinc endopeptidase thermolysin (Scheme 2.13),⁴⁰ inhibitors with X= NH moiety are evaluated and compared with phosphonate ester (X = O) moiety. The replacement of the NH-group of the ligand by -O- group reduces binding affinities by a factor of 1000, which was explained by the loss of NH...O=C hydrogen bond and repulsion of two electronegative oxygen atoms. However, when the NH group was replaced with a methylene unit (X = CH₂), experimental results shown that this compound (X = CH₂) has almost the same affinity as the phosphoramidates even though C-H...O hydrogen bonds are normally considered to be weaker than heteroatom-hydrogen bonds.⁴¹

³⁸ a) Wade, R. C.; Goodford, P. J. *Prog. Clin. Biol. Res.* **1989**, 289, 433-444. b) Davis, A. M.; Teague, S. J. *Angew. Chem. Int. Ed.* **1999**, 38, 736-749.

³⁹ Kubinyi, H., Hydrogen bonding: the last mystery in drug design? *Pharmacokinetic optimization in drug research: biological, physicochemical, and computational strategies* **2001**, 513-524.

⁴⁰ Morgan, B.; Scholtz, J. M.; Ballinger, M. D.; Zipkin, I. D.; Bartlett, P. A. *J. Am. Chem. Soc.* **1991**, 113, 297-307.

⁴¹ Horowitz, S.; Trievel, R. C., *J. Biol. Chem.* **2012**, 287, 41576-41582. b) Itoh, Y.; Nakashima, Y.; Tsukamoto, S.; Kurohara, T.; Suzuki, M.; Sakae, Y.; Oda, M.; Okamoto, Y.; Suzuki, T. *Sci. Rep.* **2019**, 9, 1-12.



Scheme 2.13. Interactions between inhibitors and thermolysin and inhibition constants K_i for binding of inhibitors to thermolysin.

Another example related to the hydrogen bonding as a key selective factor for enzymatic reaction is observed in a Gln102Arg mutant of lactate dehydrogenase.⁴² The wild type enzyme lactate dehydrogenase has a selectivity for lactate over malate of 1000:1. Due to the mutation of glutamine to arginine at position 102, a hydrogen bond is newly formed between the malate γ -carboxylate group and the arginine side chain, resulting in a selectivity change of seven orders of magnitude and the reaction rate with malate is now 10000 times faster than lactate.

2.3 Engineered T4 double mutant lysozyme as arene recognition cavity

Empty protein cavities with non-polar residues rarely exceed 50 \AA^3 in volume.⁴³ Larger cavity can be up to about 150 \AA^3 in volume and are typically solvated with water in the binding site.⁴⁴ Mutations that convert a bulky buried residue (such as Leucine or phenylalanine) to a small residue such as alanine can generate cavities in the core of a protein. Matthews and coworkers created a structurally rigid non-polar T4 lysozyme binding cavity by mutating Leu 99 to Ala. At the same time, the melting temperature of the resulting T4 lysozyme is increased by 6.0 C at $\text{pH} = 3.0$.⁴⁵ While the wild type T4 lysozyme has a cavity volume of 33 \AA^3 in the C-terminal domain adjacent to Leu 99, the L99A mutation increased this volume to about 150 \AA^3 with no solvent molecule observed in the cavity. Ligand binding interactions with T4 L99A

⁴² Wilks, H. M.; Hart, K. W.; Feeney, R.; Dunn, C. R.; Muirhead, H.; Chia, W. N.; Barstow, D. A.; Atkinson, T.; Clarke, A. R.; Holbrook, J. J. *Science* **1988**, *242*, 1541-1544.

⁴³ Matthews, B. W.; Liu, L. *Protein Sci.* **2009**, *18*, 494-502.

⁴⁴ Hubbard, S. J.; Gross, K.-H.; Argos, P. *Protein Eng.* **1994**, *7*, 613-626.

⁴⁵ a) Eriksson, A. E.; Baase, W. A.; Wozniak, J. A.; Matthews, B. W. *Nature* **1992**, *355*, 371-373. b) Eriksson, A. E.; Baase, W. A.; Zhang, X.-J.; Heinz, D. W.; Blaber, M.; Baldwin, E. P.; Matthews, B. W. *Science* **1992**, *255*, 178-183.

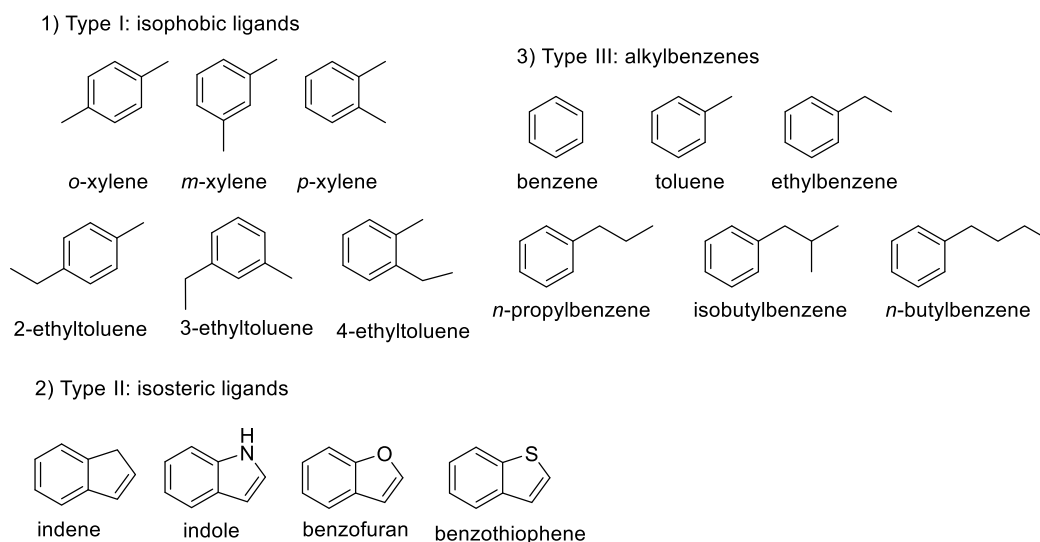
lysozyme mutant causes various amounts of reorganization of binding site based on the X-ray structure analyses of L99A-ligand complexes.⁴⁶ While the binding cavity remains rigid upon ligand binding and is mainly responsible for discrimination of ligand shapes, large conformational adjustments (large positional shifts of 1.5-2.5 Å) were found to occur in the flexible region, helix F (residue 109-113) with a significantly higher temperature factors than other regions.⁴⁷ The structure and positional shift of helix F in the C-terminal domain plays a central role in accommodating ligands and determining the interaction between the ligands and binding site.

There are three types of investigations to probe various aspects of ligand binding to the cavity of L99A T4 lysozyme mutant (Scheme 2.14):⁴⁸ 1) isophobic ligands of equivalent hydrophobicity to probe the energy cost of ligand (same hydrophobicity) packing in cavity site (Type I). 2) isosteric ligands of different hydrophobicity and its resulted difference in binding free energy (Type II). 3) alkylbenzenes with different size of side-chain length for the effect the ligand size (Type III). Isothermal titration calorimetry (ITC) measurements for the binding of ligand types I-III are listed in Table 2.2. Disubstituted ligands show a weaker binding affinity compared to their mono-substituted counterparts (xylenes vs. ethylbenzene and ethyltoluene vs. propylbenzene). There is only a rough correlation between ligand hydrophobicity and binding free energy based on the results for type II ligands. And lastly, a clear trend was indicated between the length of ligand's alkyl sidechain (type III ligands) and binding affinity of the ligand: the longer the alkyl sidechain is, the larger binding free energy was observed.

⁴⁶ Xu, J.; Baase, W. A.; Baldwin, E.; Matthews, B. W. *Protein Sci.* **1998**, *7*, 158–177.

⁴⁷ Matthews, B. W. *Biochemistry* **1987**, *26*, 6885–6888.

⁴⁸ Morton, A.; Matthews, B. W. *Biochemistry*, **1995**, *34*, 8576–8588.



Scheme 2.14. Classification of binding ligands for T4 lysozyme L99A.

Table 2.2. Binding thermodynamic data for aromatic compounds with L99A cavity.

	ΔG (kcal/mol)	K_a ($\times 10^3$ M ⁻¹)
<i>o</i> -xylene	-4.60 \pm 0.06	2.13 \pm 0.22
<i>m</i> -xylene	-4.75 \pm 0.15	2.75 \pm 0.8
<i>p</i> -xylene	-4.61 \pm 0.06	2.37 \pm 0.25
2-ethyltoluene	-4.56 \pm 0.06	1.98 \pm 0.20
3-ethyltoluene	-5.12 \pm 0.02	5.05 \pm 0.15
4-ethyltoluene	-5.42 \pm 0.01	8.33 \pm 0.08
benzofuran	-5.46 \pm 0.03	8.9 \pm 0.50
indene	-5.13 \pm 0.01	5.17 \pm 0.09
indole	-4.89 \pm 0.06	3.45 \pm 0.38
thianaphthene	-5.71 \pm 0.05	13.6 \pm 1.2
benzene	-5.19 \pm 0.16	5.7 \pm 1.7
toluene	-5.52 \pm 0.04	9.8 \pm 0.6
ethylbenzene	-5.76 \pm 0.07	14.8 \pm 1.7
<i>n</i> -propylbenzene	-6.55 \pm 0.02	55.2 \pm 2.0
isobutylbenzene	-6.51 \pm 0.06	51.0 \pm 4.9
<i>n</i> -butylbenzene	-6.70 \pm 0.02	69.8 \pm 2.9

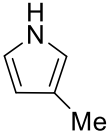
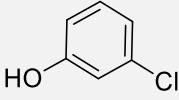
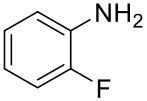
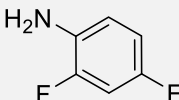
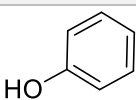
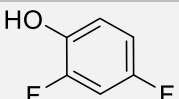
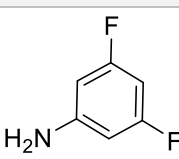
In 2002, Matthews and Shoichet introduced a second mutation in the otherwise non-polar cavity of L99A,⁴⁹ the methionine residue at 102 position was converted to a polar residue glutamine. This polar binding cavity was named T4 lysozyme double mutant L99A/M102Q. In contrast to L99A cavity that has

⁴⁹ a) Wei, B. Q.; Baase, W. A.; Weaver, L. H.; Matthews, B. W.; Shoichet, B. K. *J. Mol. Biol.* **2002**, 322, 339–355.

b) Wei, B. Q.; Weaver, L. H.; Ferrari, A. M.; Matthews, B. W.; Shoichet, B. K. *J. Mol. Biol.* **2004**, 337, 1161–1182.

been shown for binding mostly apolar small molecules (e.g. phenol and aniline are not observed to bind), polar molecules were found to bind preferentially to the cavity of L99A/M102Q. Seven ligands are known not to bind to the apolar pocket of L99A (Table 2.3). Circular dichroism (CD) was used to measure their binding affinity to the cavity L99A/M102Q; all of them were found to result in an increase of L99A/M102Q melting temperature, and none of them stabilizes L99A. In addition, it has been shown that 2-mercaptoethanol (from the crystallization buffer) and a water molecule reside in the binding pocket of the T4 lysozyme double mutant in the absence of an added ligand.⁵⁰

Table 2.3. Representative ligands bind preferentially to the polar L99A/M102Q cavity.

Compound	L99A		L99A/M102Q	
	ΔT_m (°C)	binding detected?	ΔT_m (°C)	binding detected?
	0.1	no	+2.1	Yes ^a
	-0.2	no	+2.7	Yes ^a
	0.3	no	+1.7	Yes ^a
	-0.2	no	+1.3	Yes
	-0.2	no	+1.9	Yes ^a
	0.3	no	+1.6	Yes
	0	no	+1.7	Yes ^a

^a Binding confirmed by crystallography or calorimetry.

⁵⁰ Graves, A. P.; Brenk, R.; Shoichet, B. K. *J. Med. Chem.* **2005**, *48*, 3714–3728.

Four polar ligands and toluene are further examined by ITC to determine the binding affinity K_a and thermodynamics. Whereas toluene, a nonpolar ligand binds to L99A/M102Q with K_a of $6.4 \times 10^3 \text{ M}^{-1}$, its polar isostere phenol does not bind to L99A. Aniline derivatives is another class of ligand for L99A/M102Q cavity, and the smaller nitrogen-containing heterocycle derivative 3-methylpyrrole shows a lower K_a compares to larger derivatives such as 3-chlorophenol (Table 2.4).

Table 2.4. Calorimetric analysis of ligand binding to L99A/M102Q

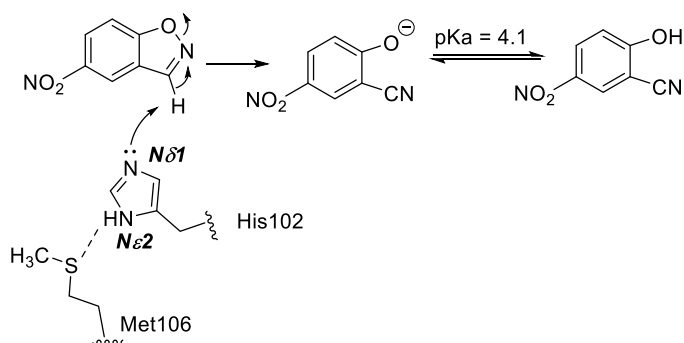
Compound	$K_a (\times 10^3 \text{ M}^{-1})^a$	ΔH (kcal/mol) ^b	N^c
3-methylpyrrole	6.3	-7	0.7
3-chlorophenol	18	-9	0.7
2-fluoroaniline	10	-8	0.6
phenol	11	-8	0.8
toluene	6.4	-6	0.8

^a Association constant ^b Calorimetric molar enthalpy

^c Apparent stoichiometry of ligand binding to L99A/M102Q lysozyme.

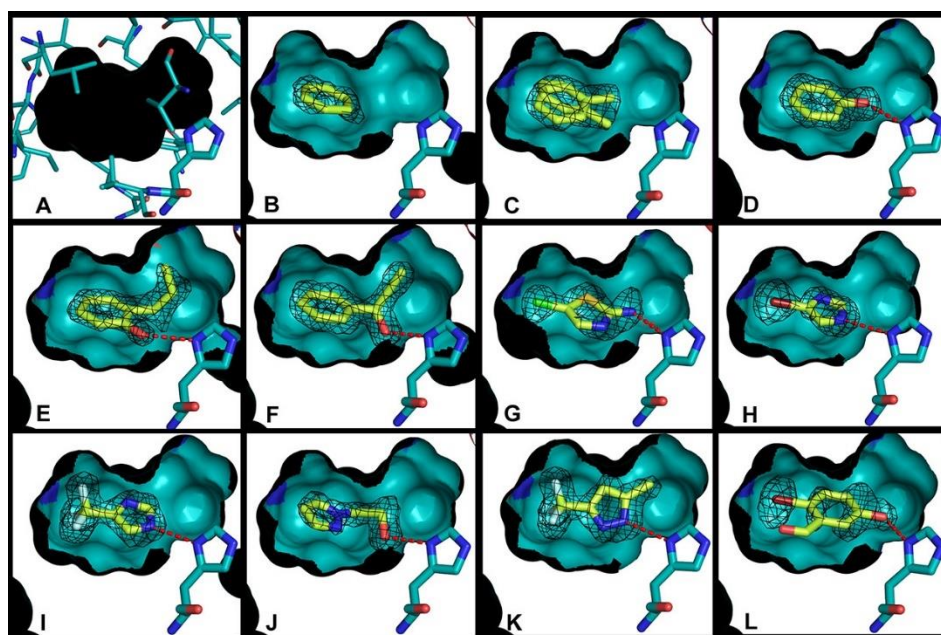
To investigate how the effects of the residue in the active site relates to ligand binding and enzyme activity, Shoichet and workers developed another T4 lysozyme double mutant L99A/M102H†, a positively charged histidine residue was introduced at the 102 methionine position of the L99A mutant into the binding pocket.⁵¹ Six stabilizing substitutions at sites distal from the cavity binding site are required to stabilize and enable the expression of this double mutant L99A/M102H†, and these distal substitutions are indicated by the dagger†. This engineered model protein cavity not only has been widely studied as a model for ligand recognition, but it also has been reported as a Kemp eliminase with k_{cat}/K_M measured to be $0.43 \text{ M}^{-1}\text{s}^{-1}$ at pH 5.0. Kemp elimination is a well-studied reaction in which a catalytic base abstract a proton from a benzisoxazole ring (Scheme 2.15). The substrate reactivity is enhanced by a polar, aprotic environment. The presence of the catalytic polar residue M102H (His102 is neutral over the range of pH 7.7 to 5.0) facilitates the enzymatic rate of the reaction.^{51a}

⁵¹ a) Merski, M.; Shoichet, B. K. *Proc. Natl. Acad. Sci.* **2012**, *109*, 16179–16183. b) Merski, M.; Shoichet, B. K. *J. Med. Chem.* **2013**, *56*, 2874–2884.



Scheme 2.15. The Kemp elimination in L99A/M102H model cavity sites.

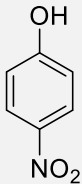
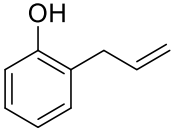
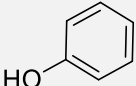
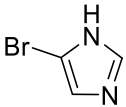
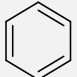
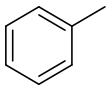
Similar to L99A, L99A/M102H[†] maintains a cavity size of approximately 150 Å³ and the site is sequestered from bulk solvent. The major difference is the construction of stabilizing disulfide bond between Cys21 and Cys142. The presumably protonated Nε2 of His102 is shown to be hydrogen bonded with Sδ of Met 106, and Nδ1 is unprotonated and is pointed into the pocket for ligand interactions (Scheme 2.15). This conformation is preserved for 11 ligand-protein complex crystallographic structures (Scheme 2.16). In its holocomplex structure, 2-mercaptoethanol (BME), a component of the crystallization buffer was present while no water molecules were observed. Hydrogen bonds was observed between the hydrogen bond donating group of the ligand and hydrogen-bond accepting Nδ1 of His102. The binding thermodynamics were also measured by isothermal titration calorimetry (ITC) for 8 ligands titrated to L99A/M102H[†] (Table 2.5). Polar ligands with hydrogen bond donating group (-OH) such as 4-nitrophenol are found to have a much higher binding affinity than non-polar ligands such as benzene or toluene in the cavity of L99A/M102H[†].



Scheme 2.16. Crystallographic poses of the L99A/M102H[†] with ligands complexes. A) L99A/M102H internal cavity. B) L99A/M102H[†] with benzene bound. C) L99A/M102H[†] with toluene bound. D) L99A/M102H[†] with phenol bound. E) L99A/M102H[†] with 2-allyl phenol bound. F) L99A/M102H[†] with 1-phenyl-2-propyn-1-ol bound. G) L99A/M102H[†] with 2-amino-5-chloro thiazole bound. H) L99A/M102H[†] with 4-bromoimidazole bound. I) L99A/M102H[†] with 4-trifluoromethyl imidazole bound. J) L99A/M102H[†] with 2-(pyrazolo-1-yl) ethanol bound. K) L99A/M102H[†] with 3-trifluoromethyl-5-methyl pyrazole bound. L) L99A/M102H[†] with 2-bromo-5-hydroxybenzaldehyde bound.

[†] indicates six stabilizing substitutions at sites distal from cavity site.

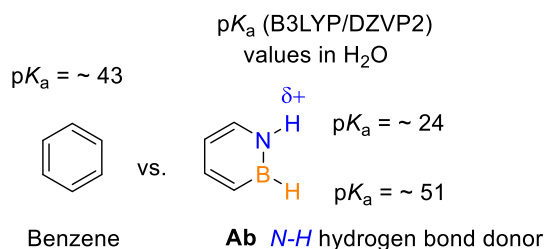
Table 2.5. Binding affinity by isothermal titration calorimetry (ITC) to L99A/M102H†^a.

Ligand	K_a (M ⁻¹)	ΔG (kcal/mol)	K_d (μ M)
4-nitrophenol 	385,500	-7.63	3
2-allyl phenol 	13,900	-5.66	72
Phenol 	9,680	-5.44	103
4-bromo imidazole 	3,155	-4.78	317
Benzene 	2,083	-4.53	480
Toluene 	1,105	-4.16	905

^a All values reflect the average of reflects the average of duplicate measurements from two separate ligand solutions.

2.4 H-bonding between 1,2-azaborine and T4 double mutant lysozyme cavity

Like benzene, 1,2-azaborine have delocalized structures consistent with aromaticity, however, unlike benzene with C–H bond pK_a of 43, the NH of 1,2-azaborines is protic and can engage in hydrogen bonding. As we previously calculated (B3LYP/DZVP2),⁵² the pK_a value of the 1,2-azaborine NH is around 24 (Scheme 2.17). The protic nature of this NH moiety is consistent with deuterium exchange with CD₃OD with a rate constant of $k = 7 \times 10^7 \text{ M}^{-1}\text{s}^{-1}$.⁵³



Scheme 2.17. Selected comparisons of pK_a values.

Our lab established a fundamental understanding of the hydrogen bonding capability of 1,2-azaborine in biological model systems-T4 lysozyme mutant. The first experimental evidence of 1,2-azaborine binding inside the nonpolar cavity of T4 lysozyme L99A as a ligand was reported as crystallographic complex structures.⁵⁴ For parental 1,2-azaborine, it binds in a very similar fashion as its carbon isosteres of benzene. There are some small differences in binding between ethyl-substituted N-ethyl-1,2-azaborine (EtAzB) and ethylbenzene. As the ethyl substituent is positioned in the bulge region of the cavity, for the two alternative modes of EtAzB, the azaborine rings are offset relative to each other by about 0.6 Å, while the two alternative modes of ethylbenzene superimpose with each other by about 0.2 Å. The Liu group also characterized the binding of ligand 1,2-azaborines as a hydrogen bond donor in the polar cavity of T4 lysozyme double mutant L99A/M102Q.⁵⁵ The X-ray structure data (Scheme 2.18) show

⁵² Marwitz, A. J. V.; Matus, M. H.; Zakharov, L. N.; Dixon, D. A.; Liu, S.-Y. *Angew. Chem. Int. Ed.* **2009**, *48*, 973–977.

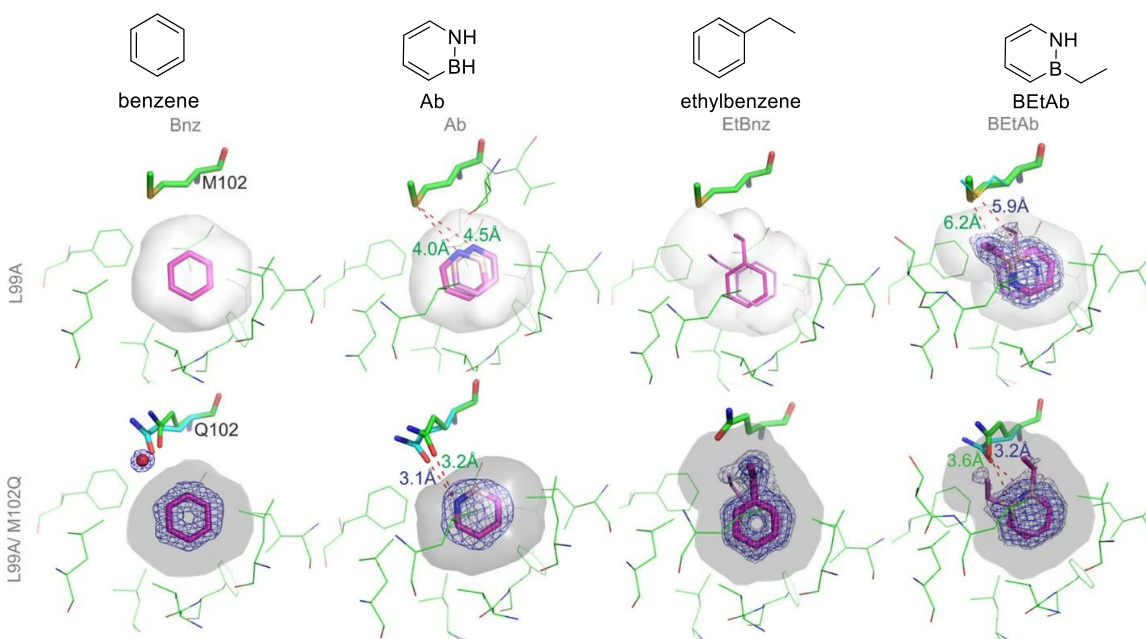
⁵³ Abbey, E. R.; Lamm, A. N.; Baggett, A. W.; Zakharov, L. N.; Liu, S.-Y. *J. Am. Chem. Soc.* **2013**, *135*, 12908–12913.

⁵⁴ Liu, L.; Marwitz, A. J. V.; Matthews, B. W.; Liu, S.-Y. *Angew. Chem. Int. Ed.* **2009**, *48*, 6817–6819.

⁵⁵ Lee, H.; Fischer, M.; Shoichet, B. K.; Liu, S.-Y. *J. Am. Chem. Soc.* **2016**, *138*, 12021–12024.

that NH group of 1,2-azaborine ligand formed hydrogen bonding with the carbonyl oxygen of the Gln 102 residue (with the distance of 3.1 and 3.2 Å for each of the protein conformations).

In a similar hydrogen bonding mode, the observed distance between the NH group of the BEtAb ligand and the Gln102 carbonyl oxygen is 3.2 Å (3.6 Å for the alternative conformation). The binding of 1,2-azaborine ligand has found to leads to a geometric change of the glutamine residue to accommodate hydrogen bonding compared to the corresponding carbonaceous ligand-bound structures.



Scheme 2.18. 1,2-Azaborines and arenes bound in the T4 lysozyme L99A and L99A/M102Q binding pockets.

To better understand the binding thermodynamics of Bnz, EtBnz, Ab, and BEtAb with L99A and L99A/M102Q T4 lysozyme mutants in aqueous solution, isothermal titration calorimetry (ITC) was used to measure the binding free energies of each complex (Table 2.6). Consistent with the more polar character of 1,2-azaborine ligands and associated higher desolvation penalty, upon binding to the nonpolar L99A cavity, azaborines lost between 0.4 and 0.5 kcal/mol in binding free energy compared to their corresponding carbonaceous analogs. Conversely, due to the favorable hydrogen bonding interaction between 1,2-azaborine and the polar L99A/M102Q cavity, we observed upon binding to the polar L99A/M102Q cavity, Ab and BEtAb gain between 0.4 and 0.2 kcal/mol of binding free energy when compared to their

carbonaceous analog benzene and ethylbenzene, respectively. The data indicate that the hydrogen bonding interaction is strong enough to overcome the desolvation penalty of the 1,2-azaborine ligand.

Table 2.6. Binding free energy and affinity determined by ITC for 1,2-azaborine ligands and its carbon analogy (Experiments were repeated five times and averaged with standard deviation error of the mean).

	L99A		L99A/M102Q	
	ΔG (kcal/mol)	K_a ($\times 10^4 M^{-1}$)	ΔG (kcal/mol)	K_a ($\times 10^4 M^{-1}$)
Bnz	-5.54 \pm 0.04	1.89 \pm 0.12	-5.96 \pm 0.04	3.95 \pm 0.29
Ab	-5.04 \pm 0.03	0.77 \pm 0.05	-6.40 \pm 0.02	8.77 \pm 0.28
EtBnz	-5.54 \pm 0.06	1.91 \pm 0.18	-5.37 \pm 0.03	1.41 \pm 0.07
BEtAb	-5.12 \pm 0.02	0.90 \pm 0.04	-5.59 \pm 0.02	2.08 \pm 0.06

2.5 The measurement of hydrogen bonding strengths

The strength of hydrogen bonding are commonly predicted and calculated by molecular modeling docking experiments and theoretical energy calculations.⁵⁶ The strength of hydrogen bonding were considered to be difficult to determine experimentally due to the challenge of dissecting the respective contributions to binding free energy of different factors including enthalpic factors like electrostatic interaction, desolvation and entropic factors such as hydrophobic effects, residual mobility and dynamics.⁵⁷

There are few representative approaches in the literature to estimate hydrogen bond strength. Fersht⁵⁸ studied the coupling of tyrosine to ATP to yield tyrosyl-AMP, which is the first step in the transfer of tyrosine to t-RNA catalyzed by the enzyme tyrosyl t-RNA synthase. Site-directed mutagenesis generated mutant enzymes that differ in their ability to form hydrogen bonds with their substrates. In the wild type enzyme active site there are eleven possible hydrogen bonds identified with its substrate and eight of them are from amino-acid side chains that can be mutated. By systematically mutating the hydrogen bond donor

⁵⁶ For selected examples, see: a) Wendler, K.; Thar, J.; Zahn, S.; Kirchner, B. *J. Phys. Chem. A* **2010**, *114*, 9529–9536. b) Dong, H.; Hua, W.; Li, S. *J. Phys. Chem. A* **2007**, *111*, 2941–2945. c) Gilli, P.; Pretto, L.; Bertolasi, V.; Gilli, G. *Acc. Chem. Res.* **2009**, *42*, 33–44. d) Sheu, S. Y.; Yang, D. Y.; Selzle, H. L.; Schlag, E. W. *Proc. Natl. Acad. Sci. U. S. A.* **2003**, *100*, 12683–12687. (e) Schwöbel, J. A. H.; Ebert, R.-U.; Kühne, R.; Schüürmann, G. *J. Phys. Org. Chem.* **2011**, *24*, 1072–1080. f) Schwöbel, J. A. H.; Ebert, R.-U.; Kühne, R.; Schüürmann, G. *J. Comput. Chem.* **2009**, *30*, 1454–1464. g) Kollman, P. A.; Massova, I.; Reyes, C.; Kuhn, B.; Huo, S.; Chong, L.; Lee, M.; Lee, T.; Duan, Y.; Wang, W. *Acc. Chem. Res.* **2000**, *33*, 889–897.

⁵⁷ a) Bronowska, A. K. *Thermodynamics of Ligand-Protein Interactions: Implications for Molecular Design, Thermodynamics - Interaction Studies - Solids, Liquids and Gases.* ISBN: 978-953-307-563-1, InTech, 2011. b) Tsai, C. J.; Norel, R.; Wolfson, H. J.; Maizel, J. V. Nussinov, R. *Protein-Ligand Interactions: Energetic Contributions and Shape Complementarity* eLS, 2001.

⁵⁸ Fersht, A. R.; Shi, J.-P.; Knill-Jones, J.; Lowe, D. M.; Wilkinson, A. J.; Blow, D. M.; Brick, P.; Carter, P.; Waye, M. M.; Winter, G. *Nature* **1985**, *314*, 235–238.

or acceptor on the sidechain, they can interrupt the formation of hydrogen bonding with either an uncharged group on the substrate or a charged group on the substrate. The kinetic methods are used here to determine the contribution of the side chains of different amino acid to binding energy of enzyme-transition state complexes (Calculated from the ratio of k_{cat}/K_M , $\Delta G = -RT \ln \{(k_{cat}/K_M)_{mut} / (k_{cat}/K_M)_{wt}\}$).

They classified the hydrogen bond interactions by two categories, hydrogen bonds with a neutral group and with a charged group. Based on their analysis, they found that a neutral-neutral hydrogen bond contributes about 0.5-1.5 kcal/mol in binding energy (equivalent to a 2- to 15-fold increase in affinity), but a hydrogen bond with a charged group contributes up to 4.5 kcal/mol (equivalent to a 3000-fold increase in affinity). Table 2.7 shown that they systematically analyzed the effects of mutation on loss and gain in hydrogen bond energy. An estimate of strength of the hydrogen bond between the hydroxy group from Tyr 34 and Phe 34 is around 0.52 kcal/mol as a weak hydrogen bonding interaction of tyrosyl OH with uncharged species (Table 2.7, entry 1). In comparison, mutation of Tyr 169 to Phe 169 resulted a loss of energy of 3.72 kcal/mol, indicating a strong hydrogen bond between the hydroxyl group of tyr169 and the ammonium ion of the substrate (Table 2.7, entry 7).

Table 2.7. Comparison of binding energies of wild-type and mutant with substrates.

entry	mutation	substrate	ΔG (kcal/mol)
1	Tyr 34* to Phe 34	Tyr	0.52
2	Cys 35* to Phe 34	ATP	1.14
3	Cys 51 to Ala 51	ATP	0.47
4	Asn 48 to Gly 48	ATP	0.77
5	His 48* to Gly 48	ATP	0.96
6	Cys 35* to Ser 35	ATP	1.18
7	Tyr 169* to Phe 169	Tyr	3.72
8	Gln 195* to Gly 195	Tyr	4.49
9	Ser 35 to Gly 35	ATP	-0.04
10	Thr51* to Ala 51	ATP	-0.44

*wild type enzymes

Williams and coworkers also estimated the hydrogen bond strength by measuring the binding constant of organic molecules in a series of NMR studies under aqueous conditions.⁵⁹ Amide-amide hydrogen bonds strength between cell wall peptides and glycopeptide antibiotics was approximated to be -0.2 to -1.7 kJ/mol. The binding free energy of the amide-amide hydrogen bond (ΔG_p) in this system is

⁵⁹ Williams, D. H.; Searle, M. S.; Mackay, J. P.; Gerhard, U.; Maple-stone, R. A. Proc. Natl. Acad. Sci. 1993, 90, 1172-1178.

estimated based on assumed energy contribution of hydrophobic effects (ΔG_h) and the assumed entropic cost per rotor restricted when peptides bind to antibiotics (ΔG_r) by applying the formula: observed binding free energy $\Delta G = \Delta G_h + \Delta G_r + \Delta G_p$ or $\Delta G_p = \Delta G - \Delta G_h - \Delta G_r$.

2.6 Introduction to isothermal titration calorimetry

Isothermal titration calorimetry (ITC), is an invaluable tool to measure the thermodynamic data.⁶⁰ A thermodynamic characterization can provide detailed information, such as the driving force (enthalpic or/and entropic contribution) for the ligand association with its target.⁶¹ During the ITC titration experiment, one binding partner is titrated into a solution containing the interaction partner, and the heat generated or absorbed during the titration can be quantified by calorimeter.⁶² A single titration experiment allows the simultaneous determination of the equilibrium binding constant (K_a) and thus the Gibbs free energy change (ΔG), the change of enthalpy (ΔH), and the stoichiometry (n) of the reaction by analyzing the resultant titration curve. The heat capacity change (ΔC_p) of the binding reaction can be accessed by performing experiments at different temperatures.⁶³

A closer look at binding process and thermodynamic parameters has its practical interest as it can provide insight for development of structure-based molecular design-strategies.⁶⁴ ΔH serves as a key indicator during hit-to-lead optimization to qualify ligands as candidates for further modifications. Thermodynamic and kinetic profiling of ligands binding to a given target protein is crucial for the hit selection as well as the hit-to-lead-to-drug discovery process.⁶⁵ The hit–target binding affinity measurement by ITC can perfectly rule out the pan-assay interference compounds, referred to as PAINS, as ITC measures directly the heat flow of the hit–target binding rather than the change of fluorescence in many

⁶⁰ a) Freyer, M. W.; Lewis, E. A. *Methods Cell Biol.* **2008**, *84*, 79-113. b) Agnieszka, K. B. *Thermodynamics-Interaction Studies-Solids, Liquids and Gases* **2011**. c) Holdgate, G. A.; Ward, W. H. *Drug Discov. Today* **2005**, *10*, 1543-1550.

⁶¹ Krimmer, S. G.; Klebe, G. *J. Comput-Aided Mol Des.* **2015**, *29*, 867-883. b) Leavitt, S.; Freire, E. *Curr. Opin. Struct. Biol.* **2001**, *11*, 560-566.

⁶² Pierce, M. M.; Raman, C.; Nall, B. T. *Methods* **1999**, *19*, 213-221.

⁶³ Perozzo, R.; Folkers, G.; Scapozza, L. J. *Recept. Signal Transduction Res.* **2004**, *24*, 1-52.

⁶⁴ Chaires, J. B. *Annu. Rev. Biophys.* **2008**, *37*, 135-151.

⁶⁵ Holdgate, G. A.; Ward, W. H. *Drug Discov.* **2005**, *10*, 1543-1550.

assays.⁶⁶ ITC supplies a powerful approach to evaluating the kinetic profiling of the hit binding to its target, no matter it is a non-covalent or covalent binder.

Recently, new ITC methods have been developed to measure the kinetic parameters of ligand–enzyme binding.⁶⁷ Thus, ITC measurements in combination with kinetic ITC technique can reveal the binding kinetics (k_{on} and k_{off}) of ligands to its target. In ITC-based kinetic experiment, the generated heat signal is plotted as a function of time and parameters such as the association rate (k_{on}) as well as the dissociation rate (k_{off}) can be obtained directly and accurately according to the curve.

ITC measurements can also be applied to obtain Michaelis-Menten parameters (k_m , k_{cat} , and V_{max}) of enzyme–substrate reactions and inhibitory constant (k_i) of the enzyme–inhibitor binding, and the instantaneous rate of enzyme catalysis can be calculated by the Michaelis–Menten equation.⁶⁸ For instance, Di Trani et al. utilized the kinetic ITC technique to successfully determine the kinetic parameters of covalent and non-covalent inhibitors binding to the prolyl oligopeptidase (POP), a drug target for treating neurodegenerative disorders.⁶⁹

2.7 Double mutant cycle analysis review

The energetic contribution factors for protein-ligand complex binding process includes a variable set of interactions such as hydrophobic effects, different electrostatic interactions such as hydrogen bonding, desolvation, etc.⁷⁰ Hence, it can be difficult to deconvolute the specific energy contribution of hydrogen bonding by simply comparing the free energy ΔG value of the interaction pair of interest, for instance hydrogen bonding interaction of benzene and 1,2-azaborine of the L99A/M102Q mutant. In 1984, Fersht proposed a general thermodynamic cycle to quantify the interaction between charged residues in a barnase mutant.⁷¹ The classic double mutant thermodynamic cycle analysis would allow the extraction of

⁶⁶ Weber, P. C.; Salemme, F. R. *Curr. Opin. Struct. Biol.* **2003**, *13*, 115-121.

⁶⁷ Su, H.; Xu, Y. *Front. Pharmacol.* **2018**, 1133.

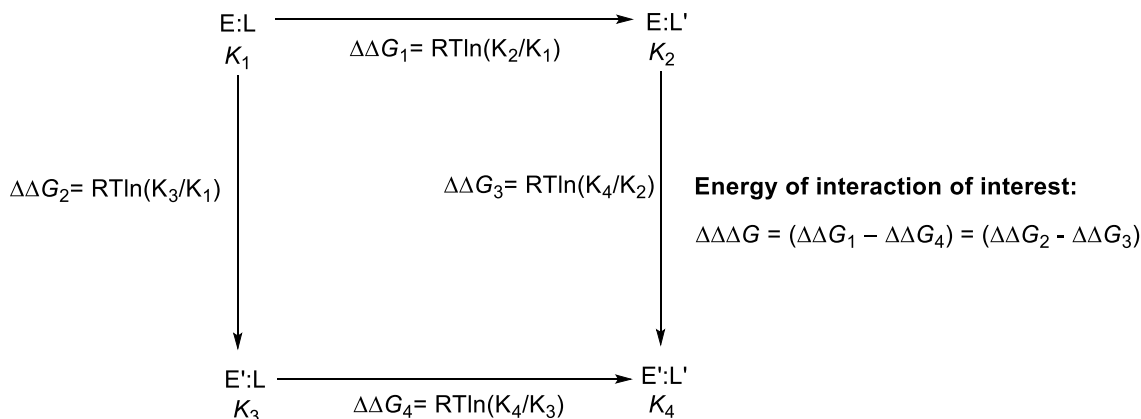
⁶⁸ Demarse, N. A.; Killian, M. C.; Hansen, L. D.; Quinn, C. F., Determining enzyme kinetics via isothermal titration calorimetry. In *Enzyme Engineering*, Springer: 2013; pp 21-30.

⁶⁹ a) Di Trani, J. M.; De Cesco, S.; O'Leary, R.; Plescia, J.; do Nascimento, C. J.; Moitessier, N.; Mittermaier, A. K. *Nat. Commun.* **2018**, *9*, 1-7. b) Garcia-Horsman, J. A.; Männistö, P. T.; Venäläinen, J. *Neuropeptides* **2007**, *41*, 1-24.

⁷⁰ Tsai, C.-J.; Norel, R.; Wolfson, H. J.; Maizel, J. V.; Nussinov, R. *Encyclopedia of Life Science*; John Wiley & Sons, Ltd.: Chichester, 2001.

⁷¹ a) Horovitz, A.; Fersht, A. R., *J. Mol. Biol.* **1990**, *214*, 613-617. b) Serrano, L.; Horovitz, A.; Avron, B.; Bycroft, M.; Fersht, A. R. *Biochemistry* **1990**, *29*, 9343-9352.

hydrogen bond interaction energy contribution from experimentally measurable binding free energy (Scheme 2.18).⁷²



Scheme 2.19. General double perturbation thermodynamic cycle. E= wild-type enzyme, E'= mutant enzyme, L= wild-type ligand, L'= mutant ligand.

As shown in Scheme 2.18, these experiments use wild-type and “mutant” versions of both the enzyme and ligand, with each “mutant” lacking the interacting groups of interest. The two horizontal arrows $\Delta\Delta G_1$ and $\Delta\Delta G_4$ accounts for the total electronic structure differences or the energy cost of removing different ligand functional group from the same enzyme cavity. And the two vertical arrows $\Delta\Delta G_2$ and $\Delta\Delta G_3$ stands for the energy cost of removing the same ligand from enzyme cavity with different residues it interacts with. Thus, the difference between these energies, $\Delta\Delta\Delta G$, is the energy of the interaction.

2.8 Exploring the strength of a hydrogen bond as a function of steric environment using 1,2-azaborine ligands and engineered T4 lysozyme receptors⁷³

2.8.1 The relationship of hydrogen bonding strength with the steric demand of the ligand

Hydrogen bonding is a fundamentally important structural organizing interaction in biomacromolecules and in biologically relevant processes. It contributes to directionality and specificity in

⁷² a) Camara-Campos, A.; Musumeci, D.; Hunter, C. A.; Turega, S. J. *Am. Chem. Soc.* **2009**, *131*, 18518-18524. b) Roth, T. A.; Minasov, G.; Morandi, S.; Prati, F.; Shoichet, B. K. *Biochemistry* **2003**, *42*, 14483-14491.

⁷³ Liu, Y.; Liu, S.-Y. *Org. Biomol. Chem.* **2019**, *17*, 7002-7006.

ligand–protein binding interactions,⁷⁴ and as a consequence, it plays an important role in the optimization of lead targets in drug design and development.⁷⁵ We anticipate that in most biologically active 1,2-azaborines, the NH group will be flanked by a boron atom that is substituted. How the size of the boron substituent influences the capability of the NH group of 1,2-azaborine to serve as a hydrogen bond donor is of fundamental interest for the development of the 1,2-azaborine motif as a pharmacophore. More generally, to the best of our knowledge, a systematic experimental and quantitative thermodynamic investigation of the strength of a hydrogen bond as a function of increasing steric environment in protein–ligand binding has not been explored.⁷⁶ The scarcity of a precedent is arguably due to the fact that the strength of the hydrogen bonding interaction is experimentally difficult to deconvolute from other factors (e.g., desolvation, hydrophobic interaction, and entropy) that contribute to the experimentally accessible overall binding free energy of the ligand to its protein target, particularly under biologically relevant aqueous conditions.⁷⁷

The isosteric relationship between 1,2-azaborines and arenes combined with the modularity of the arene recognition pocket of engineered T4 lysozymes provides a unique platform to “extract” the hydrogen bonding “enthalpy” from experimentally accessible binding free energies via the Double Mutant Cycle analysis⁷⁸ (Scheme 2.19). Here, we investigate the binding of a congeneric series of B-substituted 1,2-azaborines to L99A and L99A/M102Q mutant forms of T4 lysozymes and evaluate the strength of the NH...102Q hydrogen bonding interaction as a function of increasing steric environment at boron (H, Me, Et, *n*-Pr, and *i*-Pr). We find that the NH...102Q hydrogen bonding interaction decreases in strength with the increasing steric demand of the boron substituents. However, the observed decrease in the hydrogen bonding strength is not incremental or “continuous” but rather appears to take place in discrete steps.

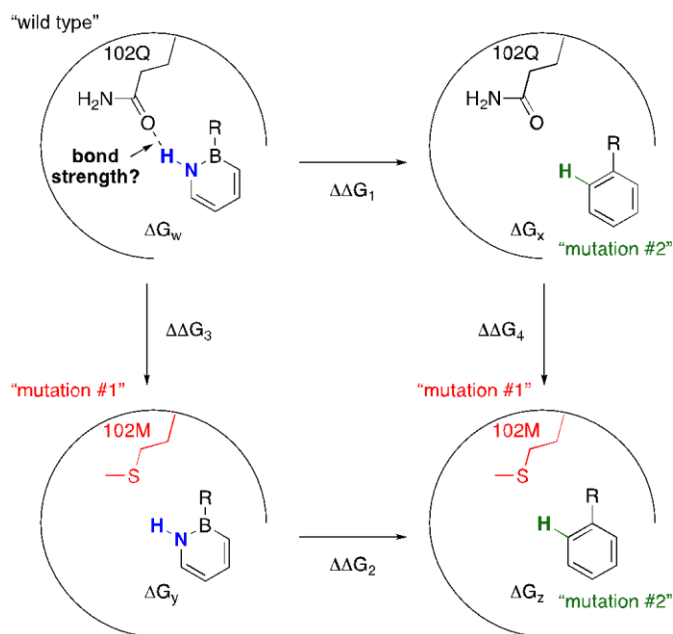
⁷⁴ a) Liu, Z.; Wang, G.; Li, Z.; Wang, R. *J. Chem. Theory Comput.* **2008**, *4*, 1959-1973. b) Fersht, A. R.; Shi, J.-P.; Knill-Jones, J.; Lowe, D. M.; Wilkinson, A. J.; Blow, D. M.; Brick, P.; Carter, P.; Waye, M. M.; Winter, G. *Nature* **1985**, *314*, 235-238.

⁷⁵ a) Hao, M.-H., *J. Chem. Theory Comput.* **2006**, *2*, 863-872. b) Foloppe, N.; Fisher, L. M.; Howes, R.; Kierstan, P.; Potter, A.; Robertson, A. G.; Surgenor, A. E. *J. Med. Chem.* **2005**, *48*, 4332-4345. c) Mills, J.; Dean, P. M. *J. Comput.-Aided Mol. Des.* **1996**, *10*, 607-622. d) Toth, G.; Bowers, S. G.; Truong, A. P.; Probst, G. *Curr. Pharm. Des.* **2007**, *13*, 3476-3493.

⁷⁶ For select examples in synthetic non-aqueous systems, see: (a) Desseyn, H.; Perlepes, S.; Clou, K.; Blaton, N.; Van der Veken, B.; Dommissie, R.; Hansen, P. *J. Phys. Chem. A* **2004**, *108*, 5175-5182. b) R. West, L. S. Whatley, M. K. T. Lee and D. L. Powell, *J. Am. Chem. Soc.*, **1964**, *86*, 3227–3229; West, R.; Powell, D. L.; Lee, M. K.; Whatley, L. S. *J. Am. Chem. Soc.* **1964**, *86*, 3227-3229. c) Berthelot, M.; Besseau, F.; Laurence, C. *Eur. J. Org. Chem.* **1998**, 925-931.

⁷⁷ a) Krimmer, S. G.; Klebe, G. *J. Comput.-Aided Mol. Des.* **2015**, *29*, 867-883. b) Tsai, C.; Norel, R.; Wolfson, H.; Maizel, J.; Nussinov, R., *Encyclopedia of Life Science*. Chichester: John Wiley & Sons, Ltd: 2001.

⁷⁸ For an overview, see: Cockroft, S. L.; Hunter, C. A. *Chem. Soc. Rev.* **2007**, *36*, 172-188.



Scheme 2.20. Evaluation of hydrogen bonding strength as a function of steric environment via double mutant cycle analysis.

Since its introduction by Fersht in 1984,⁷⁹ the thermodynamic cycle or Double Mutant Cycle analysis has established itself as a standard practice for the quantification/estimation of a specific non-covalent interaction from measurable binding free energies in proteins⁸⁰ and in synthetic chemical systems.⁸¹ The specific non-covalent interaction in question for us is the hydrogen bonding interaction (Scheme 2.19). The binding free energy ΔG_w of a “wild-type” 1,2-azaborine to the “wild-type” protein will encompass in addition to (1) the NH... 102Q hydrogen bonding also contributions from (2) desolvation of the 1,2-azaborine molecule from water, (3) the hydrophobic effect of binding of the aromatic species to the arene recognition cavity, and (4) the entropy effect of the displacement of H₂O molecules from the cavity. By measuring the additional binding free energies of “mutant” species where the hydrogen bonding interaction is absent (i.e., ΔG_x , ΔG_y , and ΔG_z), the energetic contribution from hydrogen bonding ($\Delta\Delta G = \Delta\Delta G_2 - \Delta\Delta G_1$ or $\Delta\Delta G_4 - \Delta\Delta G_3$) can be extracted. It is worth noting that a double mutation, one on the receptor and one on the ligand, each mutant lacking the interacting groups of interest, is essential for the isolation of the hydrogen bonding contribution. For example, if we were just to measure the binding

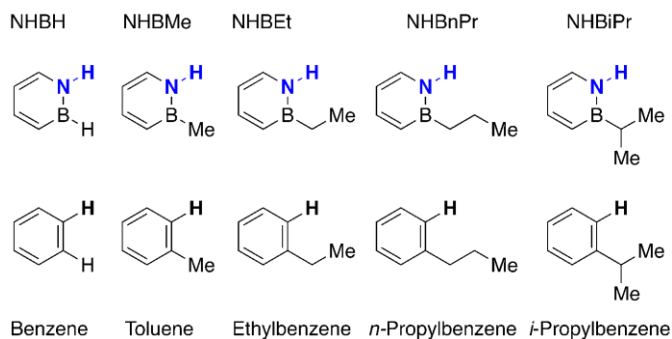
⁷⁹ Carter, P. J.; Winter, G.; Wilkinson, A. J.; Fersht, A. R. *Cell* **1984**, *38*, 835-840.

⁸⁰ Horovitz, A.; Fersht, A. R. *J. Mol. Biol.* **1990**, *214*, 613-617.

⁸¹ Camara-Campos, A.; Musumeci, D.; Hunter, C. A.; Turega, S. *J. Am. Chem. Soc.* **2009**, *131*, 18518-18524.

difference $\Delta\Delta G_1$ based on ligand mutation, i.e., 1,2-azaborine vs. benzene, we would miss the difference in energy from desolvation from water between 1,2-azaborine and benzene ($\Delta\Delta G_2$), which also needs to be accounted for. Similarly, if we were to just consider the binding difference $\Delta\Delta G_3$ based on receptor mutation, we would not account for the energetic change associated with the ligand–receptor fit ($\Delta\Delta G_4$) as a result of the change of the side chain residue.

The Double Mutant Cycle analysis was employed here to evaluate the hydrogen bonding strength as a function of the steric environment of the 1,2-azaborine ligand. Our experiments use L99A/M102Q⁸² as the wild-type protein and L99A⁸³ as the “mutant” version of the enzyme. The wild-type ligand is the 1,2-azaborine ligand, and its carbonaceous counterparts (Scheme 2.20) are the “mutant” version. The binding free energies (ΔG_w , ΔG_x , ΔG_y , and ΔG_z) were determined by isothermal titration calorimetry (ITC) experiments.⁸⁴



Scheme 2.21. A congeneric series of 1,2-azaborine ligands and their carbonaceous analogues.

We have previously reported the Double Mutant Cycle for NHBH and NHBEt. To complete the congeneric series, we report here the Double Mutant Cycle for NHBMe, NHB*n*Pr, and NHB*i*Pr (Scheme 2.21). We note that with the increasing size of the boron substituent, the solubility of the ligand decreases so that ITC conditions that differ slightly from the originally reported protocol need to be employed (see experimental section). However, the experimental conditions were kept consistent within a thermodynamic cycle. Although ITC measurements can produce numerical values for ΔG , ΔH , and ΔS , we focus our

⁸² Wei, B. Q.; Baase, W. A.; Weaver, L. H.; Matthews, B. W.; Shoichet, B. K. *J. Mol. Biol.* **2002**, *322*, 339-355.

⁸³ (a) Eriksson, A.; Baase, W.; Wozniak, J.; Matthews, B. *Nature* **1992**, *355*, 371-373.

(b) Morton, A.; Baase, W. A.; Matthews, B. W. *Biochemistry* **1995**, *34*, 8564-8575.

⁸⁴ Perozzo, R.; Folkers, G.; Scapozza, L. *J. Recept. Signal Transduction Res.* **2004**, *24*, 1-52.

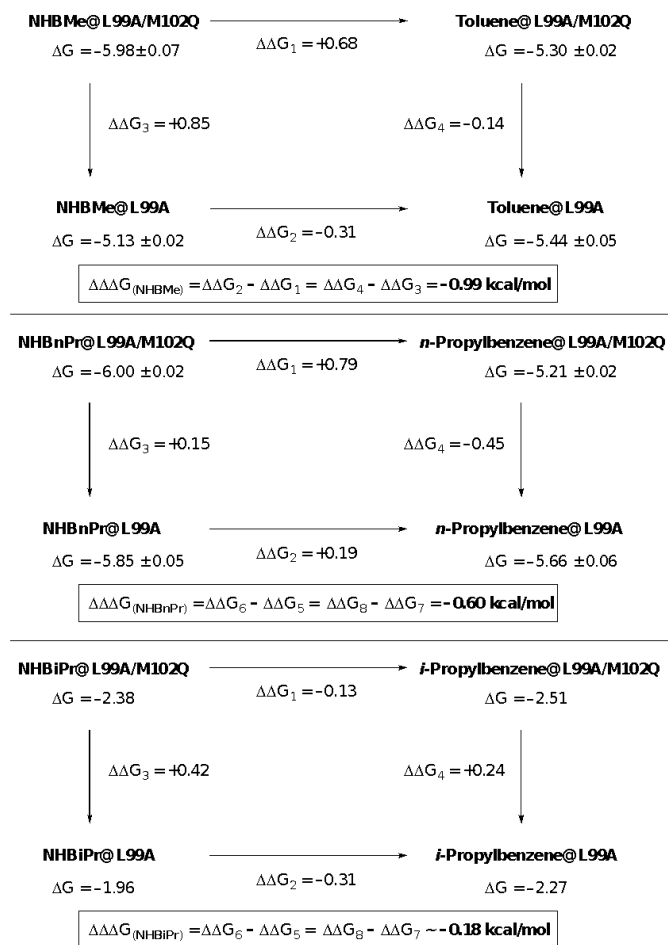
analysis only on the Gibbs free energy of binding. ITC experiments do not independently produce ΔH and ΔS values (ΔS is rather calculated from ΔG and ΔH via $\Delta G = \Delta H - T\Delta S$), thus ΔH and ΔS values from ITC experiments are perhaps more prone to misinterpretation due to the fact that they are correlated and compensate to match the measured value of ΔG .⁸⁵ For NHB*i*Pr and *i*-propylbenzene ligands, we used the ligand displacement method⁸⁶ to account for their low binding affinity.

Table 2.8 summarizes the results of the hydrogen bonding strength ($\Delta\Delta\Delta G$ from Scheme 2.21) between five congeneric 1,2-azaborine ligands and the glutamine residue of the L99A/M102Q.⁸⁷ Each binding free energy data point (reported as the average value and standard deviation of ΔG), as shown in Scheme 2.21, was obtained from a set of five titration experiments and the standard deviation of the mean for binding affinity K_a was calculated as the error bar (see experimental section), and the error range of the hydrogen bonding strength $\Delta\Delta\Delta G$, as shown in Table 2.8, was calculated by the propagation of error. The data for the low-binding affinity ligands NHB*i*Pr and *i*-propylbenzene were averaged from two data points.

⁸⁵ Klebe, G. *Nat. Rev. Drug Discov.* **2015**, *14*, 95-110.

⁸⁶ Sigurskjold, B. W. *Anal. Biochem.* **2000**, *277*, 260–266.

⁸⁷ It is noteworthy to mention that these estimated energetic values may also contain an additional electrostatic contribution between dipolar azaborine molecules and the protein binding sites.



Scheme 2.22. The double mutant cycle analysis for a congeneric ligand series.

Table 2.8. The hydrogen bonding strength

Ligand	Hydrogen bonding energy
	$\Delta\Delta\Delta G$ (kcal/mol)
NHBH	-0.94±0.08
NHBMe	-0.99±0.09
NHBet	-0.64±0.07
NHnPr	-0.60±0.08
NHBiPr	-0.18

As can be seen from Table 2.8, the evaluated NH...102Q hydrogen bonding strength for NHBH and NHBMe is about the same within the experimental error range. The hydrogen bonding interaction is weakened when the size of the boron substituent is increased from methyl to ethyl by about 0.3 kcal/mol. However, no further decrease in hydrogen bonding strength is observed when the B-ethyl substituent is replaced with a B-*n*Pr substituent. A significant decrease in the hydrogen bonding interaction is observed from a primary B-*n*Pr substituent to the more sterically encumbered secondary B-*i*Pr substituent. The lower energetic limit for a hydrogen bonding strength is considered to be 0.2 kcal/mol (e.g., for the interaction between CH₄ and FCH₃).⁸⁸ Thus, the observed hydrogen bonding strength for the NHB*i*Pr ligand (0.18 kcal/mol) can be considered negligible. In other words, the observed weak binding of NHB*i*Pr and *i*-propylbenzene to T4 lysozyme mutants (Scheme 2.21) has likely no contribution from the hydrogen bonding effects. In an IR study probing the binding interaction between ethers (serving as hydrogen bond acceptors) and phenols (hydrogen bond donors) in CCl₄ solvent, the difference in the phenol binding free energy between Et₂O and *n*Bu₂O is found to be 0.2 kcal/mol. The relatively small free energy penalty as a consequence of the increased steric demand is comparable to our observed values.

It has been reported that L99A T4 lysozyme mutants accommodate a congeneric series of substituted benzenes in three discrete conformations rather than through incremental conformational changes.⁸⁹ Specifically, protein X-ray crystallographic studies (see Figure 2.4) reveal that a “closed” conformation (purple box) of the arene recognition cavity is dominant for the benzene- and toluene-bound proteins. An “intermediate” conformation (blue box) that partially opens the cavity to bulk solvent is observed as a significant contributor for ethyl-, *n*-propyl-, *n*-butyl-, and *s*-butylbenzene-bound proteins, while for *n*-pentyl- and *n*-hexylbenzene-bound proteins an “open” conformation (green box) with a solvent exposed cavity is observed as a major contributor.

⁸⁸ a) Steiner, T. *Angew. Chem., Int. Ed.* **2002**, *41*, 48–76. b) Harris, K. D.; Kariuki, B. M.; Lambropoulos, C.; Philp, D.; Robinson, J. M. *Tetrahedron* **1997**, *53*, 8599-8612.

⁸⁹ Merski, M.; Fischer, M.; Balius, T. E.; Eidam, O.; Shoichet, B. K. *Proc. Natl. Acad. Sci.* **2015**, *112*, 5039-5044.

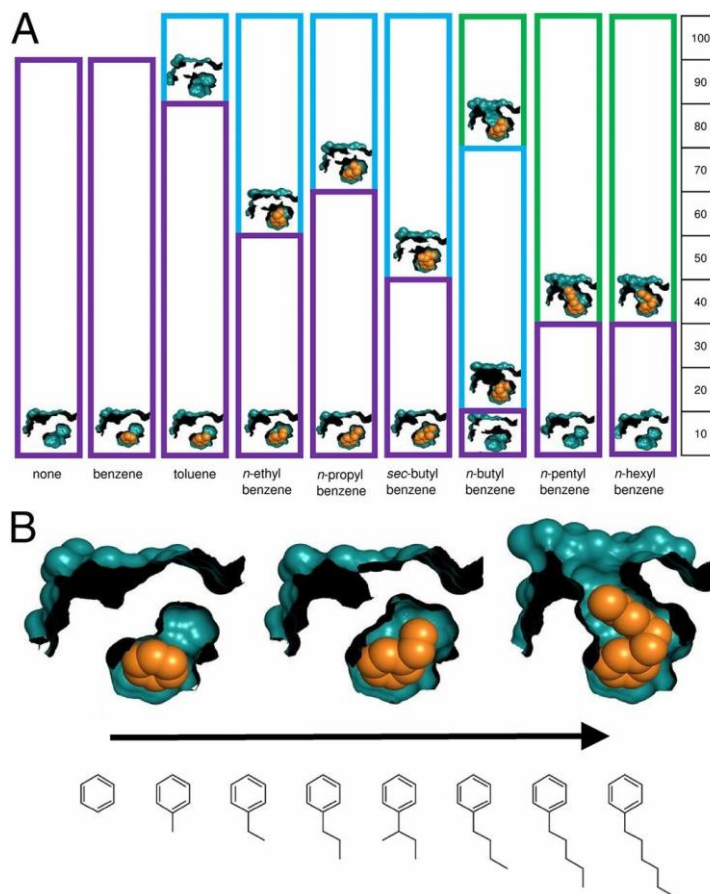


Figure 2.4. Congeneric ligand series in L99A with conformational change.⁸⁹ (A) The ligand poses assigned to their respective protein conformations. (B) Molecular surface of the cavity, ligand was shown as orange space-filling model in closed (benzene complex), intermediate (ethylbenzene complex), and open (*n*-hexylbenzene complex) conformations.

Our data in Table 2.8 indicate that changes in the strength of hydrogen bonding as a function of steric environment can also occur in discrete steps. We have previously shown that the hydrogen bonding distance between the Q102 carbonyl and NH groups of the bound parent 1,2-azaborine is 3.1 Å and 3.2 Å (there are two Q102 side chain conformations), whereas the hydrogen bonding distance for NHBET is 3.2 Å and 3.6 Å.⁹⁰ Thus, as expected, the strength of the determined hydrogen bonding interaction correlates inversely with the observed hydrogen bond distances. Overall, we believe that the observed trend, as shown in Table 2.8, is consistent with both the discrete protein conformation and the immediate local steric influence exerted by the boron substituent playing a role. In other words, the positioning of the Q102

⁹⁰ Lee, H; Fischer, M.; Shoichet, B. K.; Liu, S.-Y. *J. Am. Chem. Soc.* **2016**, *138*, 12021-12024.

residue (and as a consequence its proximity to the hydrogen bond donor on the ligand) can possibly be influenced by the protein conformation (closed, intermediate, and open; that is guided by the ligand size) and/or directly by the size of the proximal boron substituent. For NHBH and NHBMe-bound proteins, the “closed” protein conformation is likely dominant, and the local steric effect exerted by the boron substituent (H vs. Me) may be negligible, resulting in a similar observed hydrogen bonding strength. The transition from NHBMe to NHB*Et*/NHB*n*Pr may involve a protein conformational change from the “closed” to “intermediate” state, possibly influencing the positioning of the Q102 residue, which results in a weaker hydrogen bond. Finally, the local steric demand exerted by the B-*i*Pr group in the NHB*i*Pr-bound proteins may prove to be too prohibitive for hydrogen bonding to occur, irrespective of the protein conformation.

Conclusions

In summary, we evaluated the hydrogen bonding strength between a small molecule ligand and a protein as a function of ligand steric effects using a congeneric series of 1,2-azaborine ligands and the L99A/M102Q T4 lysozyme. We extracted the hydrogen bonding strength values from experimentally accessible binding free energies using the Double Mutant Cycle analysis, and we conclude that, as expected, with increasing steric demand, the hydrogen bonding interaction is weakened. However, we find that this weakening of the hydrogen bonding interaction can occur in discrete steps rather than in an incremental fashion. In view of the importance of hydrogen bonding in drug design campaign, this work provides additional fundamental reference data to help establish 1,2- azborines as a potential pharmacophore in medicinal chemistry applications.

2.8.2 Experimental details

Protein Expression and Purification

Escherichia coli strain RR1 (ATCC® 31343™) was transformed with the sub-cloned plasmids (Addgene plasmids # 18476 and 18477 from Brian Matthews lab, for T4 lysozyme WT* (L99A) and T4L mutant (S38D L99A M102Q N144D), respectively. Ampicillin-resistant transformants were isolated and

stored in 20% glycerol stock solution in (lysogeny broth) LB media. The E.coli RR1 were grown in 4.0 liters of LB media with 100mg/liter ampicillin at 37 °C within an agitating fermentor at 250 rpm. When the optical density of broth reached 0.7 at 600 nm, isopropyl- β -D-1-thiogalactopyranoside (IPTG) was added to a final concentration of 0.7mM to induce protein expression. Cell culture was incubated at 25 °C at 110 rpm shaking speed for 21hrs. Then the resulting pellet was suspended in 300 mL of a buffer solution containing 0.1 M sodium phosphate (pH= 6.6) and 0.2 M NaCl. 30 mL of 0.5 M EDTA (pH 8.0) solution was added, and the suspension was stirred for 17 h at 4 °C. To the suspension was then added 30 mL of 0.5 M EDTA (pH 8.0), and the mixture was stirred at room temperature for 8 h at 4 °C. The supernatant was collected and dialyzed into 20 mM phosphate buffer (pH 7.3) and then loaded onto a CM Sepharose Fast Flow (GE healthcare) column that was pre-equilibrated with equilibration buffer of 50 mM Tris, 1.0 mM EDTA, pH 7.3 and eluted with a linear gradient of 0 mM to 300 mM NaCl within equilibration buffer. The fractions containing pure protein were pooled and dialyzed against the degassed ITC buffer (5% to 10% PEG400, 0.5M NaCl, 0.1M sodium phosphate (pH 6.8). Specifically, 5% PEG (for NHBMe / toluene pair) and 10% PEG (for NHB*n*Pr / *n*-Propylbenzene pair, and NHB*i*Pr / *i*-Propylbenzene pair) was added into the degassed ITC buffer to make the ligand more soluble.

ITC Experiments

Isothermal titration calorimetry experiments (in a Nano ITC calorimeter from TA instruments) were carried out at 10 °C with 310 rpm stirring rate with a data collection interval of 4 min/injection. A total of volume of 100 μ l (2.5 μ l x 40 injections) ligand solution (2.66 - 3.74 mM) were injected into 320 μ l of 0.3 mM protein solution. The ligand was directly dissolved in the degassed ITC buffer from protein dialysis and ligand concentration was determined by UV-Vis against a standard calibration curve. The heat of ligand dilution was measured by titrating the ligand into the ITC buffer for each titration pairs, and the heat of dilution has been subtracted from each titration. The resulting reaction heat profiles were fit to the one binding site independent binding model with the stoichiometry *n* fixed to 1.0. All data were analyzed using NanoAnalyze software. Experiments (except *i*-Propylbenzene and NHB*i*Pr pair only repeated for 2 times) were repeated five times and averaged with standard deviation error of the mean. Representative ITC traces are shown below.

Displacement titration of *i*-Propylbenzene and NHB*i*Pr.

The competition-based method⁹¹ was utilized here for determining K_a of the low-affinity ligand (*i*-Propylbenzene and NHB*i*Pr) binding interactions with L99A and L99A/M102Q. The high affinity ligand in syringe was titrated into the protein in the cell in the presence of a large excess amount of the low-affinity ligand. The heat of dilution was accounted for by background subtraction of the heat generated by injecting the high affinity ligand into ITC buffer in the presence of the low-affinity ligand in the cell in the absence of the protein. Phenol was used for the displacement of NHB*i*Pr and *i*-Propylbenzene from the L99A/M102Q cavity. The binding affinity constant for phenol binding to L99A/M102Q was determined to be $5.03 \times 10^4 \text{ M}^{-1}$ and the concentration of the ligands (*i*-Propylbenzene and NHB*i*Pr) was 9.4 mM. Toluene was used for displacement of *n*-Propylbenzene and *i*-Propylbenzene from L99A cavity, and the binding affinity constant for toluene binding to L99A was determined to be $3.57 \times 10^4 \text{ M}^{-1}$. The ligand concentration of the low affinity ligand (*i*-Propylbenzene and NHB*i*Pr) in the cell was 10 mM.

The data was analyzed using the standard one binding site model supplied by Sigurkjold's displacement model. Binding constant K_b for our low affinity ligand was determined based on the apparent binding constant K_{app} (i.e., measured binding constant of the higher-affinity ligand to the protein in the presence of the lower-affinity ligand) and K_a (i.e., inherent binding constant of the higher-affinity ligand to the protein that was determined from independent titration experiments). [B] is the concentration of the lower-affinity ligand in the titration cell.

$$K_{app} = \frac{K_a}{(1 + K_b * [B])}$$

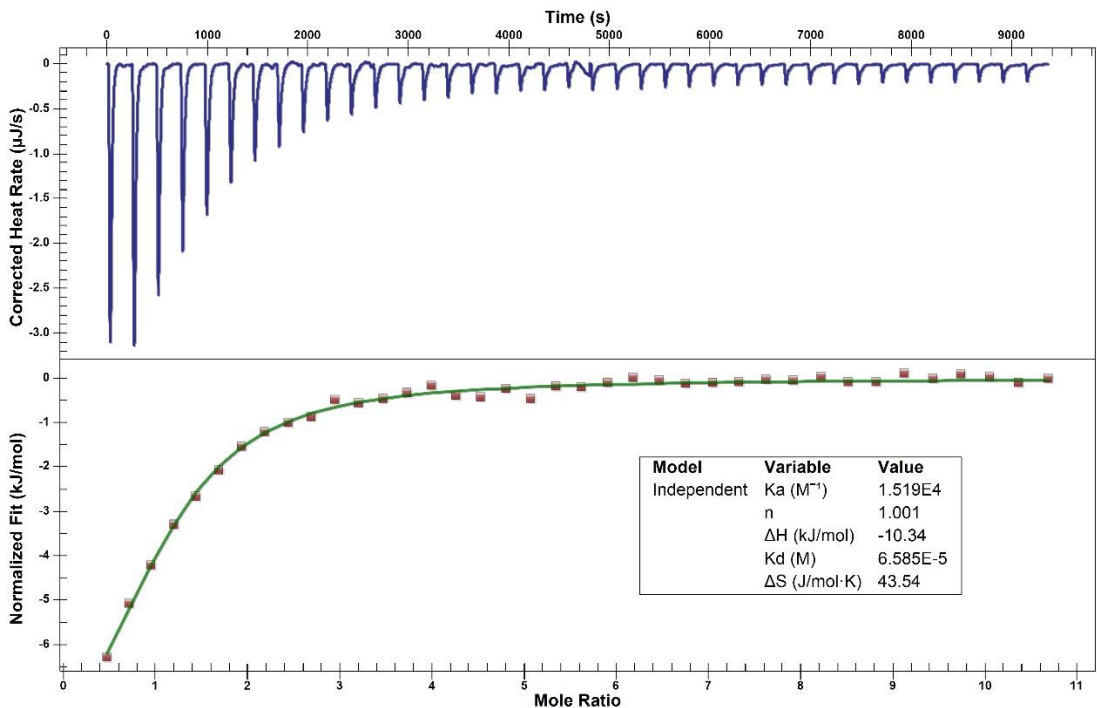
⁹¹ a) Zhang, Y.-L.; Zhang, Z.-Y. *Anal. Biochem.* **1998**, *261*, 139-148. b) B. W. Sigurkjold, *Anal. Biochem.*, 2000, *277*, 260-266. Sigurkjold, B. W. *Anal. Biochem.* **2000**, *277*, 260-266.

Table 2.9. Affinity Constant (K_a) and Binding Free Energy (ΔG) Determined by ITC.

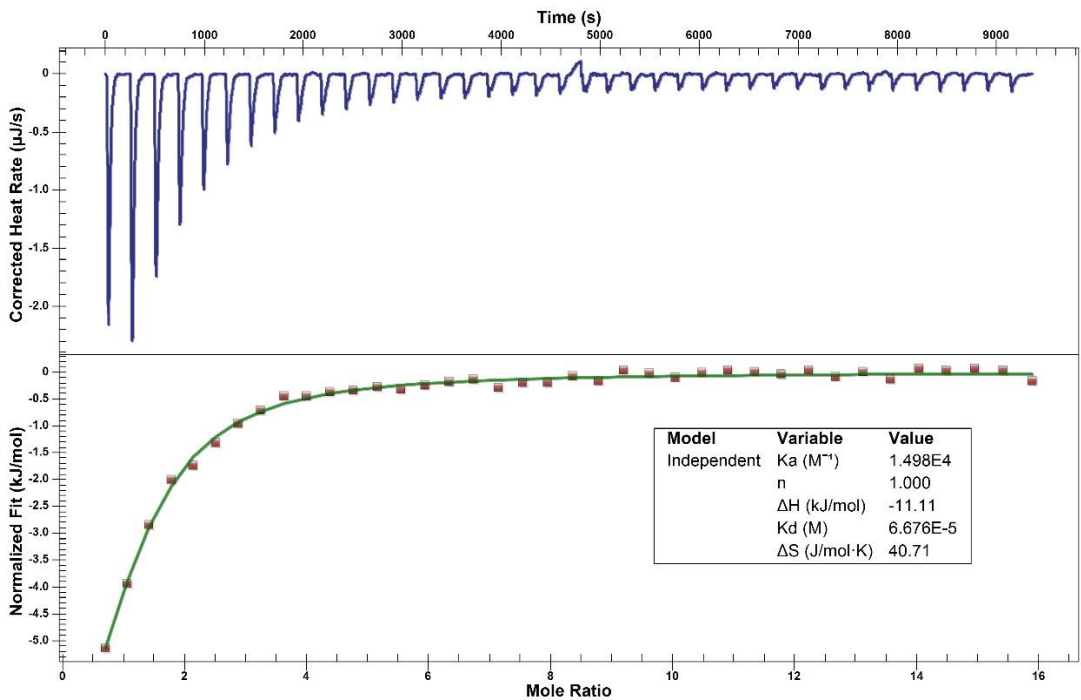
	L99A		L99A/M102Q	
	K_a ($\times 10^4 M^{-1}$)	ΔG (kcal/mol)	K_a ($\times 10^4 M^{-1}$)	ΔG (kcal/mol)
Toluene	1.59±0.15	-5.44±0.05	1.25±0.05	-5.30±0.02
NHBMe	0.93±0.09	-5.13±0.02	4.3±0.5	-5.98±0.07
<i>n</i> -Propylbenzene	2.4±0.2	-5.66±0.06	1.07±0.09	-5.21±0.02
NHBnPr	3.3±0.2	-5.85±0.05	4.3±0.1	-6.00±0.02
<i>i</i> -Propylbenzene	57 M^{-1}	-2.27	87 M^{-1}	-2.51
NHB <i>i</i> Pr	34 M^{-1}	-1.96	69 M^{-1}	-2.38

Representative ITC trace

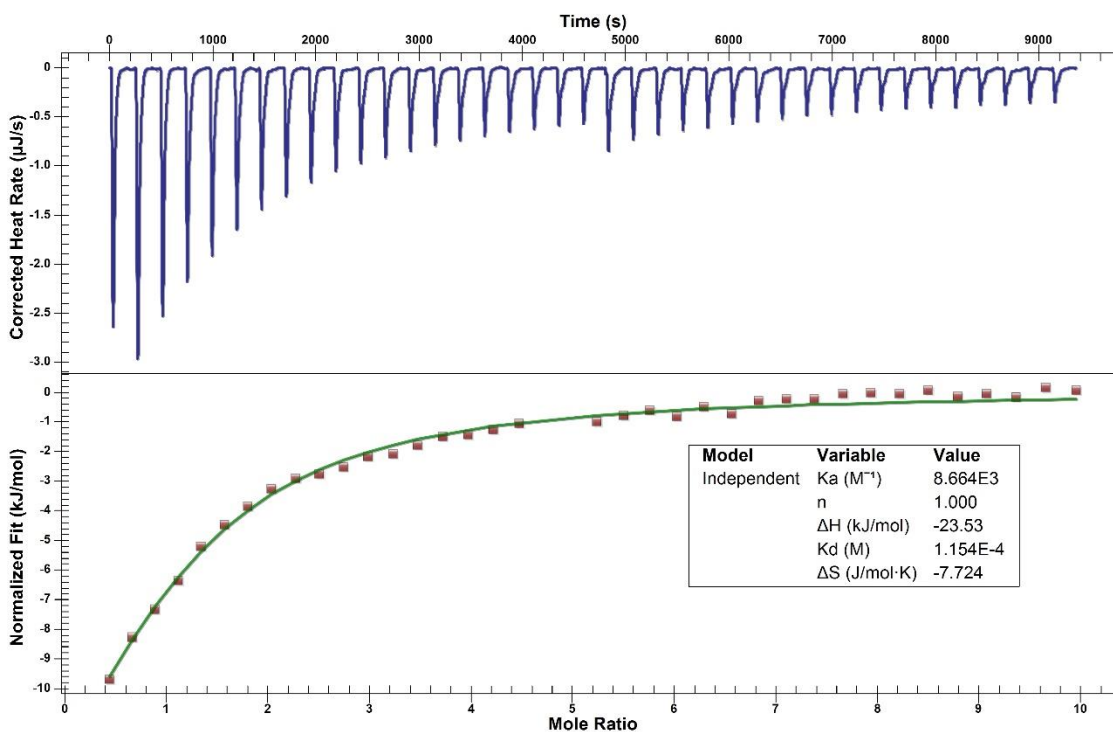
Toluene to L99A



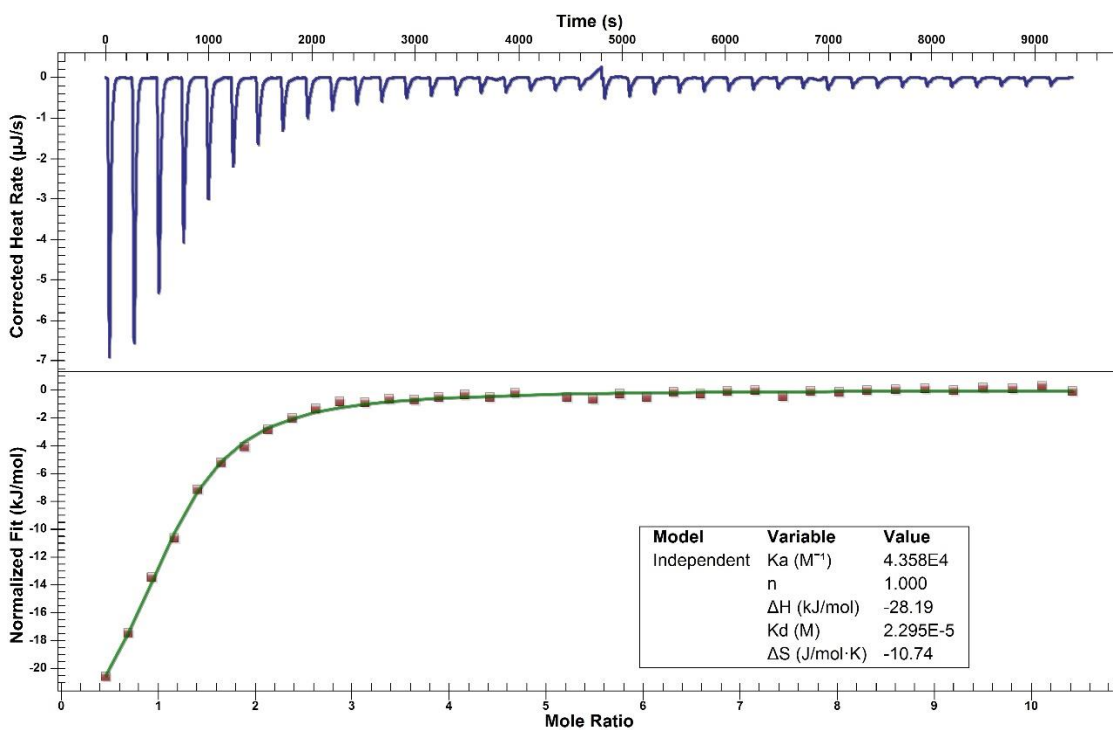
Toluene to M102Q



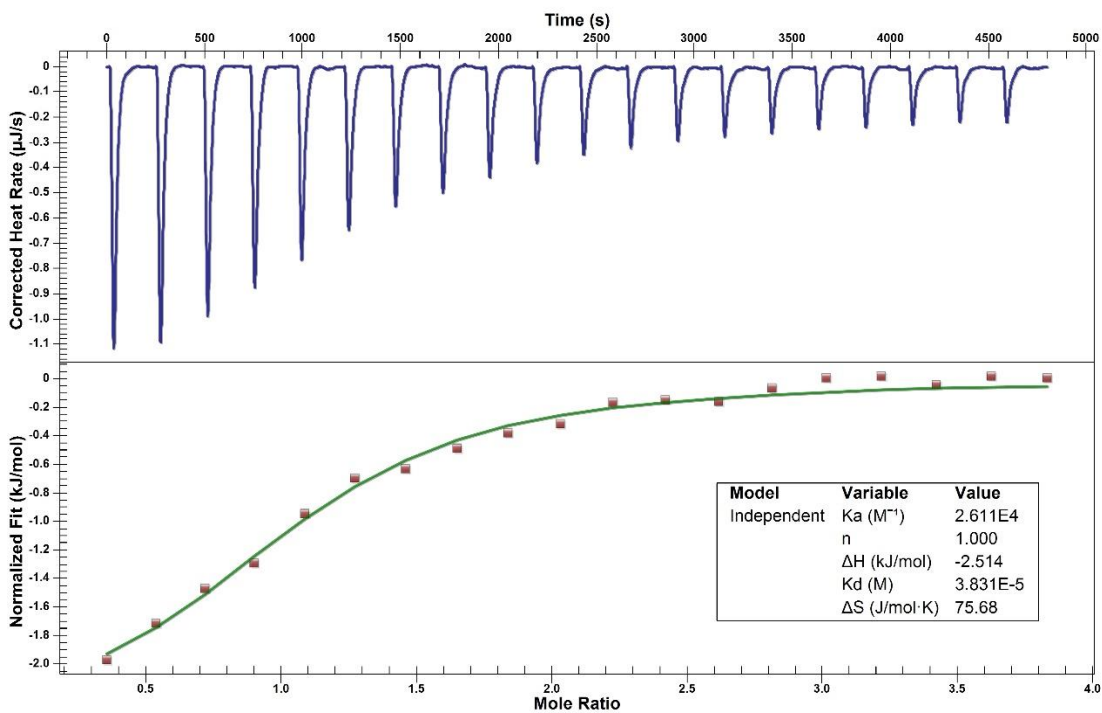
NHBMe to L99A



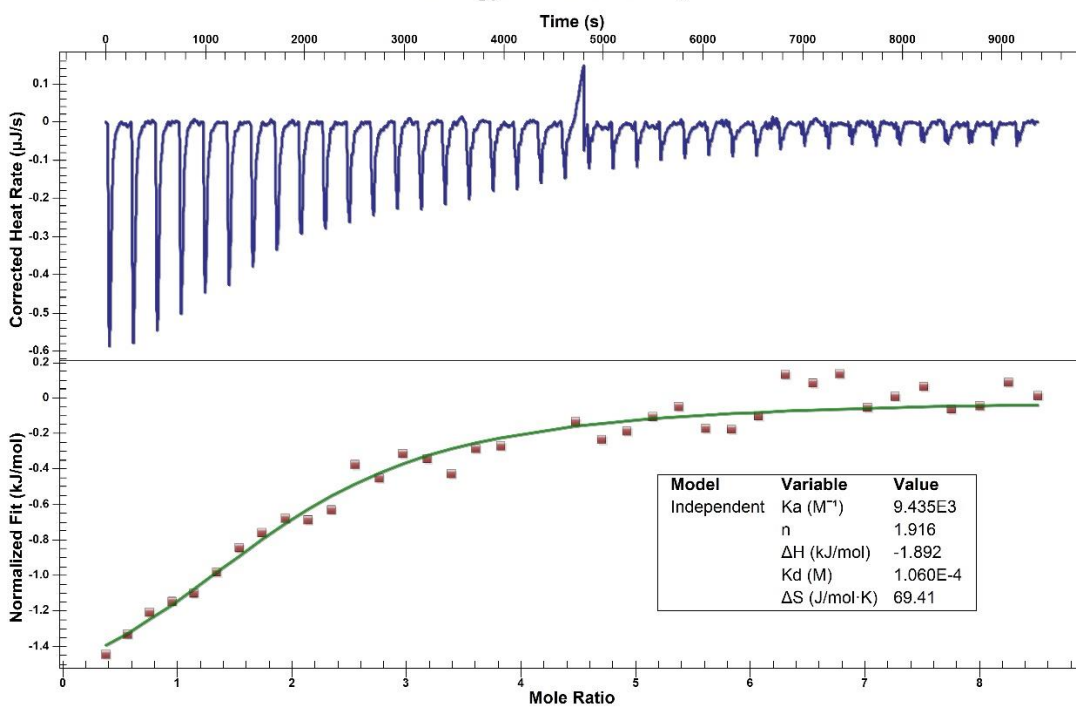
NHBMe to M102Q



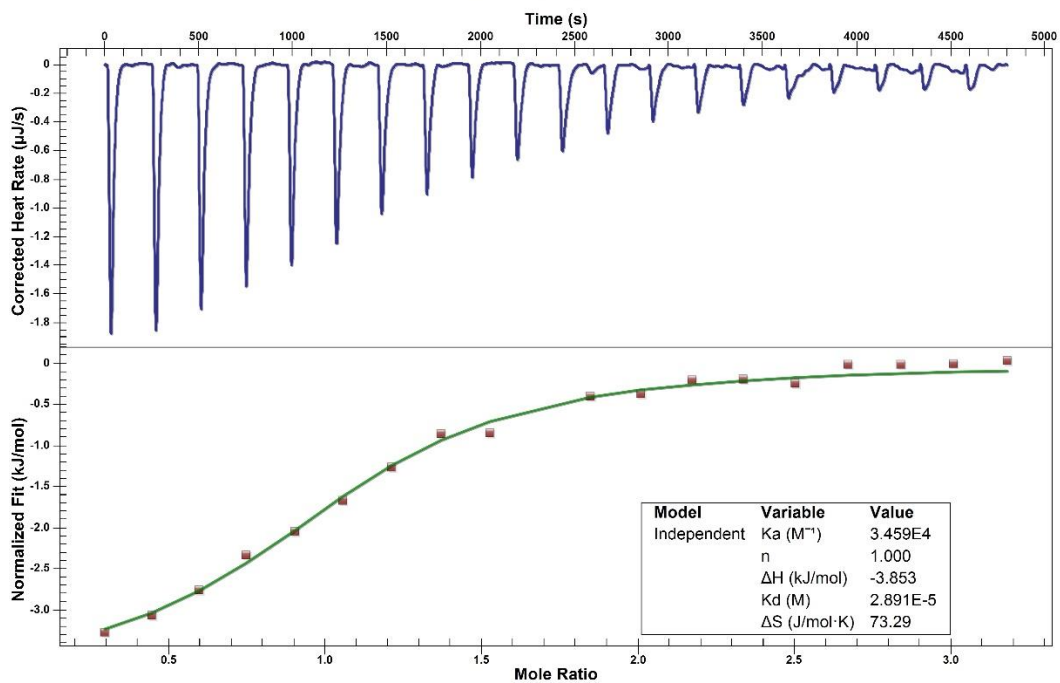
n-Propylbenzene to L99A



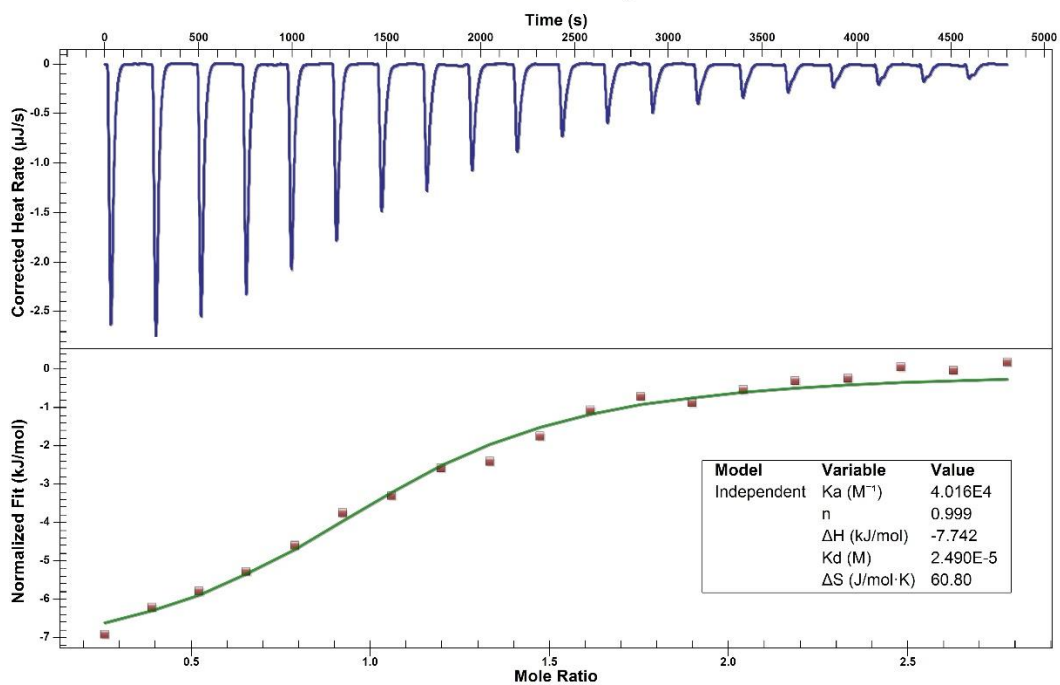
n-Propylbenzene to M102Q



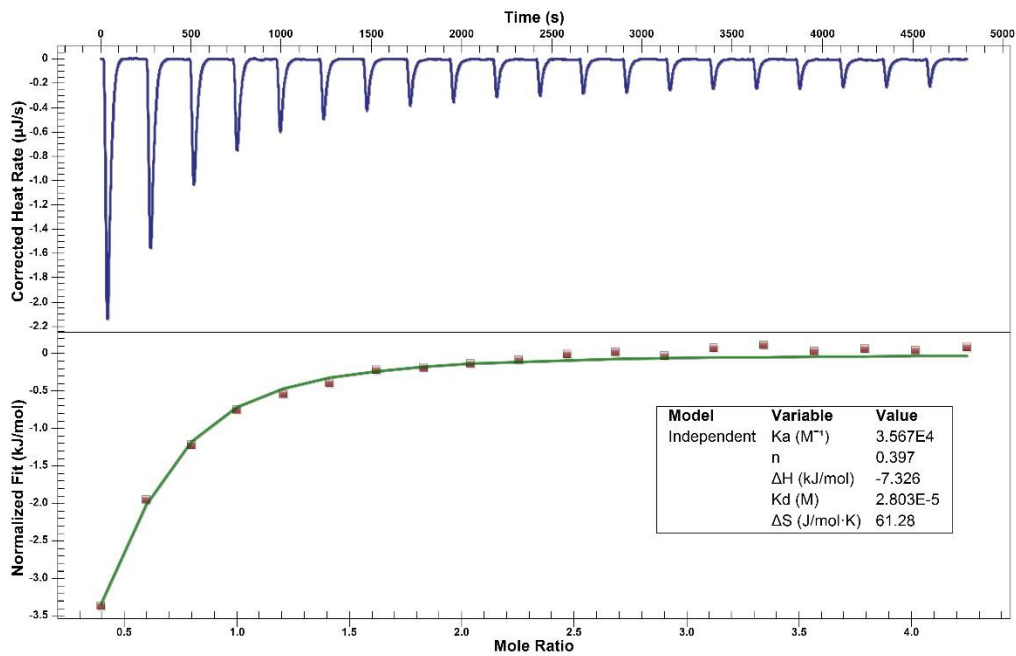
NHBnPr to L99A



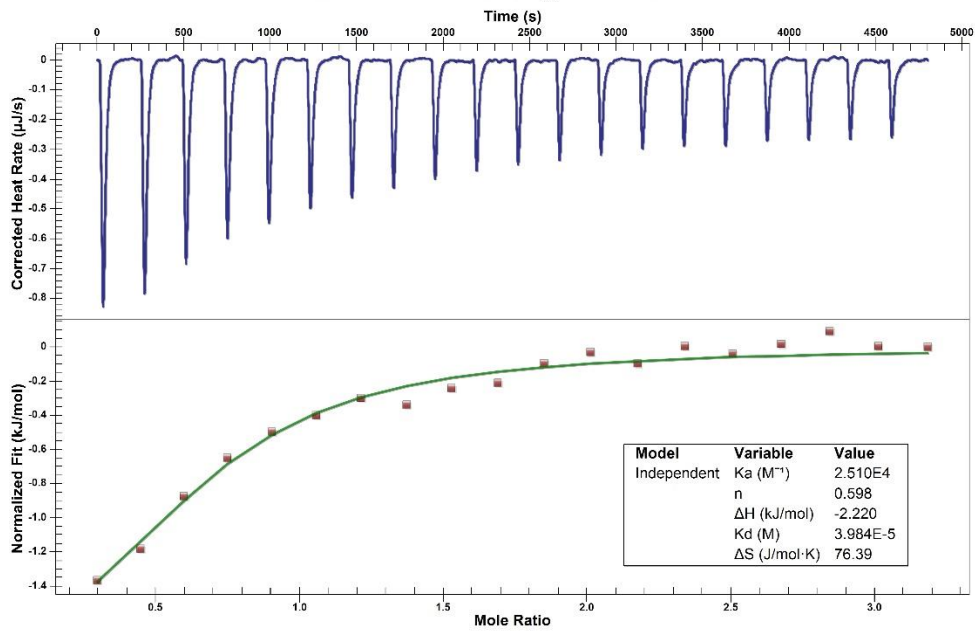
NHBnPr to M102Q



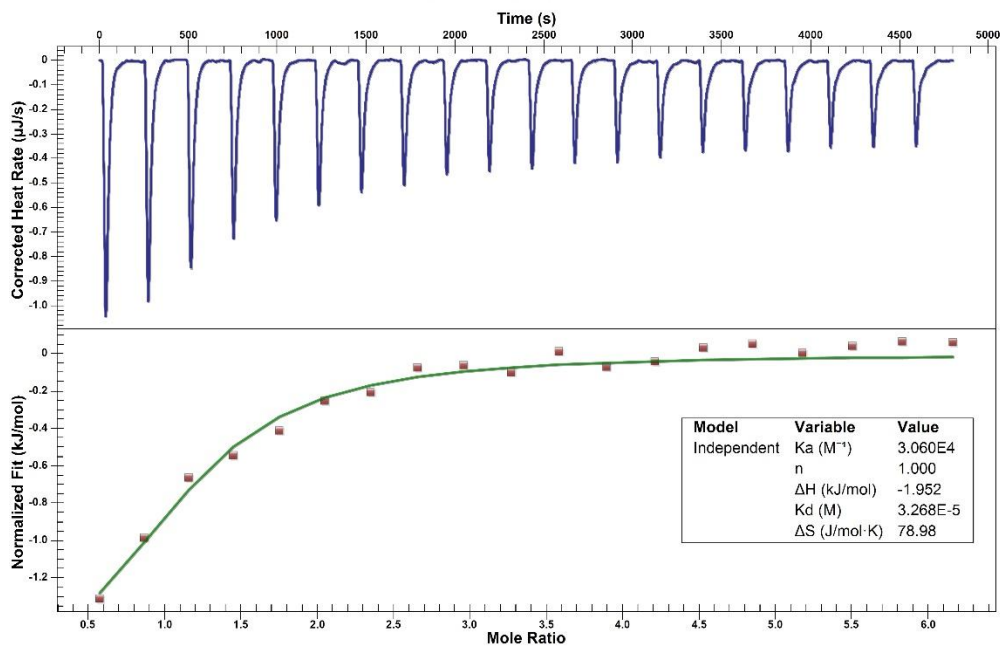
Toluene to L99A for displacement reference



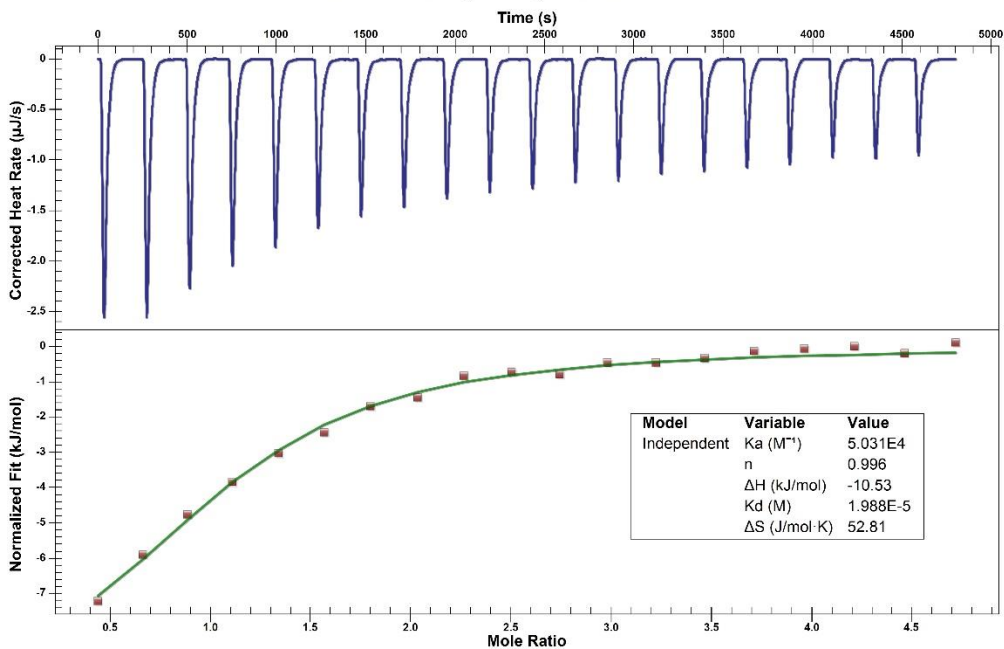
Toluene to L99A with *i*-Propylbenzene in cell



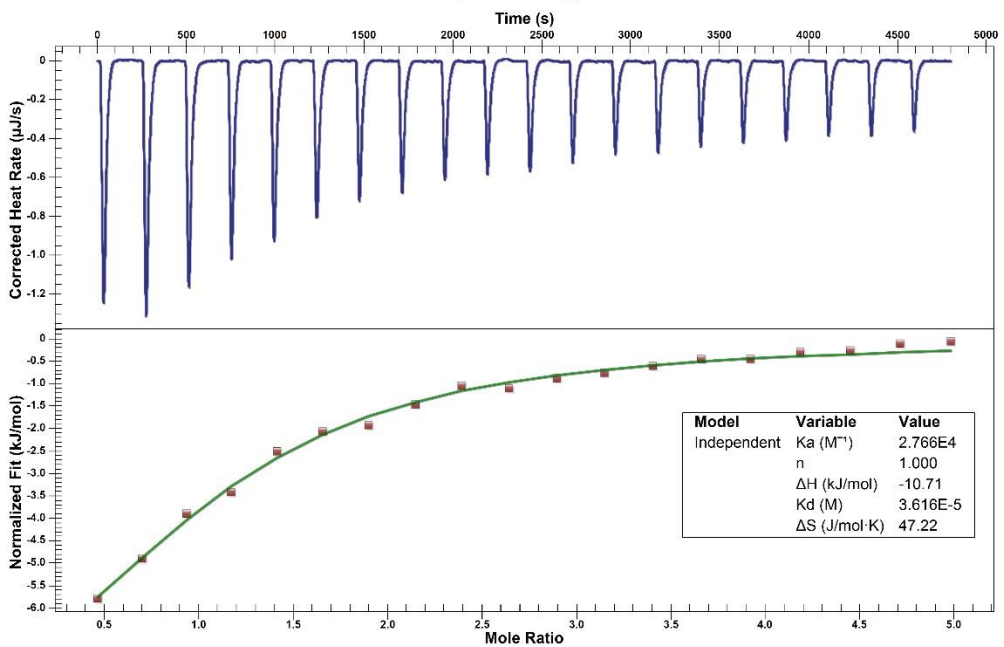
Toluene to L99A with NHBiPr in cell



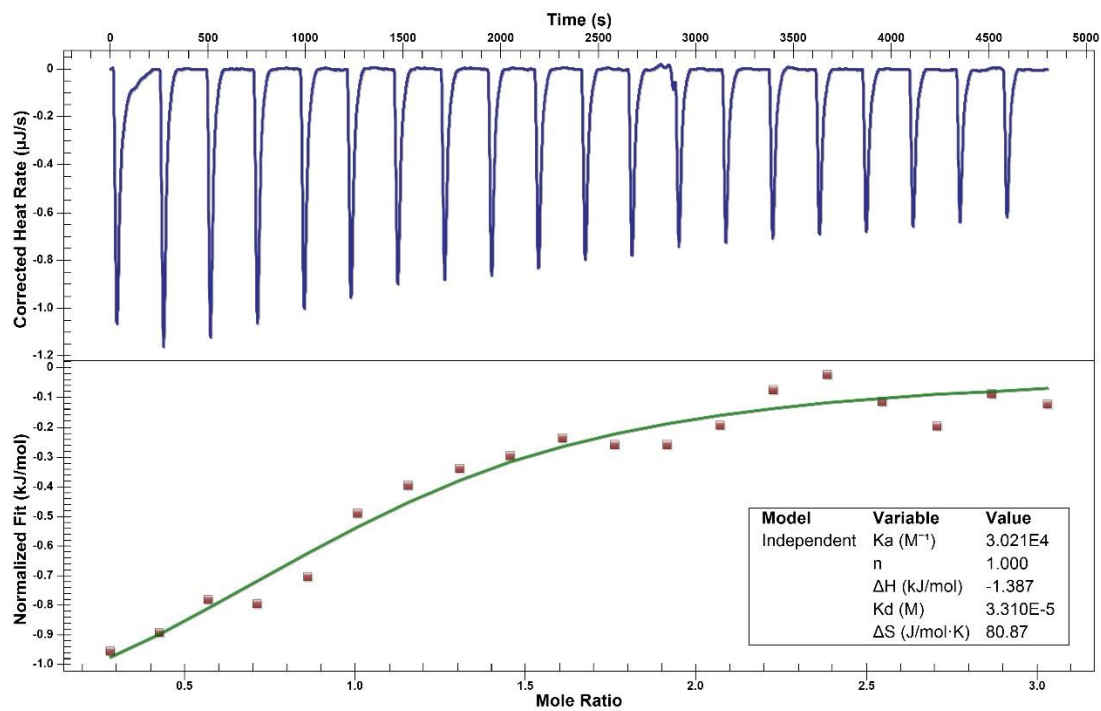
Phenol to M102Q for displacement reference



Phenol to M102Q with *i*-Propylbenzene in cell



Phenol to M102Q with NHBiPr in cell

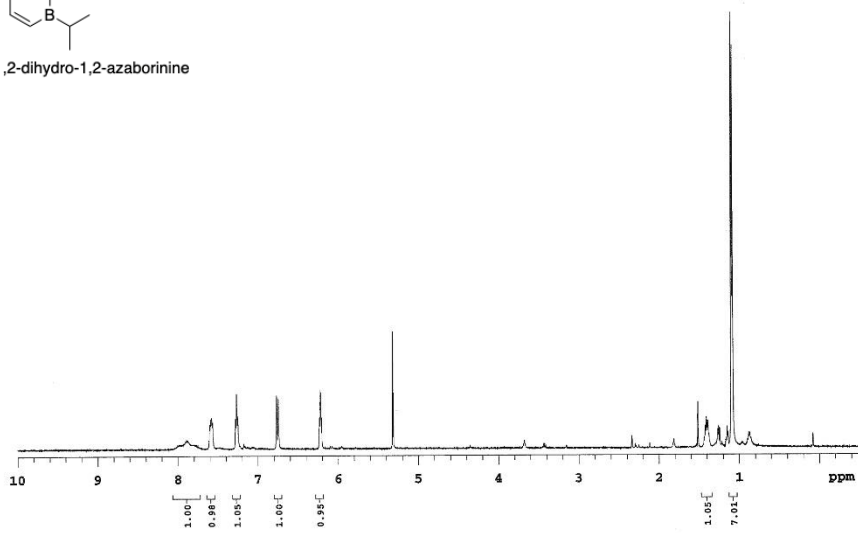




2-isopropyl-1,2-dihydro-1,2-azaborinine

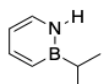
YL-02-NHBIsoopropyl_pumped

Sample Name	YL-02-NHBIsoopropyl_pumped	Acquisition	PROTON	Temperature	25	Study owner	Liu
Date collected	2018-01-05	Solvent	cd2cl2	Spectrometer	nmr18-vnmrs500	Operator	Liu



Data file: h:\nmr\18\180105\data\YL-02-NHBIsoopropyl_pumped.f2

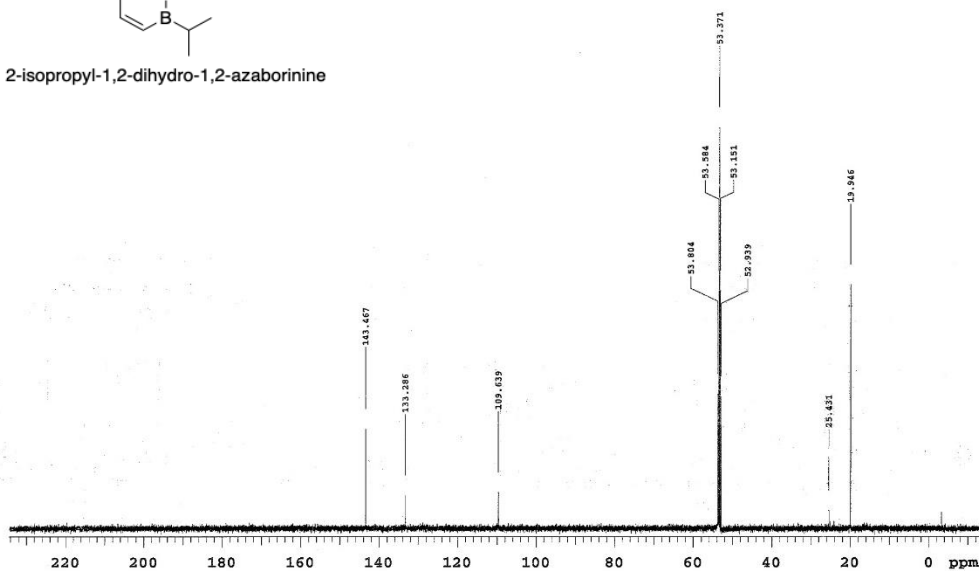
Plot date: 2018-05-01



2-isopropyl-1,2-dihydro-1,2-azaborinine

YL-01-NHBIsoopropyl-13C

Sample Name	YL-01-NHBIsoopropyl-13C	Pulse sequence	CARBON	Temperature	25	Study owner	Liu
Date collected	2018-09-11	Solvent	cd2cl2	Spectrometer	nmr18-vnmrs500	Operator	Liu

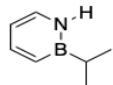


Data file: 180911

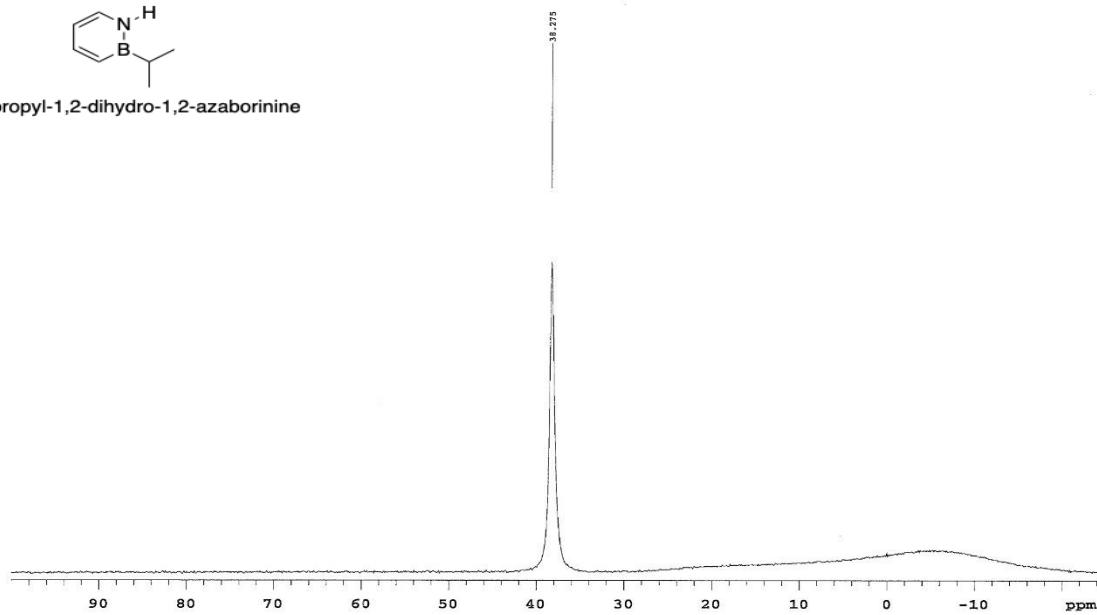
Plot date: 2018-09-11

YL-01-005-step2-11B

Sample Name: YL-01-005-step2-11B
Date collected: 2017-01-11
Pulse sequence: s2pul
Solvent: cd2cl2
Temperature: 25
Spectrometer: nmr11-inova500
Study owner: Liu
Operator: Liu



2-isopropyl-1,2-dihydro-1,2-azaborinine

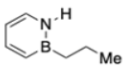


Data file: e03

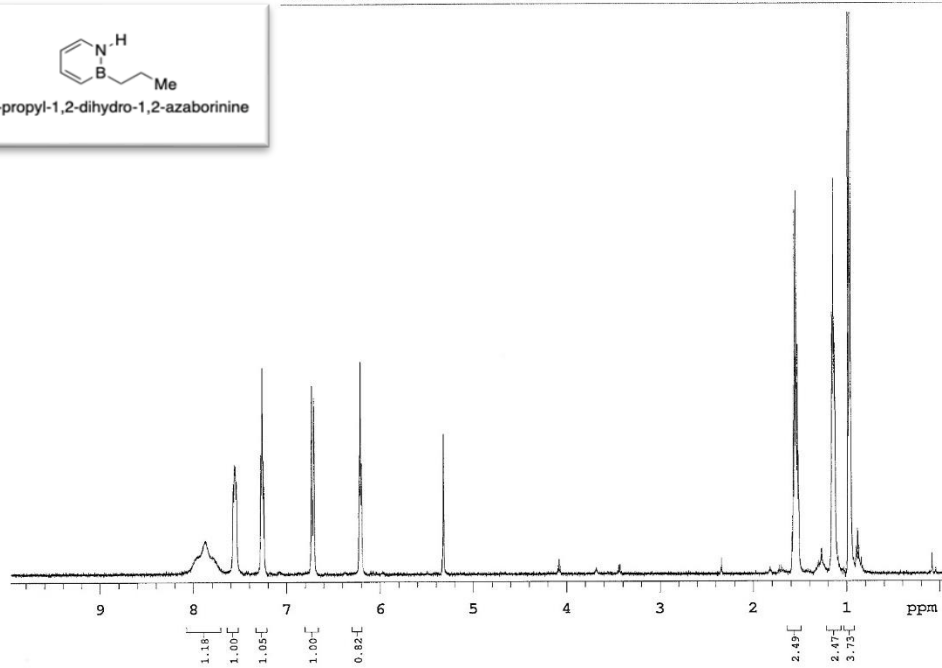
Plot date: 2017-01-11

YL-01-003-step2-1H

Sample Name: YL-01-003-step2-1H
Date collected: 2017-01-27
Pulse sequence: PROTON
Solvent: cd2cl2
Temperature: 25
Spectrometer: nmr11-inova500
Study owner: Liu
Operator: Liu



2-propyl-1,2-dihydro-1,2-azaborinine



YL-02-NHBnpr

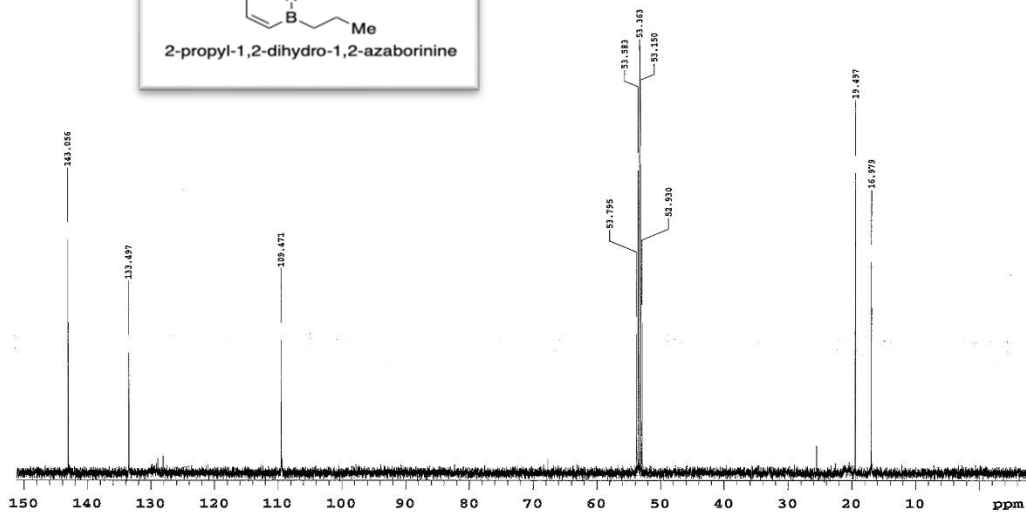
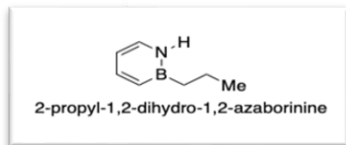
Sample Name YL-02-NHBnpr
Date collected 2017-05-22

Pulse sequence CARBON
Solvent cd2cl2

Temperature 25
Spectrometer nmr18-vnmra500

Study owner Liu
Operator Liu

yz-3-157H-2-etter



Data file exp

Plot date 2017-05-22

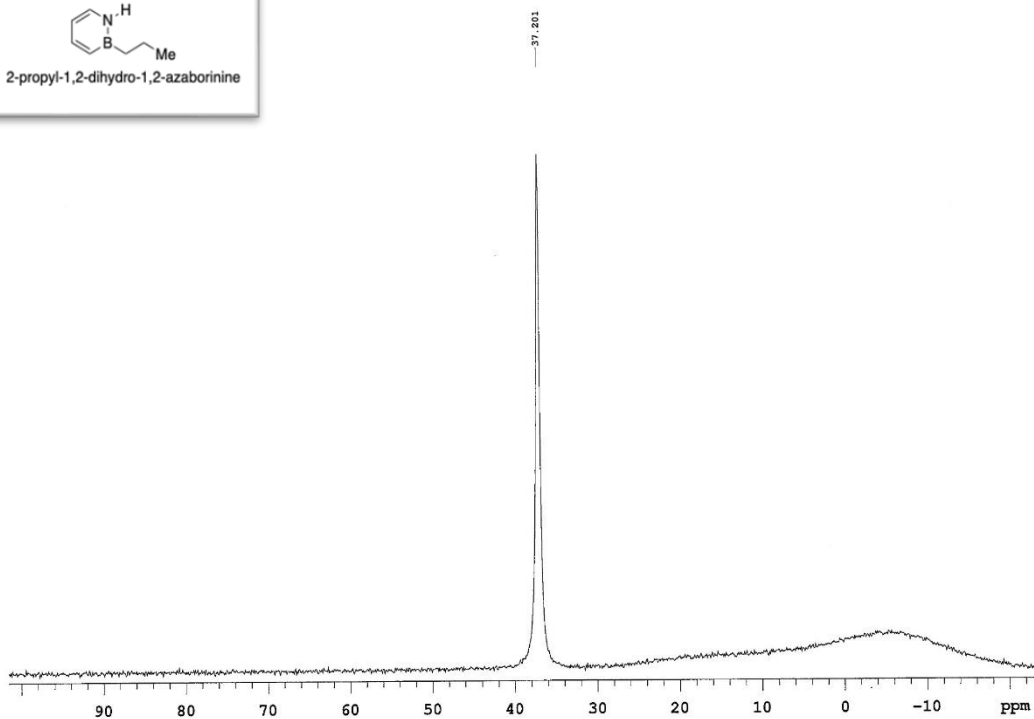
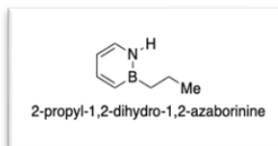
YL-01-003-step2-11B

Sample Name YL-01-003-step2-11B
Date collected 2016-06-16

Pulse sequence s2pul
Solvent cd2cl2

Temperature 25
Spectrometer nmr11-inova500

Study owner Liu
Operator Liu



Data file exp

Plot date 2016-06-16

2.9 Binding of 1,2-azaborine to L99A/M102H T4 lysozyme: the presence of a water bridge

2.9.1 The role of water bridge in the intermolecular hydrogen bonding network

Water plays an important role in virtually all biomolecular binding processes and hydrophobic association.⁹² Traditionally, ligands compete for binding site with water molecules and water contributes to the binding entropically through the hydrophobic effect.⁹³

Nevertheless, the importance of hydrogen-bond network of water was undervalued.⁹⁴ Recently, water molecules⁹⁵ have been discovered to influence protein-ligand binding kinetics or in some cases even govern the ligand selectivity.⁹⁶ Water near a nonpolar binding site is considered as more ordered than bulk water.⁹⁷ Ladbury⁹⁸ and Dunitz⁹⁹ reckoned the weakly bound water in the protein can be targeted for replacement, whereas strongly bound waters function as ligand stabilizer. Weakly bound water molecules displaced by the ligands and structured water molecules reorganized during ligand binding together determine the thermodynamics of binding process.⁹²

Water mediates the interactions between protein and ligands across the interaction interface due to their minimal size and unique ability to act as a hydrogen bond donor and acceptor.¹⁰⁰ Without the

⁹² a) Ladbury, J. E.; Connelly, P. R., *Structure-based drug design: thermodynamics, modeling and strategy*. Springer: 1997. b) Otting, G.; Liepinsh, E.; Wuthrich, K. *Science* **1991**, *254*, 974-980. c) Hummer, G.; Garcia, A. E.; Soumpasis, D. M. *Faraday discussions* **1996**, *103*, 175-189. d) Kovacs, H.; Mark, A. E.; Van Gunsteren, W. F. *Proteins: Structure, Function, and Bioinformatics* **1997**, *27*, 395-404. e) Cheng, Y.-K.; Rossky, P. J. *Nature* **1998**, *392*, 696-699. f) Israelachvili, J.; Wennerström, H. *Nature* **1996**, *379*, 219-225.

⁹³ a) Chandler, D. *Nature* **2005**, *437*, 640-647. b) Dubins, D. N.; Filfil, R.; Macgregor, R. B.; Chalikian, T. V. *J. Phys. Chem. B* **2000**, *104*, 390-401. c) Barth, A. *Biochim. Biophys.* **2007**, *1767*, 1073-1101. d) Tame, J. R.; Sleight, S. H.; Wilkinson, A. J.; Ladbury, J. E. *Nat. Struct. Biol.* **1996**, *3*, 998-1001.

⁹⁴ Darby, J. F.; Hopkins, A. P.; Shimizu, S.; Roberts, S. M.; Brannigan, J. A.; Turkenburg, J. P.; Thomas, G. H.; Hubbard, R. E.; Fischer, M. *J. Am. Chem. Soc.* **2019**, *141*, 15818-15826.

⁹⁵ a) Pearlstein, R. A.; Hu, Q. Y.; Zhou, J.; Yowe, D.; Levell, J.; Dale, B.; Kaushik, V. K.; Daniels, D.; Hanrahan, S.; Sherman, W. *Proteins* **2010**, *78*, 2571-2586. b) Pearlstein, R. A.; Sherman, W.; Abel, R. *Proteins* **2013**, *81*, 1509-1526. c) Bortolato, A.; Tehan, B. G.; Bodnarchuk, M. S.; Essex, J. W.; Mason, J. S. *J. Chem. Inf. Model.* **2013**, *53*, 1700-1713. d) Hummer, G. *Nat. Chem.* **2010**, *2*, 906-907. e) Baron, R.; Setny, P.; McCammon, J. A. *J. Am. Chem. Soc.* **2010**, *132*, 12091-12097.

⁹⁶ a) Barillari, C.; Duncan, A. L.; Westwood, I. M.; Blagg, J.; van Montfort, R. L. *Proteins* **2011**, *79*, 2109-2121. b) Robinson, D. D.; Sherman, W.; Farid, R. *ChemMedChem* **2010**, *5*, 618-627.

⁹⁷ Qiao, B.; Jiménez-Ángeles, F.; Nguyen, T. D.; De La Cruz, M. O. *PNAS* **2019**, *116*, 19274-19281.

⁹⁸ Mobley, D. L.; Gilson, M. K. *Annu. Rev. Biophys.* **2017**, *46*, 531-558.

⁹⁹ Gopal, S. M.; Klumpers, F.; Herrmann, C.; Schäfer, L. V. *Phys. Chem. Chem. Phys.* **2017**, *19*, 10753-10766.

¹⁰⁰ a) Mackman, R. L.; Katz, B. A.; Breitenbucher, J. G.; Hui, H. C.; Verner, E.; Luong, C.; Liu, L.; Sprengeler, P. A. *J. Med. Chem.* **2001**, *44*, 3856-3871. b) Biela, A.; Betz, M.; Heine, A.; Klebe, G. *ChemMedChem* **2012**, *7*, 1423-1434.

presence of water molecule, the interaction pair may only form a poor hydrogen bond or none at all.¹⁰¹ Positionally ordered water within the cavity mediates specific interactions between the ligand and the receptor.⁹² Such interacting waters can bridge between a ligand and the protein surface and would add new favorable enthalpic interactions to ligand recognition.¹⁰²

Water-ligand thermodynamics was measured in model systems such as carbonic anhydrase¹⁰³ and thermolysin.¹⁰⁴ In thermolysin (TLN) S2' binding pocket,¹⁰⁴ the crystal structures of eight TLN inhibitors showed major differences in terms of the adjacent water network. Four complexes (TLN1-4) show a water molecule capping the carboxylate group of the ligand. Another complex hosts one water molecule at a new water binding site in TLN8 is found to have stabilizing interactions (3.2 Å) with the π -system of the ligand's phenyl ring. In this case, the hydrophobic effect is paid in enthalpy.¹⁰⁵

Water molecules can have a great influence on the enthalpy (ΔH) and entropy (ΔS) contributions and as a result the free energy for protein-inhibitor binding (ΔG).¹⁰⁶ Two structurally very similar aldose reductase-ligand complexes have nearly identical binding modes and similar binding affinity(ΔG).^{106b} However, they have very different enthalpy and entropy partitions. The enthalpically more favored ligand entraps a water molecule that mediates the protein-ligand interaction, and the entropically favored ligand lacks a water bridge molecule.

Water molecules are also retained to favor ligand binding. The structure of protein surface water molecules also largely correlates with the thermodynamic signature of protein-ligand complexes. Complex contributions from enthalpy and entropy can be attributed to the disruption or stabilization of water networks.¹⁰⁷ Fisher group postulates that proteins co-evolved with the water network to discriminate for a

¹⁰¹ Maréchal, Y., *The hydrogen bond and the water molecule: The physics and chemistry of water, aqueous and bio-media*. Elsevier: 2006.

¹⁰² Balias, T. E.; Fischer, M.; Stein, R. M.; Adler, T. B.; Nguyen, C. N.; Cruz, A.; Gilson, M. K.; Kurtzman, T.; Shoichet, B. K. *Proc. Natl. Acad. Sci.* **2017**, *114*, 6839-6846.

¹⁰³ Snyder, P. W.; Mecinović, J.; Moustakas, D. T.; Thomas, S. W.; Harder, M.; Mack, E. T.; Lockett, M. R.; Héroux, A.; Sherman, W.; Whitesides, G. M. *Proc. Natl. Acad. Sci.* **2011**, *108*, 17889-17894.

¹⁰⁴ Biela, A.; Sielaff, F.; Terwesten, F.; Heine, A.; Steinmetzer, T.; Klebe, G. *J. Med. Chem.* **2012**, *55*, 6094-6110.

¹⁰⁵ Biela, A.; Nasief, N. N.; Betz, M.; Heine, A. *Angew. Chem. Int. Ed.* **2013**, *52*, 1822-1828.

¹⁰⁶ a) Petrova, T.; Steuber, H.; Hazemann, I.; Cousido-Siah, A.; Mitschler, A.; Chung, R.; Oka, M.; Klebe, G.; El-Kabbani, O.; Joachimiak, A. *J. Med. Chem.* **2005**, *48*, 5659-5665. b) Steuber, H.; Heine, A.; Klebe, G. *J. Mol. Biol.* **2007**, *368*, 618-638.

¹⁰⁷ a) Breiten, B.; Lockett, M. R.; Sherman, W.; Fujita, S.; Al-Sayah, M.; Lange, H.; Bowers, C. M.; Héroux, A.; Krilov, G.; Whitesides, G. M. *J. Am. Chem. Soc.* **2013**, *135*, 15579-15584. b) Petrova, T.; Steuber, H.; Hazemann, I.; Cousido-Siah, A.; Mitschler, A.; Chung, R.; Oka, M.; Klebe, G.; El-Kabbani, O.; Joachimiak, A. *Med. Chem.* **2005**, *48*, 5659-5665. c) Biela, A.; Nasief, N. N.; Betz, M.; Heine, A.; Hangauer, D.; Klebe, G. *Angew. Chem. Int. Ed.* **2013**, *52*, 1822-1828. d) Krimmer, S. G.; Betz, M.; Heine, A.; Klebe, G. *ChemMedChem* **2014**, *9*, 833-846.

particular ligand.¹⁰⁸ Changes made to the protein or the ligand can perturb the water hydrogen bonding network. In their work, they calculated the contribution of water network to the thermodynamic binding ability of SiaP (Haemophilus influenzae virulence protein) with several substrate ligands. A single mutation A11N caused a 1400 folds decrease in Neu5Ac affinity due to the change of the solvent network around the ligand while the ligand-binding mode and protein conformation were unaffected (see Figure 2.5).¹⁰⁷

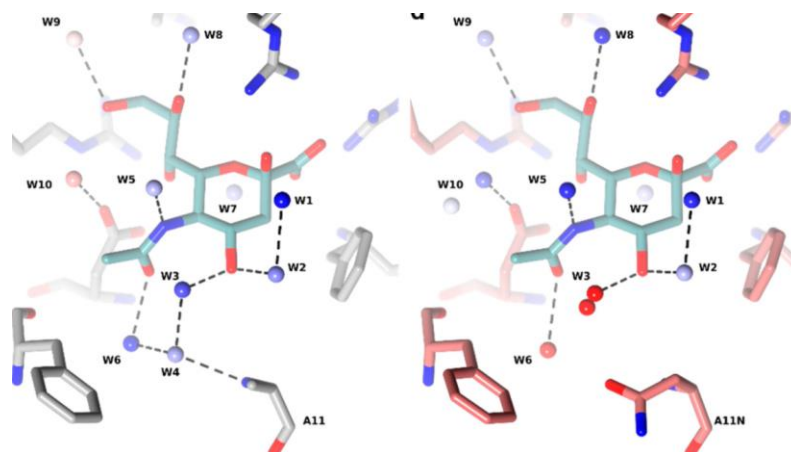


Figure 2.5. Neu5Ac (light blue sticks) in the SiaP cavity site (gray sticks) or in the site of SiaP mutant A11N (red sticks). Water molecules are numbered as W1-W10 and shown as spheres.

Hydrophobic effects often dominate the free energy of binding.¹⁰⁹ The hydrophobic effect's origin can be rationalized either from enthalpy or entropy-driven binding.¹¹⁰ The role of water in binding process has been investigated to explore the nature of the hydrophobic effects by utilizing ITC or X-ray crystallography as the experimental procedures.¹¹¹ In the structure of Human carbonic anhydrase II (HCA) with bicyclic ligands, there are three to five ordered water molecules between phenyl group and the hydrophobic wall. The hydrophobic effect has been rationalized by invoking the entropically favorable release of ordered water molecules that surrounds the hydrophobic surfaces. The changes in the structure of

¹⁰⁸ Darby, J. F.; Hopkins, A. P.; Shimizu, S.; Roberts, S. M.; Brannigan, J. A.; Turkenburg, J. P.; Thomas, G. H.; Hubbard, R. E.; Fischer, M. *J. Am. Chem. Soc.* **2019**, *141*, 15818-15826.

¹⁰⁹ Southall, N. T.; Dill, K. A.; Haymet, A. *J. Phys. Chem. B.* **2002**, *106*, 521-533.

¹¹⁰ Wang, L.; Berne, B.; Friesner, R. *Proc. Natl Acad. Sci.* **2011**, *108*, 1326-1330.

¹¹¹ Bronowska, A. K., Thermodynamics of ligand-protein interactions: implications for molecular design. In *Thermodynamics-Interaction Studies-Solids, Liquids and Gases*, IntechOpen: 2011.

water across the binding pocket of HCA determines the hydrophobic effect in biomolecular recognition of this system (Figure 2.6).¹¹²

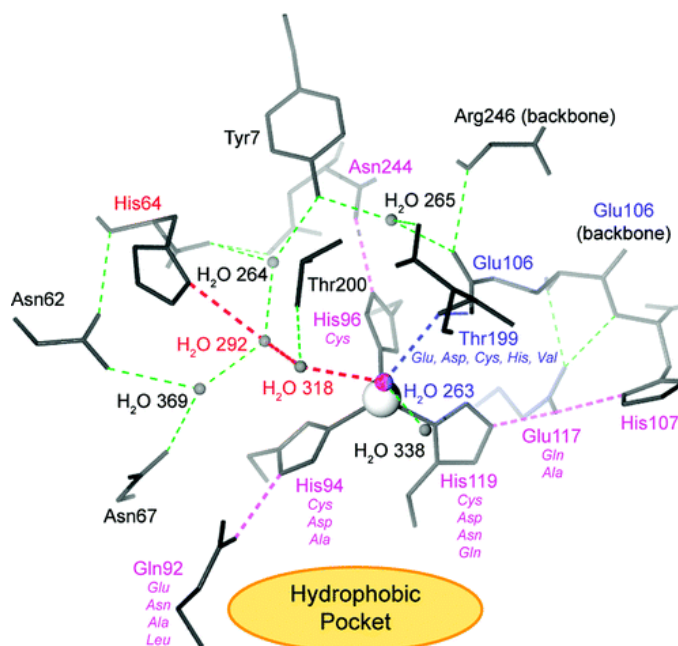


Figure 2.6. Hydrogen bonding network in the active site of HCA II. All hydrogen bonds are shown in dash lines.

2.9.2 The protein X-ray crystal structure of 1,2-azaborine in T4 lysozyme L99A/M102H cavity

We established previously that the parental 1,2-azaborines in the T4 lysozyme M102Q active site exhibits a Gln-102=O....H-N hydrogen bond and the contribution of that hydrogen bond to the net free energy binding is around -0.94 kcal/mol.¹¹³ Having demonstrated 1,2-azaborine's NH hydrogen bond donor capability, we sought out to utilize another T4 lysozyme double mutant L99A/M102H as the binding cavity model for establishing the relationship of hydrogen bond strength with different NH hydrogen bond acceptor residue. The cavity of L99A/M102H has a His102 substitution in the otherwise hydrophobic cavity.¹¹⁴ Among all the ligands of M102H that has been reported so far, no ordered water molecule has

¹¹² Krishnamurthy, V. M.; Kaufman, G. K.; Urbach, A. R.; Gitlin, I.; Gudiksen, K. L.; Weibel, D. B.; Whitesides, G. M. *Chem. Rev.* **2008**, *108*, 946-1051.

¹¹³ Lee, H.; Fischer, M.; Shoichet, B. K.; Liu, S.-Y. *J. Am. Chem. Soc.* **2016**, *138*, 12021-12024.

¹¹⁴ Merski, M.; Shoichet, B. K. *Proc. Natl Acad. Sci.* **2012**, *109*, 16179-16183.

ever been observed by protein X-ray crystallography.¹¹⁵ In the empty cavity of M102H, only 2-mercaptoethanol (BME), a component of the crystallization buffer was observed by crystal structure, It is likely that M102H cavity contains ordered water molecules when dissolved in solution.¹¹⁶ In apo binding site of M102Q, 2-mercaptoethanol from the crystallization buffer and a water molecule was observed in the pocket.⁵⁰ Upon binding of the benzene as the ligand, the 2-mercaptoethanol was displaced from the cavity, but the ordered water remained in the L99A/M102Q cavity as the water molecule is still bonded to Gln102 in the cavity via H-bond interaction. Both phenol and 4,5,6,7-tetrahydroindole also bind with an ordered water in the polar L99A/M102Q site.¹¹⁷ In the case of parental 1,2-azaborine ligand complex with M102Q, the ordered water molecule was displaced by the azaborine ligand and NH group of the ligand forms a hydrogen bond with the carbonyl oxygen of the Gln102 residue instead.¹¹³

Our crystal structure of M102H binding to NHBH ligand has revealed an opposite trend. While there may not be a water molecule in the empty cavity of M102H initially, upon 1,2-azaborine added as ligand, a water molecule was recruited into the binding cavity (shown in Figure 2.7). The water bridge was observed between 102H N δ 1 and NH of 1,2-azaborine in the cavity of L99A/M102H. The distance between water molecule and N δ 1 of 102H or NH of 1,2-azaborine are 1.8 Å and 3.2 Å, respectively. The distance between NH of 1,2-azaborine and N δ 1 of 102H is 3.7 Å. The hydrogen bond length that is considered to have energetical significance is within 3.5 Å between the donor and acceptor.¹¹⁸ In L99A/M102Q -NHBH complex, the NH group of azaborine is 3.2 Å away from the carbonyl oxygen atom of the Gln102 residue (Figure 2.8). We postulate that the water molecule here mediates the 1,2-azaborine ligand binding to M102H cavity by serving as a water bridge.

¹¹⁵ Merski, M.; Shoichet, B. K. *J. Med. Chem.* **2013**, *56*, 2874-2884.

¹¹⁶ Prabhu, N.; Sharp, K., Protein– solvent interactions. *Chem. Rev.* **2006**, *106*, 1616-1623.

¹¹⁷ Mobley, D. L.; Gilson, M. K., Predicting binding free energies: frontiers and benchmarks. *Annual review of biophysics* **2017**, *46*, 531-558.

¹¹⁸ George, J. A. *An introduction to hydrogen bonding*, Oxford University Press, Cambridge, 1997.

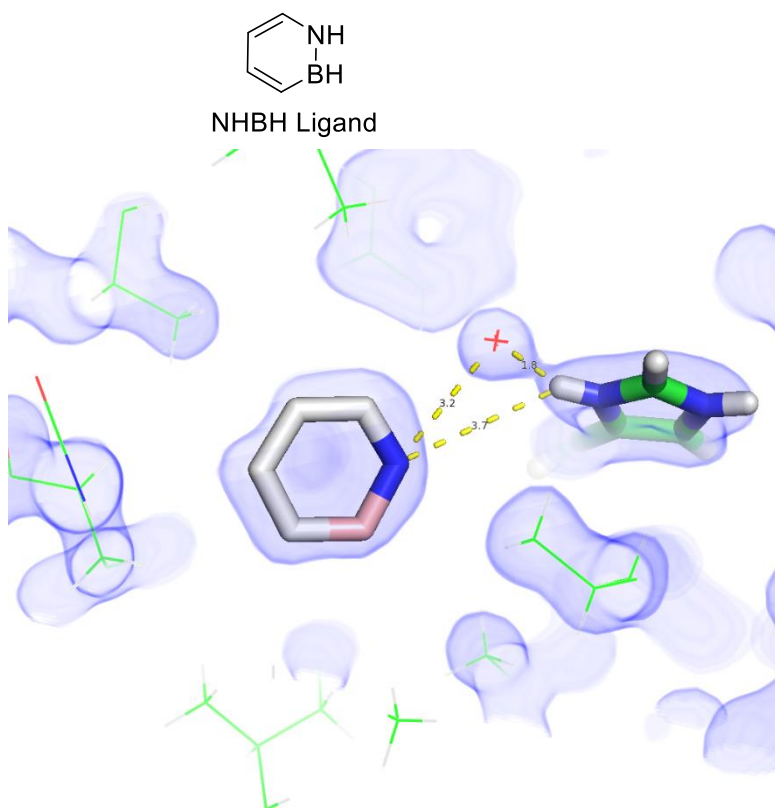


Figure 2.7. The X-ray structure of 1,2-dihydro-1,2-azaborine bound to L99A/M102H of a resolution of 1.35 Å. Parental 1,2-azaborine ligand (gray carbon backbone) in cavity of M102H. Hydrogen bonding was shown as yellow dashed bond between the water molecule and the M102H residue (green carbon backbone).

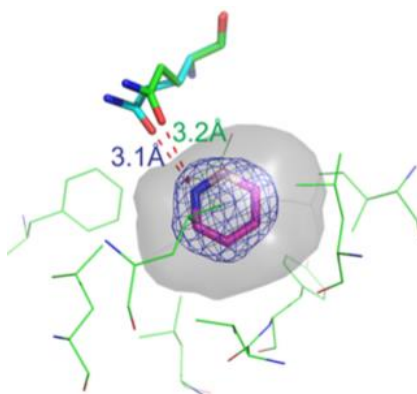


Figure 2.8. 1,2-azaborine (purple sticks) bound in the T4 lysozyme L99A/M102Q binding pockets. Distance (in Å) between ligand-N and the Gln102=O (green backbone) are illustrated in red dashes.

When we took another look at the X-ray crystal structure, there is also a possibility for the existence of a dihydrogen bonding¹¹⁹ between the boron hydride and the hydrogen of water bridge and the geometry may be a bifurcated hydrogen bonding mode between parental 1,2-azaborine and the active water molecule. The distance of boron atom of 1,2-azaborine to water molecule as shown in Figure 2.9 is 3.1 Å, which is within the distance of a dihydrogen bonding.¹²⁰ The dihydrogen bond (the negatively charged B-H atom here is the proton acceptor, while Y-H atom is the proton donor) angle B-H...H θ and Y-H ...H ψ (90-171°) and bond distance d_{HH} (1.7-2.3 Å) fall into the normal range of the conventional hydrogen bonding.¹²¹

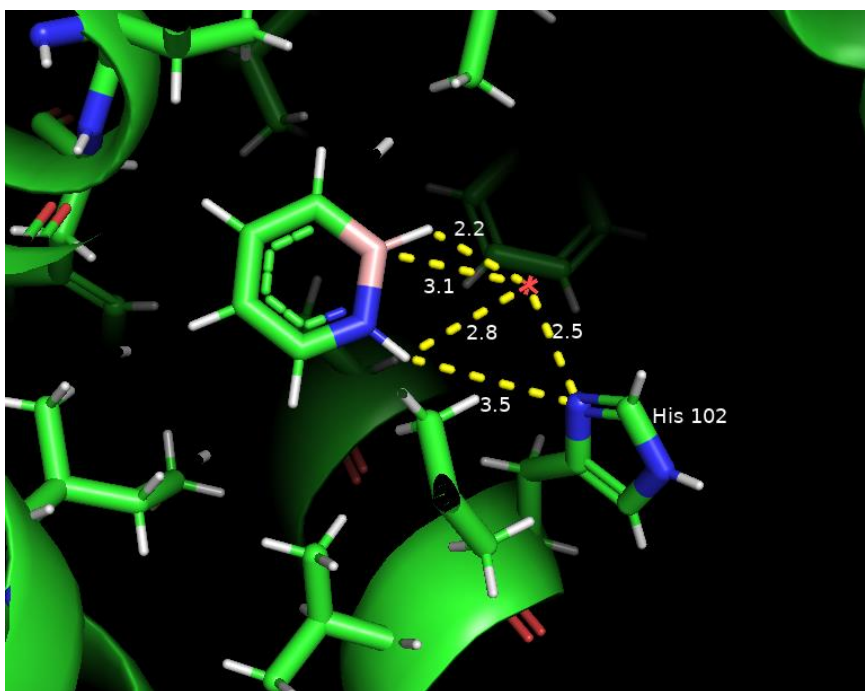


Figure 2.9. The possible B-H...H-O-H dihydrogen bonding in the cavity of L99A/M102H T4 lysozyme.

¹¹⁹ Bakhmutov, V. I., *Dihydrogen bond: principles, experiments, and applications*. John Wiley & Sons: 2008.

¹²⁰ Grabowski, S. J.; Leszczynski, J., Dihydrogen bonds: novel feature of hydrogen bond interactions. In *Practical Aspects of Computational Chemistry*, Springer: 2009; pp 255-275.

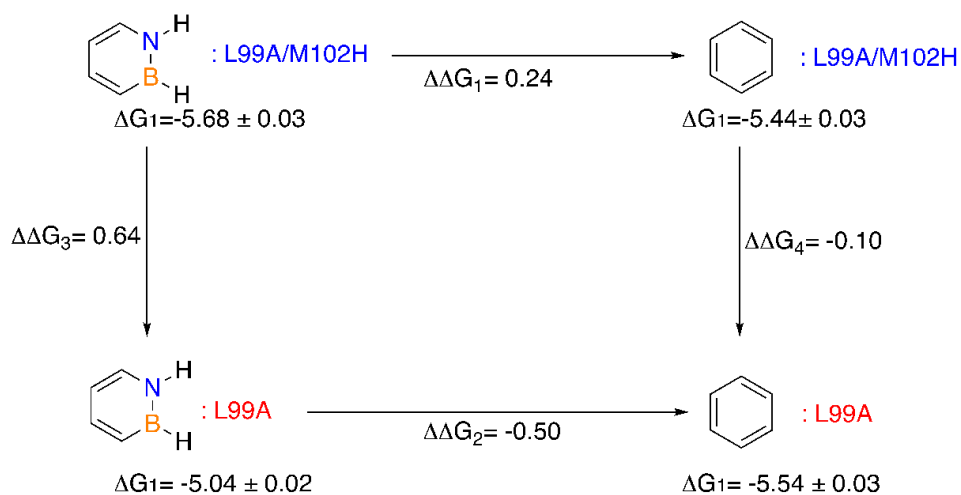
¹²¹ a) Fanfrlik, J.; Lepšik, M.; Horinek, D.; Havlas, Z.; Hobza, P. *ChemPhysChem* **2006**, *7*, 1100-1105. b) Custelcean, R.; Jackson, J. E. *Chem. Rev.* **2001**, *101*, 1963-1980. c) Kar, T.; Scheiner, S. *J. Chem. Phys.* **2003**, *119*, 1473-1482.

2.9.3 Isothermal titration calorimetry data

Ligand-receptor binding at equilibrium are typically described by thermodynamic parameters such as the Gibbs free energy of binding (ΔG), enthalpy (ΔH) and entropy (ΔS).¹²² ITC experiments can simultaneously determine the value of ΔG and ΔH for the binding process and entropy contributions can be subsequently calculated as well. Negative enthalpy and positive entropy will cause energetically favorable binding and an increase in binding affinity. In the M102H cavity, the binding affinity K_a of benzene and toluene (2.1×10^3 and $1.1 \times 10^3 \text{ M}^{-1}$) drop by 3- and 9-folds when compared to L99A cavity (5.7×10^3 and $9.8 \times 10^3 \text{ M}^{-1}$, see Table 2.2 and Table 2.5).^{48,51} On the other hand, the binding affinity K_a of phenol to M102H cavity is similar when compared to the M102Q cavity (9.7×10^3 vs. $11 \times 10^3 \text{ M}^{-1}$, see Table 2.4 and Table 2.5).^{50,51} To further investigate the binding affinities of 1,2-azaborine ligand with the M102H cavity, we utilized isothermal titration calorimetry (ITC) and the classic thermodynamic cycle analysis to estimate the specific hydrogen bonding contribution between the azaborine ligand and the water bridge/102H residue. The energy gained by hydrogen bonding of parental azaborine was -0.74 kcal/mol . In comparison, the H-bond strength of the NHBH ligand in cavity of M102Q was measured to be -0.94 kcal/mol . The slightly weaker interaction in M102H cavity may be due to the entropic cost of locking a free water molecule in the pocket. The interaction between NHBEt and M102H was measured to be -0.52 kcal/mol , also slightly lower than the same case for M102Q. The weaker hydrogen bond interaction vs. the parental NHBH ligand is likely caused by steric of the ethyl group on azaborine (Figure 2.10).¹²³

¹²² Klebe, G. *Nat. Rev. Drug Discov.* **2015**, *14*, 95-110.

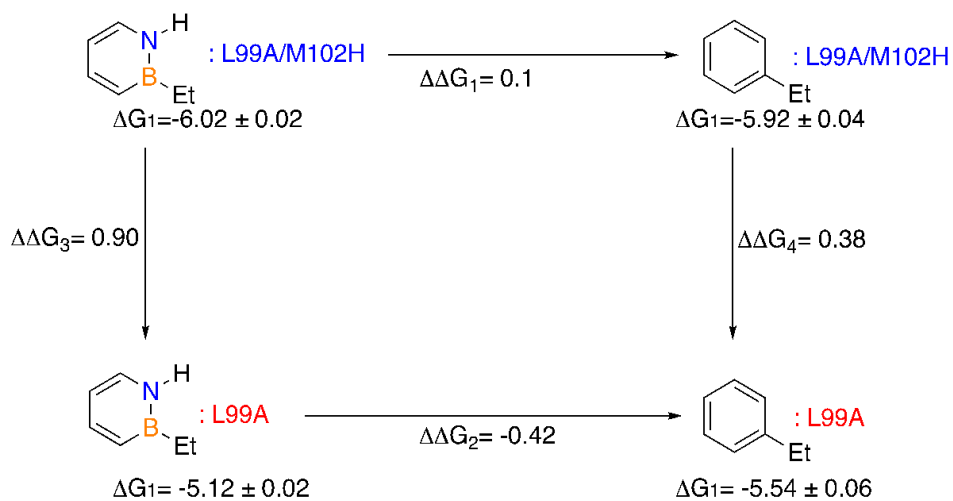
¹²³ Liu, Y.; Liu, S.-Y. *Org. Biomol. Chem.* **2019**, *17*, 7002-7006.



Energy gained by hydrogen bonding of **NHBH** to **L99A/M102Q**:

$$\Delta\Delta\Delta G = (\Delta\Delta G_2 - \Delta\Delta G_1) \text{ or } (\Delta\Delta G_4 - \Delta\Delta G_3) = -0.74 \text{ kcal/mol}$$

All the ΔG values expressed in kcal/mol.



Energy gained by hydrogen bonding of **NHBet** to **L99A/M102H**:

$$\Delta\Delta\Delta G = (\Delta\Delta G_2 - \Delta\Delta G_1) \text{ or } (\Delta\Delta G_4 - \Delta\Delta G_3) = -0.52 \text{ kcal/mol}$$

All the ΔG values expressed in kcal/mol.

Figure 2.10. The double mutant cycle analysis to estimate the H-bonding between NHBH and NHBet in the L99A/M102H T4 lysozyme cavity.

Conclusion

In summary, we have showcased the azaborine ligand binding mode in a polar cavity of M102H. The distance between the water bridge and parental azaborine ligand is 3.2Å and the water molecule has a much stronger electrostatic interaction with 102His residue as the distance is 1.8Å. The bonding interaction thermodynamics were also quantitatively described by ITC experiments. This study helped us improve our current understanding on 1,2-azaborine ligand-protein recognition mode with the L99A/M102H cavity.

2.9.4 Experimental section

Synthesis of 1,2-Azaborine Ligands

1,2-Dihydro-1,2-azaborine¹²⁴ (Ab) and B-Et-1,2-azaborine¹¹³ (BEtAb) was synthesized according to literature methods.

Protein Expression and Crystallization

E. coli BL21(DE3) cells was transformed with the subcloned plasmid from Brian Matthews lab (containing T4 phage lysozyme L99A/M102H† in pET-28). Kanamycin-resistant transformants were isolated and stored in 20% glycerol stock solution in LB media at -80°C. The protein expression procedure followed the work published by Shoichet.⁵¹ The transformed cell was grown in LB media containing kanamycin until OD600 reaches 0.6-0.8 at 37°C. And then induced with 0.5 mM isopropyl β-D-1-thiogalactopyranoside overnight at 18°C. Cells were lysed by thaw-freeze cycles for 3 times. Then centrifuged at 18000g for 20mins and suspended in 50mM phosphate buffer, pH 6.6. The suspension was purified on a nickel-nitrilotriacetic acid column at 4 °C, imidazole buffer, pH 6.8, in the presence of 5 mM 2-mercaptoethanol and the protein purity was ≥95% by SDS-PAGE. The purified protein fractions were combined and dialyzed into 200 mM KCl, 5 mM 2-mercaptoethanol, 0.02% sodium azide, 50 mM phosphate buffer, pH 6.6 once and then two more times in the same buffer without 2-mercaptoethanol or azide, and finally concentrated to 10 mg/mL, aliquoted, and flash frozen in liquid nitrogen and stored at -80 °C until needed.

For crystallization, the protein sample was dialyzed against 200 mM KCl, 5 mM 2-mercaptoethanol, 0.02% sodium azide, 50 mM phosphate buffer, pH 6.6 at 4°C overnight. 2-Mercaptoethanol (final concentration of 5 mM) was added to the dialyzed sample, and the protein solution was concentrated to 5mg/mL using Vivaspin 20 (10,000 mwco molecular weight cutout). Protein concentrations were determined by measuring absorption at 280 nm. Any precipitates was removed by spinning prior to crystallization. Crystals were grown from a 5 mg/ml solution of the protein by the hanging drop method at 4 °C over a well solution of 0.1 M sodium acetate, pH 4.5, 30% (w/v) PEG-6000, 0.3 M

¹²⁴ Abbey, E. R.; Lamm, A. N.; Baggett, A. W.; Zakharov, L. N.; Liu, S.-Y. *J. Am. Chem. Soc.* **2013**, *135*, 12908-12913.

LiSO₄, 3% trimethylamine *N*-oxide, 50 mM 2-mercaptoethanol, 50 mM 2-hydroxyethyl disulfide. Crystals grew as plates within a month. A fresh well solution with the addition of sucrose to 25% (w/v) served as a cryo solution.

Complex Preparation

Suitable crystals were picked and transferred into a microcentrifuge tube and maintained in 50 μ l of the mother liquor. Ligands were soaked into the crystals in the cryo solution at 4 °C for 1-2 days by vapor diffusion method by placing a droplet of each ligand inside of the snap-cap of the tube. The complexes were prepared in a glove box for azaborine ligands.

Isothermal titration calorimetry (ITC) Experiments

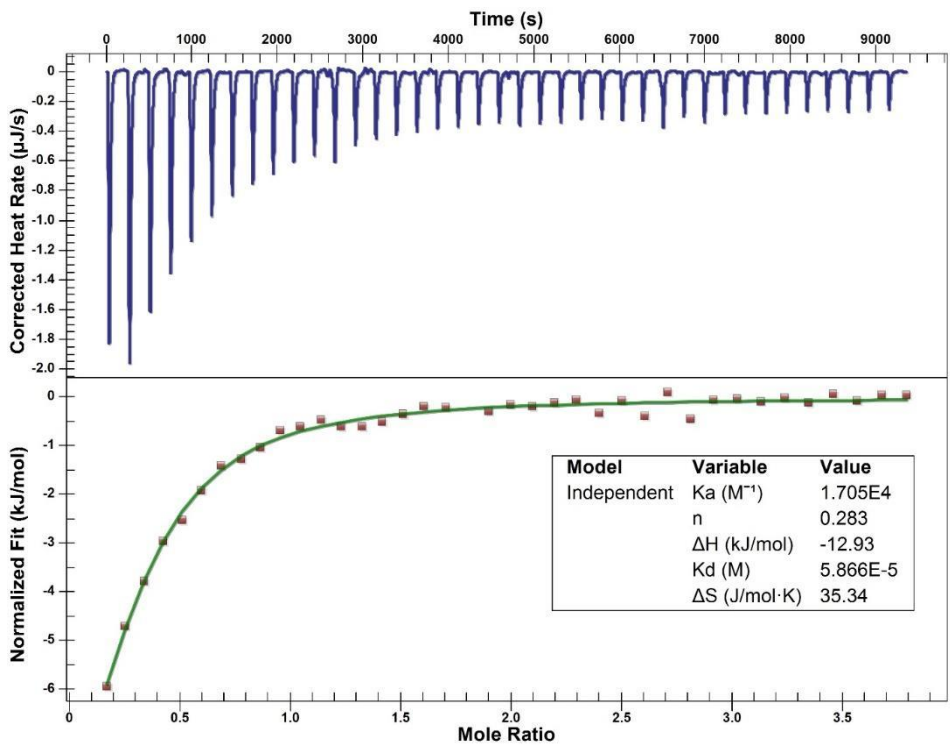
The protein solution was prepared by dialyzing against the ITC buffer of 5% PEG400, 0.5M NaCl, 0.1M sodium phosphate (pH 6.8) and the concentrations were determined by molar absorptivity at 280 nm. Both ligand and protein were in the same degassed ITC buffer solution for the ITC titration experiments to minimize the dilution heat.

Isothermal titration calorimetry experiments (in a Nano ITC calorimeter from TA instruments) were carried out at 10°C with 310 rpm stirring rate with a data collection interval of 4 min/injection. A total of volume of 100 μ l (2.5 μ l x 40 injections) ligand solution (2.66 - 3.74 mM) were injected into 320 μ l of 0.3 mM protein solution. The ligand was directly dissolved in the degassed ITC buffer from protein dialysis and ligand concentration was determined by UV-Vis against a standard calibration curve. The heat of ligand dilution was measured by titrating the ligand into the ITC buffer for each titration pairs, and the heat of dilution has been subtracted from each titration.¹²⁵ The resulting reaction heat profiles were fit to the one binding site independent binding model with the stoichiometry *n* fixed to 1.0. All data were analyzed using NanoAnalyze software. Experiments were repeated five times and averaged with standard deviation error of the mean. Representative ITC traces are shown below.

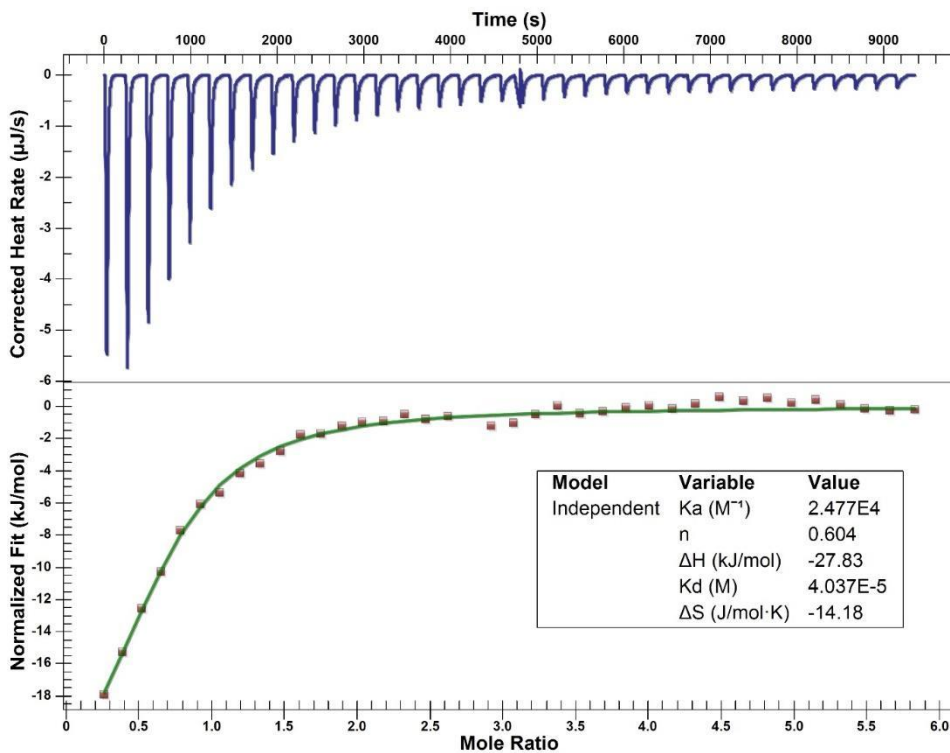
¹²⁵ Duff Jr, M. R.; Grubbs, J.; Howell, E. E. *J. Vis. Exp.* **2011**, 55, e2796.

Representative ITC Traces

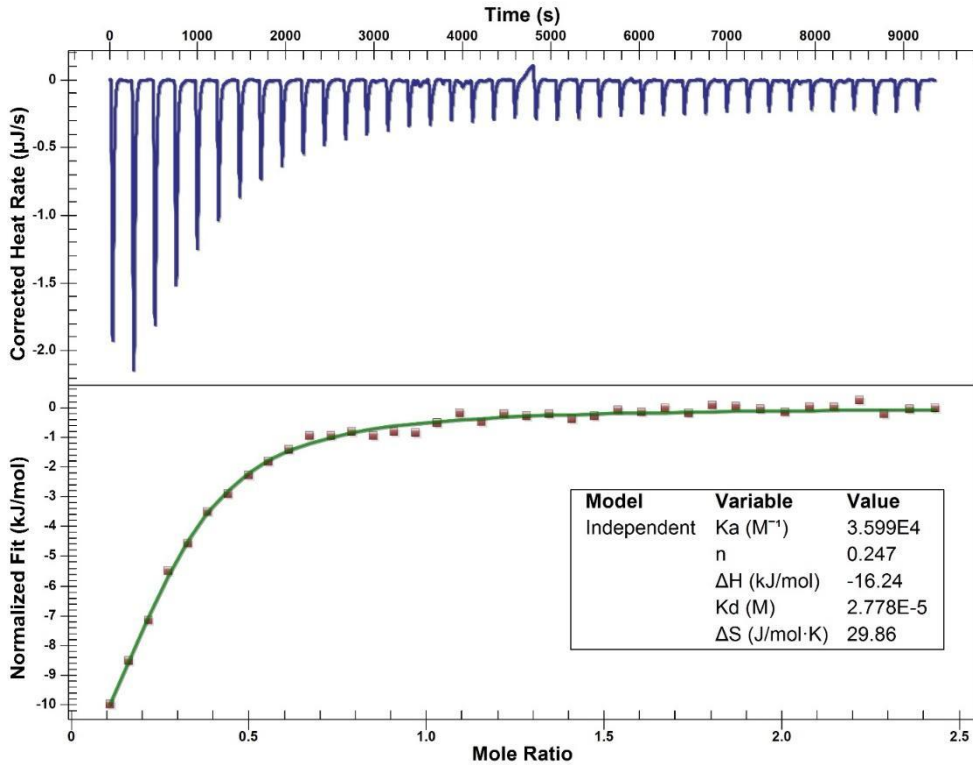
Benzene to M102H



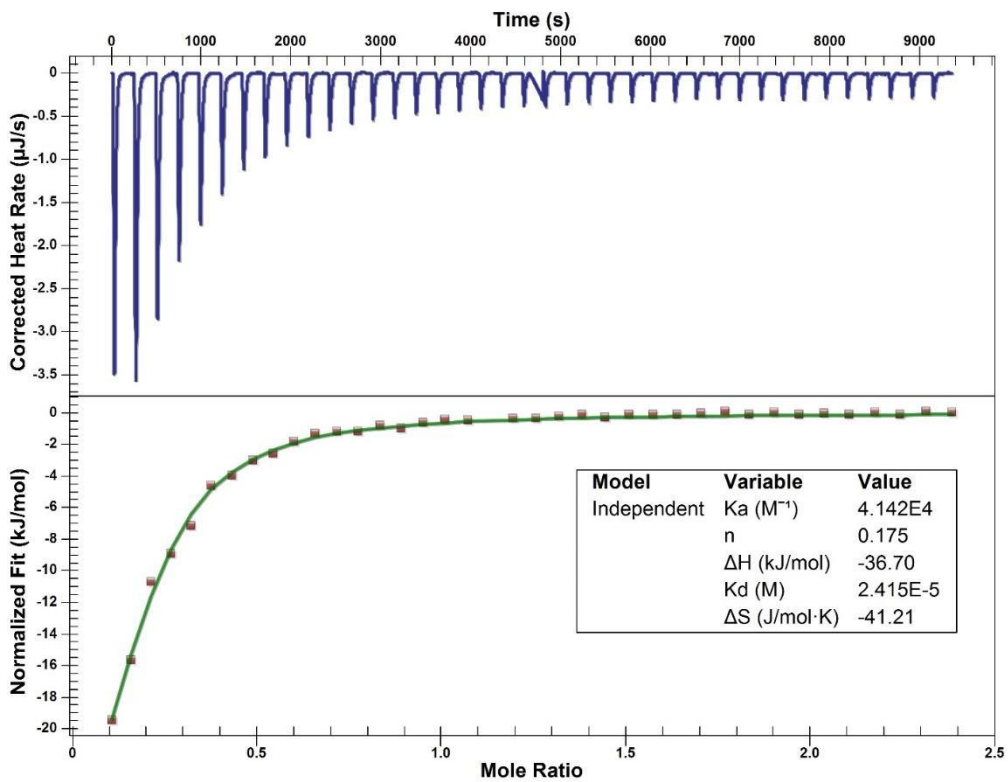
NHBH to M102H



Ethylbenzene to M102H



NHBet to M102H



X-Ray Structure Data Collection, Structure Determination and Refinement

Data sets were obtained at the ALS beamline 8.3.1. at the Advanced Light Source, Berkeley, CA. Prior to X-ray data collection the crystals were flash-frozen in liquid nitrogen with protection of N-paratone (Hampton Research).

Data were collected from beamline 8.3.1. and indexed, integrated, and scaled with XDS/XSCALE. PHENIX's AutoMR program was used to determine the structures by molecular replacement with a previously determined structure of L99A/M102H[†] in complex with 2-mercaptoethanol (4E97) with PDB code of 181L as the starting models. Ligand restraints of azaborines were generated by REEL based on knowledge of the crystal structures of the small molecules. Models were improved by rounds of manual refinement in Coot and automated refinement with PHENIX's phenix.refine program. Model quality was determined using MolProbity in PHENIX. The model M102H bound 1,2-azaborine was solved to a resolution of 1.72 Å. All structural alignments and images were generated using PyMOL (The PyMOL Molecular Graphics System, Schrödinger, LLC).

Data Deposition

The coordinates and structure factors have been deposited in the RCSB Protein Data Bank with PDB ID of 7SJ6 for L99A/M102H with 1,2-dihydro-1,2-azaborine (**Ab**).

Acknowledgements

We thank Dr. Jacob Wirth from Theobald lab, Brandeis University for solving the crystal structure of M102H/1,2-dihydro-1,2-azaborine complex, Dr. Matthew Merski for experimental advice on protein crystallization and George Meigs at Beamline 8.3.1, Advanced Light Source for data collection.

X-Ray Data Collection and Structure Refinement Statistics.

Table 1. Data collection and refinement statistics.

Parameters	M102H bound 1,2-azoborine
Wavelength	
Resolution range	48.7 - 1.721 (1.783 - 1.721)
Space group	P 1 21 1
Unit cell	48.78 75.84 52.82 90 93.223 90
Total reflections	
Unique reflections	34602 (1518)
Multiplicity	
Completeness (%)	84.90 (37.76)
Mean I/sigma(I)	
Wilson B-factor	19.35
R-merge	
R-meas	
R-pim	

CC1/2	
Reflections used in refinement	34599 (1518)
Reflections used for R-free	1770 (75)
R-work	0.1672 (0.2345)
R-free	0.2008 (0.2641)
Number of non-hydrogen atoms	3335
Macromolecules	2779
Ligands	57
Solvent	499
Protein residues	348
RMS(bonds)	0.003
RMS(angles)	0.53
Ramachandran favored (%)	98.84
Ramachandran allowed (%)	1.16
Ramachandran outliers (%)	0.00

Rotamer outliers (%)	0.68
Clashscore	0.88
Average B-factor	23.49
Macromolecules	21.61
Ligands	38.92
Solvent	32.17

Statistics for the highest-resolution shell are shown in parentheses.